

**PORTABLE PLATFORMS FOR MOLECULAR-BASED DETECTION OF
PATHOGENS IN COMPLEX SAMPLE MATRICES**

by

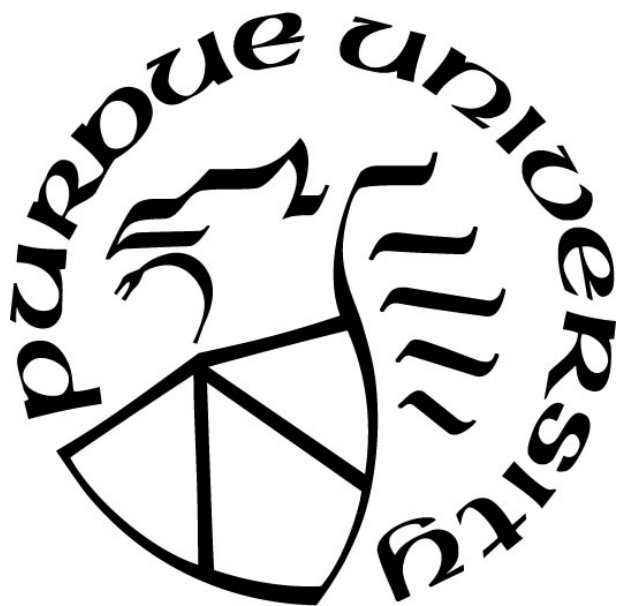
Taylor Jo Moehling

A Dissertation

Submitted to the Faculty of Purdue University

In Partial Fulfillment of the Requirements for the degree of

Doctor of Philosophy



Weldon School of Biomedical Engineering

West Lafayette, Indiana

August 2020

**THE PURDUE UNIVERSITY GRADUATE SCHOOL
STATEMENT OF COMMITTEE APPROVAL**

Dr. Jacqueline Linnes, Chair

Weldon School of Biomedical Engineering

Dr. Tamara Kinzer-Ursem

Weldon School of Biomedical Engineering

Dr. Babak Ziaie

Electrical and Computer Engineering

Dr. Afsar Ali

Department of Environmental and Global Health, University of Florida

Approved by:

Dr. George R. Wodicka

Dedicated to my parents for always challenging me to push the boundaries

ACKNOWLEDGMENTS

This work would not have been possible without the support of many individuals. First and foremost, I would like to thank my advisor Dr. Jacqueline Linnes for taking a chance on me five years ago and inviting me to join her lab. With her mentorship, I have grown both professionally and personally. Jackie has always motivated me to challenge myself and pursue my scientific, professional, and personal passions. She encouraged me to pursue a Master of Public Health in addition to my PhD in Biomedical Engineering because she understood the benefits of the additional learning experiences. Jackie is a wonderful role model and an incredible support system for her students. Still today, I am inspired by her positive energy and passion for global health and biomedical engineering and I feel fortunate to have her as a mentor.

I would also like to thank my thesis committee, Dr. Babak Ziaie, Dr. Tamara Kinzer-Ursem, and Dr. Afsar Ali. I met Dr. Babak Ziaie my first semester of graduate school in his biosensors class. This was my first exposure to the biosensor field; Dr. Ziaie and his course confirmed my decision to pursue biosensor research. I began working closely with Dr. Tamara Kinzer-Ursem in my second year of graduate school on a collaborative project with one of her graduate students. Tami has been incredibly helpful in guiding experimental design, data analysis, and manuscript writing for the particle diffusometry projects. Dr. Afsar Ali has been a critical collaborator since my first year of graduate school. Through his network, I had the opportunity to spend the summer after my first year of graduate school conducting research and learning about cholera in Haiti.

The faculty and staff in the Weldon School of Biomedical Engineering are truly exceptional. Dr. Karin (Kaisa) Ejendal was one of the best additions to our lab (and entire third floor). Kaisa's vast knowledge of fundamental science and her extensive skill set were helpful when troubleshooting research problems. She also always welcomes conversation – about research or family or recent vacations. Additionally, I am glad I had the opportunity to teach with and learn from Dr. Asem Aboelzahab during my first three years in the Weldon School of Biomedical Engineering. Tammy Siemers also deserves an acknowledgement for organizing frequent industry trips and professional development workshops for graduate students. I am also thankful for Sandy May, Jo Gelfand, Kitty Cooper, Pamela Lamb, Carla Brady, Linda Doyle, Susan Hardy, and Bill Schoenlein and all they do in terms of academic and departmental support.

I would like to thank my second home at Purdue – the Department of Public Health. After my second year in the PhD program, I enrolled in the Master of Public Health program as a dual-degree student. During my time in the Master of Public Health program, I met many individuals who shaped my professional and personal interests and values: Dr. Andrea DeMaria, Dr. Natalia Rodriguez, Dr. Laura Schwab Reese, Shauna Stapleton, Justin Phillips, Robin Wonnell, Kourtnaye Sturgeon, and Dr. Beth Meyerson. I am forever grateful for their support and patience.

The members of the Linnes Lab are creative, fun, and supportive individuals who are not only great labmates but also wonderful friends. Elizabeth, Divya, Orlando, and I will always have the shared experience of being the ‘original four’ graduate students and I am glad we could lean on each other during those first couple semesters. I would also like to thank K, Ashlee, Jay, Mindy, Somayeh, Laud Anthony, Amy, Hui, Emeka, and Emilee for their encouragement and collaboration over the years. I also had the privilege of mentoring several dedicated undergraduate students including Sonia, Jackson, Lauren, Ethan, Seba, Mariah, Meghan, and Preston.

I want to give a special shoutout to my labmate and good friend, Divya Tankasala. She has been an incredible friend and support system throughout this PhD journey. My time at Purdue was filled with many laughs, great food, and exhausting workouts because of Divya. I also want to acknowledge Katherine Clayton. Katie always pushed me to be independent in my research and challenged me to become a better scientist. Not only is Katie a phenomenal mentor and role model, but she is one of my best friends. I am grateful I can always rely on her for support. Additionally, I would like to thank my best friends from undergrad: Alli, Rachel, Nina, Jenny, and Gina. I appreciated their many visits to Purdue and our annual Spring Break trip. These strong, compassionate, and supportive women are like sisters to me.

Thank you to my parents, Chuck and Kelly Moehling, for their endless love and encouragement throughout my educational journey. I am also incredibly grateful for my brothers, grandparents, and extended family for their support and affection. My family instilled in me a strong work ethic, respect, and kindness and I always try to make them proud.

TABLE OF CONTENTS

LIST OF TABLES.....	11
LIST OF FIGURES	12
LIST OF ABBREVIATIONS.....	15
ABSTRACT.....	16
1. INTRODUCTION	17
1.1 Point-of-Care Tests	17
1.1.1 Understanding the Need	17
1.1.2 Detection Molecules for Point-of-Care Tests	17
1.1.3 Signal Transduction for Point-of-Care Tests.....	18
1.1.4 Guidance for Point-of-Care Test Development.....	18
1.1.5 Existing and Emerging Smart Handheld Platforms.....	18
1.1.6 Existing and Emerging Disposable Platforms	19
1.2 Nucleic Acid-Based Detection.....	20
1.2.1 Nucleic Acid Amplification.....	20
1.2.2 Polymerase Chain Reaction.....	20
1.2.3 Isothermal Nucleic Acid Amplification.....	21
1.3 Cholera.....	21
1.3.1 Burden, Cause, and Symptoms.....	21
1.3.2 Existing and Emerging Platforms for Detection of Cholera.....	22
1.4 HIV	23
1.4.1 Burden, Cause, and Symptoms.....	23
1.4.2 Existing and Emerging Platforms for Detection of HIV	23
1.5 Thesis Overview: Development of Molecular Detection Platforms for Pathogens in Complex Sample Matrices.....	24
2. DEVELOPMENT OF <i>V. CHOLERAE</i> LOOP-MEDIATED ISOTHERMAL AMPLIFICATION ASSAY AND DETECTION VIA LATERAL FLOW IMMUNOASSAY .	26
2.1 Rationale	26
2.2 Materials and Methods.....	27
2.2.1 Reagents.....	27

2.2.2	Bacteria Culture	28
2.2.3	Standard Loop-Mediated Isothermal Amplification (LAMP).....	28
2.2.4	Strand Displacement Loop-Mediated Isothermal Amplification (SD-LAMP)	29
2.2.5	Amplicon Analysis via Lateral Flow Immunoassay (LFIA) and Gel Electrophoresis	29
2.2.6	Statistical Analysis.....	30
2.3	Results and Discussion	30
2.3.1	<i>V. cholerae</i> Standard LAMP Reaction	30
	LAMP Assay Optimization.....	30
	LAMP Product Confirmation.....	31
	Limit of Detection of <i>V. cholerae</i> Genomic DNA	32
	Limit of Detection of <i>V. cholerae</i> Whole Cells	33
2.3.2	<i>V. cholerae</i> SD-LAMP Reaction.....	35
	Limit of Detection of <i>V. cholerae</i> Whole Cells	35
	<i>V. cholerae</i> Whole Cell Specificity.....	35
	<i>V. cholerae</i> Whole Cell Detection in Various Water Samples	36
	Limit of Detection of <i>V. cholerae</i> Whole Cells in Pond Water	37
2.4	Future Directions	39
2.5	Conclusions.....	39
3.	OPTIMIZATION OF VITRIFICATION TECHNIQUE FOR ROOM-TEMPERATURE STORAGE OF REAGENTS	40
3.1	Rationale	40
3.2	Materials and Methods.....	41
3.2.1	Reagents.....	41
3.2.2	<i>V. cholerae</i> SD-LAMP	41
3.2.3	HIV RT-LAMP.....	41
3.2.4	Reagent Drying and Storage.....	42
3.2.5	Statistical Analysis.....	42
3.3	Results and Discussion	43
3.3.1	Optimization of Vitrification for Room-Temperature Storage of LAMP Reagents..	43
3.3.2	Diffusivity of Vitrified LAMP Reagents.....	45

3.3.3	Vitrification of <i>V. cholerae</i> SD-LAMP Reagents.....	46
3.3.4	Vitrification of HIV RT-LAMP Reagents.....	48
3.4	Future Directions	51
3.5	Conclusions.....	51
4.	CREATION OF INTEGRATED PAPERFLUIDIC PLATFORMS.....	52
4.1	Rationale	52
4.2	Materials and Methods.....	53
4.2.1	Water Filtration and Bacteria Capture in Porous Membranes.....	53
4.2.2	Integrated <i>V. cholerae</i> μ PAD	55
4.2.3	Blood Separation and Virus Capture in Porous Membranes.....	56
4.2.4	Integrated microRAAD for HIV Detection	56
4.2.5	Statistical Analysis.....	57
4.3	Results and Discussion	58
4.3.1	Water Filtration and Bacteria Capture in Porous Membranes.....	58
4.3.2	Integrated μ PAD for <i>V. cholerae</i> Detection	61
4.3.3	Blood Separation and Virus Capture in Porous Membranes.....	64
4.3.4	Integration of microRAAD for HIV Detection	66
4.4	Future Directions	69
4.5	Conclusions.....	70
5.	MICROSCOPE CHARACTERIZATION OF PARTICLE DIFFUSOMETRY FOR <i>V. CHOLERA</i> E DETECTION.....	72
5.1	Rationale	72
5.2	Materials and Methods.....	74
5.2.1	LAMP	74
5.2.2	Particle Preparation.....	74
5.2.3	Particle Diffusometry Theory	75
5.2.4	Experimental Particle Diffusometry Measurements.....	77
5.2.5	Blinded Study	77
5.2.6	Water Testing.....	78
5.2.7	Statistical Analysis.....	78
5.3	Results and Discussion	79

5.3.1	Blinded Study	79
5.3.2	PD versus Fluorescence Measurements.....	80
5.3.3	Measuring the Combined Effect of Changes in Particle Size and Viscosity with PD	82
5.3.4	Environmental Water Samples	86
5.4	Future Directions	89
5.5	Conclusions.....	89
6.	TRANSLATION OF PARTICLE DIFFUSOMETRY TECHNIQUE TO SMARTPHONE PLATFORM FOR DETECTION OF <i>V. CHOLERAE</i>	91
6.1	Rationale.....	91
6.2	Materials and Methods.....	94
6.2.1	LAMP	94
6.2.2	Particle Preparation.....	94
6.2.3	Microfluidic Chip Assembly	94
6.2.4	Optics Design.....	95
6.2.5	Particle Diffusometry Theory	96
6.2.6	Smartphone-Based Platform Development	96
6.2.7	Smartphone-Based Particle Diffusometry Measurements.....	97
6.2.8	Experimental Design	98
6.2.9	Statistical Analysis.....	99
6.2.10	<i>V. cholerae</i> Concentrator User-Centered Design Study.....	99
6.2.11	<i>V. cholerae</i> Concentrator Experiments	100
6.3	Results and Discussion	101
6.3.1	Construction of Optics.....	101
6.3.2	Image Quality, Recording, and Processing.....	103
6.3.3	Limit of Detection in Pond Water	104
6.3.4	Single-Blinded Selectivity in Pond Water.....	107
6.3.5	Double-Blinded Study in Pond Water	108
6.3.6	<i>V. cholerae</i> Concentrator User-Centered Design Study	111
6.3.7	<i>V. cholerae</i> Concentrator Experiments.....	113
6.4	Future Directions	116

6.5 Conclusions.....	116
7. CONCLUSION.....	118
APPENDIX A. SUPPLEMENT TO CHAPTER 2.....	120
APPENDIX B. SUPPLEMENT TO CHAPTER 3.....	125
APPENDIX C. SUPPLEMENT TO CHAPTER 4.....	129
APPENDIX D. SUPPLEMENT TO CHAPTER 5.....	137
APPENDIX E. SUPPLEMENT TO CHAPTER 6.....	144
REFERENCES	152
PUBLICATIONS.....	169

LIST OF TABLES

Table 4.1 Absorbent wing membrane testing.	58
Table 4.2 Efficiency of membrane capture of fluorescent particles representing <i>V. cholerae</i>	59
Table 4.3 Efficiency of membrane capture of fluorescent particles representing HIV and blood cells.	65
Table 6.1 Time for each bacterial concentrator device to process 250 mL of water spiked with <i>V. cholerae</i> . (n=3).....	114
Table A.1 <i>V. cholerae</i> LAMP primers.....	120
Table A.2 <i>V. cholerae</i> LAMP target gene sequence.....	120
Table A.3 Standard LAMP master mix for <i>V. cholerae</i>	121
Table A.4 SD-LAMP master mix for <i>V. cholerae</i>	121
Table B.1 SD-LAMP vitrification master mix for <i>V. cholerae</i>	125
Table B.2 HIV RT-LAMP target gene sequence.....	125
Table B.3 HIV LAMP primers.	125
Table B.4 RT-LAMP vitrification master mix for HIV.....	125
Table C.1 Consumable components of <i>V. cholerae</i> μ PAD and cost.....	130
Table C.2 Consumable components of microRAAD and cost.	132
Table D.1 Average data from blinded study.....	137
Table E.1 Cost of the consumable components of the smartphone-based PD-LAMP system.....	147
Table E.2 Cost of the reusable components of smartphone-based PD system.	147
Table E.3 C_T values from LOD study.....	148
Table E.4 C_T values from selectivity study.....	149
Table E.5 Real-time fluorescence results and diffusion coefficients for training set samples. (n=30)	151

LIST OF FIGURES

Figure 2.1 Lateral flow immunoassay platform.....	27
Figure 2.2 <i>V. cholerae</i> LAMP assay optimization.....	31
Figure 2.3 <i>V. cholerae</i> LAMP restriction digest.....	32
Figure 2.4 <i>V. cholerae</i> LAMP LOD using genomic DNA.	33
Figure 2.5 Comparison of standard LAMP and SD-LAMP for <i>V. cholerae</i> whole cells.	34
Figure 2.6 Specificity of <i>V. cholerae</i> SD-LAMP assay.....	36
Figure 2.7 Robustness of <i>V. cholerae</i> SD-LAMP assay.....	37
Figure 2.8 LOD of <i>V. cholerae</i> SD-LAMP assay in pond water.....	38
Figure 3.1 LAMP tolerance of additives used in Hayashida <i>et al.</i>	43
Figure 3.2 Evaluation of cryoprotectants for LAMP reagent storage.....	44
Figure 3.3 Testing substrates for LAMP reagent storage.	45
Figure 3.4 Stability of vitrified <i>V. cholerae</i> SD-LAMP reagents stored at room temperature.....	48
Figure 3.5 Detection of HIV virus amplified by dried RT-LAMP reagents.....	50
Figure 4.1 <i>V. cholerae</i> LAMP in 0.22 μm PES.	60
Figure 4.2 <i>V. cholerae</i> SD-LAMP after filtering and capturing with PES.	61
Figure 4.3 Schematic of fluid flow in integrated μPAD	62
Figure 4.4 Detection of <i>V. cholerae</i> with modified μPAD	64
Figure 4.5 LFIA test band intensity of HIV RT-LAMP products after virus and blood cell separation in MF1/PES assembly.	66
Figure 4.6 Schematic of fluid flow in microRAAD.	67
Figure 4.7 Detection of HIV virus on microRAAD with reagents dried for 21 days.....	68
Figure 4.8 Operation of microRAAD.	69
Figure 5.1 PD-LAMP set-up.....	73
Figure 5.2 Relative viscosity blinded study.....	80
Figure 5.3 PD detection of <i>V. cholerae</i> amplification using purified DNA.	82
Figure 5.4 Biotinylated LAMP products measured using streptavidin-coated particles.	84
Figure 5.5 Measuring LAMP amplification from <i>V. cholerae</i> whole cells.	86
Figure 5.6 LAMP amplification from whole <i>V. cholerae</i> cells in environmental water samples.	88

Figure 6.1 Smartphone-based particle diffusometry.....	93
Figure 6.2 Smartphone-based particle diffusometry platform.....	102
Figure 6.3 Image quality comparison between smartphone and microscope.....	104
Figure 6.4 LOD of <i>V. cholerae</i> in pond water.....	106
Figure 6.5 Single-blinded selectivity in pond water.....	108
Figure 6.6 Characterization of the smartphone-based PD platform.....	110
Figure 6.7 <i>V. cholerae</i> concentrator.....	112
Figure 6.8 SUS survey data from user-centered design study with concentrator device.....	113
Figure 6.9 LAMP and PD data from <i>V. cholerae</i> concentrator experiments.....	115
Figure A.1 Schematic of standard LAMP and SD-LAMP reactions and subsequent LFIA detection.....	122
Figure A.2 Real-time amplification of <i>V. cholerae</i> genomic DNA using Yamazaki primers....	123
Figure A.3 LAMP amplification of <i>V. cholerae</i> using different reaction volumes.....	123
Figure A.4 <i>V. cholerae</i> thermal cell lysis at 65°C.....	124
Figure A.5 <i>V. cholerae</i> sample testing in Haiti.....	124
Figure B.1 LAMP reagent deposition patterns.....	126
Figure B.2 LAMP reagent drying setup.....	126
Figure B.3 LAMP tolerance of cryoprotectants and food color solutions.....	127
Figure B.4 LFIA from <i>V. cholerae</i> SD-LAMP reagent stability study.....	128
Figure B.5 HIV RT-LAMP reagents stored for 5 months at room temperature.....	128
Figure C.1 Vertical filtration setup for testing membrane capture efficiency.....	129
Figure C.2 Water filtration and bacteria capture setup.....	129
Figure C.3 <i>V. cholerae</i> μ PAD assembly.....	131
Figure C.4 Schematic of MF1/PES assembly for studies verifying red blood cell and virus separation.....	132
Figure C.5 Assembly of microRAAD μ PAD for HIV detection.....	133
Figure C.6 Fluidic testing of integrated <i>V. cholerae</i> μ PAD with large absorbent wings.....	134
Figure C.7 Fluidic testing of integrated <i>V. cholerae</i> μ PAD with small absorbent wings.....	134
Figure C.8 HIV RT-LAMP in different membranes.....	135
Figure C.9 HIV RT-LAMP assay efficiency at various temperatures.....	136

Figure D.1 Real-time fluorescence and PD measurements for DNA dilutions.	138
Figure D.2 Real-time fluorescence and PD measurements for biotinylated DNA dilutions.	139
Figure D.3 Real-time fluorescence and PD measurements for biotinylated DNA from whole <i>V. cholerae</i> cell dilutions.	140
Figure D.4 Real-time fluorescence and PD measurements for biotinylated DNA from whole <i>V. cholerae</i> cells spiked in various water samples.	141
Figure D.5 Real-time fluorescence and PD measurements for biotinylated DNA from whole <i>V. cholerae</i> cell dilutions spiked in pond water.	142
Figure D.6 Fluorescence measurements for biotinylated DNA from whole <i>V. cholerae</i> cell dilutions spiked in pond water.	143
Figure E.1 Exploded CAD model of the platform.	144
Figure E.2 System Usability Study (SUS) survey.	146
Figure E.3 Comparison of microscope and smartphone-based optical system.	148
Figure E.4 Representative real-time fluorescence curves over a 30-minute LAMP reaction for selectivity study.	149
Figure E.5 Diffusion coefficients of training set samples.	150

LIST OF ABBREVIATIONS

COP	cyclic olefin polymer
C _T	cycle threshold
<i>ctxA</i>	cholera toxin A
LAMP	loop-mediated isothermal amplification
LFIA	lateral flow immunoassay
LOD	limit of detection
microRAAD	microfluidic rapid and autonomous analysis device
NAAT	nucleic acid amplification test
NTC	no template control
PCR	polymerase chain reaction
PD	particle diffusometry
PD-LAMP	particle diffusometry + loop-mediated isothermal amplification
PES	polyethersulfone
PET	polyethylene terephthalate
POC	point of care
POCT	point-of-care test
PSA	pressure sensitive adhesive
RDT	rapid diagnostic test
RT-LAMP	reverse transcription + loop-mediated isothermal amplification
SD-LAMP	strand displacement + loop-mediated isothermal amplification
SUS	systems usability study
μPAD	microfluidic paper-based analytical device

ABSTRACT

Pathogen identification at the point of use is critical in preventing disease transmission and enabling prompt treatment. Current rapid diagnostic tests suffer from high rates of false negatives because they are not capable of detecting the inherently low concentrations of pathogens found in early stages of infection or in environmental reservoirs. The gold standard method for timely pathogen identification is a nucleic acid amplification assay called polymerase chain reaction. Although polymerase chain reaction is extremely sensitive and specific, it requires expensive laboratory equipment and trained personnel to perform the sample preparation, cyclical heating, and amplicon analysis. Isothermal nucleic acid amplification assays are better suited for field use because they operate at a single temperature and are robust to common sample matrix inhibitors. Thus, there is a need to translate isothermal amplification assays to the point of use for rapid and sensitive detection of pathogens in complex samples.

Here, I outline an approach to bring laboratory-based sample preparation, assays, and analyses to the point of use via portable platforms. First, I characterize a loop-mediated isothermal amplification assay and combine it with lateral flow immunoassay for simple, colorimetric interpretation of results. Next, I optimize an ambient-temperature reagent storage method to eliminate cold-chain requirements and precision pipetting steps. I then incorporate loop-mediated isothermal amplification, lateral flow immunoassay, and reagent drying into two different integrated paperfluidic platforms and demonstrate their ability to separately detect bacteria and viruses in complex sample matrices. Finally, I couple loop-mediated isothermal amplification with particle diffusometry to optically determine pathogen presence by tracking the Brownian motion of particles added to an amplified sample. The combined loop-mediated isothermal amplification and particle diffusometry method is first characterized on a microscope and then translated to a smartphone-based platform. Each of these portable platforms are broadly applicable because they can be easily modified for identification of other pathogens at the point of use.

1. INTRODUCTION

1.1 Point-of-Care Tests

1.1.1 Understanding the Need

There is a significant disparity between high and low resource regions of the world in terms of diagnosis of both infectious and non-infectious diseases. Disease diagnosis often depends on centralized laboratories with expensive equipment and trained technicians. In countries that report the highest mortality rates from preventable diseases, these facilities are limited in number and are often difficult to access. Other challenges in low resource areas include inadequate running water and unreliable electricity. Rapid tests for disease screening and diagnosis can improve health metrics in these regions of the world.¹

Point-of-care (POC) tests are analytical tools for near-patient testing that can be utilized in the clinic, the field, and even the patient's home. They are often designed to be inexpensive and to provide the user with rapid results whilst requiring minimal-to-no technical knowledge. In a recently published review, Yager *et al.* highlights the appeal of point-of-care tests (POCTs): the materials are easily accessible, the platforms do not require external equipment or power sources, and extensive training is not necessary.² POCTs are suitable for screening and monitoring diseases and illnesses as well as for personalized medicine. Rapid diagnostics are practical in fields of veterinary medicine, food safety, health sciences, bioterrorism, and environmental monitoring.³ The demand for *in vitro* POCTs is further demonstrated by a global market valued at \$53 billion in 2013 with an expected increase to \$75 billion by the year 2020.⁴

1.1.2 Detection Molecules for Point-of-Care Tests

Detection molecules allow specific identification of pathogens and are key for POCT evaluation. There are many types of detection molecules including antibodies, antigens, peptides, metabolites, hormones, proteins, and nucleic acids. Antibodies and antigens are the most common detection molecules for POCTs. Pathogens often cause an upregulation of unique immune response antibodies in the host or have surface antigens that can be used for infectious disease detection. However, antibodies are generally undetectable during the first few weeks of infection

and antigens often suffer from poor specificity.⁵ Metabolites, hormones, and proteins are commonly monitored by physicians and can indicate the overall health of a patient; however, they are not widely used for infectious disease screening.⁶ Direct detection of pathogens' nucleic acids provide a method for specific and sensitive early detection of infectious diseases because of the ability to amplify the nucleic acids to levels that are easily detectable.⁷

1.1.3 Signal Transduction for Point-of-Care Tests

Detection molecules need to be identified using a rapid and easy-to-read approach. Traditionally, POCTs use fluorescence, electrochemical, or colorimetric changes to determine the absence or presence of detection molecules. Both electrochemical and fluorescence signal transduction are sensitive, quantitative, and robust; however, costly and complex equipment is often necessary for signal analysis.^{3,8} Alternatively, colorimetric signal transduction does not require additional detection equipment and therefore is low-cost and easy to use. However, color changes can be difficult for the user to interpret due to background noise or a non-homogeneous color change.^{9,10}

1.1.4 Guidance for Point-of-Care Test Development

The World Health Organization (WHO) created the ASSURED criteria to streamline development of POCTs. ASSURED stands for affordable, sensitive, specific, user-friendly, rapid & robust, equipment-free, and deliverable.¹¹ The Cepheid GeneXpert is a widely used commercial molecular diagnostic system with several disease-specific cartridges that can be used for screening and diagnosis. Even though GeneXpert is completely automated and has excellent test performance, the system is not portable and the instrumentation is cost-prohibitive for low-resources settings (\$17,000).¹² Other companies and researchers have also experienced difficulties addressing all the ASSURED criteria when developing POC platforms because there is often a tradeoff between these items.¹³⁻¹⁶

1.1.5 Existing and Emerging Smart Handheld Platforms

Smart handheld POC platforms generally consist of reusable components for sample processing and output analysis and a consumable cartridge. The iSTAT is a commercial smart

handheld platform developed by Abbott in the 1990's. This portable system can provide rapid, laboratory-quality results for healthcare professionals from just a few drops of patient blood.¹⁷ The iSTAT detects disease indicators via electrochemical signal transduction and then quickly uploads results to the preferred record-keeping system. Cartridges are available to identify peptides linked to heart failure, hormones associated with pregnancy, proteins affiliated with anemia, and many more detection molecules.⁶ One in three hospitals in the U.S. currently use the iSTAT system.¹⁸

There are also many emerging smart handheld platforms. Koydemir *et al.* developed a smartphone-based fluorescence microscope to image and quantify fluorescently labeled *G. lamblia* cysts in large volumes of water. The entire process, from sample preparation to image processing and quantification, takes only one hour and has a limit of detection of 12 cysts in 10 mL of water.¹⁹ Unfortunately, this smartphone-based fluorescence microscopy technique is not suitable for detection of bacterial or viral pathogens because the system is optimized for larger microorganisms. Another group designed a smartphone platform for accurate colorimetric detection of progesterone hormone in whole blood samples.²⁰ While they managed to incorporate a miniaturized water bath for incubation steps, reagents had to be manually added by the user at each step, making this system less than ideal for POC scenarios.²⁰

1.1.6 Existing and Emerging Disposable Platforms

The most notable disposable platform is the home pregnancy lateral flow immunoassay (LFIA) test originally marketed by Warner-Chilcott in 1976.²¹ Enzymes and antibodies used to detect pregnancy-related hormones in urine are embedded in the porous membranes of the LFIA to eliminate user steps and enable long-term storage. The LFIA results are colorimetric and can be visualized with the naked eye just minutes after test initiation. The commercialization of the home pregnancy test introduced LFIA and porous membranes as viable substrates for POCTs.

Porous membranes are ideal for designing disposable platforms because they are cost-effective and easy to manufacture. Further, the inherent capillary flow of these membranes allows fluid transport without the need for external, costly pumping mechanisms. Choi *et al.* detected dengue viral nucleic acids using a disposable platform comprised of porous membranes and an LFIA.²² Although both sensitive and specific, this system relies on several user steps and requires sample processing prior to adding the sample to the platform.²² Another research group developed an inexpensive three-dimensional paper-based device to detect C-reactive protein in blood using a

colorimetric signal output.²³ The dynamic range of this paper-based device is below the clinically relevant concentrations; therefore, whole blood samples could not be used in this paper-based device without first being diluted.²³

1.2 Nucleic Acid-Based Detection

1.2.1 Nucleic Acid Amplification

When using nucleic acids as the detection molecule, amplification is required due to the inherently low concentrations of both RNA and DNA found in environmental and clinical samples.²⁴ Nucleic acid-based detection via amplification is appealing due to its exceptional sensitivity, specificity, speed, and reliability.^{25,26} Nucleic acid amplification tests (NAATs) generally require three steps to achieve successful detection of the target. First, the sample must be processed to extract and isolate the nucleic acids. Second, the nucleic acids need to be amplified to detectable levels. Finally, signal transduction must occur to detect amplified nucleic acids. Although nucleic acids are commonly used to identify disease or illness, there are some disadvantages to using this detection molecule. Because NAATs are so sensitive and can often detect a single copy of the target, cross-contamination can cause high rates of false positives.²⁵ Moreover, nucleic acids do not indicate the viability of the target and can degrade over time.²⁶

1.2.2 Polymerase Chain Reaction

The gold standard nucleic acid amplification assay is a well-defined thermal cycling method called polymerase chain reaction (PCR).^{27,28} PCR can produce 10^9 copies of specific nucleic acid segments in just 30 cycles of repeated denaturation, annealing, and extension and products can be easily detected using gel electrophoresis.²⁸⁻³⁰ However, this technique is generally not suitable for POC applications because the laboratory equipment required for the precise temperature cycling is expensive and bulky.³⁰ Several research groups have replaced this equipment with modified smartphone technology to enable translation of PCR to the POC.³¹⁻³³ The exquisite optics and computational power of modern smartphones can be utilized to evaluate results in real-time, control miniaturized thermal cyclers, and process results. These portable smartphone PCR platforms can provide sensitive, specific, and accurate detection of various pathogens.³¹⁻³³ However, these systems require nucleic acid extraction and/or purification prior to

initiation of PCR to remove inhibitors that inactivate the enzyme or prevent primer annealing necessary for amplification.³⁴⁻³⁶ This necessity for sample preparation often increases the number of user steps and complicates the platform design.

1.2.3 Isothermal Nucleic Acid Amplification

Isothermal nucleic acid amplification techniques are appealing alternatives to PCR for POC applications because they function at a single temperature and are more robust to inhibitors.³⁷ Examples of isothermal amplification assays include, but are not limited to; loop-mediated isothermal amplification (LAMP), helicase-dependent amplification (HDA), rolling circle amplification (RCA), and recombinase polymerase amplification (RPA).³⁸ LAMP provides specific and efficient amplification of nucleic acids by targeting 8 unique sequences.³⁹ Operable at a single temperature (most efficiently between 60 and 70°C),^{40,41} LAMP robustly amplifies even in the presence of complex sample matrices, further reducing sample preparation and instrumentation requirements.^{37,42,43} LAMP creates stem-loop products that serve as initiation sites for subsequent amplification so the assay can produce 10⁹ copies in under one hour.⁴⁴⁻⁴⁶ LAMP products are traditionally analyzed via gel electrophoresis, spectrophotometry, or fluorescence.⁴⁷⁻⁴⁹ Recently, there has been an increase in the number of publications that incorporate LAMP into POC platforms. The “paper machine” developed by Connelly *et al.* is a disposable layered device that includes inlets for washes, buffers, and reagents for sensitive identification of *E. coli* in human plasma in just one hour.⁵⁰ The low-cost “paper machine” incorporates cell lysis, LAMP amplification, and fluorescence detection and requires only four user steps.⁵⁰ Other researchers have demonstrated the utility of LAMP by combining the assay with smartphone technology to sensitively and specifically detect nucleic acid analytes in one hour with minimal user intervention.^{16,51,52}

1.3 Cholera

1.3.1 Burden, Cause, and Symptoms

The WHO estimates that there are up to 4 million cases of cholera each year and almost 150,000 deaths, costing more than \$220 million.⁵³ Cholera is a diarrheal disease caused by consumption of water or food contaminated with the bacterium *Vibrio cholerae* (*V. cholerae*).

Cholera causes watery diarrhea and severe dehydration and can lead to death within hours if left untreated.⁵³ In cases of inadequate sanitation infrastructure, feces containing *V. cholerae* can seep into the environment and tarnish drinking water sources. Communities with poor sanitation, insufficient access to clean water, or high population density are at risk for cholera outbreaks.⁵³ Luckily, cholera can be easily treated by immediate administration of rehydration solutions, either orally or intravenously, and antibiotics.⁵⁴

1.3.2 Existing and Emerging Platforms for Detection of Cholera

There are several commercial technologies for identification of *V. cholerae* in stool including the Crystal Vc Dipstick and the SMART Cholera O1 test.^{55,56} Both of these rapid diagnostic tests (RDTs) detect *V. cholerae* antigens directly from stool samples in less than 30 minutes using LFIA technology for a colorimetric signal output. The Crystal Vc Dipstick has a specificity of only 50% and the SMART Cholera O1 test has not been validated with concentrations less than 2×10^7 colony forming units (cfu)/mL.^{55,57} Patients infected with *V. cholerae* generally have high levels of the bacteria in their system, so these RDTs are likely sufficient for diagnostic purposes.⁵⁸ After talking with clinicians and community health workers during my summer research experience in Haiti, they revealed that cholera is easy to recognize based on symptoms alone. These commercial RDTs merely confirm the symptom-based diagnosis. Further, these medical professionals and collaborators at the Emerging Pathogens Institute in Haiti identified a greater need to detect *V. cholerae* in the environment rather than in patient samples.

There are very few examples in literature of environmental *V. cholerae* detection. The gold standard for identifying *V. cholerae* in environmental water samples is a 4-day laboratory-based method developed by Alam *et al.*⁵⁹ This technique includes enrichment, isolation, serology, and then finally PCR for nucleic acid-based detection of *V. cholerae*. This laboratory-based method is extremely sensitive and specific, but it requires expensive equipment and trained personnel. The only existing POCT for identification of *V. cholerae* in environmental water is the Cholera RDT marketed by Maternova.⁶⁰ Unfortunately, there is very little information about the test performance of this antigen-based RDT.

1.4 HIV

1.4.1 Burden, Cause, and Symptoms

The WHO estimates that there are 36.7 million people currently living with human immunodeficiency virus (HIV) and over 770,000 annual deaths from HIV-related causes.⁶¹ HIV is a retrovirus that targets and weakens the immune system and can be transmitted via blood, breast milk, semen, and vaginal secretions. HIV symptoms vary between individuals and infection stages. Many patients have influenza-like symptoms or are asymptomatic in the first few weeks after transmission. As the infection progresses, symptoms may include swollen lymph nodes, weight loss, fever, diarrhea, or cough.⁶¹ Individuals who have unprotected sex, share needles, have another sexually transmitted infection, or undergo unsafe medical procedures are at a higher risk for contracting HIV.⁶¹ Even though there is not a cure for HIV, antiretroviral drugs can suppress the viral load and prevent further transmission. Antiretroviral therapy is a lifelong treatment plan that strengthens the immune system of the infected individual. Without proper treatment, patients with HIV will develop acquired immunodeficiency syndrome (AIDS) which is diagnosed when other infections, cancer, or severe conditions emerge.⁶¹

1.4.2 Existing and Emerging Platforms for Detection of HIV

Of the millions of people living with HIV, only 79% know their status and only 58% are receiving treatment.⁶¹ Early diagnosis of HIV decreases mortality and morbidity by enabling prompt patient treatment. HIV screening is typically performed using commercial RDTs like OraQuick that are based on LFIA technology for detection of HIV antibodies from oral fluid or capillary blood.⁶² The poor sensitivity during the pre-seroconversion phase in the first four weeks of infection require that antibody-detecting RDT results are confirmed by a laboratory-based assay.⁶³ Even the fourth and fifth generation RDTs that combine antibody and antigen detection, such as the Alere HIV Combo, are less sensitive than laboratory-based assays.^{64,65} NAATs could expedite treatment response for newly infected individuals through early and direct detection of the virus. There are a few commercial tools for PCR-based detection of HIV including Cepheid Xpert Qual Assay and Alere q HIV-1/2 Detect. Although these platforms are sensitive, specific, and automated, they require cost-prohibitive (>\$17,000 for the instrument and >\$17 for the cartridge) benchtop instruments that need a stable electrical power supply.¹²

Researchers have turned to isothermal amplification methods to reduce the cost and complexity of HIV testing platforms. Gurralla *et al.* describes a portable device that can sensitively detect the pH change that occurs during reverse transcription (RT) LAMP of HIV RNA.⁶⁶ The lack of reagent storage and integrated sample preparation decreases the translatability of this device. Another group developed a smartphone platform with disposable cartridges for sensitive, real-time fluorescence detection of HIV viral RNA.¹⁶ The user is required to manually transfer precise volumes of lysed blood and reagents to the reaction chamber to initiate the isothermal assay, thus limiting the usability of this platform.¹⁶

1.5 Thesis Overview: Development of Molecular Detection Platforms for Pathogens in Complex Sample Matrices

Many existing point-of-care tests suffer from poor sensitivity and specificity, which leads to high rates of false negatives and positives. The Linnes Lab works primarily with nucleic acids and utilizes amplification to multiply low levels of DNA or RNA found in patient and environmental samples. Isothermal nucleic acid amplification assays are an excellent alternative to cyclical polymerase chain reaction because they operate at a single temperature, are robust to sample matrix inhibitors, and create millions of copies of a target sequence very rapidly. I propose the incorporation of an isothermal amplification assay into integrated, portable platforms to bring patient screening and environmental monitoring to the point of use. In Chapter 2, I develop a loop-mediated isothermal amplification (LAMP) assay targeting *Vibrio cholerae*. Existing methods for identification of *V. cholerae* in environmental water samples are less than adequate for several reasons. During the 4-day process for detection via the gold-standard laboratory method, there is risk of continued consumption of potentially contaminated water. Further, the laboratory facilities and personnel required to perform this technique are limited in low resource areas where cholera is endemic. The LAMP assay enables rapid identification of *V. cholerae* and can be combined with lateral flow immunoassay (LFIA) for colorimetric analysis. To eliminate LFIA false positives caused by dimerization of the labeled primers, I incorporate a custom designed strand displacement (SD) probe into the standard *V. cholerae* LAMP assay.⁴² I demonstrate the *V. cholerae* SD-LAMP assay specificity, robustness in various water samples, and limit of detection in pond water. In Chapter 3, I optimize a vitrification technique for room-temperature storage of LAMP reagents. Ambient-temperature reagent storage removes the need for refrigeration and allows assays to be

easily integrated into portable platforms. I explore the efficiency of *V. cholerae* SD-LAMP reagents dried for 30 days and HIV reverse transcription (RT) LAMP reagents vitrified for 21 days. In Chapter 4, I outline the creation of two integrated paperfluidic platforms: one for detection of *V. cholerae* in environmental water and the other for HIV in whole blood. These inexpensive, user-friendly paperfluidic platforms combine the inherent capillary flow of porous membranes with the efficiency, sensitivity, and robustness of LAMP amplification. Other groups have developed paperfluidic platforms for detection of various pathogens but have failed to include sample preparation^{13,14} and assay reagents,^{22,50,67} therefore, limiting the translatability of the platform. I illustrate a size-based capture and concentration method for hands-free sample preparation and incorporate the reagent vitrification technique from Chapter 3 to create portable paperfluidic platforms. These integrated platforms are ideal for in-field environmental monitoring or point-of-care screening for infectious pathogens.

The polymerization that occurs during LAMP amplification produces a change in viscosity that can be measured using an optical method called particle diffusometry (PD).⁶⁸⁻⁷⁰ In Chapter 5, I highlight the microscope characterization of the PD technique for detection of *V. cholerae*. We directly compare fluorescence and PD measurements of *V. cholerae* LAMP amplicons and analyze the limit of detection and robustness in various water samples. Because of the success of PD in determining *V. cholerae* presence, we translate the method from a microscope to a smartphone platform, thereby increasing portability and reducing cost. In Chapter 6, I describe the development and optimization of the smartphone-based PD platform. We establish the selectivity and limit of detection of this smartphone-based PD platform for *V. cholerae* in pond water and compare its sensitivity and specificity to fluorescence measurements using 132 double-blinded samples. This dissertation provides a framework for designing inexpensive and easy-to-use platforms for rapid identification of pathogens at the point of use.

2. DEVELOPMENT OF *V. CHOLERAE* LOOP-MEDIATED ISOTHERMAL AMPLIFICATION ASSAY AND DETECTION VIA LATERAL FLOW IMMUNOASSAY

2.1 Rationale

There is a critical need to rapidly detect *V. cholerae* in the environment to prevent the spread of the diarrheal disease cholera, which is caused by ingestion of the bacterium. Existing RDTs that target antigens are not capable of identifying *V. cholerae* in the environment because they cannot detect low concentrations of the bacteria typically found in water. Further, a confirmatory laboratory test is often required due to the poor specificity of these RDTs, risking continued consumption of potentially contaminated water during this extended testing period.⁷¹

NAATs have the potential to specifically and rapidly detect low concentrations of *V. cholerae* in the environment. PCR has been used to detect *V. cholerae* in water samples in a standard laboratory setting; however, the protocol requires extensive sample preparation to remove inhibitors.^{59,72} Recent advances in molecular biology include several isothermal nucleic acid amplification techniques that could reduce the complexity and number of steps required for pathogen detection.⁷³ One such isothermal amplification method, LAMP, provides specific and efficient amplification of nucleic acids by targeting 8 unique sequences.³⁹ LAMP robustly amplifies target nucleic acids even in the presence of complex sample matrices, further reducing sample processing and instrumentation requirements.^{37,42,43}

LAMP amplicons are frequently tagged for visual detection on LFIA.^{74,75} LFIA is a simple, low-cost alternative to laboratory equipment for qualitative analysis of nucleic acid amplification products. LFIAs, shown in Figure 2.1,⁷⁶ generally consist of four components. First, a small volume of sample is added to the sample pad. Reporter molecules stored in the conjugate pad are rehydrated by the sample wicking downstream via capillary flow. Reporter molecules bind to the detection molecule if it is present in the sample and the conjugates then flow into the reaction membrane, binding to immobilized capture molecules in the test band area. The control band area is located immediately downstream of the test band area and captures unbound reporter molecules, confirming successful rehydration and flow of these reporter molecules. The aggregation of these reporter molecules causes a colorimetric change visible by the naked eye. Finally, the hydrophilic absorbent pad ensures the sample wicks to the end of the LFIA. Approximately 15 minutes after

sample addition, the user can visually interpret the LFIA results. Two test bands correspond to a positive test result while one band indicates a negative test result.⁷⁷

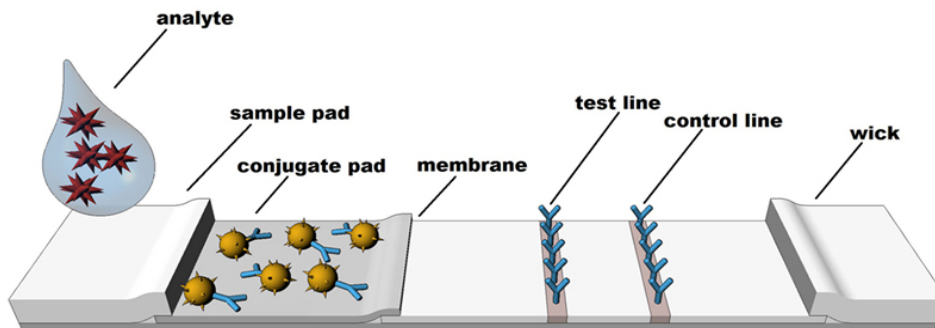


Figure 2.1 Lateral flow immunoassay platform.

LFIA regions and corresponding biology. Figure reproduced with permission from Miocevic, *et al. Front. Public Health.* 2017, 5 (133)

Here, I develop a LAMP assay for *V. cholerae* and combine it with LFIA for visual interpretation of results. I first optimize the LAMP assay, confirm amplicon size, and determine the limit of detection for *V. cholerae* genomic DNA. To eliminate LFIA false positives caused by primer hybridization, I incorporate a custom designed strand displacement probe into the LAMP reaction mixture.^{38,42} I then characterize the combined strand displacement and LAMP (SD-LAMP) assay by investigating the limit of detection for *V. cholerae* whole cells, the specificity of the assay, the robustness in various water samples, and the limit of detection in pond water. Coupling SD-LAMP with user-friendly LFIA enables rapid, sensitive, and accurate identification of *V. cholerae* in environmental water.

2.2 Materials and Methods

2.2.1 Reagents

Primers and probes, provided in Table A.1, were ordered from Integrated DNA Technology (IDT, Coralville, IA) and were resuspended in molecular biology water (Invitrogen, Carlsbad, CA). Primers and probes were designed to target the cholera toxin A (*ctxA*) gene of toxigenic *V. cholerae* strains (Table A.2).⁷⁸ There is one copy of the *ctxA* gene per *V. cholerae* genome. Loop primers were either tagged with 6-carboxyfluorescein (FAM) or biotin for LFIA detection. Other reagents used for assay development include Bst 2.0 polymerase (NEB, Ipswich, MA),

deoxynucleotide triphosphates (dNTPs) (Agilent Technologies, Santa Clara, CA), isothermal buffer (NEB, Ipswich, MA), MgSO₄ (NEB, Ipswich, MA), betaine (Millipore Sigma, Burlington, MA), *ScaI* and *DdeI* restriction enzymes (NEB, Ipswich, MA), and purified genomic DNA from *V. cholerae* N16961 (ATCC 39315D-5, Manassas, VA) maintained at 2.2 ng/μL. Water samples included molecular biology water, pond water, rain runoff, 1X phosphate buffered-saline (PBS) (Sigma-Aldrich, St. Louis, MO) pH 7.4, and laboratory tap water. Rain runoff and pond water were collected from a rain gutter and bank of a small pond, respectively, and were stored at 4 °C until LAMP was performed.

2.2.2 Bacteria Culture

Toxigenic *V. cholerae* strains N16961 (O1 serogroup) and CH-16 (altered O1 serogroup) and non-toxicogenic *V. cholerae* strains ENV-32 and NRT-36 were provided by Dr. Afsar Ali at the University of Florida. *E. coli* strain DH5α (NEB, Ipswich, MA) was also used for experimentation. All bacteria were stored at -80°C until ready to be cultured. All cultures were grown in Lysogeny Broth (LB) overnight at 37°C in a miniature incubating orbital shaker at 300 rpm (Thermo Fisher, Waltham, MA). An Ultrospec 10 (Biochrom, Cambourne, UK) cell density meter was used to measure the optical density (OD) of the cultures. Bacteria cultures were diluted to an OD₆₀₀ of 1, representing 10⁹ cells/mL of *E. coli* and 5 × 10⁸ cells/mL of all *V. cholerae* strains as determined by counting colony forming units of serially diluted cells.

2.2.3 Standard Loop-Mediated Isothermal Amplification (LAMP)

Standard LAMP reactions were 25 μL total consisting of 23 μL of LAMP master mix (Table A.3). Standard LAMP reactions utilized six primers (Table A.1); LB was labeled with FAM and LF was labeled with biotin. 2 μL of diluted template or molecular biology water (for the negative no template control (NTC)) was added prior to heating. LAMP reactions were incubated at 65°C for 30 minutes using an Applied Biosystems 7500 Real-Time PCR System (Foster City, CA) and stored at 4°C until analyzed.

2.2.4 Strand Displacement Loop-Mediated Isothermal Amplification (SD-LAMP)

SD-LAMP reactions were 25 μL total consisting of 23 μL of SD-LAMP master mix (Table A.4). SD-LAMP reactions utilized five primers (Table A.1); LB was labeled with biotin and strand displacement probe and quencher strand were annealed. The strand displacement probe and quencher strand were designed by my labmate Dr. Elizabeth Phillips and Dr. Sanchita Bhadra of the University of Texas at Austin. The strand displacement probe was tagged with FAM and annealed to a complementary strand tagged with a quencher. The single stranded regions of the FAM-labeled probe act as a toehold to initiate strand displacement and binds preferentially to true amplicons (Figure A.1).⁴² 2 μL of diluted template or molecular biology water (for the negative control (NTC)) was added prior to heating. Experiments testing the effects of various water samples on SD-LAMP consisted of 12.5 μL (50% v/v) of each water sample per SD-LAMP reaction. SD-LAMP reactions were incubated at 65°C for 30 minutes using an Applied Biosystems 7500 Real-Time PCR System (Foster City, CA) and stored at 4°C until analyzed.

2.2.5 Amplicon Analysis via Lateral Flow Immunoassay (LFIA) and Gel Electrophoresis

Dually labeled LAMP amplicons (biotin and FAM) first bind to the streptavidin-coated gold nanoparticles stored in the conjugate pad of the commercial LFIA (D003-03, Ustar Biotechnologies, Hangzhou, China). The conjugates then bind to the anti-fluorescein antibodies in the test band area. Unbound streptavidin-coated gold nanoparticles are captured by the anti-streptavidin antibodies in the control band area. A visible reddish color in both the test and control band areas, caused by the accumulation of gold nanoparticles, indicates a positive test result while a color change only in the control band area indicates a negative test result. 10 μL of amplified product was added to the sample pad of an LFIA followed by 40 μL of wash buffer. LFIA were scanned at least 1 hour after initial sample addition using a V850 Pro Scanner (Epson, Suwa, Japan). The test band was quantified using a custom MATLAB script that averages the grey-scale pixel intensity of the test band and subtracts the average background pixel intensity 30 pixels below the test band.⁷⁹ My colleague, Dr. Elizabeth Phillips, established a visual threshold through an evaluation of human subjects' instrument-free interpretation of LFIA results.⁴² This threshold serves as a guide to ensure the test band intensities are interpreted as positive by eye.

10 μ L of remaining product was combined with 2 μ L of 6X purple loading dye (NEB, Ipswich, MA) and added to a 2% agarose gel along with 10 μ L Fast DNA Ladder (NEB, Ipswich, MA) and run for 60 minutes at 100V. The 2% agarose gels were stained with ethidium bromide and imaged using an ultraviolet light gel imaging system (c400, Azure Biosystems, Dublin, CA) with UV 302 settings and a 15-second exposure.

2.2.6 Statistical Analysis

To determine the limit of detection, a one-way ANOVA *post hoc* Dunnett's was performed with multiple comparisons of the LFIA test bands of each concentration against the test bands of no template negative controls with a 95% confidence interval. A Student's unpaired, two-sided *t*-test with a 95% confidence interval was used when comparing the negative and positive samples in various water.

2.3 Results and Discussion

2.3.1 *V. cholerae* Standard LAMP Reaction

LAMP Assay Optimization

I ordered and tested two published *V. cholerae* LAMP primer sets that target the *ctxA* gene. The first primer set yielded non-specific amplification of the NTC samples (Figure A.2) after just 30 minutes of heating.⁸⁰ The second primer set from Okada *et al.* produced consistent amplification of positive samples and suppressed non-specific amplification.⁷⁸ However, amplification was slower using the Okada *et al.* primers, likely because the assay conditions were not optimal. Other researchers have optimized LAMP assays by altering the concentration of betaine and MgSO₄.^{81,82} Okada *et al.* used 0.8 M of betaine and 8 mM of MgSO₄ for their experiments.⁷⁸ In addition to these baseline concentrations, I tested 0.4 M and 1 M betaine and 4 mM and 2 mM MgSO₄. I heated an NTC and positive sample (10⁴ DNA copies/reaction) for each combination of betaine and MgSO₄ at 65°C for 45 minutes and recorded the cycle threshold (C_T) value, or time to amplification. I wanted to see fast amplification for positive samples and slow or no amplification for NTC samples. In other words, I was looking for the greatest difference between positive and NTC C_T values. Figure 2.2 illustrates that the optimal concentration of betaine and MgSO₄ is 0.8

M and 2 mM, respectively, because of the low C_T values for positive samples and large difference between positive and NTC amplification. It is important to note that the isothermal buffer used in the LAMP reactions contains 2 mM of $MgSO_4$ so additional $MgSO_4$ was not required to achieve optimal reaction conditions. During my tenure in the lab, I have also demonstrated that LAMP reactions can be uniformly scaled to total volumes of 10 μ L, 15 μ L, and 50 μ L without a significant loss in sensitivity (Figure A.3).

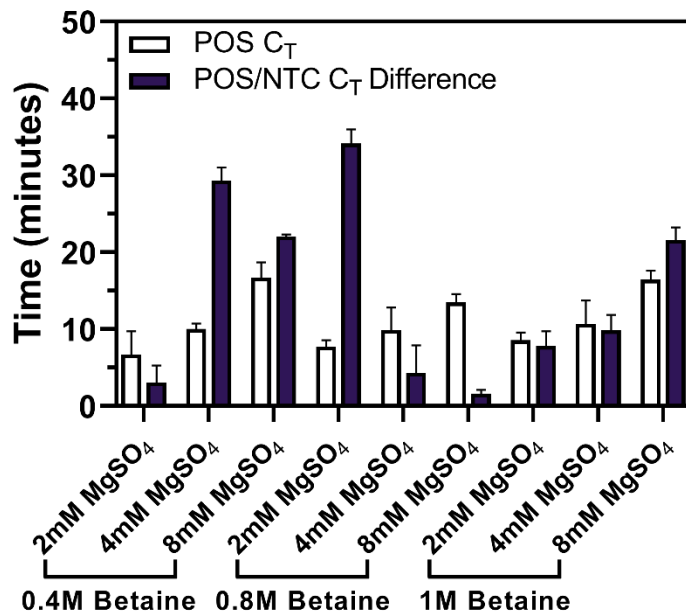


Figure 2.2 *V. cholerae* LAMP assay optimization.

Various concentrations of betaine (0.4, 0.8, 1 M) and $MgSO_4$ (2, 4, 8 mM) were tested. C_T values for both the positive and NTC samples were recorded from the real-time PCR system. The C_T values for positive samples were plotted in addition to the difference between positive and NTC C_T values. (n=2)

LAMP Product Confirmation

The *V. cholerae* LAMP primers specifically target the 193 bp sequence of the *ctxA* gene of toxigenic *Vibrio cholerae* strains.⁷⁸ I confirmed the LAMP product was indeed the amplified *ctxA* gene through an enzymatic digestion of the product with either *ScaI* or *DdeI* restriction enzymes. As predicted by LAMP restriction digest fragment analysis,⁸³ digestion with both of these enzymes resulted in smaller fragments compared to the undigested product. The *DdeI* digested product collapsed to fragments at approximately 150 bp and 250 bp as seen on the agarose gel in Figure

2.3. *ScaI* digested products were smaller fragments at approximately 50 bp and 150 bp (Figure 2.3). This experiment suggests that the primer set targets the intended region in the *ctxA* gene.

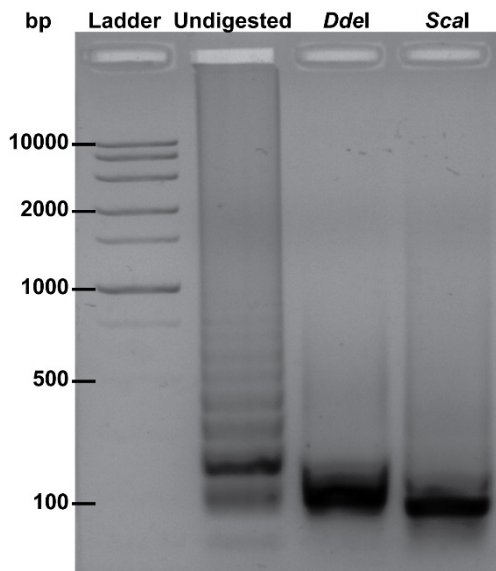


Figure 2.3 *V. cholerae* LAMP restriction digest.

2% agarose gel shows undigested and digested *V. cholerae* LAMP products.

Limit of Detection of V. cholerae Genomic DNA

The first thing I evaluated was the sensitivity of the assay using genomic DNA as template. LAMP was performed with 2 μ L of *V. cholerae* genomic DNA at concentrations ranging from 10^0 – 10^5 copies/reaction (n=3). The ladder-like banding pattern in the agarose gel indicates positive amplification and is due to the different length concatemers produced during LAMP (Figure 2.4A). The same LAMP products were added to commercial LFIA and the test band intensity was quantified to determine the limit of detection (LOD). Statistically significant differences were seen between the test band intensity of NTC compared to 10^3 , 10^4 (p-value < 0.05), and 10^5 DNA copies/reaction (p-value < 0.01) (Figure 2.4B) when using a one-way ANOVA with Dunnett's *post hoc*. This demonstrates an assay LOD of 1,000 *V. cholerae* DNA copies/reaction using LFIA. However, I noticed a faint but visible LFIA test band for low concentrations and NTC samples, but gel electrophoresis did not show amplification for these samples (Figure 2.4A and Figure 2.4B). Furthermore, the average test band intensity for these samples was above the visual threshold,

indicating that most users would interpret these samples as positive. These false positives, only observed on LFIA, are likely due to LFIA detection of primer hybrids.

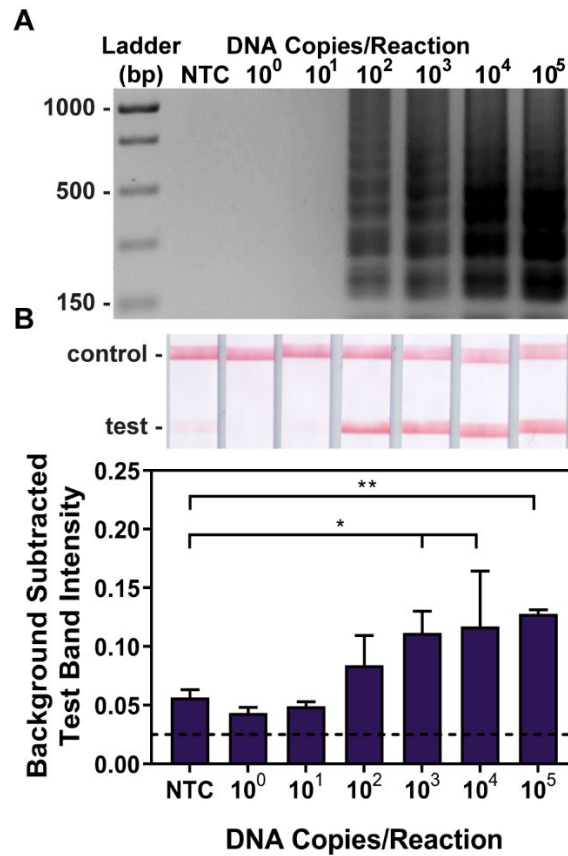


Figure 2.4 *V. cholerae* LAMP LOD using genomic DNA.

(A) Electrophoresis gel verifying amplification (contrast increased for visualization) and (B) LFIA results. LFIA test band quantification shows significance down to 1,000 DNA copies/reaction (* $p < 0.05$, ** $p < 0.01$). (n=3)

Limit of Detection of V. cholerae Whole Cells

I wanted to determine if LFIA false positives were also observed when *V. cholerae* whole cells were used as template. *V. cholerae* cells lyse at 65°C due to thermal effects, such that an additional cell lysis or DNA extraction step beyond the LAMP assay was not necessary (validated in Figure A.4). LAMP was performed with 2 µL of *V. cholerae* cells at concentrations ranging from 10⁰ – 10⁵ cells/reaction (n=3). Agarose gels confirmed amplification after the 30-minute assay (Figure 2.5A). LAMP amplicons were then added to LFIAs and the test band intensity was quantified. Statistically significant differences were seen between the test band intensity of NTC

compared to $10^2 - 10^5$ cells/reaction (p -value < 0.01) (Figure 2.5B) when using a one-way ANOVA with Dunnett's *post hoc*. This demonstrates an assay LOD of 100 *V. cholerae* cells/reaction. Similar to the genomic DNA LOD experiments, I noticed a faint test band on the LFIA for the lowest concentration and NTC samples, but gel electrophoresis did not show amplification for these samples (Figure 2.5A and Figure 2.5B). These LFIA false positives due to primer dimers are commonly reported in literature^{42,75} and can be corrected with a strand displacement probe.

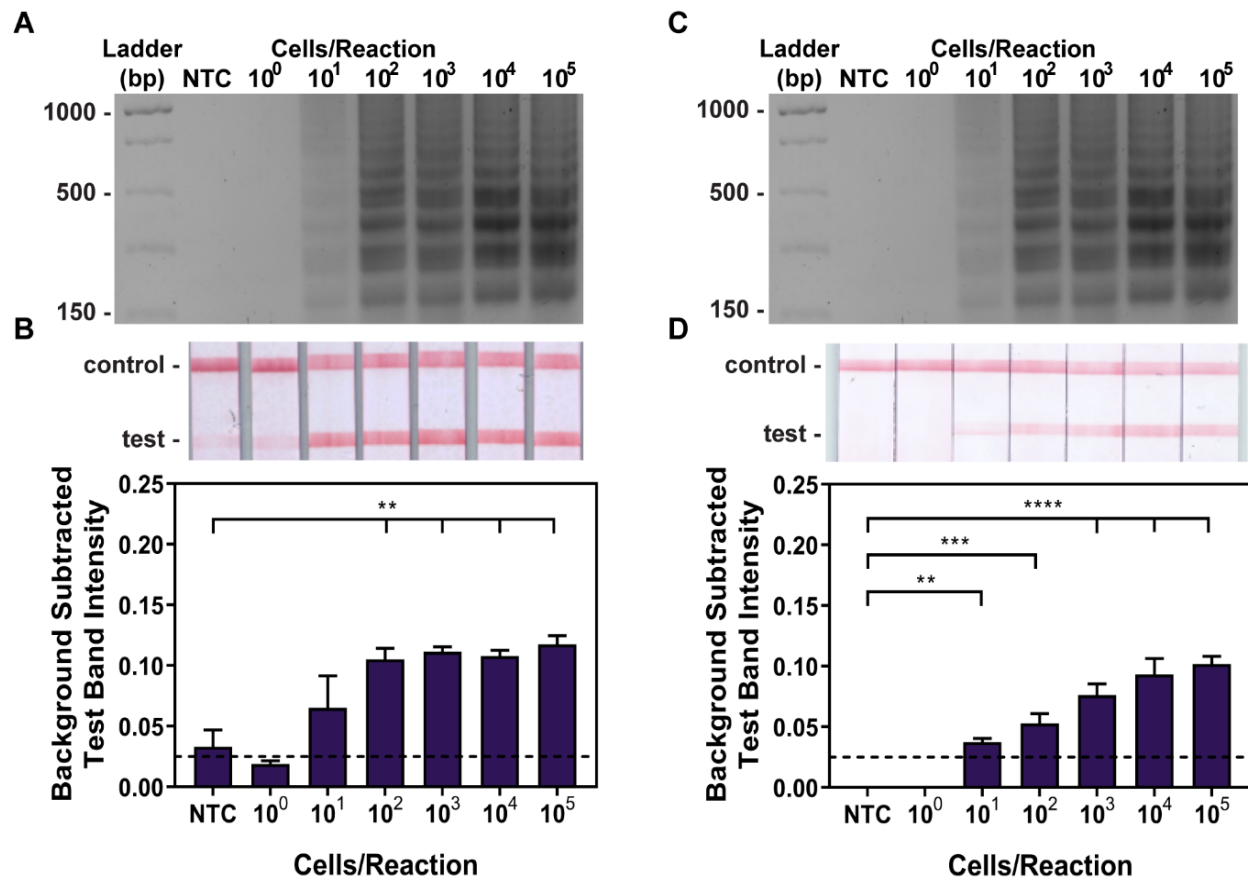


Figure 2.5 Comparison of standard LAMP and SD-LAMP for *V. cholerae* whole cells.

Standard LAMP products are visually detectable via LFIA down to 10 cells/reaction but only show significance down to 100 cells/reaction when compared to NTC. Faint test bands are visible for NTC and low concentrations. (A) Electrophoresis gel verifying amplification (contrast increased for visualization) and (B) LFIA results and test band quantification (** $p < 0.01$). (n=3) SD-LAMP products are visually detectable via LFIA and significant down to 10 cells/reaction when compared to NTC. No test bands are visible for NTC and low concentrations. (C) Electrophoresis gel verifying amplification (contrast increased for visualization) and (D) LFIA results and test band quantification (** $p < 0.01$, *** $p < 0.001$, **** $p < 0.0001$). (n=3)

2.3.2 *V. cholerae* SD-LAMP Reaction

Limit of Detection of V. cholerae Whole Cells

After incorporating the annealed SD probe into the LAMP reaction, no false positive test bands were identified (Figure 2.5D) and LFIAAs matched gel electrophoresis (Figure 2.5C). With SD-LAMP, there was a statistically significant difference between the test band intensity of 10^1 (p-value < 0.01), 10^2 (p-value < 0.001), and $10^3 - 10^5$ cells/reaction (p-value < 0.0001) compared to NTC when using a one-way ANOVA with Dunnett's *post hoc* (n=3). This demonstrates a true LOD of 10 *V. cholerae* cells/reaction. Since Dunnett's *post hoc* test computes multiple comparisons between each 'treatment' and a single 'control', eliminating the test band signal for NTC samples increases the difference between the 'treatments' and 'control' and achieves greater statistical significance. Therefore, the 10-fold improvement in the LOD with SD-LAMP is not surprising.

V. cholerae Whole Cell Specificity

Next, I wanted to confirm the specificity of the LAMP primers for toxigenic strains (with *ctxA* gene) of *V. cholerae*. I prepared SD-LAMP assays with 10^5 cells/reaction of toxigenic *V. cholerae* N16961, toxigenic *V. cholerae* CH-16, non-toxigenic *V. cholerae* ENV-32, non-toxigenic *V. cholerae* NRT-36, and *E. coli* DH5 α . The LAMP amplicons were added to LFIAAs and the test band intensity was quantified. As expected, there was only a control band on the LFIAAs of the non-toxigenic strains of *V. cholerae* and *E. coli* (Figure 2.6A), signifying no amplification of these off-target bacteria. Using an ANOVA with Dunnett's *post hoc*, there was a statistically significant difference between the test band intensity of toxigenic *V. cholerae* N16961 and toxigenic *V. cholerae* CH-16 compared to NTC (n=3, p-value < 0.0001) (Figure 2.6B). While I was working in Haiti during the summer of 2016, I tested several *V. cholerae* samples collected by the Emerging Pathogens Institute. These *V. cholerae* samples were all *ctxA*-positive (confirmed by PCR) but were isolated from various sample matrices such as patient stool samples, river water, and shrimp shells. My optimized LAMP assay successfully identified all seven *ctxA*-positive samples after just 30 minutes of heating (Figure A.5). Altogether, these results demonstrate the excellent specificity of the LAMP primers for toxigenic strains of *V. cholerae* that have the *ctxA*

gene. Further, this indicates that other bacteria found in environmental water samples, such as *E. coli*, will not interfere with the assay.

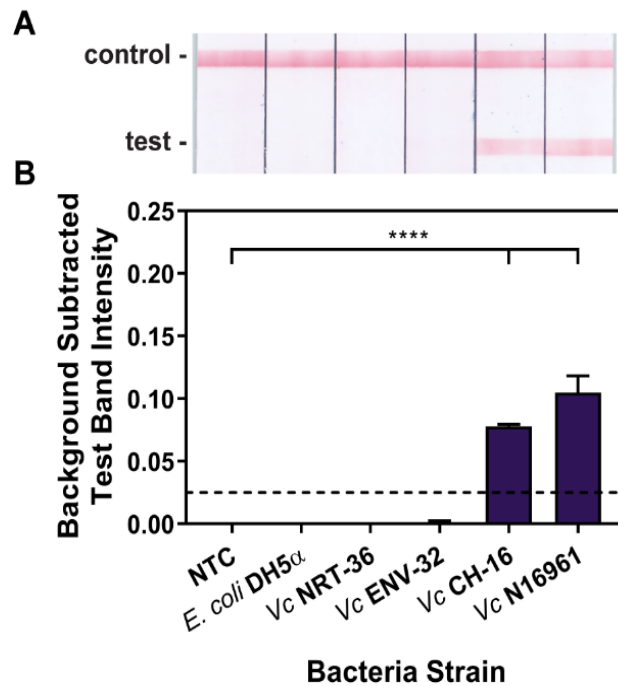


Figure 2.6 Specificity of *V. cholerae* SD-LAMP assay.

(A) Only toxigenic strains of *V. cholerae* are detectable via LFIA. (B) LFIA test band quantification shows statistical significance for *Vc* N16961 and *Vc* CH-16 when compared to NTC (**** $p < 0.0001$). (n=3)

***V. cholerae* Whole Cell Detection in Various Water Samples**

I then explored the efficiency of the SD-LAMP assay in different water samples. I prepared SD-LAMP assays with 10^5 cells/reaction of *V. cholerae* and 50% by volume of molecular biology water (control), pond water, rain runoff, PBS, and tap water. After 30 minutes of amplification, I analyzed the amplicons using LFIA (Figure 2.7A). The test band signal was strong for molecular biology water, pond water, rain runoff, and PBS. Interestingly, amplification only occurred one of three repeats in tap water. This is likely due to the presence of chlorine in city tap water which inhibits the activity of the enzyme and can even kill bacteria. When compared to their respective negative controls, there was a statistically significant difference for molecular biology water (p-value < 0.01), pond water (p-value < 0.0001), rain runoff (p-value < 0.01), and PBS (p-value < 0.01) using an unpaired *t*-test (n=3) (Figure 2.7B). These results demonstrate the robustness of the

SD-LAMP assay and indicate that common inhibitors found in environmental water samples do not prevent amplification.⁸⁴

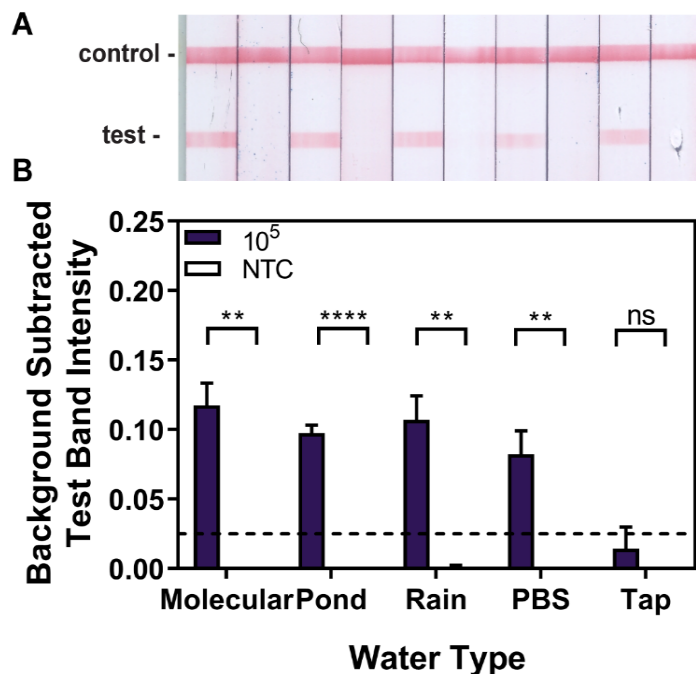


Figure 2.7 Robustness of *V. cholerae* SD-LAMP assay.

(A) LFIA results. (B) LFIA test band quantification shows statistical significance for molecular biology water, pond water, rain runoff, and PBS when compared to respective NTC samples (** $p < 0.01$, **** $p < 0.0001$, ns = no significance). (n=3)

Limit of Detection of V. cholerae Whole Cells in Pond Water

I investigated pond water further because it is an excellent surrogate for the native environment of *V. cholerae*.^{85,86} LAMP was performed by spiking serial dilutions of *V. cholerae* cells ranging from 10^0 – 10^5 cells/reaction into pond water (n=3). Both agarose gel electrophoresis (Figure 2.8A) and LFIA (Figure 2.8B) were used to confirm amplification. Statistically significant differences were seen between the test band intensity of the NTC compared to 10^2 (p-value < 0.05), 10^3 , 10^4 (p-value < 0.01), and 10^5 (p-value < 0.0001) cells/reaction (Figure 2.8B) when using a one-way ANOVA with Dunnett's *post hoc*. This demonstrates an assay LOD of 100 *V. cholerae* cells/reaction (4,000 cells/mL) in pond water, which is 10-fold less sensitive than the LOD in molecular biology water (Figure 2.5D). This slight loss in sensitivity is likely due to a change in

salt concentration between molecular biology and pond water, which can affect enzyme activity and slow the reaction.^{72,87,88} However, this experiment better simulates a field test since the pond water was collected outside the laboratory and contains natural sediment. While not statistically significant, 10^1 cells/reaction (400 cells/mL) did amplify two of three repeats, indicating that an increased assay time could improve the LOD. An LOD of 10 cells/reaction (400 cells/mL) would place the SD-LAMP sensitivity within the range of *V. cholerae* concentrations typically found in the environment (1 – 1,000 cells/mL).⁵⁹

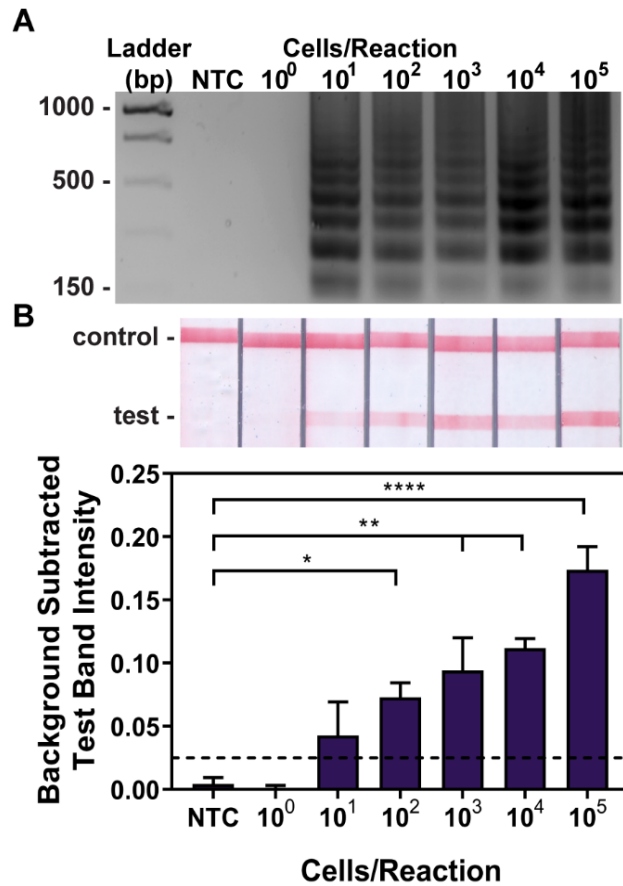


Figure 2.8 LOD of *V. cholerae* SD-LAMP assay in pond water.

(A) Agarose gel verifying amplification (contrast increased for visualization) and (B) LFIA results are consistent. LFIA test band quantification shows significance down to 100 cells/reaction (* $p < 0.05$, ** $p < 0.01$, **** $p < 0.0001$). (n=3)

2.4 Future Directions

To ensure an environmentally relevant LOD, the SD-LAMP assay time for the pond water experiments should be extended by 5-15 minutes. If unequivocal LFIA test bands are observed for 10^1 cells/reaction for each repeat, the time extension was sufficient in enhancing the LOD. If a time extension does not improve the SD-LAMP LOD in pond water, further assay optimization may be required.

2.5 Conclusions

In this chapter, I optimized and characterized an SD-LAMP assay and combined it with colorimetric LFIA detection for rapid, sensitive, and robust identification of *V. cholerae*. These studies indicate an environmentally relevant sensitivity of 10 cells/reaction (400 cells/mL) in molecular biology water. I also demonstrated that the SD-LAMP assay is specific to toxigenic strains of *V. cholerae* and that other bacteria found in water, such as *E. coli*, do not interfere with amplification or detection. Furthermore, I determined that SD-LAMP performs robustly in the presence of inhibitory sample matrices and has a LOD of 100 cells/reaction (4,000 cells/mL) in 50% pond water. Altogether, these results establish the utility of SD-LAMP combined with LFIA for the rapid, equipment-free detection of *V. cholerae* in its native environment.

3. OPTIMIZATION OF VITRIFICATION TECHNIQUE FOR ROOM-TEMPERATURE STORAGE OF REAGENTS

Parts of this chapter are reproduced from [Ref. 104](#) (Phillips & Moehling *et al.*, 2019) with permission from The Royal Society of Chemistry.

3.1 Rationale

Emerging POCTs utilizing nucleic acid amplification have the potential to revolutionize the field by enabling detection as soon as a pathogen is present and improving the sensitivity and specificity of portable platforms. However, a major obstacle that prevents the widespread translation and use of point-of-care platforms that utilize NAATs, such as LAMP, is the required cold-chain storage of reagents. Specifically, the enzyme (polymerase) and dNTPs required for amplification are unstable above freezing temperatures (-20°C).^{89,90} The most common way to dry and preserve LAMP reagents is lyophilization or freeze-drying. During the lyophilization process, water is removed from the samples by freezing, lowering the pressure, and applying heat to enable sublimation.⁹¹ Although lyophilization permits long-term room-temperature storage of most proteins and reagents, it is a laborious process that requires several rounds of optimization and a laboratory-grade lyophilizer.⁹¹ I sought to explore an alternative drying method that is less time-consuming, uses minimal equipment, and is compatible with several assays. Vitrification is the mechanism of preserving samples in a glassy state using highly concentrated cryoprotectants to prevent crystallization during the drying process.⁹² Hayashida *et al.* modified a traditional vitrification procedure for storage of LAMP reagents in the caps of PCR tubes for detection of Human African Trypanosomiasis in a standard laboratory setting.⁹³ I ultimately want to integrate dried LAMP reagents into a portable platform, so further protocol optimization is required.

In this chapter, I characterize the vitrification technique by selecting the optimal cryoprotectants, reagent deposition pattern, and substrate for reagent storage. After trial and error experimentation with LAMP reagent vitrification, I utilize transport equations to calculate the molecular diffusivity of the reagents to guide final decisions on deposition pattern and rehydration. Finally, I use the optimized vitrification protocol to store both SD-LAMP and RT-LAMP reagents at room temperature. I compare the assay efficiency of fresh and vitrified reagents and determine the limit of detection using reagents stored for several weeks.

3.2 Materials and Methods

3.2.1 Reagents

In addition to items outlined in **2.2.1 Reagents**, diethyl pyrocarbonate (DEPC) water (Invitrogen, Carlsbad, CA), sucrose (IBI Scientific, Dubuque, IA), trehalose dihydrate (Thermo Fisher, Waltham, MA), glycerol (Thermo Fisher, Waltham, MA), and Triton X-100 (Sigma-Aldrich, St. Louis, MO) were used for experiments in this chapter.

3.2.2 *V. cholerae* SD-LAMP

SD-LAMP reactions remain unchanged from **2.2.4 Strand Displacement Loop-Mediated Isothermal Amplification (SD-LAMP)** except for the addition of cryoprotectants to the 25 μ L reactions (Table B.1). 2 μ L of diluted template or molecular biology water (for NTC) was added prior to heating. *V. cholerae* was grown according to **2.2.2 Bacteria Culture**. For time point studies, SD-LAMP reactions were incubated at 65°C for 45 minutes. Amplicons were characterized via gel electrophoresis and LFIA as described in **2.2.5 Amplicon Analysis via Lateral Flow Immunoassay (LFIA) and Gel Electrophoresis**.

3.2.3 HIV RT-LAMP

LAMP primers were devised by my colleague Dr. Karin Ejendal using Primer Explorer v5. The primers target a 201 bp region of the *gag* gene of HIV-1 (Table B.2) and loop primers were labeled with FAM and biotin for detection via commercial LFIA (Ustar Biotechnologies, Hangzhou, China). The primer sequences are provided in Table B.3. To allow for both reverse transcription and amplification of the HIV-1 target, we used Bst 3.0 polymerase, which includes reverse transcriptase capabilities, in addition to the buffers and dyes listed in Table B.4. 4 μ L of non-infectious HIV-1 virus (AccuSpan Linearity Panel, SeraCare Life Sciences, Milford, MA) diluted in plasma (SeraCare Life Sciences, Milford, MA) or plasma alone (NTC) was added to 21 μ L of RT-LAMP master mix to make 25 μ L reactions. RT-LAMP was performed at 65°C for 60 minutes and amplicons were characterized via gel electrophoresis and LFIA as described in **2.2.5 Amplicon Analysis via Lateral Flow Immunoassay (LFIA) and Gel Electrophoresis**.

3.2.4 Reagent Drying and Storage

Following the Hayashida *et al.* protocol,⁹³ I separated LAMP reagents into a primer and enzyme mixture to prevent false priming and primer extension that can occur when primers and enzymes are mixed and left at room temperature for an extended period of time.⁹⁴ Moreover, I tested the effects of common cryoprotectants (sucrose and trehalose) and a surfactant (Triton X-100) on LAMP amplification. Three reagent deposition patterns (Figure B.1) were tested in addition to storage substrates such as PCR strip tube caps (1402-4700, USA Scientific, Ocala, FL), 0.22 μm polyethersulfone (PES) (Millipore Sigma, Burlington, MA), 60 μm cyclic olefin polymer (COP) (Zeonor, Tokyo, Japan), self-seal pressure sensitive adhesive (PSA) (GBC, Lake Zurich, IL), and polyethylene terephthalate (PET) (Apollo, Lake Zurich, IL).

After optimization was complete, the following finalized protocol was used for vitrification of both *V. cholerae* SD-LAMP and HIV RT-LAMP reagents. The primer mixture (Table B.1 and Table B.4) containing sucrose, glycerol, Triton X-100, and primers was deposited by hand on a 1 \times 1 cm piece of PET in two parallel lines (Figure B.2). After drying in a sterile biosafety cabinet under continuous air flow for 60 minutes at room temperature, the enzyme mixture (Table B.1 and Table B.4) containing the polymerase, sucrose, and dNTPs was deposited directly on top of the dried primer mixture in parallel lines and set out to dry for another 60 minutes (Figure B.2). After deposition and initial drying, the PET squares were packaged in opaque Mylar bags with silica gel desiccant (Uline, Pleasant Prairie, WI) and stored at room temperature. The dried LAMP reagents were reconstituted by adding the PET squares to PCR tubes containing the rehydrating mixture (Table B.1 and Table B.4) and template (either *V. cholerae* or HIV). LAMP was performed according to protocol and amplicons were characterized via gel electrophoresis and LFIA as described in **2.2.5 Amplicon Analysis via Lateral Flow Immunoassay (LFIA) and Gel Electrophoresis.**

3.2.5 Statistical Analysis

To analyze the effect of reagent storage on the LOD for the *V. cholerae* SD-LAMP assay, a two-way ANOVA *post hoc* Dunnett's was performed with a confidence level of 95%. The two-way ANOVA investigated how the length of time reagents were stored at room temperature affected the vitrified enzyme's activity and assay LOD as determined by LFIA test band quantification.

A Student's unpaired, two-sided *t*-test with a 95% confidence interval was used when comparing the negative and positive controls and fresh and dried samples during the initial testing of 21-day dried HIV RT-LAMP reagents. To determine the limit of detection of 21-day dried HIV RT-LAMP reagents, a one-way ANOVA *post hoc* Dunnett's was performed with multiple comparisons of the LFIA test bands of each concentration against the test bands of NTC with a 95% confidence interval.

3.3 Results and Discussion

3.3.1 Optimization of Vitrification for Room-Temperature Storage of LAMP Reagents

It is well known that cryoprotectants are necessary to stabilize both proteins and oligonucleotides during the drying process;⁹¹ however, it is important that these additives do not decrease amplification efficiency. I first examined the effects of sucrose, trehalose, and Triton X-100 on amplification using concentrations from Hayashida *et al.*⁹³ I established that the *V. cholerae* LAMP assay can tolerate 165 mM (~8% v/v) of both sucrose and trehalose and 0.007% Triton X-100 (Figure 3.1). After further investigation, I found that LAMP can sustain 10% (v/v) of both

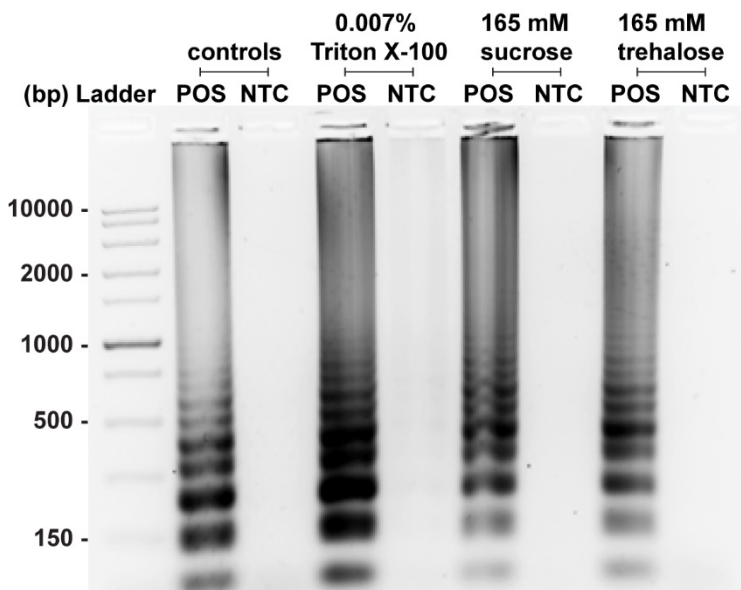


Figure 3.1 LAMP tolerance of additives used in Hayashida *et al.*

After 30 minutes of heating, LAMP is not inhibited by 0.007% Triton X-100 or 165 mM sucrose or trehalose (final concentrations). Positive samples were spiked with 10^5 *V. cholerae* cells/reaction. (n=1)

sucrose and trehalose (Figure B.3A) and 10% (v/v) of yellow food color solution (Figure B.3B). Food color solutions may be helpful for machine alignment when scaling up reagent deposition to printing mechanisms. After establishing that the additives do not affect my *V. cholerae* LAMP reaction, I replicated the Hayashida *et al.*⁹³ protocol in PCR tube caps using the reagent deposition pattern seen in Figure B.1A. I used sucrose as the cryoprotectant for the first group of samples and trehalose for the second group. As seen in Figure 3.2, both sucrose and trehalose adequately protect LAMP proteins and oligonucleotides during the vitrification process and the 24-hour room-temperature storage period. I decided to move forward with sucrose because it is less expensive

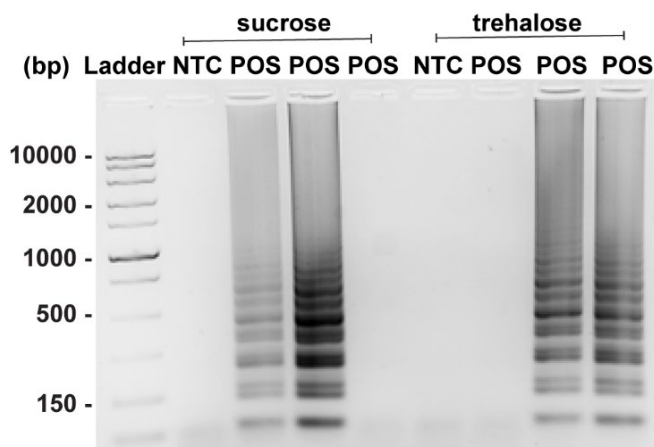


Figure 3.2 Evaluation of cryoprotectants for LAMP reagent storage.

Sucrose and trehalose were added to both the primer and enzyme mixture according to the protocol. LAMP reagents were stored at room temperature for 24 hours before reconstituting with the rehydrating mixture and water (NTC) or 10^5 *V. cholerae* cells/reaction (positives). (n=1)

and more accessible. I also tested variations of the reagent deposition pattern from Hayashida *et al.* (Figure B.1B and Figure B.1C) and concluded that the striped reagent deposition pattern (Figure B.1C) produced the best results after three days of room-temperature storage (data not shown). Finally, I used the striped reagent deposition pattern to store *V. cholerae* LAMP reagents for three days at room temperature on various substrates (all 1×1 cm squares). Figure 3.3 indicates that LAMP reagents can be vitrified and stored for three days on PES (Figure 3.3A), COP (Figure 3.3A), self-seal PSA (Figure 3.3B), and PET (Figure 3.3C). Rehydration of the LAMP reagents vitrified on PES and self-seal PSA was difficult due to the porosity and adhesiveness of the substrates, respectively. Conversely, the vitrified reagents were easily reconstituted from the smooth surfaces of both COP and PET. Both COP and PET produced promising results, but I

selected PET for further experimentation since it is significantly less expensive than COP. In summary, the fully optimized vitrification protocol utilizes sucrose as the cryoprotectant, the striped reagent deposition pattern (Figure B.1C), and PET as the substrate.

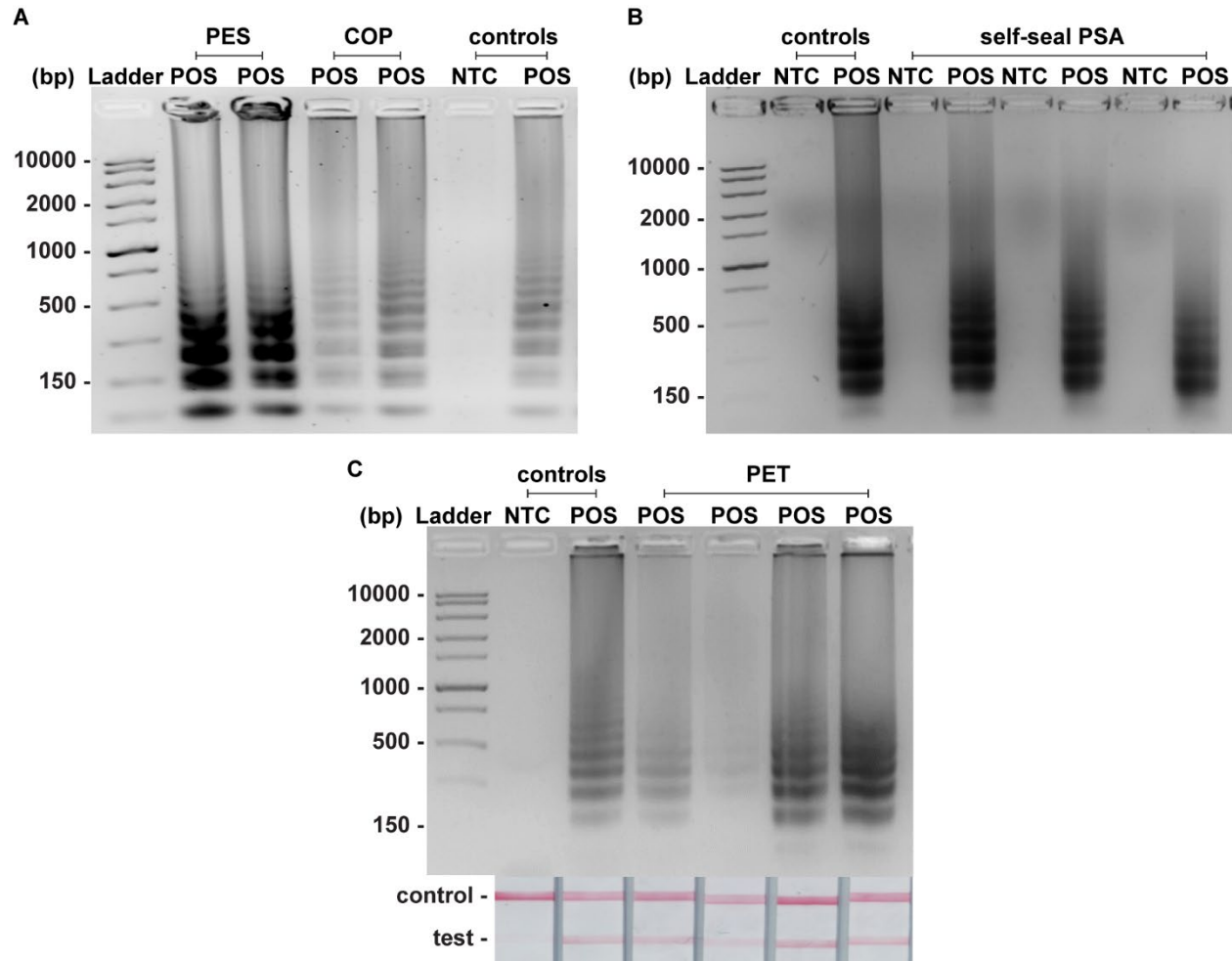


Figure 3.3 Testing substrates for LAMP reagent storage.

LAMP reagents were stored for three days at room temperature on (A) PES and COP, (B) self-seal PSA, and (C) PET. Fresh controls were prepared for each experiment. Samples were reconstituted with the rehydrating mixture and water (NTC) or 10^5 *V. cholerae* cells/reaction (positives). LFIA analysis was only conducted with LAMP reagents stored on PET (C). (n=1)

3.3.2 Diffusivity of Vitrified LAMP Reagents

When I extended the storage period beyond three days using the optimized vitrification protocol, I noticed a decrease in efficiency of the *V. cholerae* LAMP reaction when compared to freshly prepared controls. I hypothesized that separating the primers and enzyme might result in

diffusion-limited amplification; therefore, I explored how the reagent deposition pattern affects diffusion and mixing of reagents upon rehydration.

Prior to beginning the stability studies, I calculated the molecular diffusivity of reconstituted reagents using the Stokes-Einstein equation⁹⁵ and Renkin equation.^{96,97} The hydrodynamic radius, a , was calculated for the largest molecule in both the primer mixture (inner primer) and enzyme mixture (polymerase). Using Equation 3.1, I then calculated the bulk diffusivity, D , for each molecule where R is the gas constant, T is the reaction temperature, η is the viscosity of the solution, and N_A is Avogadro's number.

$$D = \frac{RT}{6\pi\eta a N_A} \quad \text{Equation 3.1}$$

Since the molecule diffusion will eventually occur from the PET to a porous amplification membrane, I then calculated pore diffusivity, D_m , using Equation 3.2.

$$D_m = DK(a/r) \omega_r(a/r) \quad \text{Equation 3.2}$$

Where r is the pore radius, $K(a/r)$, the partition coefficient, is equal to $(1 - a/r)^2$, and the hydrodynamic drag, $\omega_r(a/r)$, is equal to $[1 - 2.1(a/r) + 2.09(a/r)^3 - 0.95(a/r)^5]$. The calculated pore diffusivity indicates that it will take the reconstituted reagents approximately 10 minutes to diffuse 1 mm into the porous amplification membrane at 65°C. Using this information, I decided to layer the primer and enzyme mixture during the drying process (Figure B.2) to minimize the distance which the reconstituted reagents would have to diffuse to ensure proper and rapid mixing for subsequent amplification.

3.3.3 Vitrification of *V. cholerae* SD-LAMP Reagents

I experimentally evaluated the stability of vitrified *V. cholerae* SD-LAMP reagents stored at room temperature for 10, 20, and 30 days. The LOD of *V. cholerae* in 50% pond water was determined using dried reagents at each time point and compared to the LOD using freshly prepared SD-LAMP reagents. I reconstituted the dried SD-LAMP reagents with rehydrating mixture and serial dilutions of *V. cholerae* from $10^0 - 10^5$ cells/reaction or water (NTC) (n=3).

Control reactions using freshly prepared reagents (0-day dried) were heated simultaneously. After 45 minutes of amplification, vitrified samples and fresh controls from each time point were analyzed via LFIA. The SD-LAMP assay was extended to 45 minutes due to a slight loss in activity of the dried enzyme, resulting in slower amplification (data not shown).

After 10 days of room-temperature reagent storage, there was noticeable decrease in LFIA test band intensity at each concentration compared to 0-day dried reagents (n=3) (Figure B.4A and Figure 3.4A). However, there was still statistical significance down to 10^0 cells/reaction for both 0- and 10-day dried reagents when compared to their respective NTC (p-value < 0.001 and p-value < 0.05, respectively) (Figure 3.4B). The improvement in LOD from Chapter 2, 10^2 cells/reaction (Figure 2.8B) to 10^0 cells/reaction (Figure 3.4B), is likely due to the lengthening of the amplification period to 45 minutes. The LFIA test band intensity was even weaker after 20 days of room-temperature reagent storage (n=3) (Figure B.4B and Figure 3.4A). While there was a statistical difference down to 10^1 cells/reaction for 0-day dried reagents when compared to NTC (p-value < 0.0001), there was only significance at 10^5 cells/reaction for reagents stored for 20 days at room temperature (p-value < 0.01) (Figure 3.4C). After 30 days of ambient-temperature storage, the test band intensity dropped to just above the visual threshold for 10^3 , 10^4 , and 10^5 cells/reaction and was more or less zero for other concentrations (n=3) (Figure B.4C and Figure 3.4A). There was a statistical difference down to 10^1 cells/reaction compared to NTC (p-value < 0.0001) for 0-day dried reagents; however, for 30-day dried reagents there was only significance at 10^5 cells/reaction (p-value < 0.05) (Figure 3.4D). Even though there was not statistical significance at low concentrations of *V. cholerae* beyond 10 days of room-temperature storage, the quantified test band intensity remains above the visual threshold down to 10^2 cells/reaction after 20 days of storage and 10^3 cells/reaction at 30 days (Figure 3.4A). This is important because LFIA is ultimately interpreted by the user in a binary (yes/no) manner. From this stability study, it seems the vitrification process is somewhat detrimental to enzyme activity or primer efficiency. Other groups have similarly reported a loss in reaction efficiency of both lyophilized¹⁶ and vitrified⁹⁸ LAMP reagents stored at room temperature when compared to freshly prepared controls.

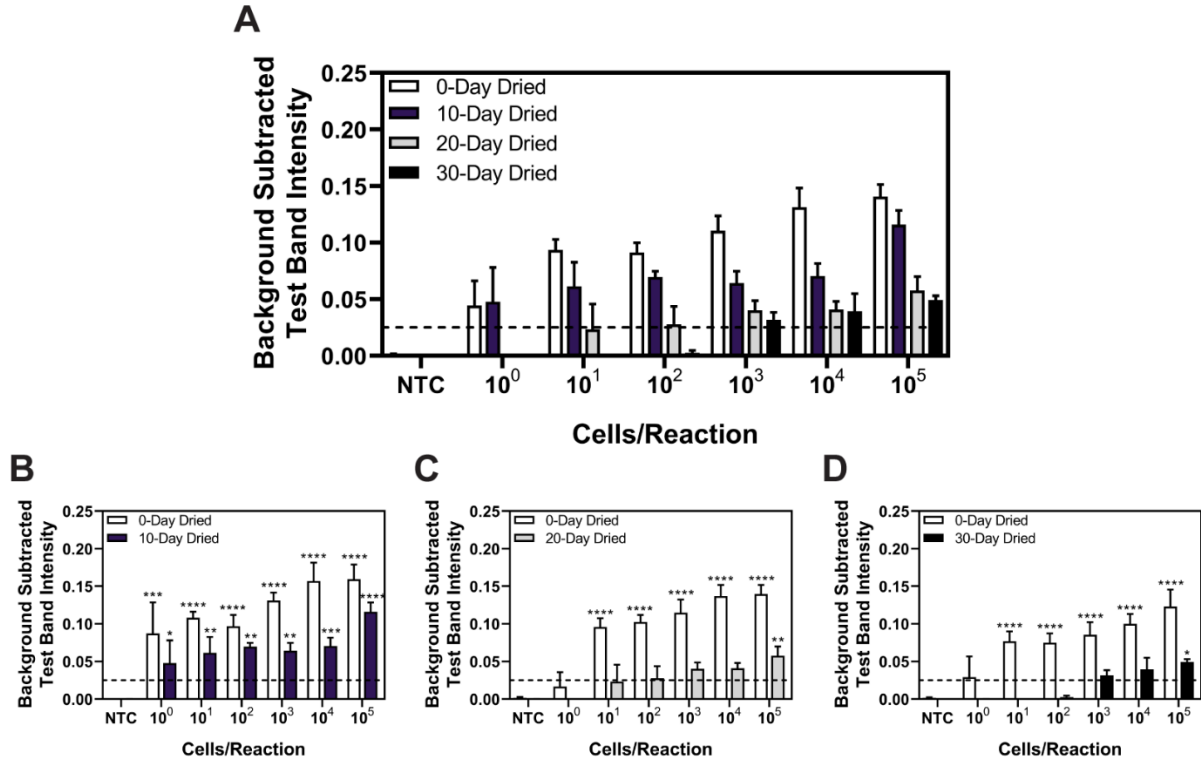


Figure 3.4 Stability of vitrified *V. cholerae* SD-LAMP reagents stored at room temperature.

(A) Average LFIA test band intensity at each time point (0, 10, 20, and 30 days) with concentrations of *V. cholerae* ranging from 10^0 – 10^5 cells/reaction. (B) Direct comparison between 0 and 10 days of room-temperature reagent storage. The 0-day dried group shows significance at 10^0 (** $p < 0.001$) and 10^1 – 10^5 (**** $p < 0.0001$) cells/reaction compared to NTC. The 10-day dried group demonstrates statistical significance at 10^0 (* $p < 0.05$), 10^1 , 10^2 , 10^3 (** $p < 0.01$), 10^4 (** $p < 0.001$), and 10^5 (**** $p < 0.0001$) cells/reaction compared to NTC. (C) Direct comparison between 0 and 20 days of room-temperature reagent storage. The 0-day dried group shows significance at 10^1 – 10^5 (**** $p < 0.0001$) cells/reaction compared to NTC. The 20-day dried reagent group demonstrates statistical significance only at 10^5 (** $p < 0.01$) cells/reaction compared to NTC. (D) Direct comparison between 0 and 30 days of room-temperature reagent storage. The 0-day dried group shows significance at 10^1 – 10^5 (**** $p < 0.0001$) cells/reaction compared to NTC. The 30-day dried reagent group demonstrates statistical significance only at 10^5 (* $p < 0.05$) cells/reaction compared to NTC. Statistical analysis (B-D) was a two-way ANOVA with Dunnett’s *post hoc* relative to respective NTC samples (n=3). Note: n=9 for 0-day dried group graphed in (A).

3.3.4 Vitrification of HIV RT-LAMP Reagents

After determining that vitrification was successful for room-temperature storage of SD-LAMP reagents, I explored whether the vitrification process could be translated to a LAMP assay without an SD probe. Along with undergraduate researcher Lauren Jankowski, I conducted the next set of experiments with the HIV RT-LAMP assay developed in our lab. We reconstituted 21-

day dried RT-LAMP reagents with rehydrating mixture and HIV-1 at 10^5 virus copies/reaction diluted in water or water alone (NTC). Positive and negative control reactions using freshly prepared reagents were heated simultaneously. After the 60-minute amplification period, all samples were analyzed via LFIA (Figure 3.5A). The LFIA test band intensity of positive samples using 21-day dried reagents was not statistically significantly different than that of the test band of the freshly prepared positive controls, indicating that the drying process did not damage enzyme or primer activity. As expected, LFIA results of positive samples were statistically differentiable from NTC samples for both the dried and fresh reagent groups (p -value < 0.001) (Figure 3.5A).

To compare the amplification efficiency of dried and freshly prepared reagents, the LOD of HIV-1 in 16% plasma was determined using 21-day dried RT-LAMP reagents ($n=3$). There was a statistically significant difference between the test band intensity of the 10^5 and 10^6 virus copies/reaction compared to NTC (p -value < 0.05 and p -value < 0.01 , respectively) (Figure 3.5B). While not significant, samples containing 10^4 and 10^3 virus copies did amplify in some cases: two of three repeats for 10^4 and one of three repeats for 10^3 virus copies/reaction. There is a slight loss in sensitivity when using the dried reagents (LOD of 10^5 versus 10^4 virus copies/reaction (data not shown)); however, the LOD can likely be improved with further assay optimization such as RT and polymerase enzyme selection and primer design. Hayashida *et al.* established that vitrified LAMP reagents designed for DNA targets have the same sensitivity as freshly prepared reagents after seven months of storage at room temperature.⁹³ These findings in combination with my preliminary evaluation of limited HIV RT-LAMP reagents stored for five months at room temperature, shown in Figure B.5, give reason to believe that I can increase the storage period of the HIV RT-LAMP reagents far beyond 21 days.

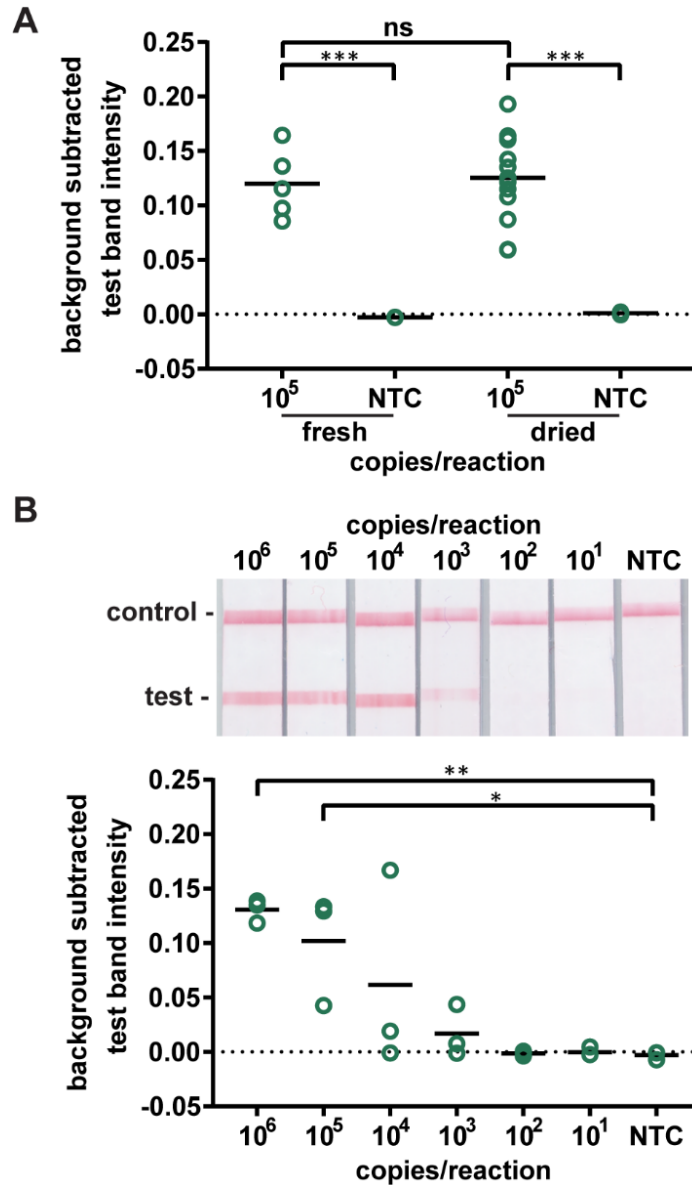


Figure 3.5 Detection of HIV virus amplified by dried RT-LAMP reagents.

(A) There is no significant difference in test band intensity of amplification products detected on LFIA after amplification with fresh RT-LAMP reagents compared to amplification with reagents dried for 21 days. (n=5 fresh, n=13 dried) (***p* < 0.001) (B) There is a statistically significant difference in LFIA test band intensity of RT-LAMP products from as few as 10⁵ HIV virus copies in 16% plasma as compared to NTC. Representative LFIA (top) and test band quantification (bottom). (n=3) (***p* < 0.01, **p* < 0.05)

3.4 Future Directions

For ambient-temperature reagent storage via vitrification beyond 30 days, it is likely that both assays will have to be re-optimized. Specifically, the concentrations of cryoprotectants may require adjustment to better protect the proteins and oligonucleotides in the mixtures. Moreover, we recently purchased a small lyophilizer so lyophilization could be investigated as an alternative to vitrification for long-term (>3 months) reagent storage for both SD-LAMP and RT-LAMP. Future work also includes modeling LAMP reagent diffusivity using COMSOL Multiphysics to better understand the mixing that occurs upon rehydration and heating. The 3D model should consider molecule diffusion through a porous media (membrane), how the assay temperature affects molecular diffusion, and microfluidic modeling via CFD.

3.5 Conclusions

I have demonstrated a simple and equipment-free vitrification method to store LAMP reagents at room temperature. I selected appropriate cryoprotectants, characterized the reagent deposition pattern, and tested various substrates for reagent storage. With the optimized vitrification protocol, I illustrated that *V. cholerae* SD-LAMP reagents can be dried and stored at room temperature for 30 days and HIV RT-LAMP reagents for 21 days before use. The ability to dry reagents eliminates the need for cold chain storage and enables translation of molecular assays, such as LAMP, into portable POC platforms. Moreover, integrated reagents reduce the potential for user error by removing precision pipetting steps and decrease the training requirements to operate POC platforms.

4. CREATION OF INTEGRATED PAPERFLUIDIC PLATFORMS

Parts of this chapter are reproduced from [Ref. 104](#) (Phillips & Moehling *et al.*, 2019) with permission from The Royal Society of Chemistry.

4.1 Rationale

Nucleic acid amplification tests generally require three steps: sample processing, amplification, and detection. Most NAATs are not suitable for the POC because they require separate sample preparation units, cold-chain storage of amplification reagents, expensive analysis equipment, and trained laboratory personnel.^{99,100} Recent efforts have been focused on translating these extremely sensitive and accurate NAATs to portable platforms that can be used by minimally trained individuals at the point of use.^{12,100} As discussed in **1.1.6 Existing and Emerging Disposable Platforms**, paperfluidic platforms consisting of porous membranes and LFIA are ideal for the POC because they are inexpensive, manufacturable, and easy to use and their inherent capillary flow enables fluid transport without external equipment. However, integrating sample preparation, nucleic acid amplification, and detection into a single paperfluidic platform has proven challenging.¹⁰¹ Tang *et al.* developed an integrated paper-based device for sensitive detection of *S. typhimurium* from complex sample matrices.¹⁰² The device incorporates nucleic acid extraction, isothermal amplification, and LFIA detection but it requires four time-sensitive user steps.¹⁰² Another group designed a disposable paperfluidic test for rapid identification of human papillomavirus (HPV) DNA directly from cervical samples; however, there are six distinct operational steps within the 1 hour testing period.¹³

To address the lack of integrated paperfluidic NAATs that are also fully automated, our lab has developed several tools to facilitate the advancement of these platforms. My colleague, Dr. Elizabeth Phillips, characterized thermally actuated wax valves to control fluid flow in paperfluidic platforms.^{103,104} My labmates Orlando Holett and K Byers designed a temperature control circuit and flexible microheaters to supply heat for isothermal amplification assays and wax valve actuation.^{104,105} In Chapter 3, I discussed the utility of vitrification as a reagent drying technique to eliminate cold-chain storage requirements for LAMP reagents. I propose combining these tools with appropriate sample preparation, LAMP amplification, and LFIA detection to create fully integrated and automated paperfluidic platforms.

In this chapter, I outline the development of two paperfluidic platforms: one for detection of *V. cholerae* in pond water and another for identification of HIV from whole blood samples. The *V. cholerae* microfluidic paper-based analytical device (μ PAD) combines bacterial concentration from 1 mL of environmental water, rapid amplification of DNA from lysed cells via SD-LAMP, and equipment-free, colorimetric detection of amplicons via LFIA. The entire process can be performed in just 70 minutes by a minimally trained individual. The HIV platform is a fully-integrated sample-to-answer device that leverages porous membranes' wicking abilities and size discriminating pores to isolate HIV viral particles from human blood cells, amplify RNA from the viral particles using pre-dried RT-LAMP reagents that target the highly conserved *gag* gene of HIV-1, and automatically transport RT-LAMP amplicons to an integrated LFIA for simple, visual interpretation of results within 90 minutes of sample application. This microfluidic rapid and autonomous analysis device (microRAAD) demonstrates the potential for simple and low-cost HIV detection at the point of use.

4.2 Materials and Methods

4.2.1 Water Filtration and Bacteria Capture in Porous Membranes

I tested both Grade 3 chromatography paper (Whatman, Marlborough, MA) and gel blotting paper (Grade GB003, Whatman, Marlborough, MA) as potential membranes to filter the 1 mL pond water sample. I cut three 2 cm \times 2 cm squares of each membrane, added 150 μ L of MilliQ water to each square, and recorded the time to absorb the entire volume.

Fluorescent particles were used to characterize and quantify size-based membrane capture. *V. cholerae* was represented by particles of two different sizes due to its rod-shaped appearance: 0.3 μ m diameter green (Ex468/Em508 nm) particles (Fluoro-Max, Thermo Fisher, Waltham, MA) and 1 μ m diameter Flash Red (Ex660/Em690 nm) particles. A calibration curve correlating particle concentration to fluorescence was created by serially diluting both particle solutions and measuring dilutions in a SpectraMax M5 microplate reader (Molecular Devices LLC, San Jose, CA) at an excitation of 468 nm and 660 nm for the 0.3 μ m and 1 μ m particles, respectively. Along with undergraduate researcher Ethan Pollack, I tested several materials to determine their particle capture efficiency: 0.1 μ m PES (PALL, Port Washington, NY), 0.22 μ m PES (Millipore Sigma, Burlington, MA), 0.22 μ m nylon (GVS Filter Technology, Sanford, ME), 0.45 μ m

polytetrafluoroethylene (PTFE) (Millipore Sigma, Burlington, MA), and 0.6 μm isopore polycarbonate (PC) (Millipore Sigma, Burlington, MA). A 7 mm hole punch was used to cut each membrane into circular pieces. The membranes were then sandwiched between two O-rings and placed into a commercial miniprep spin column (Figure C.1) (Qiagen, Hilden, Germany). The spin column was then placed into a clear 2 mL collection tube. Next, 150 μL of either the 0.3 μm (at 10^{11} particles/mL) or 1 μm particles (at 10^8 particles/mL) was pipetted into the spin column containing the membrane of interest. The tubes were then centrifuged for 60 seconds at 0.5 rcf and the fluorescence of the eluent was measured using the microplate reader. The fluorescence of unfiltered particles (10^{11} particles/mL and 10^8 particles/mL) was also measured and used to determine the proportion of particles that passed through the membrane. Capture efficiency was calculated by subtracting the proportion of particles in the eluent from 1 and multiplying by 100%.

To determine whether LAMP amplification could be performed within the pores of the bacteria capture membrane, I added 1 cm \times 1 cm squares of the membrane to PCR tubes containing the LAMP master mix and template (serial dilutions of *V. cholerae* from 10^0 – 10^5 cells/reaction or water). The membrane completely absorbed the 25 μL solution; therefore, I was confident that amplification happened within the pores of the membrane rather than in residual (unabsorbed) liquid in the tube. Samples and controls (reactions without membrane) were heated for 30 minutes at 65°C. Amplification was confirmed via gel electrophoresis (membranes were loaded into wells of an agarose gel).

I tested the combined filtration and capture mechanism with *V. cholerae* whole cells spiked into pond water. The setup is pictured in Figure C.2, where the bacteria capture membrane (1.5 cm \times 1.5 cm) is centered on top of the absorbent wings. The absorbent wings were carefully sized to absorb 1 mL of liquid (\pm 5%). Negative samples were simply 1 mL of pond water. For positive samples, I spiked *V. cholerae* in 1 mL of pond water at 100 cells/mL. After filtering the 1 mL sample, the bacteria capture membrane was removed from the setup with tweezers and placed into PCR tubes containing the SD-LAMP master mix. The bacteria capture membrane served as the template for the assay. Positive (100 *V. cholerae* cells/reaction) and negative controls contained SD-LAMP reagents and an unused membrane. SD-LAMP was performed for 30 minutes at 65°C. Amplification was confirmed via gel electrophoresis.

4.2.2 Integrated *V. cholerae* μ PAD

Components of the μ PAD (Table C.1) were designed in Adobe Illustrator and cut with a CO₂ laser (VLS 3.5, Universal Laser Systems, Scottsdale, AZ) with help from my labmate Amy Sritong. Valves were prepared by printing 1.25 mm wide lines of solid wax-ink (Black ColorQube ink, Xerox, Norwalk, CT) onto cellulose membranes (Chr1, GE Healthcare, Pittsburgh, PA) using a Xerox ColorQube 8570 (Norwalk, CT). Cellulose membranes were then heated for twelve minutes at 85°C in a table-top oven (VWR, Radnor, PA) and cut into 1 cm long strips with the laser cutter to create closed valves.¹⁰³ Commercially available LFIA (Ustar Biotechnologies, Hangzhou, China) were modified by cutting off the sample pad. Glass fiber conjugate pad (1.5 cm \times 1 cm, Millipore Sigma, Burlington, MA) was used to hold the wash buffer. Once prepared, all components were hand assembled (Figure C.3) and laminated on top and bottom with self-seal PSA (GBC, Lake Zurich, IL) to minimize evaporation during heating.

Diluted food color solutions were used to test the fluidics in the assembled μ PAD. First, 1 mL of yellow food color solution (mimics environmental sample) was added to the sample inlet and allowed to filter through the bacteria capture membrane and into the absorbent wings. Then, 75 μ L of green food color solution was deposited into the wash buffer inlet followed by 23 μ L of blue food color solution into the sample inlet (simulates the rehydrating mixture). Both inlets were then sealed with adhesive (Microseal Seals, Bio-Rad, Hercules, CA). The amplification zone was then locally heated to 65°C for 45 minutes using an 3.8 Ω silver ink microheater.¹⁰⁵ After the incubation, the wax valves were simultaneously heated to 80°C for 1 minute using a hot block. After allowing 30 minutes for LFIA flow control band development, the entire μ PAD was imaged using a desktop scanner (Epson V850 Pro Scanner).

Due to heating and contact issues with the microheaters, a modified μ PAD (without absorbent wings) was used for preliminary testing. *V. cholerae* (10^5 cells/reaction) was spiked into 50 μ L SD-LAMP reactions containing 50% (v/v) pond water. The SD-LAMP reactions were incubated in tubes on a hot block at 65°C for 45 minutes. Green food color solution was added to the modified μ PAD as the wash buffer to ensure there was no fluid leakage past the valve. SD-LAMP amplicons were then deposited into the μ PAD sample inlet before sealing both the wash and sample inlets. Wax valves were heated for 1 minute to allow amplicons to flow into the LFIA. The μ PAD was scanned approximately 15 minutes after opening the valves and the test band was

quantified using a custom MATLAB script that averages the grey-scale pixel intensity of the test band and subtracts the average background pixel intensity 30 pixels below the test band.⁷⁹

4.2.3 Blood Separation and Virus Capture in Porous Membranes

As an initial proof of concept of size-based separation, two sizes of fluorescent particles (Bangs Laboratories, Fishers, IN) were used in a vertical flow filtration setup to allow quantification of both separation and capture in porous membranes (Figure C.1). The 0.11 μm diameter Dragon Green (Ex480/Em520 nm) particles represented HIV-1 virus and the 7.32 μm diameter Suncoast Yellow (Ex540/Em600 nm) particles represented blood cells. Along with my colleague Dr. Laud Anthony Basing, I tested two membranes: a blood separation membrane (MF1, GE Healthcare, Chicago, IL) and an amplification membrane (0.22 μm PES, Millipore Sigma, Burlington, MA). The 0.11 μm particles were added to the spin column containing the membrane of interest at a concentration of 10^{11} particles/mL and the 7.32 μm particles at 10^6 particles/mL. The experimental protocol for determining capture efficiency is detailed in **4.2.1 Water Filtration and Bacteria Capture in Porous Membranes**.

MF1 and 0.22 μm PES membranes were then used to confirm size-based separation of blood from virus in a lateral flow format. The 0.22 μm PES (1 cm \times 1 cm) was overlapped with MF1 (1 cm \times 1 cm) to form the amplification and filtering segments of the integrated device (Figure C.4). Next, 1.2 μL of 2.5×10^5 virus copies per μL of HIV-1 was mixed with 12 μL of human whole blood and deposited onto the MF1 membrane of the MF1/PES assembly, followed by 61.8 μL of rehydrating mixture (Table B.4) (final concentration of 4×10^6 virus copies per mL). After 1 minute of capillary flow, the PES was removed from the assembly and added to a PCR tube with the enzyme and primer mixtures (Table B.4). The samples were amplified for 60 minutes at 65°C. Amplification was confirmed by placing the PES membranes into wells of an agarose gel and performing gel electrophoresis. The remaining solution in the PCR tube that had not saturated the PES membrane was added to a LFIA followed by 40 μL of wash buffer.

4.2.4 Integrated microRAAD for HIV Detection

The microRAAD for HIV detection is composed of the reusable temperature control circuit, silver ink microheaters, and plastic housing and a single use laminated μPAD . The

components of the single use μ PAD were designed and laser cut by my labmate, Dr. Elizabeth Phillips. More details about the materials can be found in Table C.2 and the publication.^{104,106} Once prepared, we assembled the components by hand (Figure C.5) and laminated them with self-seal PSA (GBC, Lake Zurich, IL) to minimize evaporation during the assay.

Seventy-five (75) μ L of RT-LAMP master mix or rehydrating mixture (Table B.4) containing HIV-1 virus (at a final concentration of 4×10^6 virus copies per mL) was loaded into the sample inlet of the μ PAD and sealed with a 1 cm \times 1 cm square of self-seal PSA. When testing whole blood samples spiked with HIV-1 virus, 1.2 μ L of 2.5×10^5 virus copies per μ L of HIV-1 was mixed with 12 μ L of human whole blood and loaded into the sample inlet, followed by 61.8 μ L of RT-LAMP master mix or rehydrating mixture (final concentration of 4×10^6 virus copies per mL). Then, 130 μ L of green food color solution (for visualization of flow) was added to the wash inlet and the inlet was sealed. The loaded μ PAD was then adhered to the acrylic lid with double-sided adhesive. Microheaters¹⁰⁵ were adhered to the backside of the μ PAD, aligned with the two valves and amplification zone, and faced such that the silver traces would contact the pogo pins of the temperature control circuit inside the plastic housing. Two plastic brackets were slid over the acrylic lid and plastic housing to ensure proper contact within microRAAD. Heating was initiated via the temperature control circuit: 1) 65°C for the middle microheater for 60 minutes (amplification) and 2) 80°C for the outer microheaters for 2 minutes (valve actuation). After 30 minutes of LFIA development (1.5 hours after initiating the heating), the μ PAD was imaged using a desktop scanner (Epson, Suwa, Japan). The LFIA test band was quantified using a custom MATLAB script that averages the grey-scale pixel intensity of the test band and subtracts the average background pixel intensity 25 pixels below the test band.⁷⁹

4.2.5 Statistical Analysis

A Student's unpaired, two-sided *t*-test with a 95% confidence interval was used when comparing the test band intensity of NTC and positive samples evaluated in the μ PAD (*V. cholerae*) and integrated microRAAD (HIV).

4.3 Results and Discussion

4.3.1 Water Filtration and Bacteria Capture in Porous Membranes

When testing environmental water samples for bacteria, it is important to collect and perform measurements on a sample volume that is representative of the entire source.¹⁰⁷ Based on my experience, I decided that 1 mL of water is feasible to filter within a small paperfluidic platform and still characteristic of the source. After selecting the two most absorbent membranes in lab, I tested their wicking rate. As seen in Table 4.1, blotting paper absorbed the water two times faster, on average, than the chromatography paper. Therefore, the absorbent wings in the integrated μ PAD will be made of gel blotting paper.

Table 4.1 Absorbent wing membrane testing.

Time to absorb 150 μ L of water was recorded for each 2 cm \times 2 cm squares membrane. (n=3)

	<u>Grade 3 Chromatography</u>	<u>Gel Blotting Paper</u>
Repeat 1	20.3 sec	6.8 sec
Repeat 2	19.4 sec	9.1 sec
Repeat 3	14.4 sec	8.3 sec
<i>Average</i>	<i>18.0 sec</i>	<i>8.0 sec</i>

Using the vertical flow filtration setup in Figure C.1, we quantitatively determined the particle capture efficiency of several membranes. As seen in Table 4.2, the selected membranes were generally effective at trapping the 1.0 μ m fluorescent particles. The 0.6 μ m PC was the only membrane with a capture efficiency less than 98%; therefore, we decided not to test the PC membrane further. We also chose not to move forward with the 0.45 μ m PTFE membrane because it is extremely delicate and prone to tears. The 0.1 μ m PES, 0.22 μ m PES, and 0.22 μ m nylon membranes all effectively captured the smaller 0.3 μ m fluorescent particles, though the 0.1 μ m PES and 0.22 μ m nylon membranes have considerably higher capture efficiencies (Table 4.2). These results indicate that both PES membranes and the nylon membrane would provide sufficient size-based capture of *V. cholerae* bacteria.

Table 4.2 Efficiency of membrane capture of fluorescent particles representing *V. cholerae*.

All membranes except for PC trapped the 1.0 μm particles effectively. The 0.1 μm PES and 0.22 μm nylon membranes captured the small (0.3 μm) particles very efficiently. (n=3)

<u>Particle Size</u>	<u>Membrane</u>	<u>Fluorescence (RFU)</u>	<u>Capture Efficiency</u>
1.0 μm	None	2945.5 \pm 98.3	0.0%
	0.1 μm PES	32.7 \pm 44.8	98.9%
	0.22 μm PES	0.0 \pm 0.0	100.0%
	0.22 μm nylon	9.0 \pm 9.2	99.7%
	0.45 μm PTFE	11.3 \pm 6.2	99.6%
	0.6 μm PC	2053.3 \pm 136.9	30.3%
0.3 μm	None	2565.3 \pm 104.6	0.0%
	0.1 μm PES	64.0 \pm 64.2	97.3%
	0.22 μm PES	545.0 \pm 76.0	77.3%
	0.22 μm nylon	189.3 \pm 36.2	93.6%

Since the *V. cholerae* bacteria will be trapped on top of or within the pores of these capture membranes, it makes sense to perform LAMP in the capture membrane where all the bacteria are localized. Therefore, I needed to investigate whether LAMP amplification was possible within the pores of these capture membranes. Based on previous work in our lab and by other research groups suggesting the compatibility of PES with isothermal amplification techniques,¹⁰⁸ I decided to explore the two PES membranes first. I started with the 0.1 μm PES membrane since it efficiently captured both sizes of fluorescent particles (Table 4.2). After adding the 0.1 μm PES membrane to the tube with LAMP master mix and template and heating for 30 minutes, I found the 0.1 μm PES membrane completely inhibited LAMP amplification (data not shown for *V. cholerae*). When I tested the 0.22 μm PES membrane, I was able to visualize LAMP amplicons via gel electrophoresis down to 10^1 cells/reaction (Figure 4.1A). The same detection limit is observed for the controls (reactions without PES membrane) (Figure 4.1B). I wanted to better understand the discrepancy between the two PES membranes in terms of amplification performance, so I searched for their product specification documents. I discovered that the membranes are manufactured by two different companies (PALL – 0.1 μm and Millipore – 0.22 μm) who have their own proprietary surface treatments. Unfortunately, Millipore does not sell PES membranes with smaller pores, so the 0.22 μm PES is the best available material for this application. The 0.22 μm PES membrane sufficiently captures both sizes of particles that represent the *V. cholerae* bacteria and does not

hinder LAMP; therefore, it is the best candidate for the bacteria capture and amplification membrane. As a note: I did not test LAMP amplification in the pores of the 0.22 μm nylon membrane, but it would be worth exploring in the future.

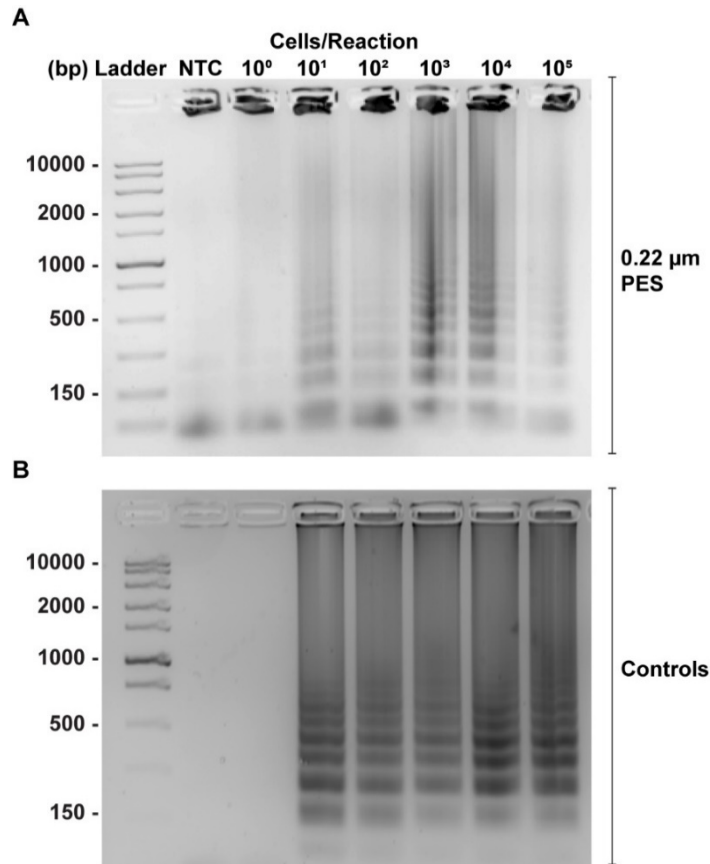


Figure 4.1 *V. cholerae* LAMP in 0.22 μm PES.

(A) Agarose gel displaying banding pattern indicative of LAMP amplification down to 10^1 cells/reaction when assay performed in pores of PES membrane. (B) Amplification down to 10^1 cells/reaction for controls (reactions without PES membrane). (n=1) Note: (A) and (B) are different agarose gels hence the difference in appearance.

Finally, I tested the combined water filtration and bacteria capture mechanism with *V. cholerae* cells spiked in pond water at 100 cells/mL. This concentration was selected because the LOD of the *V. cholerae* SD-LAMP assay in pond water is 100 cells/reaction (Figure 2.8). If cells are not effectively concentrated in the bacteria capture membrane, the SD-LAMP assay (performed in the bacteria capture membrane) will not be able to target and amplify *V. cholerae* DNA. After filtering the pond water sample through the setup in Figure C.2 and adding the 0.22 μm PES membrane to PCR tubes with master mix, I analyzed the samples on an agarose gel. As expected, the negative control did not amplify while the positive control showed the banding pattern

indicative of LAMP amplification (Figure 4.2). Moreover, one of three positive replicates that underwent water filtration and bacteria capture amplified (Figure 4.2), indicating that purification and enrichment is possible with this setup. Further exploration of this water filtration and bacteria capture mechanism is required to determine the *V. cholerae* concentration factor. Traditionally, researchers perform bacteria enrichment via centrifugation or pressure-based separation but these methods are not optimal for use at the POC.^{109–111} One group demonstrated gravity-driven separation and enrichment of *E. coli* from 1 mL of urine prior to performing PCR in a portable POC device.¹¹² Similarly, the filtration and capture setup described here could serve as an equipment-free sample preparation mechanism for target molecules in large sample volumes to improve the sensitivity of portable NAATs.

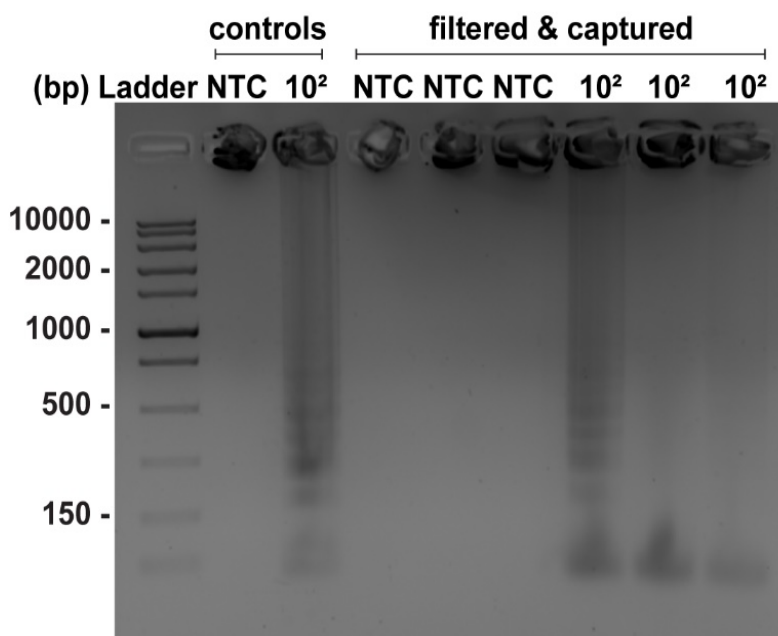


Figure 4.2 *V. cholerae* SD-LAMP after filtering and capturing with PES.

PES can be used to capture *V. cholerae* spiked into 1 mL of pond water. PES served as the template for the SD-LAMP reaction. The banding pattern indicative of amplification is seen in the positive control and one of three sample replicates. (n=1)

4.3.2 Integrated μ PAD for *V. cholerae* Detection

Figure 4.3 outlines the proposed workflow of the integrated μ PAD. First, the water sample is added to the sample inlet. *V. cholerae* are trapped in the PES membrane while excess water filters into the absorbent wings (Figure 4.3A). The wash buffer is deposited, the sample and wash

buffer inlets are sealed, and the amplification zone is heated to 65°C for 45 minutes (Figure 4.3B). Next, both wax valves are opened by heating them to 80°C, allowing the solution in the amplification zone to flow into the LFIA (Figure 4.3C) for colorimetric analysis (Figure 4.3D).

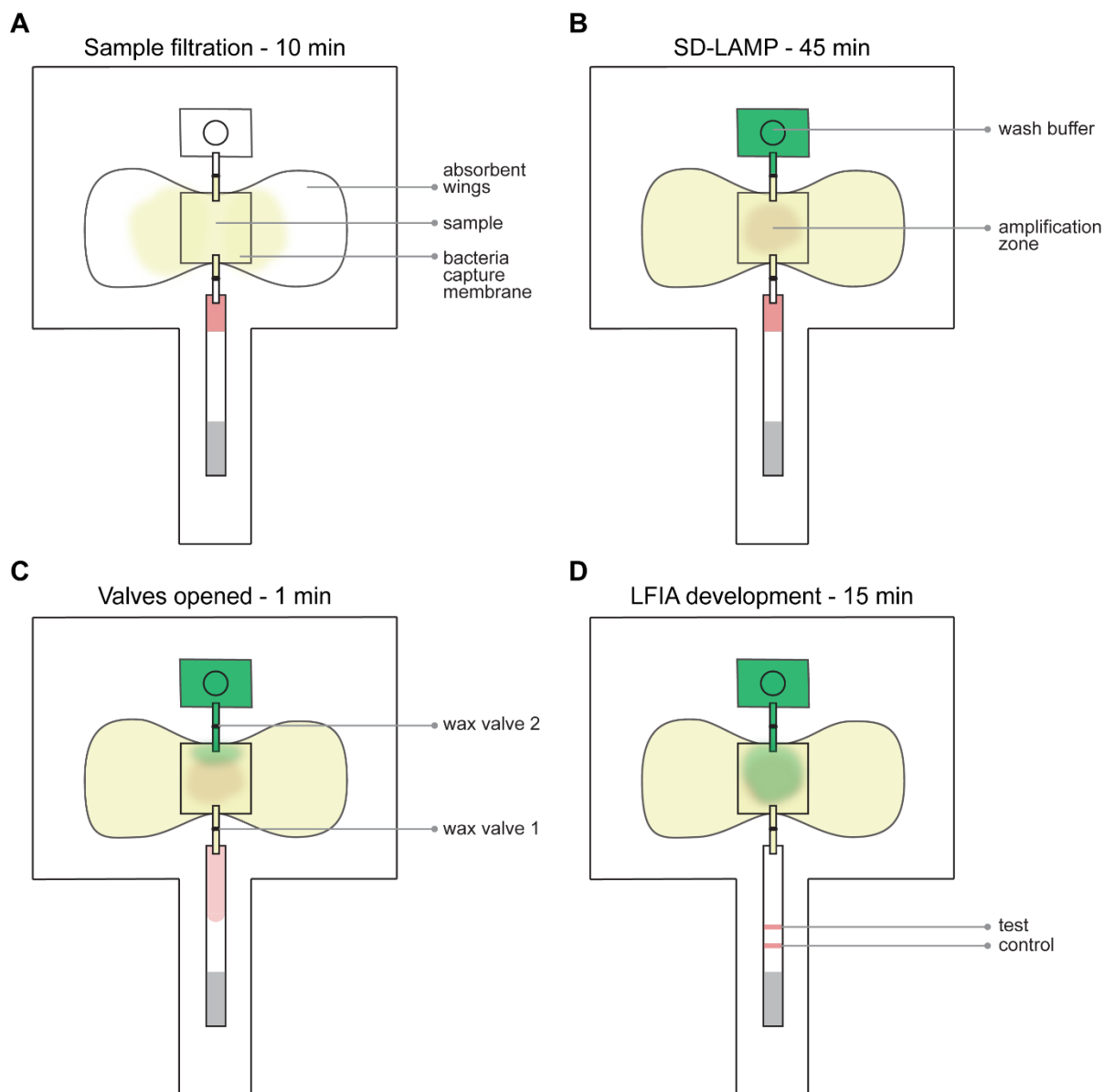


Figure 4.3 Schematic of fluid flow in integrated μ PAD.

(A) The water sample filters into the absorbent wings while *V. cholerae* is trapped in the bacteria capture membrane (PES). (B) The wash buffer (green) and SD-LAMP reagents are constrained during amplification by closed wax valves. (C) Upon thermally actuating the valves, wash buffer is released to the amplification zone and the SD-LAMP products migrate to the (D) LFIA for visual analysis.

To test the fluidics of the integrated μ PAD, I used food color solutions. I noticed that the 1 mL yellow food color solution efficiently filtered through the PES bacteria capture membrane

and wicked into the absorbent wings and that the wax valves withstand the fluid pressure from sample and wash buffer addition. Moreover, the blue food color solution that imitates the rehydrating mixture remained in the PES membrane where it was deposited. This is important because the reagents in the rehydrating mixture are necessary for LAMP amplification so the mixture must remain localized in the bacteria capture and amplification membrane. After heating the amplification zone to 65°C for 45 minutes to simulate LAMP, the two wax valves were opened. However, the green solution in the amplification zone (mix of yellow and blue) never migrated into the LFIA (n=2) (Figure C.6). I hypothesized that 1 mL did not fully saturate the absorbent wings; therefore, the rehydrating mixture diffused outwards into the absorbent wings over time, leaving no liquid in the amplification zone for subsequent LFIA detection. Diffusion can be minimized if a membrane is fully wetted,^{113,114} so I decided to decrease the size of the absorbent wings to ensure full saturation with 1 mL of sample.

After halving the total area of the absorbent wings, I tested the fluidics again. It was obvious that the wings were fully saturated after depositing the 1 mL yellow food color solution. After all solutions were added to their appropriate inlets and the amplification zone was heated, the valves were opened. Within 10 minutes, the green solution from the amplification zone (mix of yellow and blue) migrated the full length of the LFIA, enabling visualization of the control band (n=3) (Figure C.7). Confident I understood the μ PAD fluidics, I wanted to test the integrated device with *V. cholerae* and SD-LAMP reagents.

I verified the detection capabilities of the modified μ PAD with *V. cholerae* SD-LAMP products in 50% pond water. Samples containing as few as 10^5 cells/reaction in pond water resulted in strong test bands (Figure 4.4A) while NTC samples yielded negative LFIA results. There was a statistically significant difference between the test band intensity of 10^5 cells/reaction compared to NTC (p-value < 0.01) (Figure 4.4B). Once the temperature control circuit is completed, I can test the entire process from water filtration and bacteria capture to amplification and LFIA detection in the fully integrated μ PAD. To the best of my knowledge, there are no portable devices to identify *V. cholerae* in environmental water. The equipment-free enrichment, low cost (\$2.83, Table C.1), and simplicity (three user steps) of the fully integrated *V. cholerae* μ PAD make it ideal for rapid, specific, and sensitive field-based detection of *V. cholerae* directly from environmental water samples.

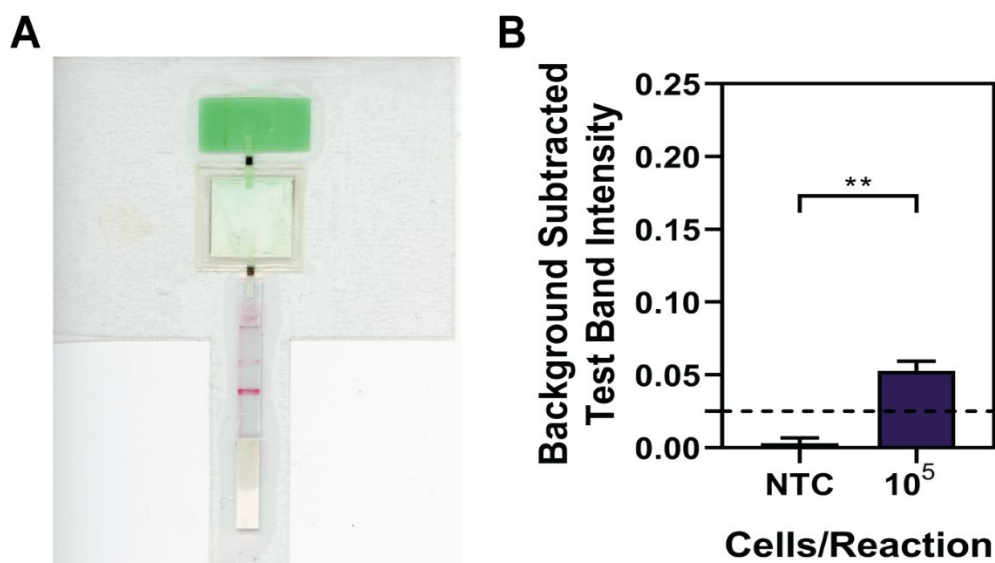


Figure 4.4 Detection of *V. cholerae* with modified μPAD.

(A) Representative positive μPAD imaged 15 minutes after wax valves were opened. (B) SD-LAMP products with initial concentration of 10^5 *V. cholerae* cells/reaction in pond water are detectable by the μPAD and are statistically significantly different (** $p < 0.01$) than NTC samples. (n=3)

4.3.3 Blood Separation and Virus Capture in Porous Membranes

As the RT-LAMP assay was only shown to be robust in up to 20% whole blood, we required the removal of most blood cells that would inhibit the reaction. We developed a simple quantitative method to experimentally test the size-based capture of blood cells and virus in membranes. As seen in Table 4.3, the 7.32 μm particles, representative of blood cells, were captured in the MF1 membrane at an efficiency of 98.6% while 30% of the 0.11 μm particles, representative of the virus, were captured by MF1 (n=3). This implies that MF1 can be used for size-based separation of blood cells from the virus, although some virus will remain in the MF1 membrane, thereby reducing detection sensitivity. Further, 47.6% of the 0.11 μm particles were trapped in the PES membrane (n=3) (Table 4.3), indicating that the PES could localize nearly half of the smaller particles within the amplification zone. Despite the PES membrane having a reported 0.22 μm pore diameter, we suspect that a fraction of the smaller diameter particles were trapped in the PES and the MF1 membranes due to a combination of properties. Because of the membrane heterogeneity, a portion of the pores may be smaller than the nominal pore size, allowing particles to be physically trapped. Furthermore, the tortuosity of the membranes may prevent particle

migration through the membrane.¹¹⁵ Lastly, the proprietary surface chemistries of both membranes may create a charge-based attraction that causes particles to adhere to the membranes. Experimental results indicate future designs could leverage these factors; extending the PES membrane could enable a filtration and localization of the virus for more sensitive detection from higher sample volumes.

Table 4.3 Efficiency of membrane capture of fluorescent particles representing HIV and blood cells.

As expected, MF1 trapped the 7.32 μm particles effectively. PES efficiently captured the 7.32 μm particles and trapped approximately half the 0.11 μm particles. (n=3)

<u>Particle Size</u>	<u>Membrane</u>	<u>Fluorescence (RFU)</u>	<u>Capture Efficiency</u>
0.11 μm	None	4007.6 \pm 165.0	0%
	MF1	2810.9 \pm 193.0	30.0%
	0.22 μm PES	1986.8 \pm 103.2	47.6%
7.32 μm	None	275.1 \pm 12.2	0%
	MF1	2.3 \pm 1.3	98.6%
	0.22 μm PES	0.9 \pm 0.2	81.9%

After the characterization with particles in a vertical format, we confirmed that blood cells would be trapped in the MF1 membrane while the virus would flow into the 0.22 μm PES membrane for subsequent amplification in a lateral flow format. We spiked HIV-1 virus into human whole blood and added the mixture onto the MF1 membrane which overlapped with the PES membrane and chased the sample with rehydrating mixture. After removing the PES from the MF1/PES assembly and amplifying the trapped virus in the PES membrane, the amplicons were analyzed via LFIA. As depicted in Figure 4.5, the test band intensity is strong, implying that the virus is indeed dispersed throughout the PES yet accessible for amplification. The membrane amplification results are consistent with previous findings that have also shown that LAMP and other isothermal amplification methods can be performed within the pores of 0.22 μm PES.¹⁰⁸ However, it seems that amplification is only possible in Millipore 0.22 μm PES. We tried performing HIV RT-LAMP in 0.1 μm PES from PALL since its nominal pore size is smaller than

the virus particles; however, amplification was unsuccessful likely due to proprietary membrane surface treatments (Figure C.8).

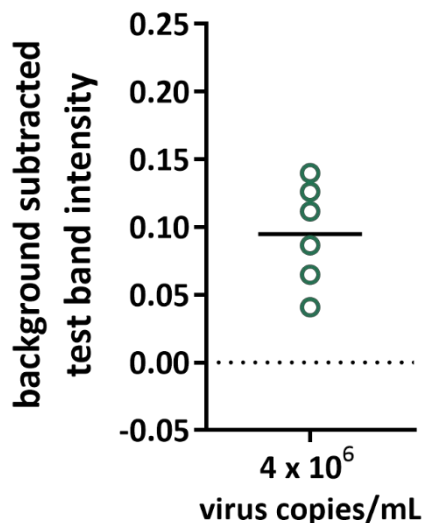


Figure 4.5 LFIA test band intensity of HIV RT-LAMP products after virus and blood cell separation in MF1/PES assembly.

HIV was diluted in blood and applied to the MF1 of MF1/PES assembly. Rehydrating mixture was applied afterwards. The PES was removed from assembly and amplified in RT-LAMP master mix. (n=6)

4.3.4 Integration of microRAAD for HIV Detection

During heating, we observed that the amplification zone reached 65°C within seconds of initiation and remained at $65 \pm 2^\circ\text{C}$ throughout the 60-minute heating period which is adequate for efficient amplification (Figure 4.6A). In separate experiments, we determined that even low concentrations of template can amplify at temperatures between 62°C and 71°C (Figure C.9). The temperature control circuit automatically terminated the amplification zone heating and initiated simultaneous heating of the wax valves. Upon initiation of valve heating, the green food color solution flowed past valve 1 to the MF1 and the heated sample flowed past valve 2 into the LFIA portion of the μPAD (Figure 4.6B). Within 5–10 minutes of the valves opening, test and control bands were consistently observed on the LFIA (Figure 4.6C). We found that both a laptop and a cellphone provided sufficient current to power the temperature control circuit for the duration of the assay and yielded comparable results.

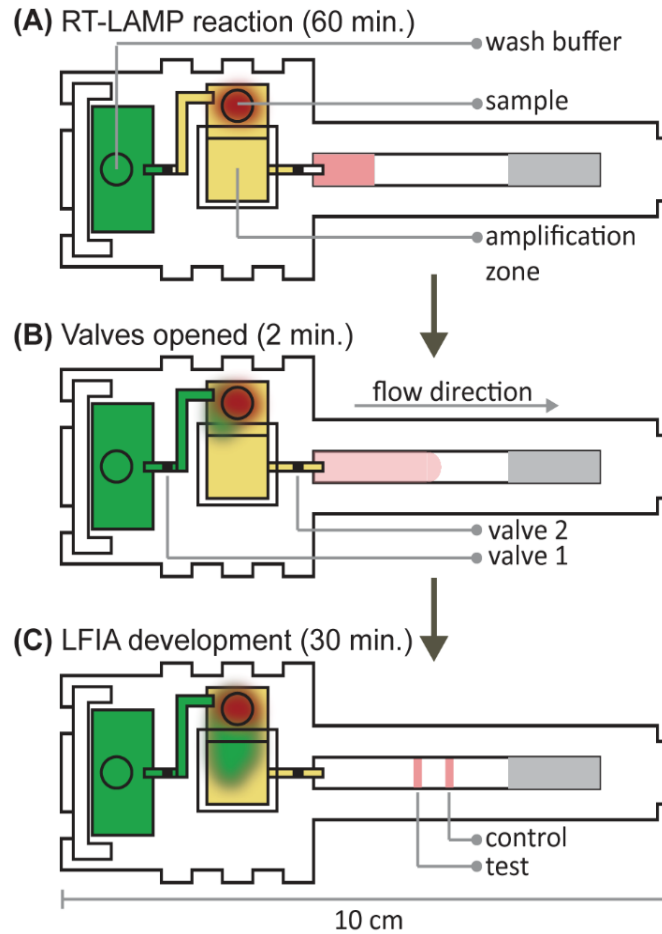


Figure 4.6 Schematic of fluid flow in microRAAD.

(A) The wash buffer (green) is constrained from flowing to the amplification zone and the sample (red blood cells and yellow plasma) is constrained from flowing to the LFIA by closed valves. (B) Upon thermally actuating the valves, wash buffer is released to the amplification zone and the RT-LAMP products migrate to the LFIA for (C) test band development.

To verify the amplification functionality of microRAAD, we initiated the automated detection using 21-day dried RT-LAMP reagents and rehydrating buffer containing HIV-1 virus osmotically lysed in water. Samples containing as few as 3×10^5 virus copies per reaction resulted in unequivocally positive test bands and samples containing no template (NTC) yielded negative test results (p -value < 0.05) (Figure 4.7A). The test band intensity at a concentration of 3×10^5 virus copies per reaction using the dried reagents in microRAAD was comparable to the test band intensity of the same concentration in a tube reaction with the dried reagents (Figure 4.7A and Figure 3.5A).

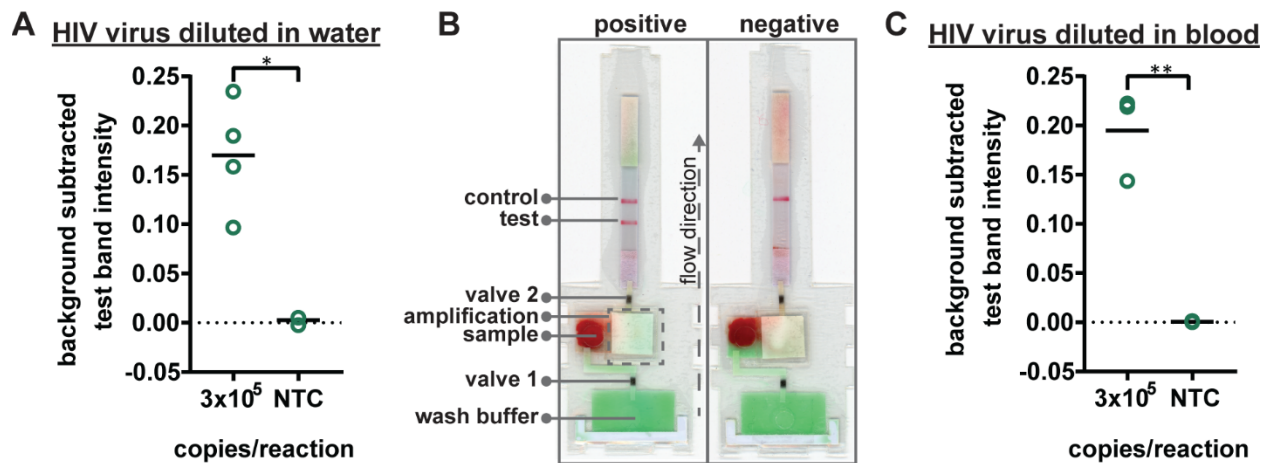


Figure 4.7 Detection of HIV virus on microRAAD with reagents dried for 21 days.

(A) 3×10^5 HIV osmotically lysed virus copies are detectable by microRAAD prepared with RT-LAMP reagents dried for 21 days. (n=4) (B) Representative μ PADs imaged 90 minutes after blood (with and without HIV virus) deposited into microRAAD's sample inlet. After capillary migration of HIV from sample inlet to amplification zone and subsequent heating, the valves are automatically heated, releasing solution to LFIA for detection. (C) As few as 3×10^5 HIV intact virus copies in blood are detectable by microRAAD prepared with RT-LAMP reagents dried for 21 days. (n=3) (* $p < 0.05$, ** $p < 0.01$)

Finally, we performed the detection in the integrated microRAAD using 21-day dried amplification reagents and HIV-1 virus in whole blood. As expected, and seen in Figure 4.7B, the red blood cells remained in the MF1 directly below the sample inlet while the remaining plasma and buffer solution with virus migrated to the PES for amplification. Following amplification, we visually observed positive test bands on the LFIA within 5–10 minutes after valves opened. There was a statistically significant difference between the test band intensity of the 3×10^5 virus copies per reaction compared to NTC (p-value < 0.01) (Figure 4.7C). Notably, the sensitivity using microRAAD for HIV-1 viral detection in blood using dried reagents is comparable to the sensitivity of standard tube reactions with similar conditions (Figure 4.7C and Figure 3.5B). Other groups have similarly reported only 5 to 10-fold reductions in sensitivity when translating manual assays into automated sample-to-answer devices.^{14,74,116} Damhorst *et al.* developed a microfluidic chip for blood cell lysis and modified a smartphone for real-time detection of HIV-1 virus with an LOD of 1.7×10^4 virus copies per reaction.¹⁶ However, the user is required to transfer the lysed blood and freshly prepared RT-LAMP reagents to the reaction chamber for amplification.¹⁶ Even though this platform is 10-fold more sensitive than microRAAD, we believe that the full automation of microRAAD, which reduces sample handling and exposure to bloodborne pathogens, makes it an advantageous system for rapid HIV testing at the POC.

Our initial studies of this integrated sample-to-answer device demonstrate its potential to provide simple, affordable, and rapid detection of HIV from blood samples at the point of use (Figure 4.8). The consumable components of microRAAD (membranes, LFIA, adhesive, reagents) cost only \$2.23 per assay (Table C.2) while the reusable components (temperature control circuit and housing) cost \$70.08. The price is comparable to other rapid HIV tests developed for resource-limited settings and will decrease as we scale-up the manufacturing of the device.¹¹⁷ While low component cost does not guarantee a low price point for consumers, it remains a critical feature of research and development.¹¹⁸

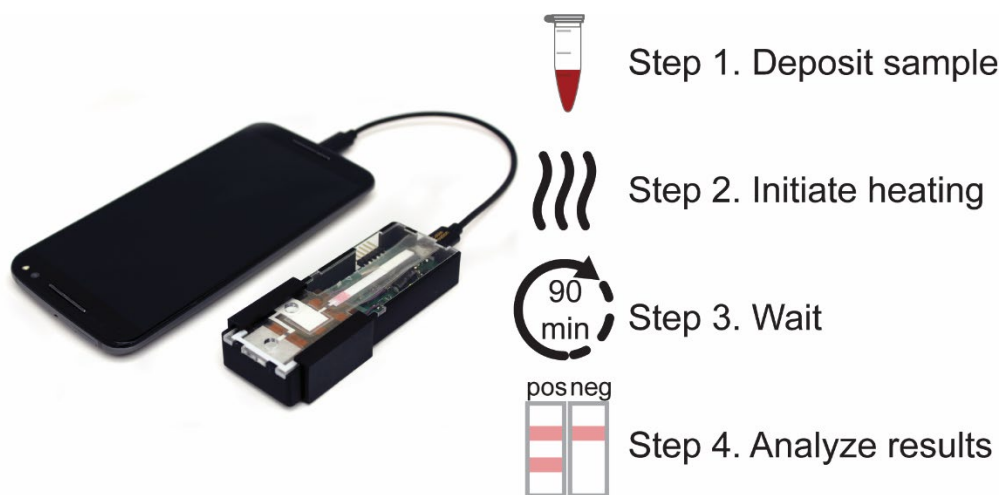


Figure 4.8 Operation of microRAAD.

Photo of microRAAD connected to a phone to power the temperature control circuit. To operate, user 1) deposits sample and wash buffer into inlets, 2) initiates heating by connecting microRAAD to phone, 3) waits 90 minutes for automated sample incubation and fluid delivery within μ PAD, and 4) analyzes LFIA results.

4.4 Future Directions

The next steps for the integrated *V. cholerae* μ PAD include testing the fully integrated device with 30-day dried reagents. First, a comparison between the LFIA test band intensity of pond water samples containing 10^5 and 0 (NTC) cells/mL is necessary. The limit of detection of *V. cholerae* in the integrated μ PAD utilizing 30-day dried SD-LAMP reagents can then be determined by spiking $10^0 - 10^5$ *V. cholerae* cells into 1 mL of pond water and evaluating the

μ PAD LFIA test band intensity. Additionally, including an internal amplification control into the μ PAD could differentiate negative from invalid results.

Even though microRAAD has many advantages over comparable diagnostic tools, there remain some limitations. The sensitivity of this integrated prototype is 3×10^5 virus copies per reaction, or 2.3×10^7 virus copies per mL of whole blood, which falls at the high end of the clinical range, 10^7 virus copies per mL at peak infection.¹¹⁹ This inadequate sensitivity may be due to the thermal lysis performed within microRAAD that bypasses nucleic acid purification and concentration steps. We expect that improvements in primer design, enzyme selection, and the addition of virus concentration from larger volumes of sample could further improve the device's sensitivity and enhance clinical utility. Specifically, the incorporation of a smaller pore-sized membrane could enable size-based capture of the virus and isolation from inhibiting blood components. Incorporating these improvements along with extended device storage and usability studies will enable clinically relevant detection and early diagnosis of HIV at the POC.

4.5 Conclusions

I have shown that the modified *V. cholerae* μ PAD is capable of detecting SD-LAMP amplicons. There are only three user steps for the proposed integrated μ PAD: add sample, rehydrating mixture, and wash buffer; seal inlets; and introduce heat to amplification zone. Because of the simplicity of operation and colorimetric analysis, this test can be performed by a minimally trained individual unlike the laboratory method typically used to detect *V. cholerae* from water samples. The integrated and equipment-free filtering mechanism enables the μ PAD to process large sample volumes (1 mL) while locally concentrating the bacteria for isothermal amplification and subsequent LFIA detection. The *V. cholerae* μ PAD is completely disposable and costs only \$2.83 per test. Altogether, this portable μ PAD has the potential to transform field-based monitoring of environmental water sources for *V. cholerae* presence.

We have demonstrated microRAAD, an autonomous and fully integrated sample-to-answer device, for the specific detection of HIV-1 from human whole blood. After sample addition, the LFIA can be visualized within 90 minutes. Moreover, the user is required to perform only four steps to initiate testing: load sample and rehydrating mixture, add wash buffer, seal the inlets with adhesive, and initiate the temperature control circuit by connecting a power source. One of the most noteworthy aspects of microRAAD is the complete automation from blood-in to

results-out, eliminating sample preparation and other time-critical steps by the user. Furthermore, we have demonstrated that RT-LAMP reagents can be dried and stored at room temperature for three weeks before use in the integrated device. The ability to dry reagents eliminates the need for cold chain storage and increases the usability and portability of the device, especially in resource-limited settings. The sensitivity of this integrated prototype is 3×10^5 virus copies per reaction, or 2.3×10^7 virus copies per mL of whole blood, which is comparable to the viral load at peak infection. Moreover, microRAAD requires only \$2.23 worth of consumable components, making it an affordable detection tool. MicroRAAD combines robust and selective molecular techniques with elegant capillary fluidics and resilient heating controls into a single, portable platform for rapid pathogen detection at the POC.

5. MICROSCOPE CHARACTERIZATION OF PARTICLE DIFFUSOMETRY FOR *V. CHOLERAE* DETECTION

This chapter is reproduced from [Ref. 43](#) (Clayton & Moehling *et al.*, 2019) with permission from Springer Nature via [Creative Commons license](#). All work presented in this chapter was performed equally with my co-author, Dr. Katherine Clayton.

5.1 Rationale

Environmental pathogen detection presents unique challenges in the development of novel biosensing mechanisms due to the exceedingly low concentrations of pathogens in their native environments. The current gold standard for detection of *V. cholerae* in water samples is a 4-day process involving bacteria enrichment and culture prior to performing PCR.¹²⁰ Despite being one of the most sensitive laboratory detection methods, PCR is still not robust or sensitive enough to directly detect *V. cholerae* from the environment.¹²¹ Hence, there is a need for a biosensor that can rapidly detect pathogens, such as *V. cholerae*, directly from their native environment.

Next generation mechanical, electrical, and optical signal transducers have the potential to detect pathogens and biomolecular species with high sensitivity. For example, mechanical micro- and nano-cantilever systems have been used extensively to detect *E. coli* in the range of 1-100 cells/mL.¹²²⁻¹²⁶ Electrical and electrochemical transducers, such as impedance-based sensing of carbon nanotubes where the signal change is caused by *E. coli* binding to the surface, have been shown to have a LOD of 50 cfu/mL.¹²⁷ Further, optical biosensing techniques have been used for dark-field imaging of *E. coli* functionalized with gold nanoparticles to detect as few as 10⁴ cfu/mL of bacteria in only 30 minutes.¹²⁸ However, these methods require extensive pre-processing to purify or label samples prior to detection.

Due to their exquisite sensitivity, nucleic acid amplification methods such as PCR and LAMP, provide excellent target DNA enrichment for biosensor detection. LAMP is a particularly attractive amplification method because it operates at a single temperature and provides rapid and robust amplification even in complex sample matrices.³⁷ Researchers have demonstrated successful LAMP amplicon detection using fluorescence, visual, and electrochemical methods.^{47,50,129} Okada *et al.* showed that LAMP is robust enough to identify *V. cholerae* in clinical rectal swabs.⁷⁸ The promising results from Okada *et al.* indicate that LAMP can be used for the detection of *V. cholerae* in complex sample matrices.

In this chapter, we develop a highly accurate and sensitive biosensing technique for the rapid detection of *V. cholerae* in environmental water samples by pairing LAMP with particle diffusometry (PD) (Figure 5.1A). PD involves rapid optical measurements of particle Brownian motion following amplification.^{68–70} When *V. cholerae* is present in the solution, the LAMP assay polymerizes DNA targets into a variety of base pair lengths up to 25 kilobases.⁴⁵ This polymerization causes the particle Brownian motion to decrease (Figure 5.1B).⁶⁹ We calculate the change in the particle Brownian motion with PD using correlation-based algorithms of the particle images.⁶⁸ We show the applicability of PD to detect the presence of *V. cholerae* down to 1 cell/reaction, which is 100-fold more sensitive than fluorescence-based measurements, and 10 cells/reaction in complex sample matrices.

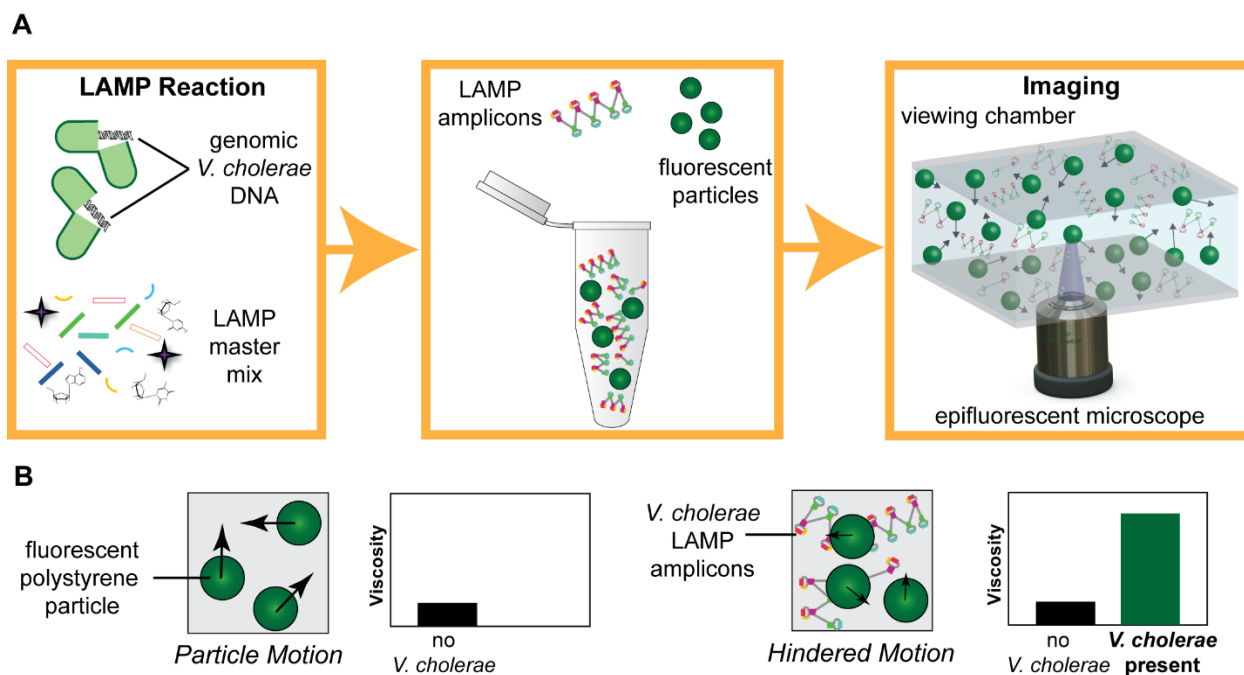


Figure 5.1 PD-LAMP set-up.

(A) The LAMP assay is performed in the presence of *V. cholerae* DNA (left). LAMP amplicons combined with fluorescent polystyrene particles (middle) are imaged under fluorescence microscopy (right). (B) Relationship of particle motion and viscosity. Particles undergo Brownian motion in a solution (left). In the presence of LAMP amplicons, the viscosity of the solution increases and particles experience hindered motion, indicating the presence of *V. cholerae* DNA in the sample (right).

5.2 Materials and Methods

5.2.1 LAMP

The LAMP primers (B3, F3, BIP, FIP, LB, LF, LF-Biotin) and standard master mix from previous chapters were also used here (Table A.1 and Table A.3). 2 μ L of template (purified *V. cholerae* DNA or whole cells) or molecular biology water (NTC) was added just prior to heating. LAMP was performed at 65°C for 20, 25, or 35 minutes using an Applied Biosystems 7500 Real-Time PCR System (Foster City, CA) and samples were stored at 4°C until analyzed with PD.

LAMP was performed with *V. cholerae* purified genomic DNA or whole cells. *V. cholerae* strain N16961 was grown according to **2.2.2 Bacteria Culture**. 10-fold serial dilutions of template (both DNA and cells) were prepared for experimentation in molecular biology water. Real-time fluorescence data was collected for each experiment to visually track the amplification progress. LAMP amplicons were analyzed via gel electrophoresis using a 2% agarose gel at 100 V for 60 minutes, stained with ethidium bromide, and imaged using an ultraviolet light gel imaging system (c400, Azure Biosystems, Dublin, CA). All gel images were collected using the Azure cSeries software and settings of UV302 with an exposure time of 15 seconds.

5.2.2 Particle Preparation

For viscosity measurements, red fluorescent 200 nm polystyrene particles (Fluoro-max red dyed aqueous spheres, Thermo Fisher, Waltham, MA) were combined with the LAMP products. Polystyrene particles were chosen because they are similar in density to water, making them relatively neutrally buoyant, allowing the effects of gravity to remain negligible for particle diffusometry measurements. Further, the 200 nm particle size was chosen to achieve more sensitive measurements as smaller particles exhibit greater changes in diffusivity. These particles were washed three times in MilliQ water by centrifugation at $13,000 \times g$ for 15 minutes. Following, the particles were added to the LAMP products at a final concentration of 6×10^9 particles/mL and stored at 4°C until imaging.

For combined size and viscosity measurements (i.e. diffusivity), streptavidin coated 220 nm green polystyrene fluorescent particles were used (Bangs Labs, Fishers, IN) to maintain a particle diameter as close as possible to the 200 nm unmodified polystyrene particles used for viscosity measurements. Due to supplier constraints, 220 nm was the nearest particle diameter with

streptavidin-modified surface chemistry. Particles were washed three times in MilliQ water by centrifugation at $13,000 \times g$ for 15 minutes. Washed particles were added to the LAMP products at a final concentration of 1.49×10^9 particles/mL (note that the final concentrations of the 200 and 220 nm particles differ due to their size to eliminate hindered diffusion). Particles and LAMP amplicons were incubated at 4°C by gentle rotation for two hours to allow binding of the biotinylated LAMP products to the streptavidin particles and then imaged.

5.2.3 Particle Diffusometry Theory

PD involves recording a series of images of fluorescent particles undergoing Brownian motion in a quiescent volume and calculating the particle diffusion coefficient using correlation analysis.⁶⁸ Each individual image is partitioned into smaller interrogation areas where the size of each interrogation area is defined such that 8-10 particles, on average, are present.¹³⁰ Within these interrogation areas, autocorrelations and cross-correlations of the images are computed for the entire image stack. Cross-correlation involves correlating two sequential images, for example taken at time t and at time $t + \Delta t$ (where Δt is a function of the frame rate). Greater particle displacement, during the elapsed time Δt , creates broader cross-correlation peaks.¹³¹ The cross-correlation peak width, s_c (pixels) at a height of $1/e$, is used to calculate the diffusion coefficient.¹³² Further, autocorrelation is performed by correlating an image captured at time t with itself. The autocorrelation peak width, s_a at a height of $1/e$, is taller and narrower when compared to the cross-correlation peak.¹³¹ With autocorrelation and cross-correlation, the diffusion coefficient, D , can be calculated by the equation derived by Olsen and Adrian:¹³³

$$D = \frac{s_c^2 - s_a^2}{16M^2\Delta t} \quad \text{Equation 5.1}$$

where M is the magnification of the microscope objective. Because the peak width is in units of pixels, using Equation 5.1, we see that the squared difference in the peak widths, $s_c^2 - s_a^2$, corresponds to the change in the cross-sectional area of the correlation peak at $1/e$. By experimentally determining the diffusion coefficient, D , from the series of particle images, the Stokes-Einstein relationship can be algebraically rearranged (Equation 5.2) to calculate the viscosity, η , of a solution.^{95,134}

$$\eta = \frac{kT}{6\pi D a} \quad \text{Equation 5.2}$$

Here, k is the Boltzmann constant, T is the absolute temperature, and a is the hydrodynamic radius of fluorescent particles that are imaged. It is important to note that smaller diameter particles will provide a greater signal-to-noise ratio in solutions where there are only modest changes in viscosity.

We are specifically interested in characterizing how the presence of LAMP amplicons affects diffusivity of particles for pathogen detection. The change in diffusivity in this context is due to changes in solution viscosity and/or particle size. Therefore, we compute the relative solution viscosity or the combined relative size and solution viscosity, forgoing the magnitude in either case. Algebraic manipulation of Equation 5.2, where η_0 is the viscosity of the LAMP solution without *V. cholerae* template (still includes primers and fluorescent particles), depicts the relative viscosity (η/η_0).

$$\frac{\eta}{\eta_0} = \frac{\eta a}{\eta_0 a_0} = \frac{D_0}{D} \quad \text{Equation 5.3}$$

Further, Equation 5.2 can be manipulated to include relative size. In Equation 5.3, a_0 is the size of unbound particles and a is the size of the particles after binding to biotinylated LAMP products. This approach is optimal in binary situations, where an investigator is interested in the presence or absence of pathogens in a solution.

Sample-to-sample variation often occurs in the quantitative measurements of LAMP assays due to the polymerization process.⁸⁴ Therefore, when measuring the change in the diffusion coefficient as a function of the initial concentration of *V. cholerae*, we calculate the change (Δ) in the signal. This approach is used when comparing fluorescence measurements with PD measurements. In Equation 5.4 the signal change (ΔSignal) is a function of the signal after amplification (*final measurement*) and before amplification (*initial measurement*).

$$\Delta \text{Signal} = \frac{\text{final measurement} - \text{initial measurement}}{\text{final measurement}} + 1 \quad \text{Equation 5.4}$$

5.2.4 Experimental Particle Diffusometry Measurements

A fluid well for the LAMP-particle solution was made by punching a 6 mm diameter hole through double-sided adhesive (120 μm thickness) (Therm-O-Web, Wheeling, IL) which was then adhered to a cover glass slide (Thickness No. 1, Thermo Fisher, Waltham, MA). The 3 μL LAMP-particle solution was added to the fluid well and sealed with a second cover glass slide to limit convective evaporation during imaging.

The LAMP-particle solutions were imaged at room temperature using an inverted fluorescence microscope (Nikon TE-2000U, Nikon, Japan) equipped with an X-cite lamp and 40X magnification objective using PCO Camware software (PCO, Kelheim, Germany). Images were recorded using a PCO 1600 CCD camera (PCO, Kelheim, Germany) using an 802×802 pixel² imaging window with 2×2 binning at 13.3 fps. Individual pixels were $7.4 \times 7.4 \mu\text{m}^2$. For imaging of the 200 nm red polystyrene particles, a Q-Dot 585 filter cube was used (Chroma, Bellows Falls, VT) and for the 220 nm green polystyrene particles, a B3-A filter cube was used (Nikon, Japan).

Particles were imaged at the mid-plane of the chip to ensure the effects of hindered diffusion caused by the proximity of particles to any wall were avoided. We analyzed particles which were located in the depth of correlation, 4.2 μm , by using an expression derived by Meinhart *et al.*^{135,136} Therefore, particles located within the depth of correlation form the correlation function and the remainder of particles contribute to the background signal.

Particle images were processed and auto- and cross-correlation analysis was performed using an in-house MATLAB code. 64×64 pixel² interrogation areas contain, on average, 8-10 particles per 100 image frame stacks (~8 seconds of data). This allowed for a high signal-to-noise ratio while maintaining a statistically relevant number of data points. Nine measurements, of which 100 images constituted one measurement, were performed for every sample. A two-dimensional Gaussian curve fit was used to calculate the auto- and cross-correlation peak widths for both the XZ- and YZ-planes. The width of the correlation peak is defined by $1/e$ and the width of the XZ- and YZ-Gaussian curves are averaged as one peak width value.¹³²

5.2.5 Blinded Study

Control samples contained (1) no *V. cholerae* DNA that underwent the 65°C heating for 20 minutes ((-) heat), (2) genomic *V. cholerae* DNA that did not undergo heating ((+) no heat),

and (3) no *V. cholerae* DNA that did not undergo heating ((-) no heat). The experimental sample contained genomic *V. cholerae* DNA and was amplified at 65°C for 20 minutes ((+) heat). The four samples were blinded to the researcher performing the PD testing to obtain unbiased measurements. The four samples contained 200 nm red fluorescent unmodified polystyrene particles that were added to the samples after amplification and were imaged with fluorescence microscopy. Data was represented in terms of relative viscosity.

5.2.6 Water Testing

All LAMP reactions in various water samples were prepared using the standard master mix and the LF-Biotin primer and were performed for 25 minutes. The different water samples were 50% by volume of the total LAMP reaction. Water samples included laboratory tap water, autoclaved 1X PBS (Sigma-Aldrich, St. Louis, MO) pH 7.4, rain runoff, pond water, and molecular biology water. In the experiment that investigated the limit of detection of whole *V. cholerae* cells in pond water, the LAMP assay was run for a total of 35 minutes due to the slight delay in amplification caused by inhibitors in pond water.⁷²

5.2.7 Statistical Analysis

The blinded study was statistically analyzed with a one-way ANOVA with multiple comparisons using a 95% confidence interval, comparing data represented in terms of relative viscosity. In measuring the 10-fold dilutions and determining the LOD, data was represented in terms of Δ *Viscosity* or Δ *Diffusivity*. When comparing a series of 10-fold dilutions, a one-way ANOVA *post hoc* Dunnett's test was performed with multiple comparisons against a no template negative control (NTC) with a 95% confidence interval. To compare Δ *Fluorescence* and Δ *Viscosity*, the Pearson's correlation coefficient was calculated. A Student's paired *t*-test with a 95% confidence interval was used when comparing the negative and positive samples in different water, with data again represented in terms of relative viscosity. Box-and-whisker plots were made for the PD and fluorescence data for the 10-fold dilutions where the upper and lower bounds represent the 75th and 25th percentile about the median, respectively, and the minimum and maximum values are represented by the upper and lower whiskers.

5.3 Results and Discussion

5.3.1 Blinded Study

To validate that PD measurements of relative solution viscosity could be used to detect successful LAMP amplification, a series of blinded studies were performed. The sample containing the amplified genomic *V. cholerae* DNA was correctly identified with statistical significance (p-value < 0.0001) in every circumstance (n=3). Data from one representative blinded study is presented in Figure 5.2 and averaged data from all 3 repeats is in Table D.1. The sample containing amplified genomic *V. cholerae* DNA had the greatest relative viscosity (η/η_0 , calculated from Equation 5.3) compared to the control samples, meaning that the presence of polymerized LAMP amplicons in the solution increased the fluid viscosity (Figure 5.2B). Successfully identifying *V. cholerae* LAMP amplicons in blinded studies demonstrated that viscosity measurements are a feasible approach in determining pathogen presence.

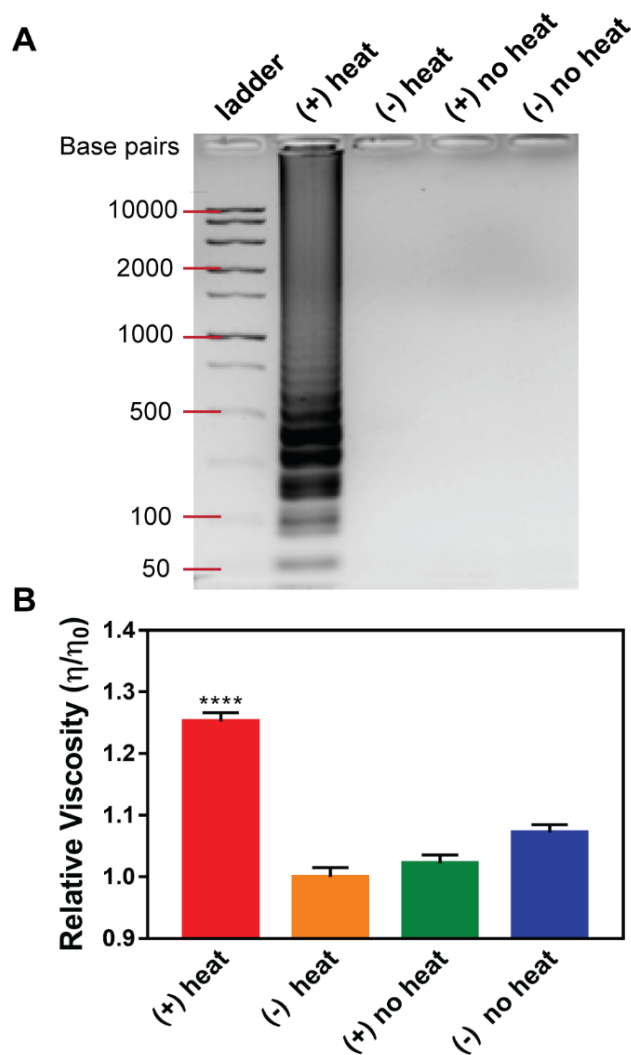


Figure 5.2 Relative viscosity blinded study.

Here, genomic *V. cholerae* DNA that underwent the 65°C heating of LAMP is represented as (+) heat, no genomic *V. cholerae* DNA that underwent the 65°C heating of LAMP is (-) heat, genomic *V. cholerae* DNA that did not undergo heating is (+) no heat, and no genomic *V. cholerae* DNA that did not undergo heating is (-) no heat. (A) A 2% agarose gel of a representative blinded test to show DNA amplification in the (+) heat sample. (B) Relative PD results show the (+) heat sample is statistically significantly more viscous than control samples (**** p-value < 0.0001). Nine PD measurements were collected for each sample.

5.3.2 PD versus Fluorescence Measurements

LAMP was performed with genomic *V. cholerae* DNA at concentrations ranging from 10^0 – 10^5 DNA copies/reaction (n=3, data of repeats in Figure D.1). As expected, real-time visualization of the change in fluorescence showed that LAMP samples with higher initial

concentrations of genomic *V. cholerae* DNA amplify more rapidly (Figure 5.3A). Samples with lower concentrations showed slower, if any, amplification and resulted in a lower fluorescence signal at the end of the 20-minute period (corresponding C_T values presented in Figure 5.3B). Gel electrophoresis was used to confirm amplification of the DNA (Figure 5.3C). The change in EvaGreen/Rox ($\Delta EvaGreen/Rox$), the signal measured at 0 minutes and 20 minutes, was calculated by Equation 5.4 (Figure 5.3D). The data indicated that a higher initial concentration of DNA corresponds to a greater $\Delta EvaGreen/Rox$ signal at 20 minutes. We performed a one-way ANOVA with Dunnett's *post hoc* against the NTC sample and saw statistically significant differences for samples 10^2 , 10^3 , 10^4 , and 10^5 DNA copies/reaction (p-value < 0.001 for 10^2 and p-value < 0.0001 for 10^3 , 10^4 , and 10^5 DNA copies/reaction).

PD was used to measure the change in the viscosity of the same *V. cholerae* samples after the 20-minute LAMP reaction (data for individual repeats is presented in Figure D.1). Similar to the change in fluorescence, we found that as the initial concentration of *V. cholerae* DNA increased, there was a greater change in viscosity ($\Delta Viscosity$, Figure 5.3E, calculated with Equation 5.4). Like the fluorescence measurements, statistically significant differences were seen between the $\Delta Viscosity$ of NTC compared to 10^2 , 10^4 , and 10^5 DNA copies/reaction (p-value < 0.05 and p-value < 0.0001) (Figure 5.3E).

Correlation between the $\Delta Viscosity$ (PD) and $\Delta EvaGreen/Rox$ (fluorescence) measurements confirmed agreement between the two methods. The correlation plot demonstrated in Figure 5.3F, with a calculated Pearson correlation coefficient (R) of 0.81, indicates that the two methods are strongly positively correlated with one another.¹³⁷ A slight discrepancy between measurements is expected since the polymerized DNA chains produced in each LAMP reaction vary in length.⁸⁴ Chain length has a major effect on solution viscosity,¹³⁸ and in turn the PD measurement.⁶⁹ However, the strong positive correlation between the two measurements demonstrated the feasibility of PD as a measurement technique for detection of *V. cholerae*.

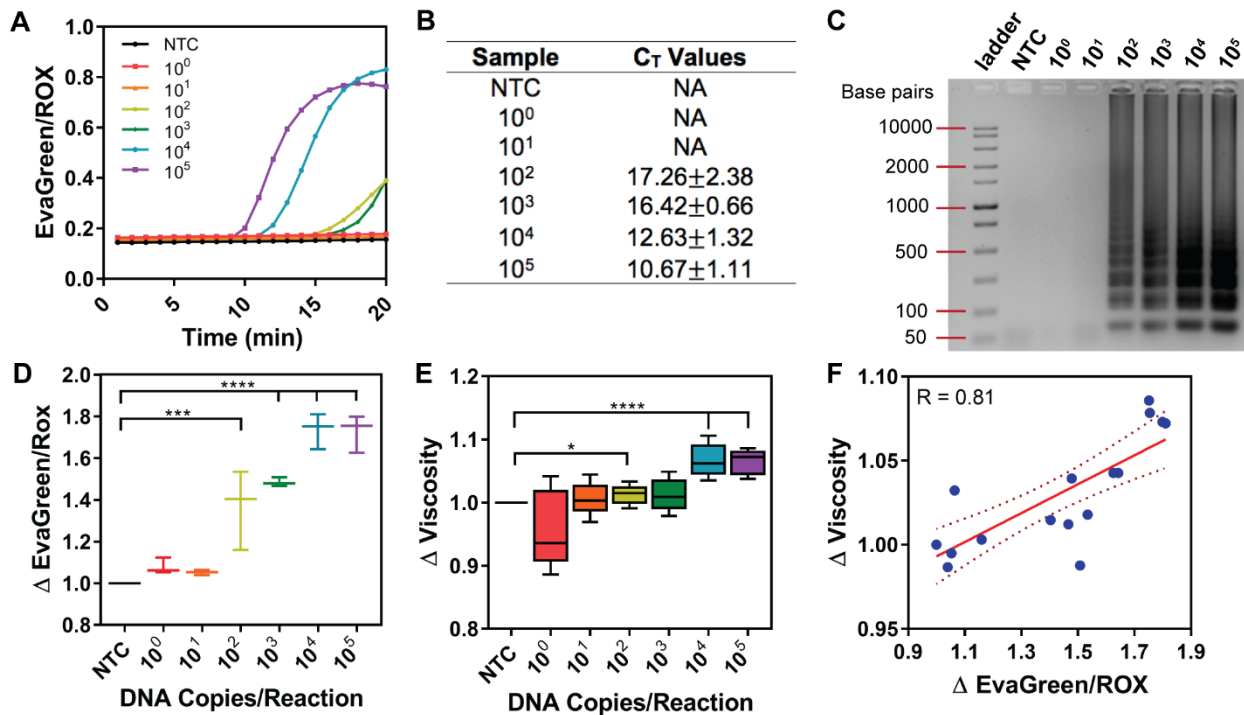


Figure 5.3 PD detection of *V. cholerae* amplification using purified DNA.

(A) Real-time fluorescence was monitored over a 20-minute LAMP reaction for initial DNA concentrations between 10^0 – 10^5 DNA copies/reaction. (B) The corresponding C_T values were recorded for each sample and are not available (NA) for samples that did not amplify. (C) A 2% agarose gel confirms amplification and presents the banding pattern indicative of LAMP amplification. (D) Box plots of the average change in fluorescence (Δ EvaGreen/Rox) shows a trend of a greater change in fluorescence signal at higher initial *V. cholerae* DNA concentrations with statistical differences for samples 10^2 (***) p -value < 0.001), 10^3 , 10^4 , and 10^5 (**** p -value < 0.0001) DNA copies/reaction when compared to NTC. (E) Particle diffusometry measurements of the viscosity change of LAMP reactions show statistically significant measurements for 10^2 (* p -value < 0.05), 10^4 , and 10^5 (**** p -value < 0.0001) DNA copies/reaction when compared to NTC. (D and E) Statistical analysis was a one-way ANOVA with Dunnett's *post hoc* relative to NTC. ($n=3$) (F) A positive correlation between change in fluorescence and PD yields a Pearson's correlation coefficient of 0.81.

5.3.3 Measuring the Combined Effect of Changes in Particle Size and Viscosity with PD

Despite successful detection of as few as 10^4 DNA copies/reaction, we sought to improve the sensitivity of the of the PD measurements by combining detection of the change in viscosity with change in the hydrodynamic radius of the particles. Particle diffusivity (Equation 5.2) is a function of both viscosity of the solution (η) and the size of the measured particles (a). Similar to Tian *et al.*,¹³⁹ we used streptavidin conjugated polystyrene particles and a biotinylated primer (LF) to allow binding of the polymerized biotinylated LAMP products to the streptavidin polystyrene

particles, creating multi-particle aggregates (Figure 5.4A). First, we sought to experimentally validate that biotin-streptavidin induced aggregation occurs as a response only to *V. cholerae* DNA amplification (Figure 5.4B and Figure 5.4C). In the negative sample (NTC), the streptavidin conjugated particles were uniformly distributed in the image (Figure 5.4B, top). However, when particles were added to a positive sample after amplification, a cluster of particles was seen by observing the increase in fluorescence in regions of the image (Figure 5.4B, bottom). Quantitative analysis showed that there was a narrower distribution of particle size, around 10 pix², in the negative samples and greater variability in the positive samples (Figure 5.4C).

To quantify the relative change in particle motion upon changes in both viscosity and particle size, we measured the change in diffusivity ($\Delta Diffusivity$, Equation 5.4). We measured the $\Delta Diffusivity$ in samples containing $10^0 - 10^5$ DNA copies/reaction (n=4, data of repeats in Figure D.2). The data showed a similar trend as observed in the uncoated particles; a higher initial DNA concentration leads to a higher $\Delta Diffusivity$ measurements (Figure 5.4D). Further, there was an increase in the baseline signal when streptavidin conjugated particles were used compared to the uncoated 200 nm polystyrene particles (comparing the y-axis in Figure 5.3E to Figure 5.4D in which $\Delta Diffusivity$ is directly proportional to $\Delta Viscosity$). This baseline shift occurred as both the particle size and solution viscosity were considered (Equation 5.2). There was a statistically significant difference for the 10^3 , 10^4 and 10^5 DNA copies/reaction samples (p-value < 0.05 and p-value < 0.0001) when compared to NTC using a one-way ANOVA with a *post hoc* Dunnett's test.

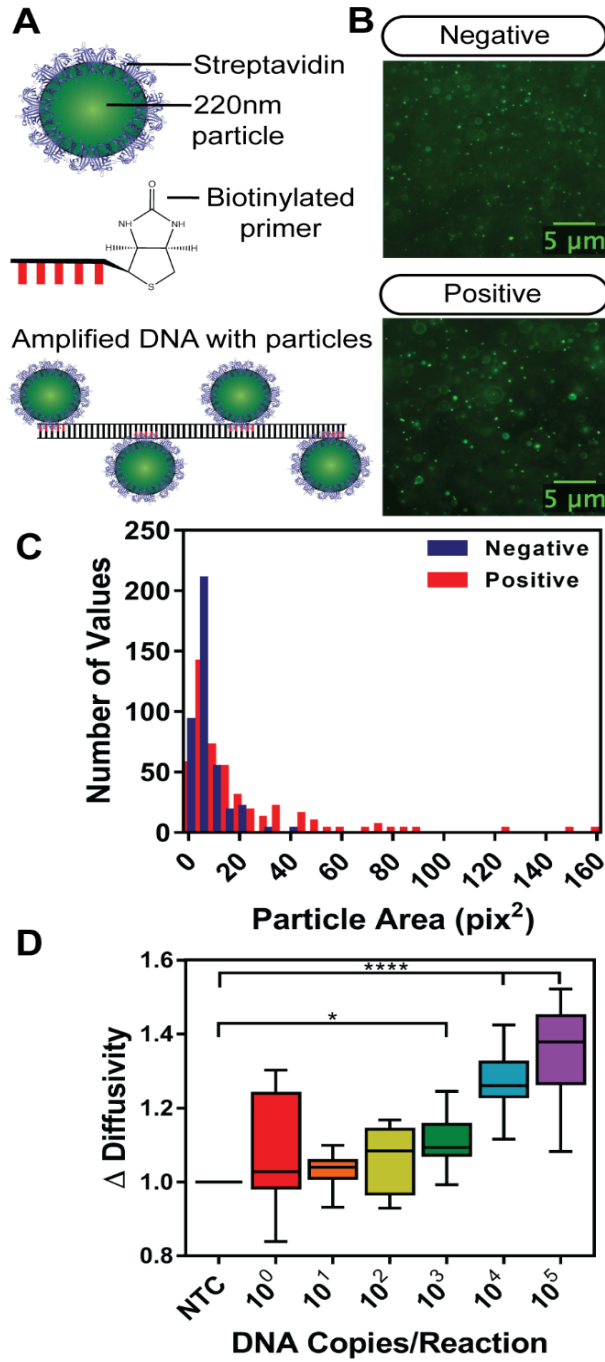


Figure 5.4 Biotinylated LAMP products measured using streptavidin-coated particles.

(A) Schematic of fluorescent streptavidin-coated polystyrene particles combined with biotinylated LAMP products. (B) Representative images of fluorescent particles in a negative and positive LAMP sample. (C) Images in (B) are processed to quantify particle area (in pix²) for negative and positive LAMP samples. (D) Measurement of diffusivity of amplified *V. cholerae* DNA is statistically significant for 10³ (* p-value < 0.05), 10⁴, and 10⁵ (**** p-value < 0.0001) DNA copies/reaction compared to NTC. Statistical analysis was a one-way ANOVA with Dunnett's *post hoc* relative to NTC. (n=4)

We wanted to determine if changes in diffusivity could be measured after amplification of DNA from whole cells. The cell lysate contained extra proteins that may potentially alter solution viscosity or cause changes in particle stability. It is important to note that *V. cholerae* cells, like other gram-negative bacteria, lysed due to thermal effects alone at 65°C,¹⁴⁰ such that an additional cell lysis step beyond the LAMP assay was not necessary. LAMP assays with a biotin primer and varying concentrations of whole *V. cholerae* cells ($10^0 - 10^5$ cells/reaction) were performed and the Δ Diffusivity of streptavidin particles was measured with PD. As the initial concentration of *V. cholerae* cells increased, both the Δ EvaGreen/Rox and Δ Diffusivity of the solutions also increased (Figure 5.5). Real-time fluorescence curves and PD measurements for each repeat are presented in Figure D.3. There was a statistically significant difference in the Δ Diffusivity down to 10^0 cells/reaction when compared to NTC (p-value < 0.01). In contrast, the Δ EvaGreen/Rox measurements showed statistically significant differences only down to 10^2 cells/reaction when compared to NTC (p-value < 0.01). Interestingly, the PD technique demonstrated an LOD three orders of magnitude lower using whole cells versus purified DNA (compare Figure 5.5B with Figure 5.4D). These results are in agreement with Linnes *et al.* showing a 10-fold improvement in the limit of detection when using isothermal amplification on whole cell *Chlamydia trachomatis* samples as compared to purified DNA.¹⁵ Relative to fluorescence measurements, the PD measurements were 100-fold more sensitive (comparing Figure 5.5A to Figure 5.5B). This is promising in the implementation of PD as a pathogen detection technique considering that environmental samples collected for testing would contain very low concentrations of *V. cholerae* cells.

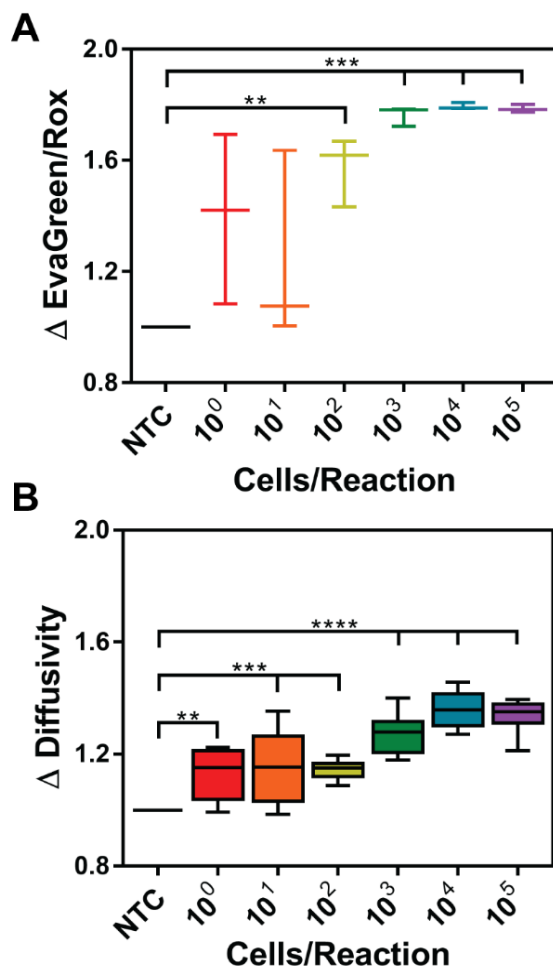


Figure 5.5 Measuring LAMP amplification from *V. cholerae* whole cells.

Cells were spiked into LAMP reactions at concentrations ranging from 10^0 – 10^5 cells/reaction. The change in (A) EvaGreen/Rox is significant at 10^2 (** p-value < 0.01), 10^3 , 10^4 , and 10^5 (***) p-value < 0.001) cells/reaction. (B)

The change in diffusivity measurements show an increasing trend as a function of starting cell concentration with significance at 10^0 (** p-value < 0.01), 10^1 , 10^2 (***) p-value < 0.001), 10^3 , 10^4 , and 10^5 (**** p-value < 0.0001) cells/reaction. Statistical analysis was a one-way ANOVA with Dunnett's *post hoc* relative to NTC. (n=3)

5.3.4 Environmental Water Samples

V. cholerae is a pathogen found in environmental water samples,^{59,141} thus it is essential to perform PD of cells in complex matrices other than molecular biology water. LAMP was performed in 1X PBS, tap water, rain runoff, pond water, and molecular biology water (as a control) with 10^5 *V. cholerae* cells (positive samples) or no cells (negative control) spiked into each reaction

prior to the 25-minute heating. These water samples presented three potential challenges for accurate PD detection of DNA amplification: (1) inhibition of the LAMP assay, (2) adverse effects to the particles during the measurement including degradation or aggregation, and (3) unaccounted changes in apparent size or viscosity that may occur due to excess sediment that may non-specifically bind to the particles.

Gel electrophoresis (Figure 5.6A) and fluorescence measurements (Figure D.4) showed little DNA amplification in tap water. We measured the relative diffusivity using PD to investigate this difference (D_0/D , Equation 5.3, repeat data presented in Figure D.4). There was no statistically significant difference in relative diffusivity of positive samples in tap water compared to the negative controls (Figure 5.6B, p-value > 0.05, Student's *t*-test). This was to be expected because city tap water contains chlorine, which likely inhibited the activity of the Bst 2.0 enzyme required for the LAMP assay.³⁶

Since *V. cholerae* can be harbored in sea water, we performed LAMP in 1X PBS to determine whether salt affects the LAMP assay or PD measurements. LAMP assays performed in 1X PBS did not show any inhibition when analyzing both fluorescence measurements and gel electrophoresis (Figure D.4 and Figure 5.6A). There was a statistically significant difference in PD measurements (Figure 5.6B, p-value < 0.0001, Student's *t*-test) between the negative and positive PBS samples. This confirmed that salt did not inhibit the LAMP assay or PD measurements.

Using PD, we also analyzed LAMP assays performed in rain runoff and pond water, both which contained sediment and therefore added to sample matrix complexity. PD measurements showed a statistically significant difference in the relative diffusivity of rain runoff samples spiked with *V. cholerae* cells compared to its negative control (Figure 5.6B, p-value < 0.0001, Student's *t*-test). This is extremely promising given that the water sample was collected outside of the laboratory space. In contrast, LAMP assays conducted in pond water demonstrated a decreased amplification signal (Figure D.4). This was supported with the faded banding pattern in the agarose gel (Figure 5.6A). Due to the minimal amplification, PD reflected little-to-no change in the diffusivity between the negative and positive *V. cholerae* samples in pond water (Figure 5.6B, p-value > 0.05, Student's *t*-test).

Further characterization of PD in pond water was performed, as this sample is the best surrogate of the native environment for *V. cholerae*.^{85,86} Varying concentrations of whole *V.*

cholerae cells ($10^0 - 10^5$ cells/reaction) were spiked into pond water (where 50% of the total LAMP reaction volume was pond water). The $\Delta Diffusivity$ of streptavidin particles in the presence of LAMP products was measured with PD. Because the debris and ions in pond water slightly inhibit amplification,⁷² the LAMP assay was extended to 35 minutes. As the initial concentration of *V. cholerae* cells increased, the $\Delta EvaGreen/Rox$ and $\Delta Diffusivity$ of the solutions also increased (Figure D.5 and Figure 5.6C). There was a statistically significant difference in the $\Delta Diffusivity$ down to 10 cells/reaction when compared to NTC (p-value < 0.01). Real-time fluorescence curves and $\Delta Diffusivity$ for each repeat are presented in Figure D.5. In contrast, $\Delta EvaGreen/Rox$ measurements showed statistically significant differences down to 10^2 cells/reaction when compared to NTC (Figure D.6, p-value < 0.05). Relative to fluorescence measurements, PD measurements were 10-fold more sensitive (Figure 5.6C and Figure D.6).

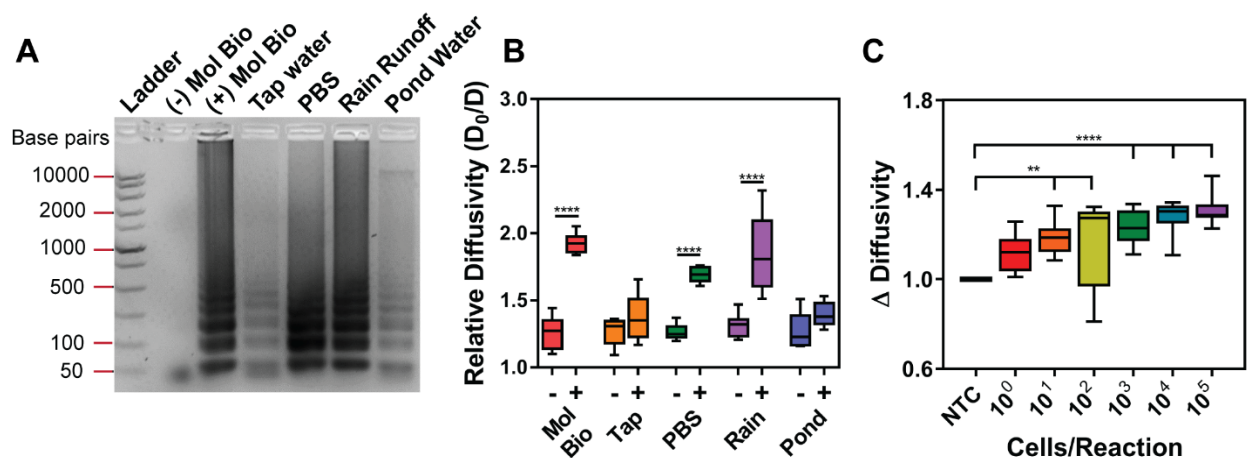


Figure 5.6 LAMP amplification from whole *V. cholerae* cells in environmental water samples.

Different water samples were used in the LAMP reactions for (A) and (B). Molecular biology water (Mol Bio) was used as a control ((-) no *V. cholerae* cells, (+) *V. cholerae* cells) in (A) and (B). (A) Gel electrophoresis shows less amplification in pond and tap water compared to other water samples. (B) PD measurement of relative diffusivity shows a statistically significant difference between negative and positive samples for molecular biology water, PBS, and rain runoff groups (**** p-value < 0.0001). (C) *V. cholerae* cells were spiked into pond water at concentrations ranging from $10^0 - 10^5$ cells/reaction. The change in diffusivity measurements show an increasing trend as a function of starting cell concentration with significance at 10^1 , 10^2 (** p-value < 0.01), 10^3 , 10^4 , and 10^5 (**** p-value < 0.0001) cells/reaction.

Statistical analysis was a one-way ANOVA with Dunnett's *post hoc* relative to NTC. (n=3)

5.4 Future Directions

PD is pathogen agnostic; it is not limited to *V. cholerae* identification, but it can serve as a method for detection of a wide variety of pathogens. Due to the success in detecting *V. cholerae*, we envision PD as an effective mechanism to identify nucleic acid amplification products of other infectious diseases. Specifically, we want to investigate whether PD can be used to detect bloodborne pathogens such as malaria. The Brownian motion of particles in solutions containing blood will likely be different than particle Brownian motion in pond water because of the high viscosity of blood. Therefore, we may need to calibrate the PD technique or perform blood separation prior to amplification and PD analysis. Moreover, we want to translate the PD technique to a handheld device. This is plausible considering that PD involves only a microscope, camera, and computer. Miniaturization and integration of these components would allow for the translation of a field deployable biosensor for pathogen detection.

5.5 Conclusions

In this work, we demonstrate that PD can be used as a rapid, sensitive, and robust method for the detection of *V. cholerae* LAMP products in environmental water samples. PD is particularly attractive due to the passive nature of the method (optically recording Brownian motion) compared to current DNA detection techniques that require chemical reactions involving fluorophore intercalation or colorimetric or turbidimetric readouts derived from magnesium products or electrochemical techniques. In blinded studies, PD could identify the presence of *V. cholerae* DNA with 100% accuracy. Additionally, there is a strong, positive correlation between $\Delta \text{EvaGreen}/\text{Rox}$ (fluorescence) and $\Delta \text{Viscosity}$ (PD). The studies indicate that PD can detect as few as 1 cell/reaction of *V. cholerae* DNA from cells lysed *in situ* during a 20-minute reaction in molecular biology water without the need for additional sample preparation. This method is 100-fold more sensitive than gold-standard fluorescence detection of nucleic acid amplification products. Furthermore, we demonstrate that PD is robust enough to identify 10 *V. cholerae* cells/reaction in pond water in just 35 minutes. This is the first study directly comparing fluorescence and PD detection of LAMP products. These results establish the utility of combining both changes in size and viscosity for improved signal-to-noise measurements with PD for the rapid identification of *V. cholerae* LAMP products. PD is an alternate method to fluorescence detection for nucleic

acid amplification products that has a significant improvement in sensitivity and is robust enough to identify the amplified products in their native sample matrix.

6. TRANSLATION OF PARTICLE DIFFUSOMETRY TECHNIQUE TO SMARTPHONE PLATFORM FOR DETECTION OF *V. CHOLERAE*

This chapter is reproduced from Ref. 165 (Moehling & Lee *et al.*, 2020) which is currently under review by Elsevier. All smartphone work presented in this chapter was performed equally with my co-author Dong Hoon Lee and concentrator work was in collaboration with Jordan Florian of OmniVis LLC. OmniVis LLC is a spinout company of Purdue University that is translating the smartphone PD-LAMP technology into a commercial product.

6.1 Rationale

In the past decade, many pathogen detection biosensors have emerged by translating standard optical methods onto portable platforms. Notably, smartphones possess both advanced computational power and quality image sensors that previously could only be found in expensive laboratory equipment.^{142,143} Along with these technical improvements, the usability and accessibility of smartphone technology are attractive features that promote translation of cumbersome optical techniques from the laboratory to the point of use.¹⁴⁴ For example, Zeng *et al.* combined smartphone technology with surface-enhanced Raman scattering (SERS) optical detection modality to enable detection of analytes down to 10^{-5} M at the point of use. This portable Raman spectrometer allows rapid, real-time analysis; however, its applications are limited due to poor sensitivity and specificity.¹⁴⁵ Wu *et al.* developed a dark-field smartphone microscope to be used in combination with an immunoassay for rapid and specific detection of *E. coli* in water samples down to 10 cells/10 mL after filtration.¹⁴⁶ Although sensitive, immunoassays involve several time-sensitive user steps that limit the usability of such platforms in the field. Koydemir *et al.* utilized a smartphone-based fluorescence microscope for imaging and quantifying fluorescently labeled *G. lamblia* cysts in large volumes of water. The entire process, from sample preparation to image processing and quantification, takes only one hour and has a limit of detection of 12 cysts in 10 mL of water.¹⁹ Unfortunately, this smartphone-based fluorescence microscopy technique is not suitable for detection of bacterial or viral pathogens because the system is optimized for larger microorganisms. Alternatively, integrating optical techniques with nucleic acid amplification assays allows for detection of a multitude of pathogens with excellent sensitivity and specificity.¹⁴³

Nucleic acid amplification techniques efficiently target and produce millions of copies of a nucleic acid sequence during a thermal process with high accuracy and sensitivity.¹⁴³ Researchers have demonstrated the utility of an isothermal amplification technique called LAMP, by combining the assay with smartphone technology to sensitively detect nucleic acid analytes in one hour with minimal user intervention.^{16,51,52} Even though LAMP is a selective and rapid amplification technique, current fluorescence detection methods depend on relative measurements to adjust for the variation between repeats.^{40,147}

By integrating LAMP with particle imaging, we can minimize the variability between repeats and take advantage of the high selectivity of LAMP and the sensitivity of particle imaging. The polymerization that occurs during LAMP produces a change in viscosity that can be measured using an optical detection method called particle diffusometry.^{43,68–70} PD can also measure changes in size; by labeling a LAMP primer with biotin and combining streptavidin-coated nanoparticles with the LAMP products, the inherent binding causes an increase in particle size and enhances PD measurements. After recording a video of the Brownian motion of nanoparticles that are added to the amplification products (Figure 6.1A), the images can be extracted (Figure 6.1B) and auto- and cross-correlated (Figure 6.1C) to calculate a diffusion coefficient for the sample. The diffusion coefficient quantifies the Brownian motion of nanoparticles in solution and is affected by both sample viscosity and particle size (Figure 6.1D). In our previous proof-of-concept work using a fluorescence microscope (Chapter 5), we demonstrated that PD could be used to detect LAMP amplicons with a 10-fold improvement in sensitivity over end-point fluorescence detection.⁴³ We also established that PD is a statistically robust detection method; three diffusion coefficients are calculated for each sample.

Here, we demonstrate a portable smartphone-based PD platform for the rapid and specific detection of *V. cholerae* in environmental water samples using LAMP. We perform a 30-minute LAMP assay using a biotinylated primer and add 400 nm streptavidin-coated fluorescent nanoparticles to induce a change in particle size that alters PD measurements along with changes in solution viscosity. Using a 30-second video recording of the nanoparticles in solution, the smartphone algorithm computes the diffusion coefficient in less than one minute. The resulting diffusion coefficient suggests the presence of *V. cholerae* when diffusivity of the nanoparticles is low and absence of the pathogen when diffusivity is high. We establish the robustness of this smartphone-based PD platform, determine its selectivity and LOD for *V. cholerae* in pond water,

and compare its sensitivity and specificity to real-time fluorescence detection using 132 blinded samples.

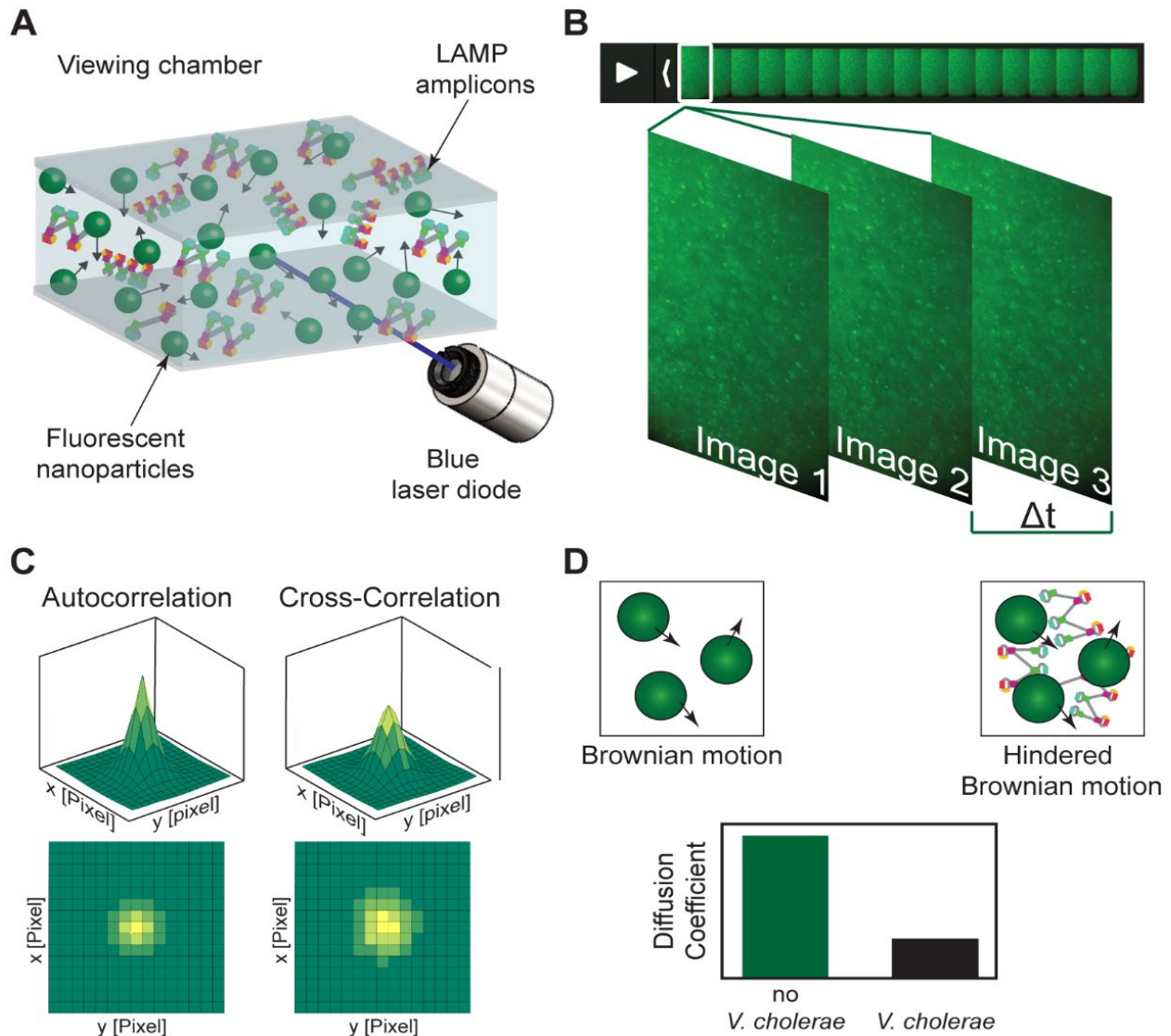


Figure 6.1 Smartphone-based particle diffusometry.

(A) 400 nm streptavidin-coated fluorescent nanoparticles are combined with LAMP amplicons and excited with a blue laser diode. (B) Brownian motion of the nanoparticles is recorded using sequential images from an iPhone 6 with a frame extraction rate of 15 frames per second. (C) 3D and 2D correlation peaks of sequential frames. (D) Relationship between nanoparticle motion and diffusion. In the presence of LAMP amplicons, nanoparticles experience hindered Brownian motion and decreased diffusivity, indicating the presence of *V. cholerae* in the sample.

6.2 Materials and Methods

6.2.1 LAMP

The LAMP primers (B3, F3, BIP, FIP, LB, LF-Biotin) and standard master mix from previous chapters were also used here (Table A.1 and Table A.3). LAMP reactions were 15 μL total, consisting of the LAMP master mix and 7.5 μL (50% v/v) of pond water. Pond water was collected from a local small (100 m wide and 200 m long) water source. 1.2 μL of template or molecular biology water (for the negative control (NTC)) was spiked into the reactions prior to heating. Cultures of *V. cholerae* N16961, *V. cholerae* NRT-36, and *E. coli* DH5 α were grown according to **2.2.2 Bacteria Culture**. LAMP reactions were incubated at 65°C for 30 minutes using an Applied Biosystems 7500 Real-Time PCR System (Foster City, CA). Real-time fluorescence data was collected to track amplification. LAMP samples were stored at 4°C until analyzed with the smartphone-based PD platform. LAMP amplicons were also characterized via gel electrophoresis at 100 V for 60 minutes. The 2% agarose gels were stained with ethidium bromide and imaged using an ultraviolet light gel imaging system (c400, Azure Biosystems, Dublin, CA) with UV 302 settings and a 15-second exposure.

6.2.2 Particle Preparation

Streptavidin-coated 400 nm Dragon green polystyrene fluorescent nanoparticles (Ex480/Em520 nm) were purchased from Bangs Laboratories (Fishers, IN). We used streptavidin-coated nanoparticles because they strongly bind to the biotin-labeled amplicons causing a change in both viscosity and size; therefore, improving sensitivity.⁴³ Nanoparticles were added to the 15 μL LAMP reaction at a final concentration of 1.84×10^9 particles/mL. The LAMP-nanoparticle solution was incubated at room temperature for 10 minutes to allow binding of the biotinylated amplicons to the streptavidin-coated nanoparticles.

6.2.3 Microfluidic Chip Assembly

The microfluidic chips were designed as a drawing exchange format (.dxf) in Autodesk Fusion 360 software and translated to the Silhouette Studio 2.0 Software (Silhouette America, Lindon, UT). Microfluidic chips were composed of four layers: 2 layers of 188 μm cyclic olefin

polymer (COP) (Zeonor, Tokyo, Japan), 1 layer of 60 μm COP (Zeonor, Tokyo, Japan), and 1 layer of 120 μm double-sided tape. The 188 μm COP was cut with the Silhouette Cameo Craft Cutter (Silhouette America, Lindon, UT) with two passes using a 10-blade, force of 19, and a speed of ten (arbitrary units within the Silhouette software). The COP pieces were cleaned after cutting with 1) a MilliQ rinse and 2) a two-minute sequential sonication in acetone, isopropanol, methanol, and MilliQ. After cleaning and drying with a nitrogen stream, the two layers of 188 μm COP were bonded together by thermal fusion using a Carver 4386 hydraulic press (Carver Inc., Wabash, IN) with 1.2 tons of pressure at 120°C. Double-sided tape with a 3.175 mm hole served as the sample well. The 60 μm COP was placed on top of the double-sided tape to enclose the sample and prevent evaporation. The assembled microfluidic chips were 25.4 mm by 22.10 mm and 0.556 mm thick.

6.2.4 Optics Design

My co-author, Dong Hoon Lee, used three different elements to develop the optics within the smartphone-based PD platform: a spherical BK7 borosilicate lens with 500 μm diameter (Edmund Optics, Barrington, NJ), a blue laser diode (Laserland, Wuhan, China) powered by a lithium ion polymer battery (Adafruit, New York, NY), and #12 straw Cinegel film filter (Roscolux, Stamford, CT).

The spherical 500 μm diameter BK7 lens has a 117 μm back focal length, 160 μm field of view, and produces a 68X magnification. All lens calculations were adapted from Cybulski *et al.*¹⁴⁸ The iPhone 6 camera lens system used in this platform has a CMOS with one blue, one red, and two green pixel sensors (Bayer array). Because there are twice as many green pixel sensors than blue or red, the smartphone camera lens system can detect green light most effectively.¹⁴⁹ Therefore, Dragon green (Ex480/Em520 nm) 400 nm streptavidin-coated nanoparticles were selected for imaging. The size of the nanoparticles was selected based on the fixed optics of the iPhone 6 camera lens system and magnification provided by the spherical lens; 400 nm was the smallest particle size visible using the smartphone optics. These nanoparticles then dictated the laser and filter combination. To excite the nanoparticles, a 445 nm laser with an 80-mW power capacity (12 mm diameter and 35 mm length) was selected. Any light with a wavelength below 470 nm was filtered out by the straw film filter. This straw film filter was selected after reviewing the color spectrums of all green and yellow Roscolux film filters.¹⁵⁰ Roscolux provides

inexpensive cinematic lighting films that have been shown to be effective low-cost fluorescence filters for portable devices.¹⁴⁸

6.2.5 Particle Diffusometry Theory

PD involves recording a series of images of fluorescent particles undergoing Brownian motion in a quiescent volume and calculating the particle diffusion coefficient using correlation analysis.⁶⁸ Each individual image is partitioned into smaller interrogation areas (64×64 pixel²) containing, on average 8-10 particles.¹³⁰ Within these interrogation areas, autocorrelation and cross-correlation of the images are computed for the entire series of images. Cross-correlation (s_c) involves correlating two temporally sequential images and autocorrelation (s_a) is performed by correlating a captured image with itself.¹³² Using both autocorrelation and cross-correlation, the diffusion coefficient, D , can be calculated by Equation 6.1 derived by Olsen and Adrian¹³³

$$D = \frac{s_c^2 - s_a^2}{16M^2\Delta t} \quad \text{Equation 6.1}$$

where M is the magnification and Δt is the time step between images. Equation 6.2 shows the relationship between the diffusion coefficient, viscosity (η), and hydrodynamic radius (a).

$$D \sim \frac{1}{\eta a} \quad \text{Equation 6.2}$$

LAMP produces polymerized DNA strands that cause a change in the viscosity of the surrounding solution. We use streptavidin-coated fluorescent nanoparticles that bind directly to the biotin-labeled LAMP amplicons to provide a change in size, in addition to viscosity. The change in both viscosity and size produces a more substantial difference in the diffusion coefficient measurements.

6.2.6 Smartphone-Based Platform Development

The smartphone-based PD platform is composed of a 3D printed platform that houses the optics and a smartphone application built for the iPhone 6. The platform was designed by my co-author, Dong Hoon Lee, to incorporate the optics and power source, secure the smartphone and

microfluidic chip, and exclude external light during imaging. The smartphone application was also created by Dong Hoon Lee using Apple's development platform, XCode.

The platform, composed of six parts, was designed using SolidWorks (Figure E.1). Five parts were 3D printed with a Fortus 400mc 3D printer (Stratasys, Eden Prairie, MN) using acrylonitrile butadiene styrene (ABS). The aluminum plate that holds the external ball lens was machined. The platform was developed following Apple's accessory design guidelines to ensure the iPhone 6 fit securely into the platform. The external ball lens is situated directly below the camera lens system which aligns with the sample well of the microfluidic chip. The platform also contains a slot with a z-axis stage to insert the microfluidic chip; a bolt and nut (McMaster-Carr, Elmhurst, IL) with a 3D printed knob were used to adjust the z-axis stage to ensure the microfluidic chip was within the focal length of the external ball lens.

The smartphone application was developed following the principles of PD introduced in Clayton *et al.*⁷⁰ Both Swift and Objective-C programming languages were used in the smartphone application development. The iOS application takes advantage of the iPhone's capability to record a 30 frames per second (FPS) video. By reducing the frame rate to 15 FPS, 300 frames on average are extracted from a 30-second video recording, leaving a 21-second video for analysis. The center 800×800 pixel² region is used for processing to minimize the distortion effects around the edges from the external ball lens. A 2×2 binning is then applied for signal improvement. This binning allowed for a high signal-to-noise ratio while maintaining a statistically relevant number of data points. Frames were processed, and auto- and cross-correlation analysis was performed using the in-house smartphone algorithm. Native software development kits (SDK) and application programming interfaces (API) were used to perform image processing and PD analysis. All steps were verified by comparing the code with the previously developed MATLAB code.

6.2.7 Smartphone-Based Particle Diffusometry Measurements

A 1.5 μL aliquot of the LAMP-nanoparticle solution was added to the sample well within the microfluidic chip and a 1×1 cm² piece of 60 μm COP was placed over the sample well to seal the sample, preventing evaporation. Three 1.5 μL aliquots from each sample were loaded into three separate microfluidic chips for intra-sample measurement validation. Each microfluidic chip was inserted into the smartphone-based PD platform for imaging at room temperature on a stabilizing optical table to minimize external vibration. After turning the laser on, a 30-second video of

nanoparticle Brownian motion was recorded. After the 60-second image analysis, three diffusion coefficients were displayed for each microfluidic chip. Three diffusion coefficient measurements from three different microfluidic chips were collected for each biological repeat (nine measurements), highlighting the statistical robustness of PD.

6.2.8 Experimental Design

For all studies presented in this work, three individuals prepared biological samples and performed LAMP and three different individuals measured the PD of the samples on the smartphone-based platform. For the LOD experiments, 10-fold serial dilutions ($6 \times 10^0 - 6 \times 10^4$ cells/reaction) of *V. cholerae* N16961 whole cells were prepared and added to LAMP reactions. For the selectivity experiments, *V. cholerae* N16961, *V. cholerae* NRT-36, and *E. coli* DH5 α were all used as the template. *V. cholerae* NRT-36 was chosen to ensure that LAMP is only selective for toxigenic strains of *V. cholerae*. *E. coli* DH5 α was tested because it is also found in environmental water sources and we wanted to ensure no cross-reactivity of PD-LAMP.¹⁵¹ The bacteria were added to separate LAMP reactions at a concentration of 10^3 cells/reaction. The three individuals measuring PD on the smartphone-based platform were blinded to the sample contents for the selectivity experiments. All nine diffusion coefficients were plotted for each biological repeat for both experiments.

We wanted to compare smartphone-based PD with real-time fluorescence detection of LAMP to determine the sensitivity, specificity, and accuracy of the smartphone-based PD platform. The data were split into a training and test set. The 30 samples used in the training set were ordered by diffusion coefficient to determine the positive and negative diffusion coefficient thresholds. Real-time fluorescence results were recorded for each sample in the training set. For the test set, we used a double-blinded study design to approximate a field study. Neither the individual who performed LAMP nor the individual who performed PD on the smartphone-based platform knew the contents of the samples. A total of 132 samples, ranging from 0 cells/mL to 3.5×10^8 cells/mL, were used in the test set. If the relative fluorescence increased ten standard deviations above the baseline (the auto-threshold setting on real-time PCR system) by the end of the 30-minute amplification period, the individual that performed LAMP recorded that sample as positive by real-time fluorescence. If the relative fluorescence did not increase ten standard deviations above the baseline, the sample was considered negative by real-time fluorescence. We confirmed

fluorescence results via gel electrophoresis. Each sample was then measured on the smartphone-based PD platform and the diffusion coefficients were recorded. The average of all nine diffusion coefficients was used to describe each sample for this double-blinded study.

6.2.9 Statistical Analysis

For the LOD study, a one-way ANOVA *post hoc* Dunnett's test was performed with multiple comparisons against a negative control with no template (NTC) using a 95% confidence interval. For the selectivity experiments, a one-way ANOVA *post hoc* Dunnett's test was conducted with multiple comparisons against the positive control (toxigenic *V. cholerae*) with a 95% confidence interval. Quartile box-and-whisker plots were generated for the PD data for both studies where the upper and lower bounds represent the 75th and 25th percentile about the median, respectively, and the minimum and maximum values are represented by the upper and lower whiskers. Individual data points for each sample were plotted on the quartile box-and-whisker plots.

A single, averaged diffusion coefficient (from 9 measurements) for each of the 132 test set samples from the double-blinded study was plotted and fitted with a bimodal Gaussian distribution curve. A 2×2 contingency table was created to directly compare the smartphone-based PD platform and real-time fluorescence measurement of LAMP. From this contingency table, we calculated the sensitivity, specificity, accuracy, positive predictive value, and negative predictive value of the smartphone-based PD platform.¹⁵² We created a receiver operating characteristic (ROC) curve to demonstrate the tradeoff between sensitivity and specificity and indicate the accuracy of the platform.¹⁵³ All figures were created using GraphPad Prism 7.

6.2.10 *V. cholerae* Concentrator User-Centered Design Study

To test the usability of the bacterial concentrator device developed by Jordan Florian of OmniVis LLC, 30 volunteers over the age of 18, with and without technical backgrounds, were asked to assemble the device using an instructional video and complete a Systems Usability Study (SUS) survey.¹⁵⁴ The SUS survey covers the effectiveness, efficiency, and satisfaction of using a particular system through ten questions: five of which are negative (i.e. unnecessarily complex, cumbersome to use, or inconsistent) and the other five are positive (i.e. wanting to use frequently,

easy to use) (Figure E.2). Responses were collected using a 5-point Likert scale where 1 is Strongly Disagree and 5 is Strongly Agree. The user-centered design study was performed in accordance to Purdue University's Human Research Protection Program. Responses for each of the ten SUS survey questions were averaged across all participants and plotted with standard deviation. An overall SUS score was calculated for each volunteer by summing the normalized score for each of the ten SUS survey questions. Normalization for positive SUS survey questions was achieved by subtracting one from the raw score and multiplying by 2.5; normalization for negative SUS survey questions was achieved by subtracting the raw score from five and multiplying by 2.5. A one-way ANOVA *post hoc* Tukey's test was performed to determine whether technical background (formal training in science, technology, engineering, or math) influenced volunteers' overall SUS score for the bacterial concentrator device.

6.2.11 *V. cholerae* Concentrator Experiments

V. cholerae N16961 cells were grown according to **2.2.2 Bacteria Culture** and added to 250 mL of MilliQ water at a concentration of 10^6 cells/mL. Although the bacterial concentrator device was designed to filter 1 L of water, we observed leaking during preliminary testing, so we used a lower volume to minimize pressure due to gravity and we expect that the results will scale. After letting the 250 mL filter through the assembled system, the 1 L bottle (Nalgene, Rochester, NY) was disconnected from the 3D printed bacterial concentrator device. The 0.8 μm nylon membrane (47 mm diameter, GVS Filter Technology, Sanford, ME) was removed from the bottom layer of the concentrator device and six nylon pieces were collected using a 6 mm biopsy punch (Miltex, York, PA). Four-10 μL samples were gathered from the fluid reservoir in the bottom layer of the bacterial concentrator device. These nylon pieces and fluid reservoir samples serve as template for subsequent LAMP reactions. Several controls were run alongside the test samples: a positive control (10^6 cells/25 μL reaction), a negative control (no template added), a positive nylon control (10^6 cells/reaction with 6 mm diameter nylon membrane), and a negative nylon control (no template added with 6 mm diameter nylon membrane). LAMP reactions were incubated at 65°C for 45 minutes. LAMP was monitored in real-time and amplicons were analyzed via gel electrophoresis as explained in **6.2.1 LAMP**. The same samples were measured on the smartphone-based PD platform as described in **6.2.7 Smartphone-Based Particle Diffusometry**

Measurements. This entire process was repeated three times using three different bacterial concentrator devices.

6.3 Results and Discussion

6.3.1 Construction of Optics

High resolution optics and robust construction are critical for PD measurements on a portable device. Therefore, we developed a 3D printed platform to house the optics for nanoparticle visualization that is perpendicular to the axis of gravity to improve platform stability. An external ball lens was incorporated to enhance the magnification of the iPhone 6 camera lens system to visualize the nanoparticles. The external ball lens diameter is inversely related to magnification; thus, the 500 μm spherical glass ball lens provides a magnification of 68X which is sufficient for this application. The external ball lens back focal length (BFL) is 117 μm ; therefore, the topmost layer of the microfluidic chip must be less than the BFL.¹⁴⁸ We selected optically transparent 60 μm COP as the top layer of the microfluidic chip. Lastly, a 445 nm blue laser diode was used to excite the fluorescent nanoparticles and a (yellow filter was placed between the external ball lens and camera lens system to act as a high-pass filter, transmitting wavelengths above 470 nm to the iPhone 6 camera (Figure 6.2A). Four hundred (400) nm fluorescent particles (Ex480/Em520 nm) are greater than four pixels in diameter under imaging conditions, which minimizes the diffractive effects and maximizes the signal-to-noise ratio.¹⁵⁵

The external ball lens, iPhone 6 camera lens system, microfluidic chip, and blue laser diode were first aligned using the virtual construction tool in SolidWorks. The computer-aided design (CAD) model of the laser was placed at a 15° incident angle and fixed in position by designing the surrounding structure to support the laser (Figure 6.2B). At the 15° incident angle, the fluoresced and scattered light is focused into the iPhone 6 camera lens system.¹⁵⁶ The light passes through the optically transparent COP microfluidic chip containing the LAMP sample with nanoparticles and then through the external ball lens. We ensured the microfluidic chip fit snugly into the platform by designing a slot to match the width of the microfluidic chip and incorporating a z-axis stage. The z-axis stage also allows adjustment of the optical focus (Figure 6.2C).

After confirming alignment in SolidWorks, the external ball lens was carefully placed in a metal plate and secured using epoxy. The collimator on the 445 nm blue laser diode was glued into

the 3D printed platform. The body of the laser was screwed into the stationary collimator. The combined effect of fluorescence and scattering of the nanoparticles makes this optical system ideal for imaging small fluorescent nanoparticles.^{148,156} Scattered light reduces the background noise by filtering out the oblique illumination on the sample plane.¹⁵⁶ Further, the short working distance of the optical system keeps the platform compact. The cost of the consumables for the smartphone-based PD-LAMP system is \$0.78 (Table E.1) and the reusable components of the platform cost less than \$265 (Table E.2).

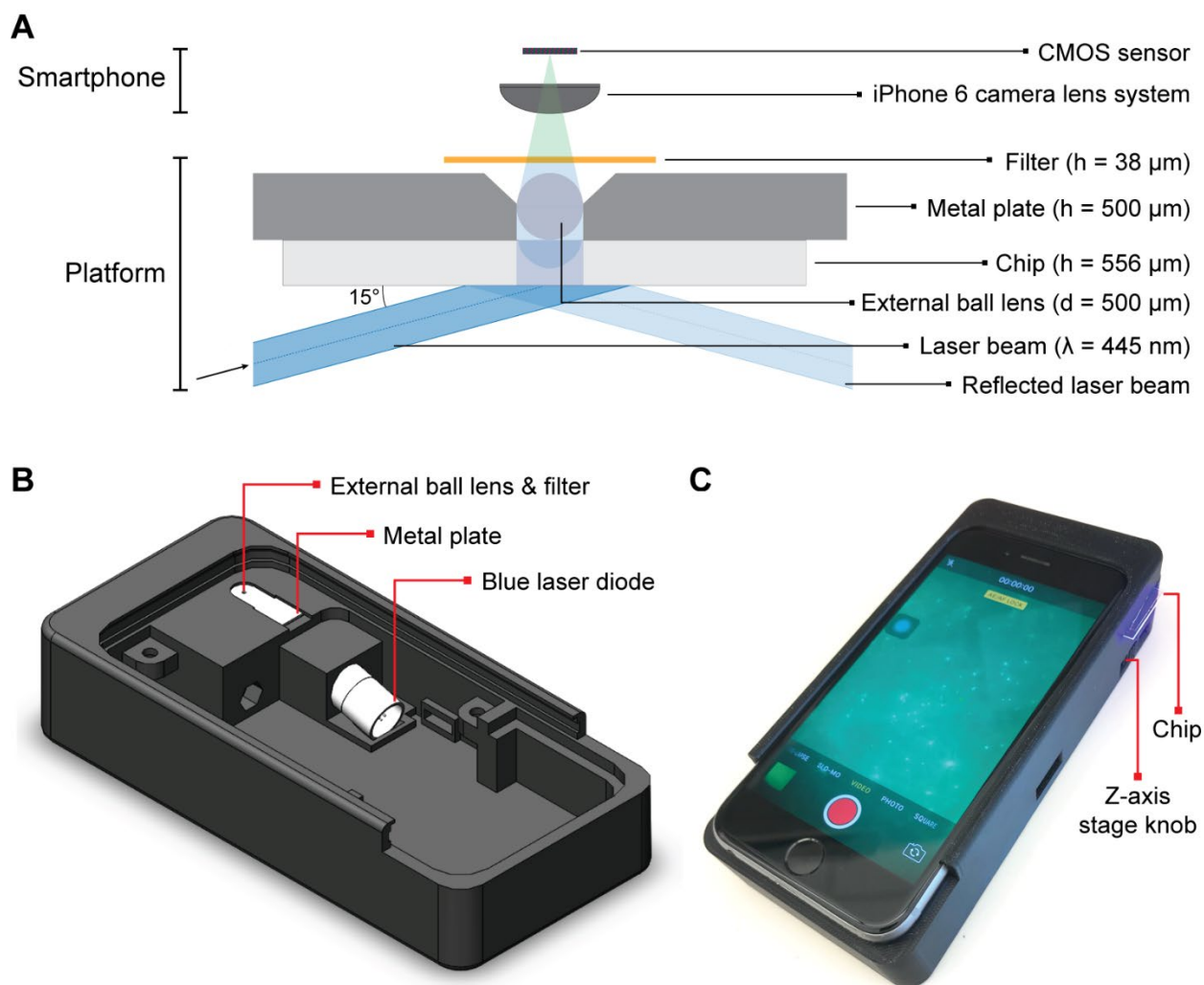


Figure 6.2 Smartphone-based particle diffusometry platform.

(A) Optics setup within the platform includes an external ball lens, filter, complementary metal-oxide-semiconductor (CMOS) sensor, iPhone 6 camera lens system, and laser at a 15° incident angle. (B) Schematic of the platform that incorporates the blue laser diode, metal plate, external ball lens, and filter. (C) Image of the integrated smartphone-based PD platform recording Brownian motion of 400 nm streptavidin-coated fluorescent nanoparticles in the microfluidic chip.

6.3.2 Image Quality, Recording, and Processing

We designed a smartphone application to process the images captured with the optical system to perform PD analysis. Videos recorded on an iPhone 6, using high definition settings, have a resolution of 1920×1080 pixel².¹⁵⁷ Therefore, the resulting images depict the 400 nm streptavidin-coated fluorescent nanoparticles with high contrast and minimal background noise (Figure 6.3A). The center 800×800 pixel² region is used for analysis to minimize distortion effects around the edges of the images from the external ball lens (Figure 6.3B). This central region is processed to further differentiate nanoparticles from background noise (Figure 6.3C). The images are then auto- and cross-correlated within the smartphone application to generate diffusion coefficients. All image processing was performed independently by the smartphone application without external processing support (network or hardwired). Next, we imaged the same nanoparticle solution using 40X magnification on an inverted epifluorescence microscope (Figure 6.3D and Figure 6.3E). We compared image quality and resulting diffusion coefficient measurements on the smartphone-based optical system ($9.83 \times 10^{-13} \text{ m}^2/\text{s} \pm 1.83 \times 10^{-14} \text{ m}^2/\text{s}$) with results obtained on the microscope ($1.02 \times 10^{-12} \text{ m}^2/\text{s} \pm 1.57 \times 10^{-14} \text{ m}^2/\text{s}$) and saw no significant difference ($p > 0.05$) (Figure E.3).

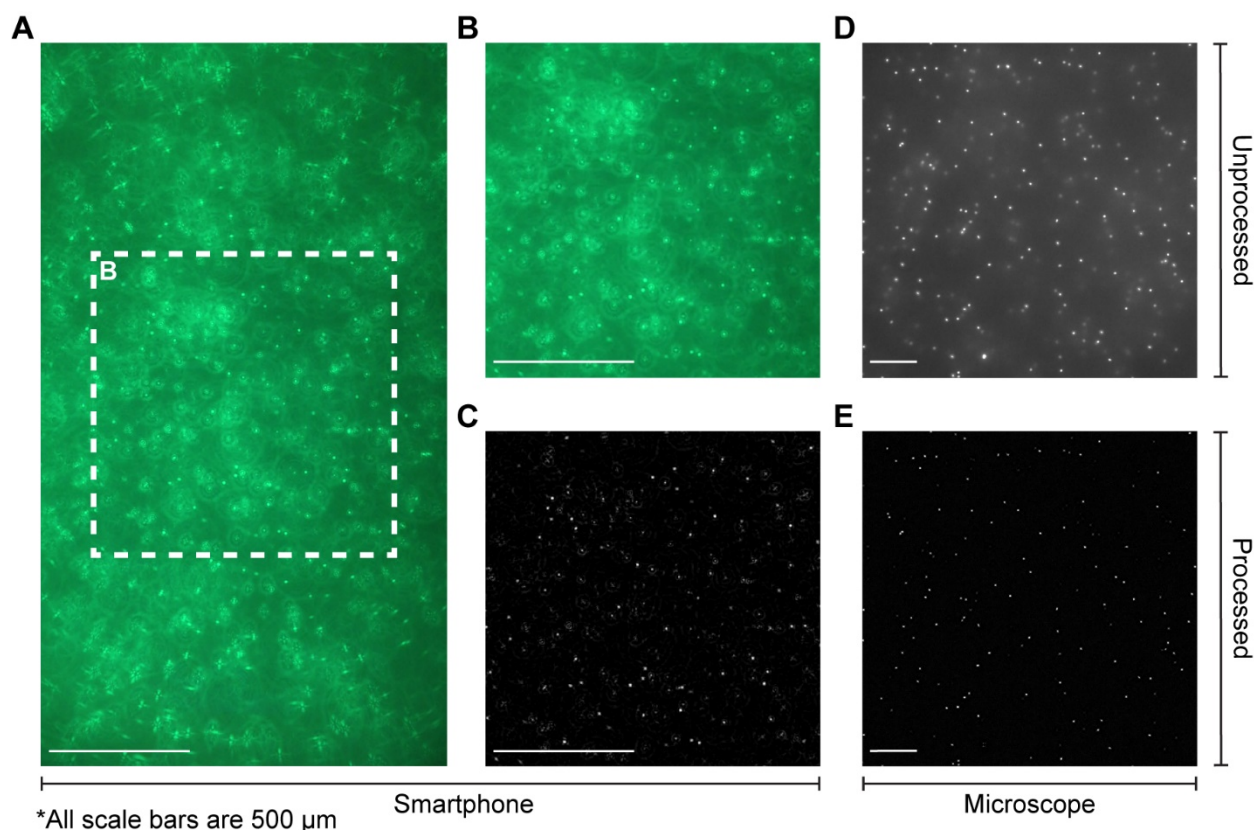


Figure 6.3 Image quality comparison between smartphone and microscope.

(A) Raw image of 400 nm streptavidin-coated fluorescent nanoparticles in water using smartphone-based optical system. (B) Central 800×800 pixel² used for analysis. (C) Final processed image taken with the smartphone. (D) Image of the same streptavidin-coated fluorescent nanoparticle solution using a 40X objective on an inverted epifluorescence microscope. (E) Resulting image from the microscope after processing. Note: all scale bars are 500 μm .

6.3.3 Limit of Detection in Pond Water

After measuring the diffusion coefficient of the nanoparticles in water, we performed PD on whole cells in environmental pond water. The pond water contains some sediment and other debris which add to sample matrix complexity and simulates the natural environment where *V. cholerae* is found.^{43,59,86,141} If we use environmental samples with excessive amounts of sediment in the future, we may need to filter the water samples prior to performing PD measurements. We incorporated multiple users in the experimental design to demonstrate the repeatability of smartphone-based PD; three users performed LAMP and three different users executed measurements on the smartphone-based PD platform. LAMP assays were prepared with 6×10^0

– 6×10^4 cells/reaction in pond water (where 50% of the total LAMP reaction volume was pond water). Fluorescence visualization of LAMP performed in a real-time PCR system demonstrated that samples with higher initial concentrations of *V. cholerae* amplify more rapidly than samples with lower initial concentrations (Figure 6.4A) as indicated by the lower C_T values (Table E.3). Gel electrophoresis was used to confirm amplification (Figure 6.4B). There was a statistically significant difference in the diffusion coefficients from 6×10^0 – 6×10^4 cells/reaction (0.66 aM to 6.6 fM) when compared to NTC (p-value < 0.01 for 6×10^0 and p-value < 0.0001 for 6×10^1 , 6×10^2 , 6×10^3 , and 6×10^4 cells/reaction) (Figure 6.4C). This LOD of 6 cells/reaction, 0.66 aM or 400 cells/mL, falls within the concentration range that is commonly found in the environment (10 – 1000 cells/mL).⁵⁹ This environmentally relevant LOD suggests the applicability of this handheld smartphone-based PD platform for future point-of-use applications. The sub-attomolar concentration of *V. cholerae* measured on the smartphone-based PD platform is equivalent to the microscope results in previous work;⁴³ however, unlike the microscope, the smartphone platform used here is both portable and low-cost.

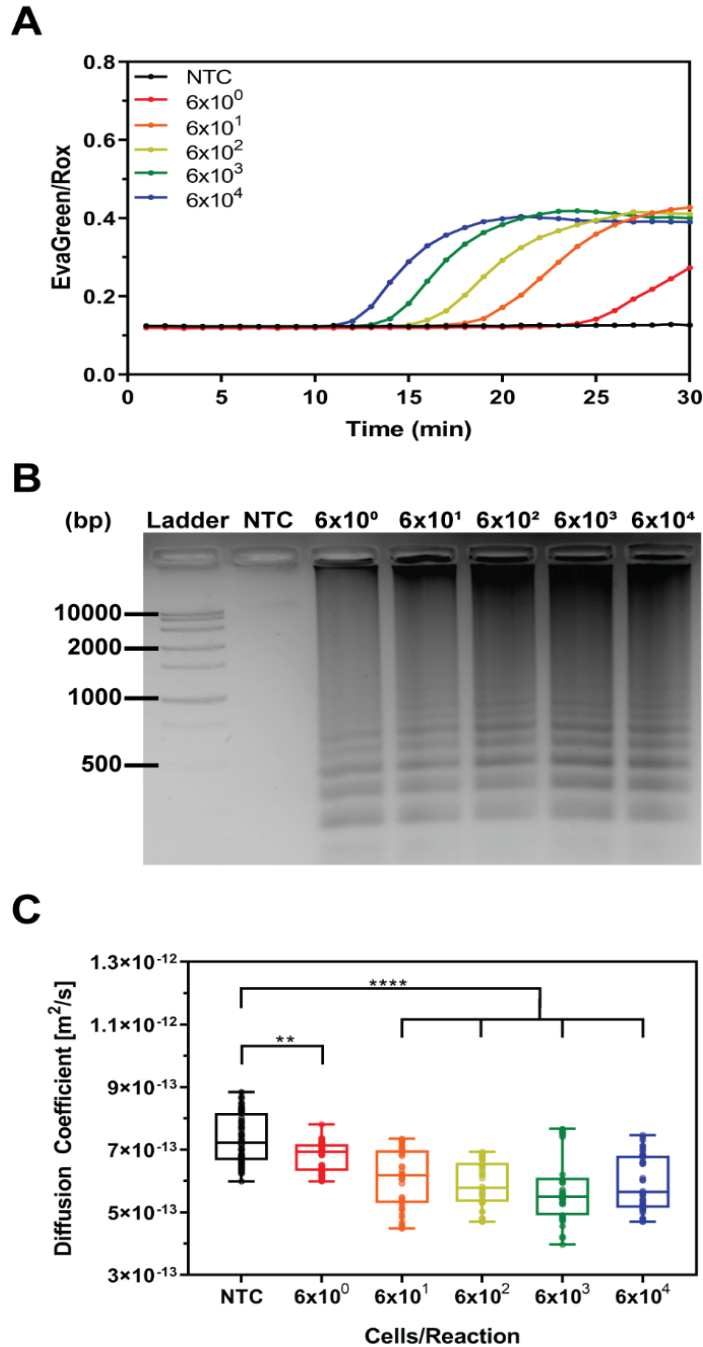


Figure 6.4 LOD of *V. cholerae* in pond water.

V. cholerae cells were spiked into pond water at concentrations ranging from 6×10^0 – 6×10^4 cells/reaction. (A) Real-time fluorescence was monitored over a 30-minute LAMP reaction. (B) A 2% agarose gel confirms amplification and presents the banding pattern indicative of LAMP amplification for positive samples. (C) The diffusion coefficient measurements show a decreasing trend as a function of starting cell concentration with significance at 6×10^0 (** $p < 0.01$), 6×10^1 , 6×10^2 , 6×10^3 , and 6×10^4 (**** $p < 0.0001$) cells/reaction. Statistical analysis was a one-way ANOVA with Dunnett's *post hoc* relative to NTC. (N=5, n=9)

6.3.4 Single-Blinded Selectivity in Pond Water

After establishing the LOD, we confirmed the selectivity of the PD technique by ensuring only toxigenic *V. cholerae* was detected and other environmental bacteria that may be present in water samples were not. We used *E. coli* and non-toxigenic *V. cholerae* to measure selectivity since both bacteria are commonly found in the same environment as toxigenic *V. cholerae*.¹⁵¹ It is important to note that non-toxigenic *V. cholerae* lacks the *ctxA* gene targeted by the LAMP primers, and therefore, cannot produce the toxin responsible for severe symptoms and disease outbreaks in humans.⁵⁴

We prepared LAMP assays with 10^3 cells/reaction of *E. coli*, non-toxigenic *V. cholerae*, and toxigenic *V. cholerae* in 50% pond water. To measure selectivity, we performed a single-blinded experiment with six different users to remove the potential for measurement bias. The three users performing LAMP knew the contents of each sample; however, the sample details were blinded to the three individuals taking measurements on the smartphone-based PD platform. There was no amplification of samples with *E. coli* or the non-toxigenic strain of *V. cholerae* as indicated by gel electrophoresis (Figure 6.5A) and fluorescence data (Figure E.4 and Table E.4). These results demonstrate the selectivity of LAMP and coincide with previous literature regarding the target efficiency of LAMP primers.^{78,158,159} There was a statistically significant difference in the diffusion coefficient of the NTC, *E. coli*, and non-toxigenic *V. cholerae* samples when compared to toxigenic *V. cholerae*, which resulted in a much lower diffusion coefficient than the off-target samples (Figure 6.5B, p-value < 0.0001). This illustrates that off-target bacteria that may be present in a water sample will not interfere with diffusion coefficient measurements. Moreover, incorporating six users in the study design speaks to the repeatability of smartphone-based PD measurements.

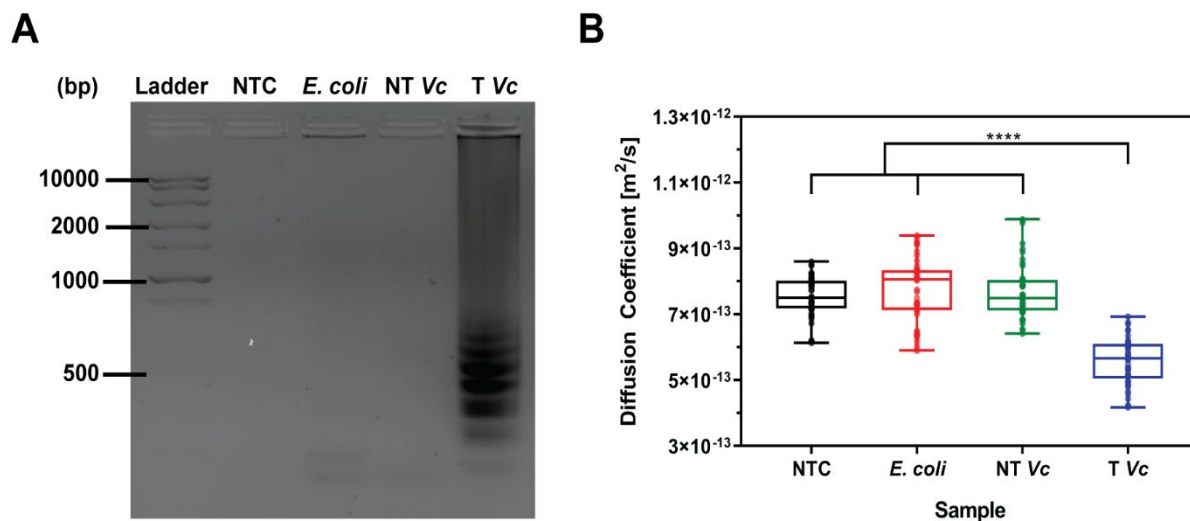


Figure 6.5 Single-blinded selectivity in pond water.

E. coli, non-toxicogenic (NT) *V. cholerae*, and toxicogenic (T) *V. cholerae* cells were spiked into pond water at 10^3 cells/reaction. (A) A 2% agarose gel confirms amplification and presents the banding pattern indicative of LAMP amplification only for toxicogenic *V. cholerae*. (B) The diffusion coefficient measurements show a statistically significant difference between NTC, *E. coli*, and non-toxicogenic *V. cholerae* (**** $p < 0.0001$) when compared to toxicogenic *V. cholerae*. Statistical analysis was a one-way ANOVA with Dunnett's *post hoc* relative to toxicogenic *V. cholerae*. (N=5, n=9)

6.3.5 Double-Blinded Study in Pond Water

To determine the sensitivity, specificity, and accuracy of the smartphone-based PD platform, we directly compared it to real-time fluorescence detection of LAMP amplicons. The data were split into a training and test set. The training set (n=30) was used to determine the positive and negative diffusion coefficient thresholds. Using the PD (Figure E.5) and real-time fluorescence (Table E.5) data collected for the training set, we determined that test set samples with an average diffusion coefficient less than $7.0 \times 10^{-13} \text{ m}^2/\text{s}$ would be considered positive for *V. cholerae* while samples with an average diffusion coefficient greater than $7.2 \times 10^{-13} \text{ m}^2/\text{s}$ would be considered negative for *V. cholerae*. From the training set and other preliminary testing on the smartphone-based PD platform, we realized that there was a small range of diffusion coefficients, from $7.0 \times 10^{-13} \text{ m}^2/\text{s}$ to $7.2 \times 10^{-13} \text{ m}^2/\text{s}$, for which results were inconclusive.

The test set was validated using a double-blinded study design in which all 132 samples (varying concentrations of *V. cholerae*) were unknown to all individuals performing LAMP and collecting smartphone-based PD data. We included multiple users in this study; three users

performed LAMP and three different users conducted measurements on the smartphone-based PD platform. The frequency of test set samples plotted in a histogram over a range of averaged diffusion coefficients follows a bimodal Gaussian distribution (Figure 6.6A). Using the thresholds identified from the training set, we determined that 59 samples were positive when measured by the smartphone-based PD platform while 65 were considered negative. PD measurements for 8 of the 132 samples (6.1%) fell into the inconclusive range (Figure 6.6A). The percentage of samples determined to be inconclusive was similar to clinical trial results of several commercial devices that also have a pre-determined inconclusive range.¹⁶⁰ As we analyze more samples on the smartphone-based PD platform, we expect to narrow or even eliminate this inconclusive range.

To directly compare the smartphone-based PD platform and real-time fluorescence measurements, we constructed a 2×2 contingency table, seen in Figure 6.6B. Overall, there were 56 true positives (TP), 3 false positives (FP), 5 false negatives (FN), and 60 true negatives (TN). The data indicates that false negatives are slightly more common than false positives using smartphone-based PD. Both false negatives and false positives can be mitigated in the future by altering the thresholds or improving the optics within the smartphone-based PD platform. From the true and false negatives and positives, we calculated a sensitivity of 91.8% and a specificity of 95.2% for the smartphone-based PD platform.¹⁶¹ For comparison, the commercialized Crystal Vc Rapid Diagnostic Test for detection of *V. cholerae* in stool has a published sensitivity of 93.1% but a specificity of only 49.2%.⁵⁷ The characterization of the smartphone-based PD platform demonstrates its ability to sensitively and specifically detect low concentrations of *V. cholerae* found in the environment.

Lastly, we created a ROC curve, as seen in Figure 6.6C, to further evaluate the sensitivity and specificity of the smartphone-based PD platform when compared to real-time fluorescence data. ROC curves depict the tradeoff between sensitivity and specificity of a device. In the case of this smartphone-based PD platform, both sensitivity and specificity are high indicating that there is not a significant tradeoff. The area under the curve (AUC) is 0.943, or 94.3%, which represents the accuracy of the platform.¹⁶² Others have demonstrated comparable ROC curve analyses for smartphone platforms.^{163,164} Combined, these results highlight the excellent sensitivity, specificity, and accuracy of the smartphone-based PD platform for measuring LAMP amplicons.

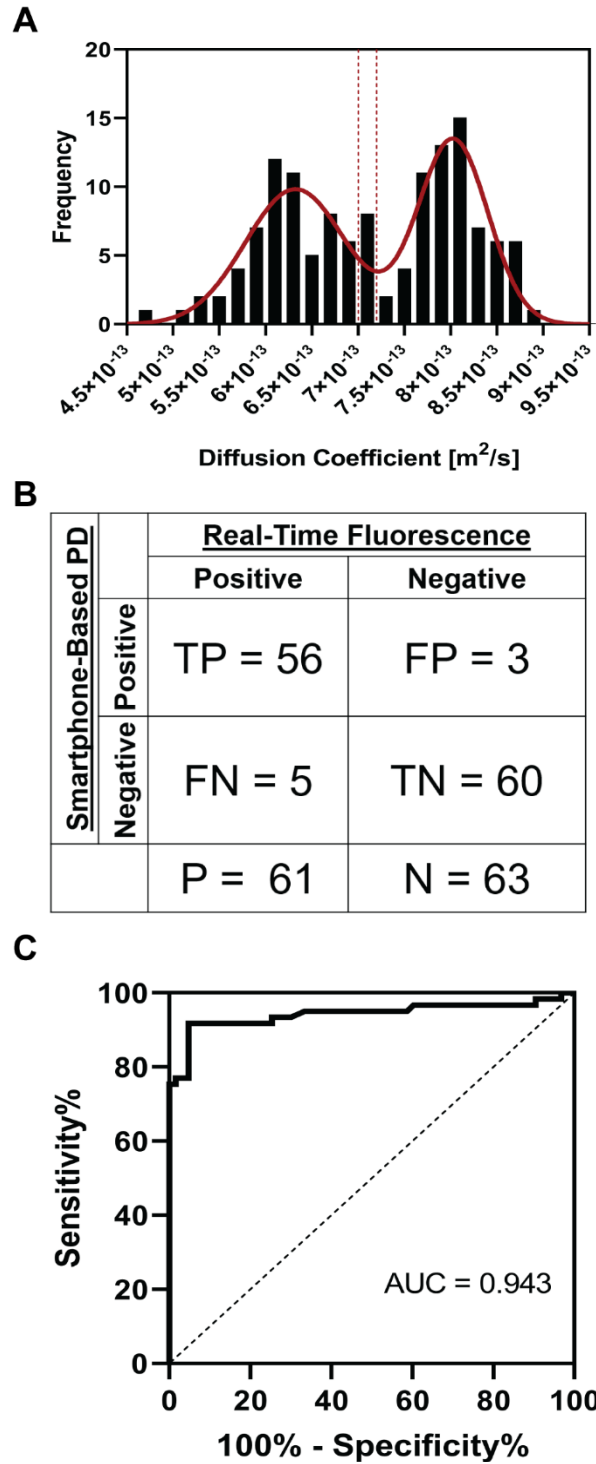


Figure 6.6 Characterization of the smartphone-based PD platform.

(A) Distribution of averaged diffusion coefficients for 132 samples in the double-blinded study. The red solid line demonstrates that this data follows a bimodal Gaussian distribution while the red dashed lines outline the inconclusive range. (B) 2×2 contingency table used to calculate sensitivity and specificity that is confirmed by (C) the ROC curve with an AUC of 0.943.

6.3.6 *V. cholerae* Concentrator User-Centered Design Study

Even though the LOD of the smartphone-based PD platform can be mathematically converted from 6 cells/reaction to 400 cells/mL, the smartphone-based PD platform is not compatible with volumes greater than 25 μ L. Volumes on the microliter scale are not representative of an environmental water source; therefore, we sought to develop a bacterial concentrator device. The goal was to create a device that could process 1 L of water and concentrate the *V. cholerae* bacteria into a volume that is compatible with the smartphone-based PD platform. The bacterial concentrator device (designed by Jordan Florian of OmniVis LLC) consists of three layers: the top layer (Figure 6.7A) incorporates a 50 mm diameter wire mesh screen to remove large sediment, the middle layer (Figure 6.7B) includes a 100 μ m pore size nylon membrane to trap small organisms or small sediment, and the bottom layer (Figure 6.7C) contains a 0.8 μ m pore size nylon membrane to capture and concentrate the *V. cholerae* bacteria. We were interested in gaining perspective from non-team members regarding the usability of the bacterial concentrator device, so we conducted a user-centered design study with 30 individuals. After study participants successfully assembled the concentrator device (Figure 6.7D), they were asked to complete the SUS survey.

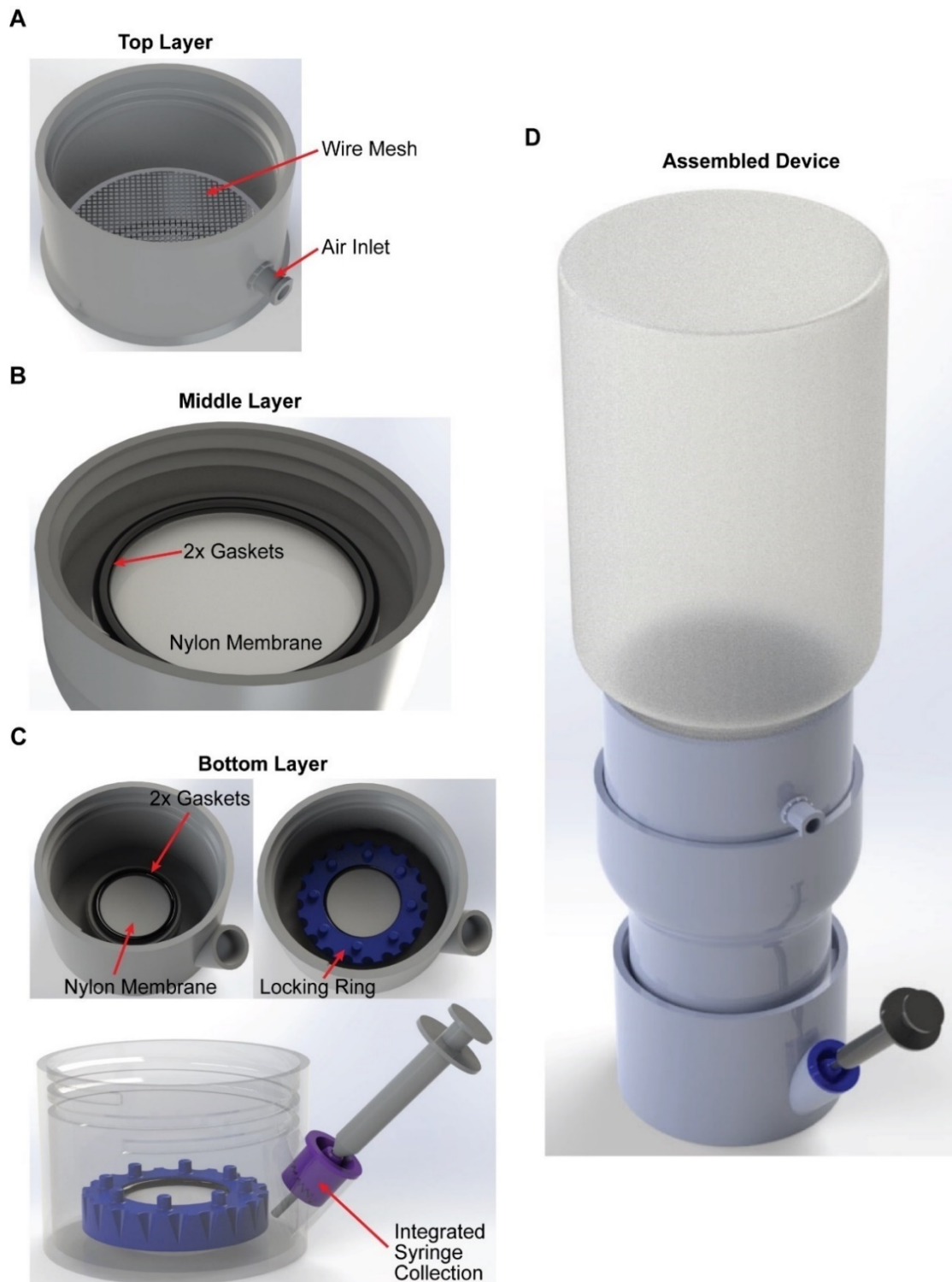


Figure 6.7 *V. cholerae* concentrator.

(A) Top layer removes large sediment, (B) middle layer traps small sediment and small organisms such as copepods, and (C) bottom layer captures the *V. cholerae* bacteria. Bottom layer includes a collection port for sample extraction via syringe. (D) Assembled *V. cholerae* concentrator attached to a Nalgene bottle.

Figure 6.8A demonstrates the SUS survey responses from all 30 participants. The top five categories display low scores, which is promising because very few participants found the concentrator device cumbersome, inconsistent, or complex or thought they needed to learn more or required technical assistance for use. In contrast, the study participants ranked the concentrator device high in terms of user confidence, ability to learn quickly, integration, ease-of-use, and likeability. The bacterial concentrator device received an average overall SUS score of 77.7% (Figure 6.8B) which was well above the ‘usable’ threshold of 68%. Because we had participants with both technical and non-technical backgrounds, we were interested in evaluating whether the individual’s background was associated with their overall SUS score for the bacterial concentrator device. Interestingly, there was no statistically significant difference between the overall SUS score of the two participant groups (77.7% for technical, 77.5% for non-technical, Figure 6.8B); both found the concentrator device quite usable. This is very promising, because it seems that background is not correlated with the usability rating of the bacterial concentrator device.

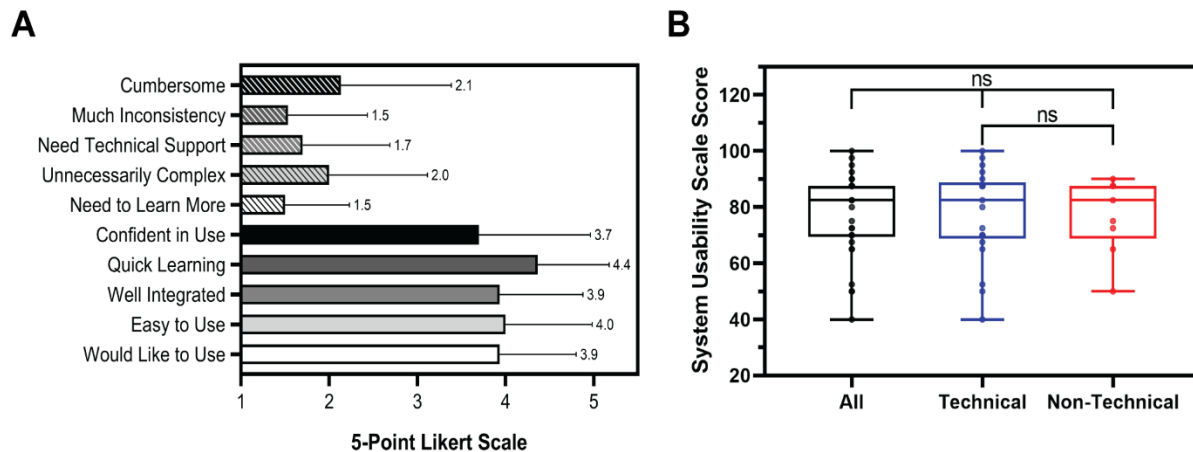


Figure 6.8 SUS survey data from user-centered design study with concentrator device.

(A) Results from each question on the SUS survey are plotted as the mean (value to the right of bar) with standard deviation. (B) Overall SUS scores were plotted for all participants (n=30), individuals with technical backgrounds (n=21), and those with non-technical backgrounds (n=9). There was no statistically significant difference between any of the groups ($p > 0.05$, ns = no significance). Statistical analysis was a one-way ANOVA with Tukey’s *post hoc*.

6.3.7 *V. cholerae* Concentrator Experiments

To test the functionality of the concentrator device, 10^6 *V. cholerae* cells/mL were spiked into 250 mL of MilliQ water and the mixture was added to a Nalgene bottle. After connecting the

Nalgene bottle to the 3D printed bacterial concentrator device, the mixture processed through the device via gravity filtration. Even though the experimental setup was consistent between repeats, we observed vastly different flow rates (indicated by the time to process the mixture, Table 6.1). The heterogeneity of the printing resin and insufficient tolerance of the 3D printer could have led to minor differences between each bacterial concentrator device, causing the variation in flow rate.

Table 6.1 Time for each bacterial concentrator device to process 250 mL of water spiked with *V. cholerae*. (n=3)

Repeat	Device	Time (min:sec)
1	3	14:03
2	1	30:06
3	5	23:08

After collecting the nylon pieces and fluid reservoir samples from the disassembled bacterial concentrator device, LAMP was performed on these samples along with controls for 45 minutes. As expected, the negative controls (NTC and NTC nylon) did not amplify (seen in real-time and gel electrophoresis, Figure 6.9A and Figure 6.9B) while the positive control (10^6 cells/reaction) consistently amplified (Figure 6.9A and Figure 6.9B). We observed that the nylon membrane somewhat inhibited fluorescence measurements by the real-time PCR system (Figure 6.9A, blue lines); however, we saw clear banding in the agarose gel (Figure 6.9B). All samples collected from the fluid reservoir exhibited strong amplification (Figure 6.9A, green lines and Figure 6.9B), indicating that *V. cholerae* cells may have been enriched as intended. We do expect some bacteria loss to occur because the nylon membrane in the bottom layer has $0.8\ \mu\text{m}$ pores and *V. cholerae* bacteria can be as small as $0.3\ \mu\text{m}$ in diameter and $1\ \mu\text{m}$ in length. The nylon was selected because it has a reasonable flow rate and the ability to capture majority of the bacteria.

The samples were then analyzed with the smartphone-based PD platform. The aliquots from the fluid reservoir produced the lowest diffusion coefficients for all three repeats and the greatest statistical significance when compared to NTC (p-value < 0.001) (Figure 6.9C). From previous work, we know that diffusivity decreases as initial pathogen concentration increases.^{43,165} Therefore, it is likely that *V. cholerae* bacteria are indeed being enriched by the concentrator device because the positive control (10^6 cells/reaction) had higher diffusion coefficients than the fluid reservoir samples (reservoir contained 4 mL concentrated from 250 mL mixture with 10^6 cells/mL).

However, we must perform further testing and analysis with the bacterial concentrator device to prove *V. cholerae* enrichment and determine the concentration factor. Specifically, we want to repeat these experiments with lower concentrations of *V. cholerae* spiked into the Nalgene bottle.

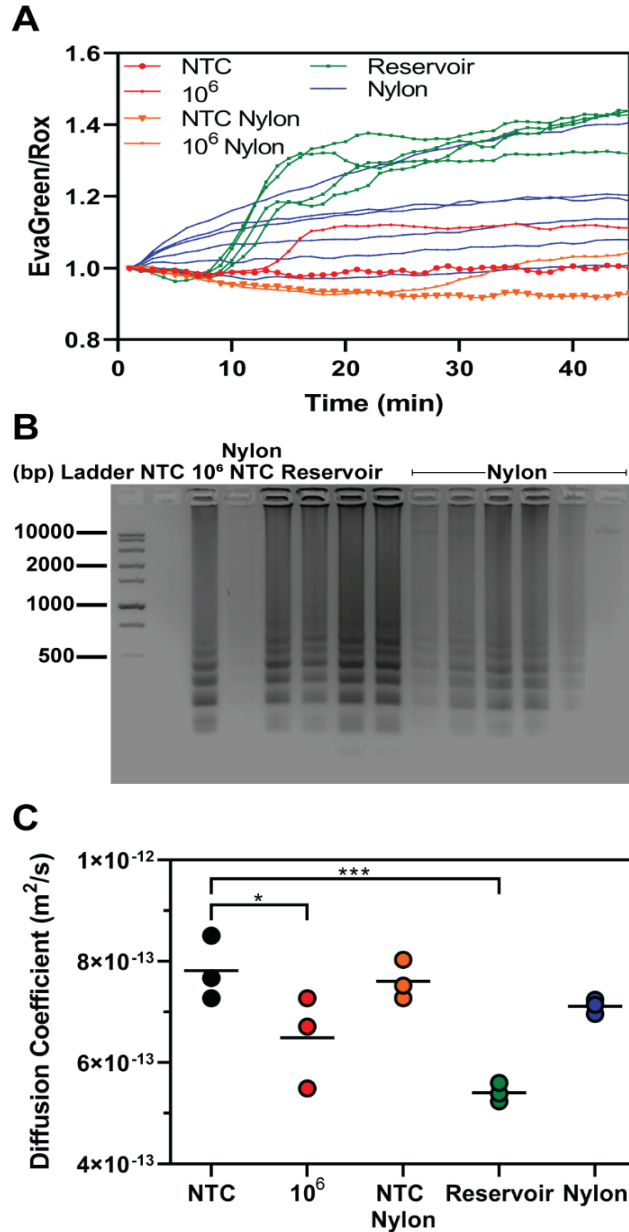


Figure 6.9 LAMP and PD data from *V. cholerae* concentrator experiments.

V. cholerae cells were spiked into MilliQ water at 10^6 cells/mL and processed through the concentrator device. (A) Real-time fluorescence was monitored over a 45-minute LAMP reaction. (B) A 2% agarose gel confirms amplification and presents the banding pattern indicative of LAMP amplification for positive samples. (C) The diffusion coefficient measurements show significance for 10^6 cells/reaction (* $p < 0.05$) and fluid reservoir samples (***) when compared to NTC. Statistical analysis was a one-way ANOVA with Dunnett's *post hoc* relative to NTC. (n=3)

6.4 Future Directions

Future development of the smartphone-based PD platform includes incorporating a heating unit to perform LAMP amplification so the entire PD-LAMP technique can be executed continuously on the portable platform. A fully integrated smartphone-based PD-LAMP platform will enable rapid sample-to-answer detection of pathogens at the point of use. Beyond qualitatively identifying the presence or absence of a target pathogen, we are interested in correlating diffusion coefficient measurements with pathogen concentration in hopes of developing a quantitative PD-LAMP system. This would be extremely beneficial, for example, in monitoring the viral load of an individual living with HIV.

Even though the bacterial concentrator device was well-received by all participants in the user-centered design study, there are improvements we would like to make. First, we want to explore pressure-driven flow within the bacterial concentrator device because gravity-based filtration is impractical for field applications due to the length of time needed to process 1 L of water. Second, the bacterial concentrator device needs to seamlessly integrate with the smartphone-based PD platform to enable a truly sample-to-answer detection platform.

6.5 Conclusions

The portable and compact optical system combines an external ball lens, iPhone 6 camera lens system, blue laser diode, and high-pass filter. This optical system produces a 68X magnification, sufficient for imaging the Brownian motion of 400 nm streptavidin-coated fluorescent nanoparticles bound to biotin-labeled amplification products. The smartphone application efficiently processes the recorded images and computes a diffusion coefficient for each sample that indicates the presence or absence of pathogens. Smartphone-based PD is incredibly sensitive, detecting as few as 6 *V. cholerae* cells/reaction (0.66 aM) in pond water in just 35 minutes. Smartphone-based PD selectively identified toxigenic *V. cholerae* while off-target waterborne pathogens such as *E. coli* and non-toxigenic *V. cholerae* did not interfere with measurements. When directly compared to real-time fluorescence detection of LAMP amplicons in a double-blinded study, smartphone-based PD had an overall sensitivity of 91.8%, 95.2% specificity, and accuracy of 94.3%. Furthermore, this portable platform requires only \$0.78 of consumables, making it affordable for low-resource areas. Altogether, these results demonstrate

that smartphone-based PD is accurate, sensitive, and robust for detection of *V. cholerae* LAMP amplicons in pond water.

Participants in a user-centered design study gave the bacterial concentrator device an overall SUS score of 77.7% which is almost 10% above the ‘usable’ threshold. Moreover, we were able to enrich *V. cholerae* cells from 250 mL of water in less than 30 minutes with the bacterial concentrator device, amplify the enriched solution via LAMP, and measure the presence of *V. cholerae* LAMP products on the smartphone-based PD platform.

7. CONCLUSION

This dissertation outlined several tools for detection of pathogens in complex sample matrices as well as strategies to translate these tools to the point of use. Nucleic acid amplification methods have excellent sensitivity, specificity, and accuracy compared to other detection mechanisms. The most common nucleic acid amplification method, polymerase chain reaction, is not ideal for point-of-care applications due to its precise temperature requirements and abundance of inhibitors in pathogen sample matrices. In this dissertation, I detailed the development of two paperfluidic platforms and a smartphone platform that all incorporate an isothermal amplification technique called loop-mediated isothermal amplification (LAMP). In Chapter 2, I described the characterization of a strand displacement LAMP (SD-LAMP) assay for rapid detection of *Vibrio cholerae*. The SD-LAMP assay is highly specific to toxigenic strains of *V. cholerae* and robust enough for direct identification in environmental pond water. The vitrification technique reported in Chapter 3 allows room-temperature storage of the *V. cholerae* SD-LAMP reagents up to 30 days. I also dried reverse transcription LAMP (RT-LAMP) reagents for HIV and noted little difference in the assay limit of detection after storing reagents for 21 days when compared to freshly prepared reagents. Room-temperature reagent storage eliminates cold-chain requirements and enables integration of assays, such as LAMP, into portable devices. In Chapter 4, I detailed the creation of two integrated paperfluidic platforms: one for detection of *V. cholerae* in pond water and the other for HIV in whole blood. Both platforms take advantage of the inherent capillary flow of porous membranes, the speed of LAMP amplification, and the simplicity of colorimetric lateral flow immunoassay analysis. The HIV device even incorporates vitrified RT-LAMP reagents to eliminate precision pipetting steps and improve automation.

Chapter 5 outlined the characterization of the combined LAMP and particle diffusometry (PD) technique on a laboratory microscope for identification of *V. cholerae*. We showed a strong correlation between fluorescence and PD measurements and demonstrated that PD is 10-fold more sensitive than gold-standard fluorescence detection of *V. cholerae* LAMP products in pond water. We then translated the PD technique to a smartphone-based platform as described in Chapter 6. The smartphone-based PD platform can detect as few as 6 cells/reaction in pond water in just 35 minutes and is highly selective to toxigenic strains of *V. cholerae*. When directly compared to real-

time fluorescence detection of LAMP amplicons in a double-blinded study, smartphone-based PD had an overall sensitivity of 91.8%, 95.2% specificity, and accuracy of 94.3%.

The molecular tools and strategies for platform development reported in this dissertation provide a framework for designing inexpensive and easy-to-use devices for rapid identification of pathogens at the point of use. Integrated pathogen detection platforms have the potential to impact communities around the world by improving time to treatment and reducing unnecessary disease transmission.

APPENDIX A. SUPPLEMENT TO CHAPTER 2

Table A.1 *V. cholerae* LAMP primers.

Primers targeting a 193 bp sequence of the *ctxA* gene of *Vibrio cholerae*.

Primer	Sequence (5' – 3')
B3	GTGGGCACTTCTCAAAC
F3	TCGGGCAGATTCTAGACC
BIP	TCAACCTTTATGATCATGCAAGAGGGGAAACATATCCATCATCGTG
FIP	TTGAGTACCTCGGTCAAAGTACTTCCTGATGAAATAAAGCAGTCA
LB	AACTCAGACGGGATTTGTTAGG
LF	CCTCTTGGCATAAGACCACC
LB-FAM	/56-FAM/AACTCAGACGGGATTTGTTAGG
LB-Biotin	/5Biosg/AACTCAGACGGGATTTGTTAGG
LF-Biotin	/5BiosG/CCTCTTGGCATAAGACCACC
Strand displacement probe	/56-FAM/CTGCAGGTGGTCTTATGCCAAGAGGACAGAGTG/3InvdT/
Quencher (displaced) strand	TCTTGGCATAAGACCACCTGCAG/3IABkFQ/

Table A.2 *V. cholerae* LAMP target gene sequence.

Gene Name	Sequence (5' – 3')
<i>V. cholerae ctxA</i>	GTTTGGATCAATTATTTTCTGTAAACAAAGGGAGCATTATATGGTAAAGA TAATATTTGTGTTTTTTATTTTCTTATCATCATTTTCATATGCAAATGATGAT AAGTTATATCGGGCAGATTCTAGACCTCCTGATGAAATAAAGCAGTCAGGT GGTCTTATGCCAAGAGGACAGAGTGAGTACTTTGACCGAGGTAAGTCAAATG AATATCAACCTTTATGATCATGCAAGAGGAACTCAGACGGGATTTGTTAGG CACGATGATGGATATGTTTCCACCTCAATTAGTTTGAGAAGTGCCCACTTAG TGGGTCAAACATATTTGTCTGGTCATTCTACTTATTATATATATGTTATA

Table A.3 Standard LAMP master mix for *V. cholerae*.

Reagent	Final Concentration
Isothermal Buffer	1.0X
dNTPs	1.4 mM
Betaine	800 mM
F3 Primer	0.2 μ M
B3 Primer	0.2 μ M
FIP Primer	1.6 μ M
BIP Primer	1.6 μ M
LF Primer	1.6 μ M
LB Primer	1.6 μ M
EvaGreen Dye	0.4X
ROX Reference Dye	0.5X
Bst 2.0 Polymerase	8.0 U
Template	2 μ L
Molecular Bio H ₂ O	Fill to 25 μ L

Table A.4 SD-LAMP master mix for *V. cholerae*.

Reagent	Final Concentration
Isothermal Buffer	1.0X
dNTPs	1.4 mM
Betaine	800 mM
F3 Primer	0.2 μ M
B3 Primer	0.2 μ M
FIP Primer	1.6 μ M
BIP Primer	1.6 μ M
LB-Biotin Primer	1.6 μ M
SD Probe (1 μ M FAM:5 μ M Quench)	1.0X
Bst 2.0 Polymerase	8.0 U
Template	2 μ L
Molecular Bio H ₂ O	Fill to 25 μ L

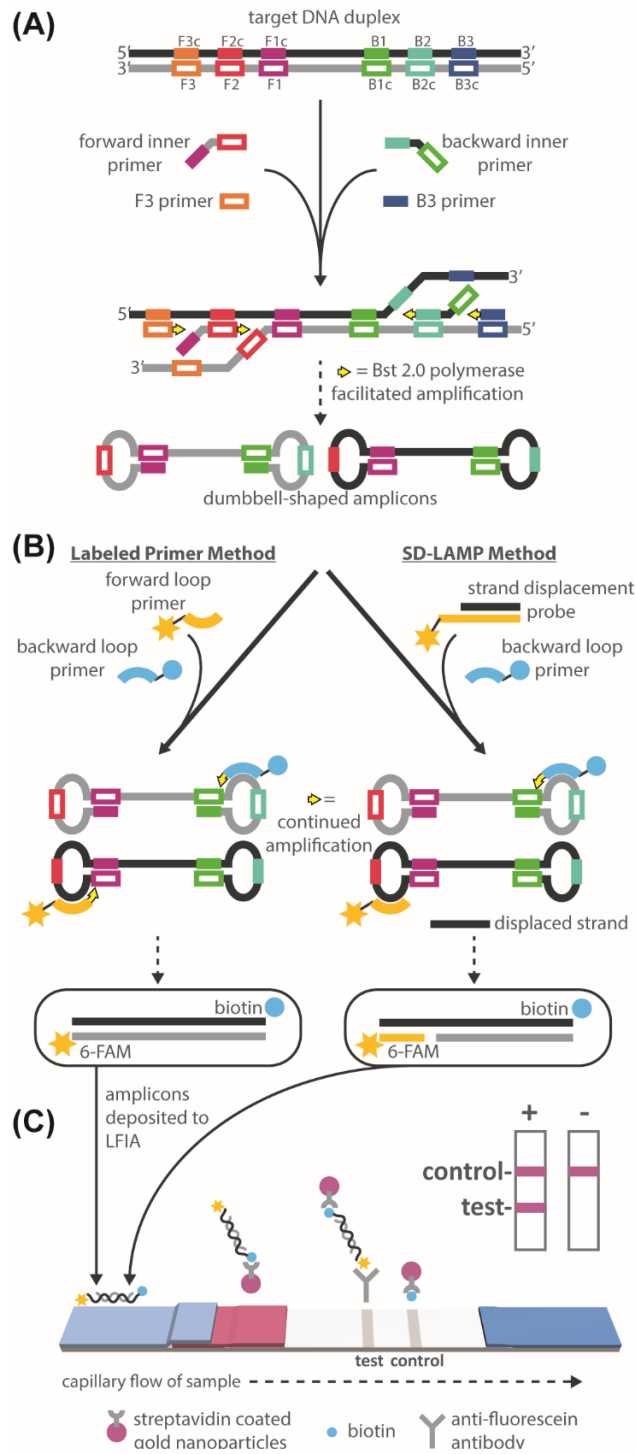


Figure A.1 Schematic of standard LAMP and SD-LAMP reactions and subsequent LFIA detection.

(A) The noncyclic step of both reactions in which F3, B3, and inner primers bind to a double-stranded target sequence and polymerase generates dumbbell-shaped products. (B) Dumbbell-shaped products enter the cyclic amplification step during which loop primers accelerate amplification. Products can be labeled by either standard tagging of each loop primer or by SD-LAMP, which uses one labeled loop primer along with a tagged strand displacement probe that hybridizes to the amplicons' loop region. (C) Labeled amplicons visualized on a standard LFIA strip.

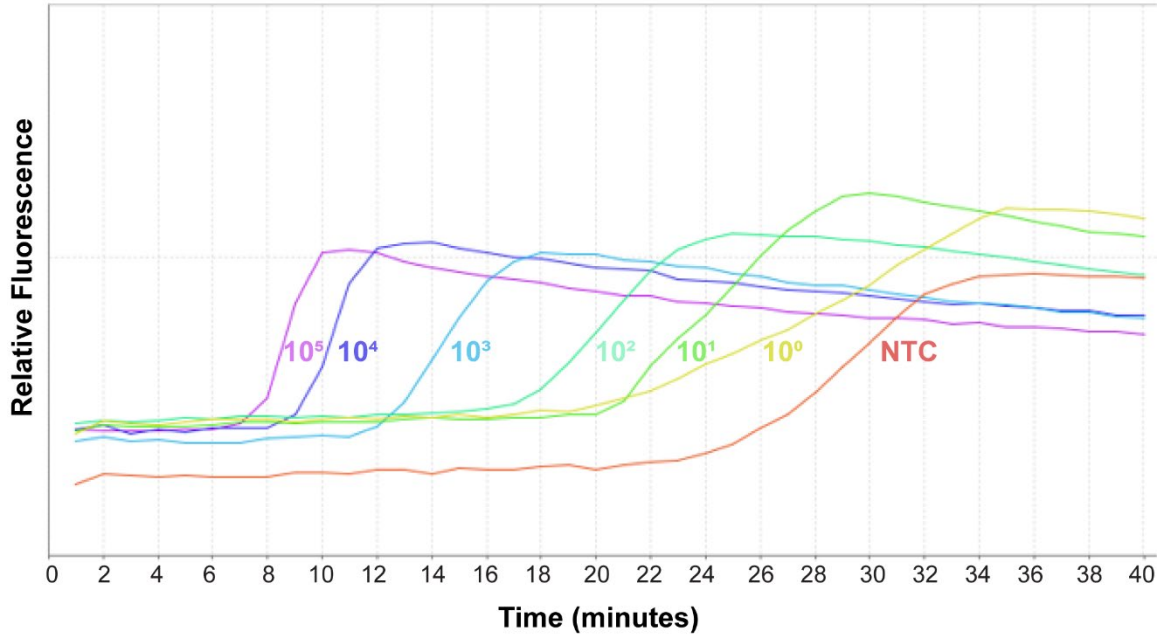


Figure A.2 Real-time amplification of *V. cholerae* genomic DNA using Yamazaki primers.

Real-time relative fluorescence data demonstrates faster amplification for higher concentrations of *V. cholerae* genomic DNA (concentrations in DNA copies/reaction). However, the NTC samples consistently amplified after approximately 30 minutes of heating, indicating these primers induce non-specific amplification. (n=1)

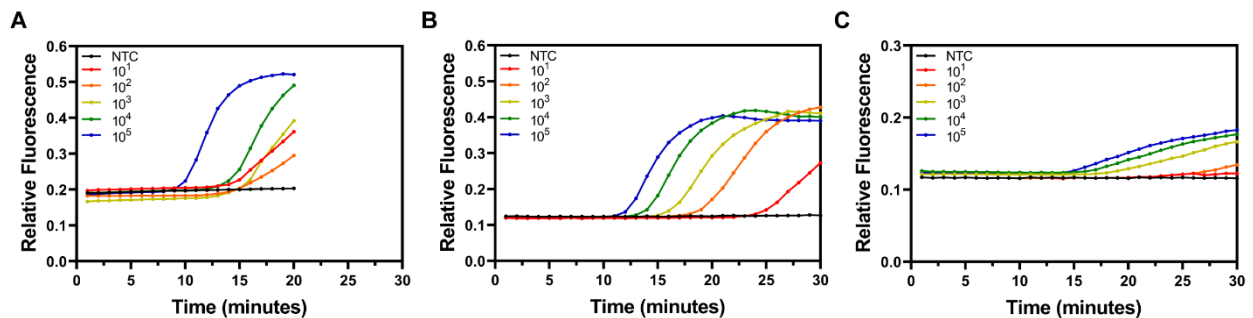


Figure A.3 LAMP amplification of *V. cholerae* using different reaction volumes.

Real-time relative fluorescence data show amplification of *V. cholerae* at concentrations of 10¹, 10², 10³, 10⁴, and 10⁵ cells/reaction in total LAMP reaction volumes of (A) 10 μL, (B) 15 μL, and (C) 50 μL. Note: LAMP assay in (A) was stopped after 20 minutes of heating.

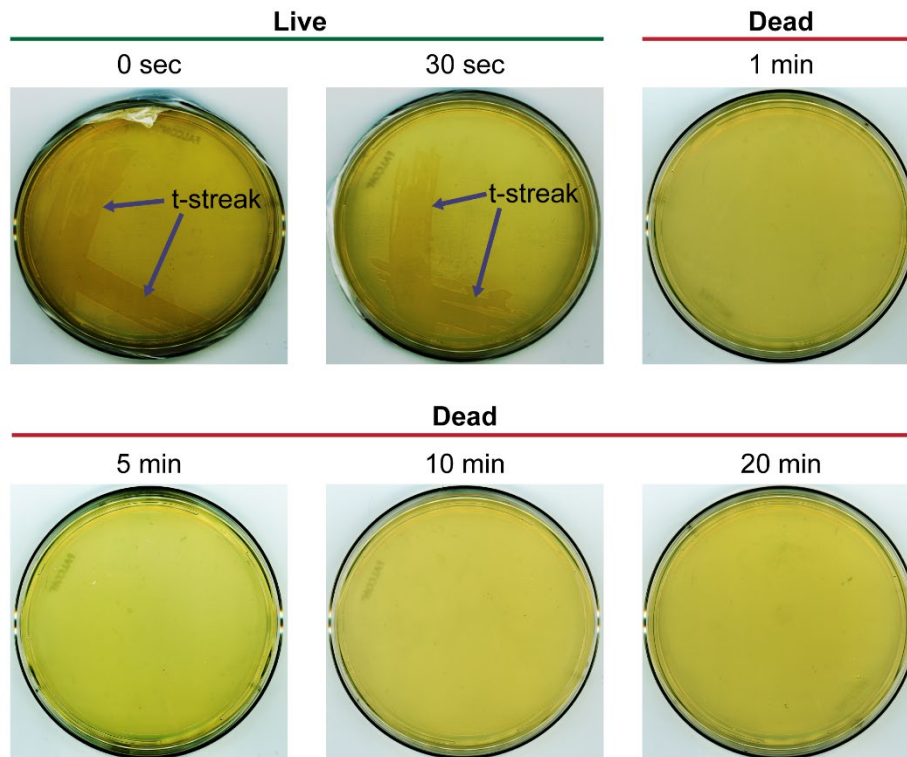


Figure A.4 *V. cholerae* thermal cell lysis at 65°C.

25 μ L aliquots of *V. cholerae* were subject to heating at 65°C for various lengths of time (0 sec, 30 sec, 1 min, 5 min, 10 min, and 20 min) and then immediately streaked onto an LB agar plate. After a 9-hour incubation at 37°C, images were taken; *V. cholerae* cell lysis occurs between 30 seconds and 1 minute of heating. This can be seen from the cluster of colonies seen in the 0 and 30 second plates (marked by “t-streak” in the image) and the absence of these colonies at heating times of 1 minute or greater. (n=1)

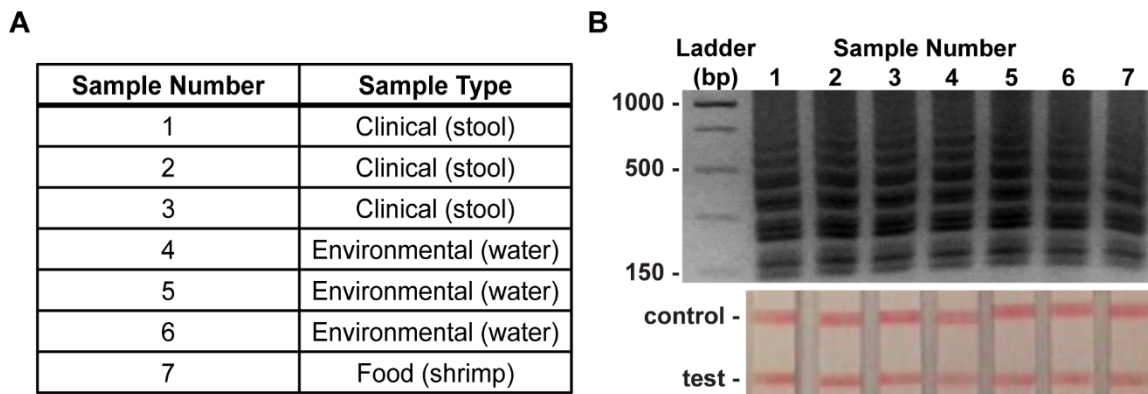


Figure A.5 *V. cholerae* sample testing in Haiti.

(A) *ctxA*-positive *V. cholerae* samples collected by the Emerging Pathogens Institute in Haiti. *V. cholerae* was isolated from patient stool samples, river water, and shrimp shells. (B) Electrophoresis gel verifying amplification (contrast increased for visualization) and LFIA results (image taken with iPhone) are consistent indicating that primers can detect various *ctxA*-positive strains. (n=1)

APPENDIX B. SUPPLEMENT TO CHAPTER 3

Table B.1 SD-LAMP vitrification master mix for *V. cholerae*.

Reagents are combined into one master mix for fresh reactions and separated into three mixtures for the reagent drying process. All reactions are 25 μ L total.

Primer Mixture	Enzyme Mixture	Rehydrating Mixture
44.8 mM Sucrose	120 mM Sucrose	1.0X Isothermal Buffer
0.007% Triton X-100	1.4 mM dNTPs	800 mM Betaine
0.28% Glycerol	8.0 U Bst 2.0 Polymerase	Molecular Bio H ₂ O
0.2 μ M F3/B3		Pond H ₂ O
1.6 μ M FIP/BIP/LB		2 μ L template
1.0X SD Probe		

Table B.2 HIV RT-LAMP target gene sequence.

Gene Name	Sequence (5' – 3')
HIV-1 <i>gag</i> (201 bp target region)	TCAGCATTATCAGAAGGAGCCACCCACAAAGATTTAAACACCATGCTAAAC ACAGTGGGGGACATCAAGCAGCCATGCAAATGTTAAAAGAGACCATCAA TGAGGAAGCTGCAGAATGGGATAGAGTGCATCCAGTGCATGCAGGGCCTA TTGCACCAGGCCAGATGAGAGAACCAAGGGGAAGTGACATAGCAGGAACT

Table B.3 HIV LAMP primers.

Primers targeting a 201 bp sequence of the *gag* gene of HIV-1.

Primer	Sequence (5' – 3')
B3	AGTTCCTGCTATGTCCTTC
F3	TCAGCATTATCAGAAGGAGC
BIP	ATGAGGAAGCTGCAGAATGGGCCCTTGTTCTCTCATCTG
FIP	GGTCTCTTTTAAACATTTGCATGGCTTTAAACACCATGCTAAACACA
LB-FAM	/56-FAM/AGTGCATGCAGGGCCTATTG
LF-Biotin	/5-Biosg/TGCTTGATGTCCCCCAC

Table B.4 RT-LAMP vitrification master mix for HIV.

Reagents are combined into one master mix for fresh reactions and separated into three mixtures for reagent drying process. All reactions are 25 μ L total.

Primer Mixture	Enzyme Mixture	Rehydrating Mixture
44.8 mM Sucrose	120 mM Sucrose	1.0X Isothermal Buffer II
0.007% Triton X-100	1.5 mM dNTPs	200 mM Betaine
0.28% Glycerol	4.0 U Bst 3.0 Polymerase	DEPC H ₂ O
0.2 μ M F3/B3		4 μ L template
1.6 μ M FIP/BIP		
0.8 μ M LF/LB		

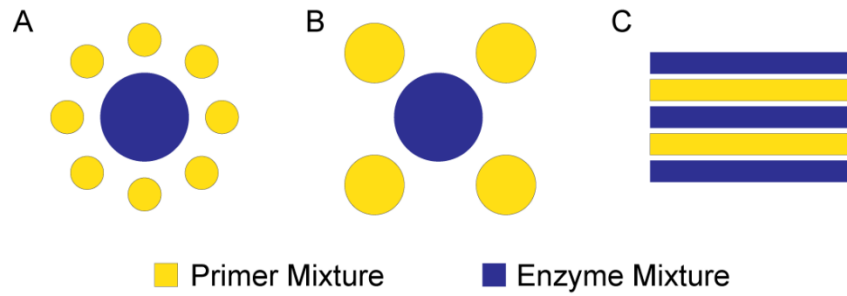


Figure B.1 LAMP reagent deposition patterns.

LAMP primer and enzyme mixture deposition patterns (A, B, C) tested during initial optimization of the vitrification protocol.

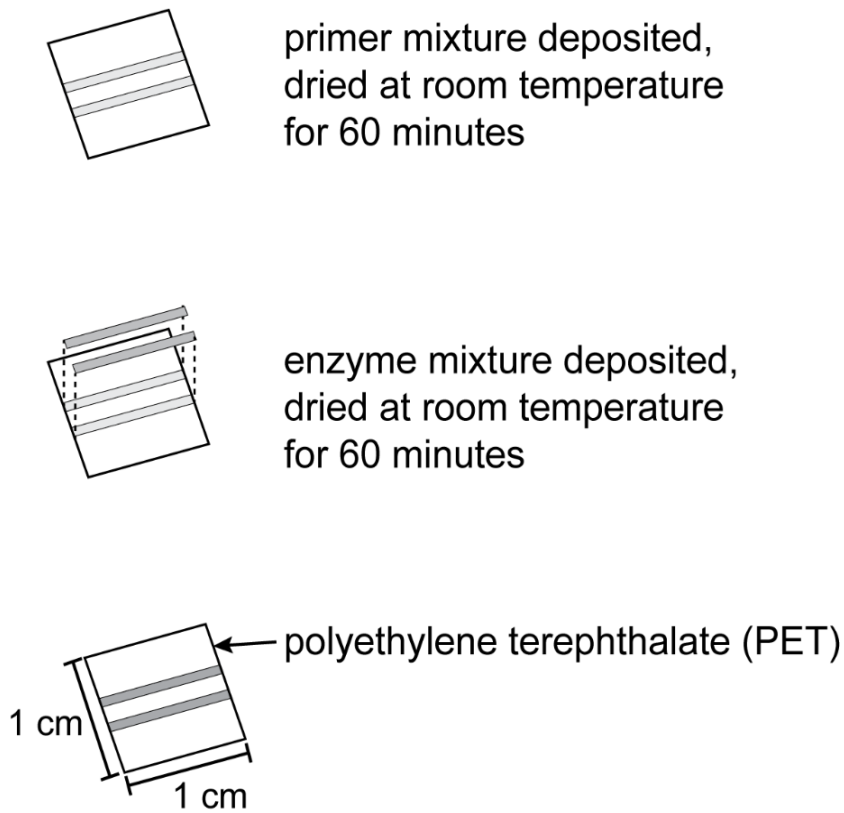


Figure B.2 LAMP reagent drying setup.

The primer mixture is deposited onto 1 × 1 cm PET squares in parallel lines and dried at room temperature under continuous air flow for 60 minutes. The enzyme mixture is then deposited directly on top the dried primer mixture and dried for another 60 minutes under continuous air flow.

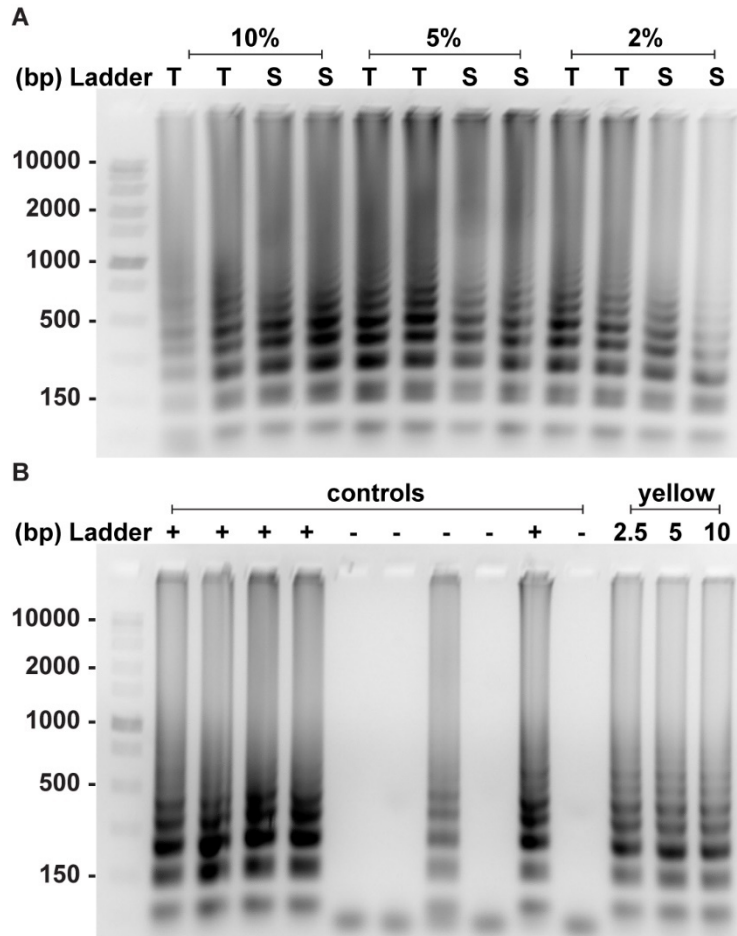


Figure B.3 LAMP tolerance of cryoprotectants and food color solutions.

(A) Trehalose (T) and sucrose (S) were added to LAMP reactions at 10% (v/v), 5% (v/v), and 2% (v/v) concentrations and (B) yellow food color solution was added at 2.5% (v/v), 5% (v/v), and 10% (v/v) concentrations to determine the maximum of each additive that LAMP can withstand. Yellow was the only food color dye that did not inhibit LAMP (data not shown). All positive samples were spiked with 10^5 *V. cholerae* cells/reaction. (n=1)

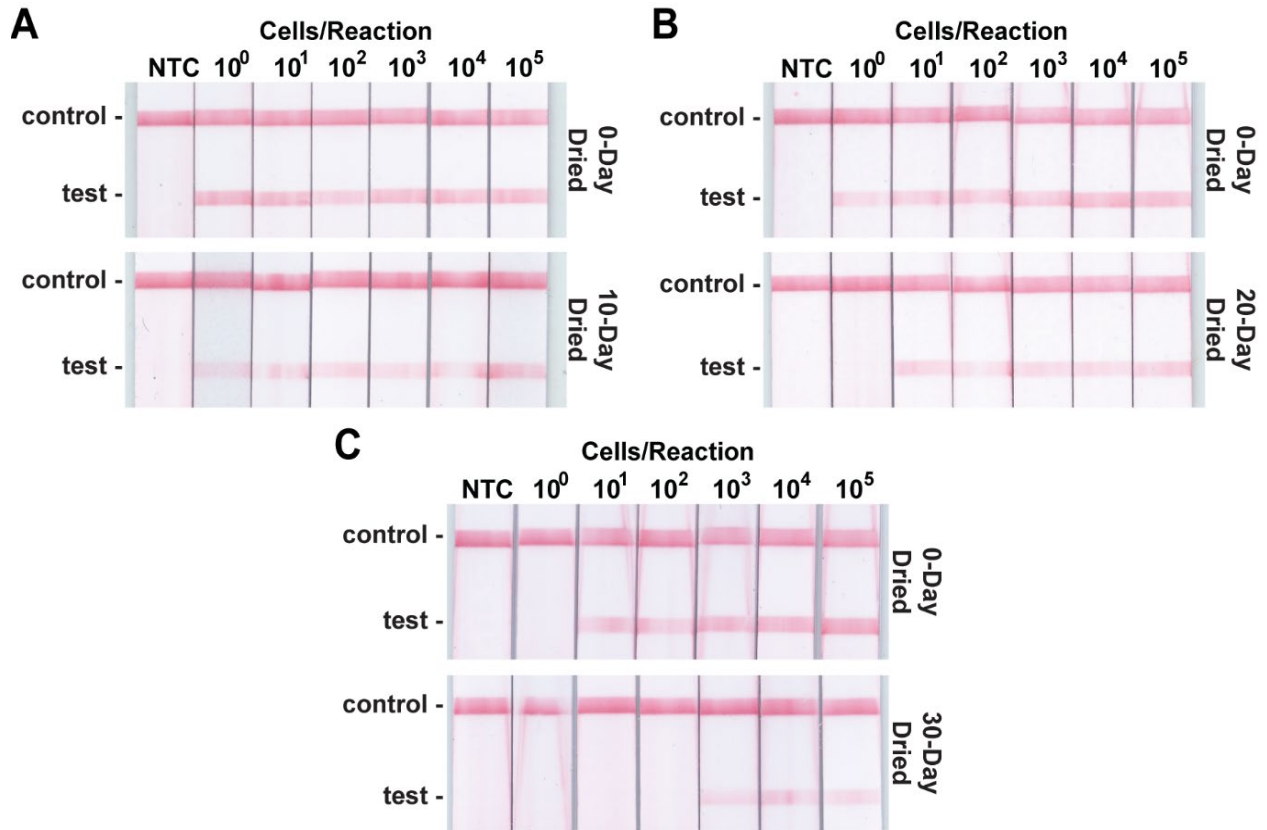


Figure B.4 LFIAs from *V. cholerae* SD-LAMP reagent stability study.

(A) Representative LFIAs at 10-day dried and respective fresh controls (0-day dried). (n=3) (B) Representative LFIAs at 20-day dried and respective fresh controls (0-day dried). (n=3) (C) Representative LFIAs at 30-day dried and respective fresh controls (0-day dried). (n=3) LFIA test band intensity decreases as reagent storage time increases.

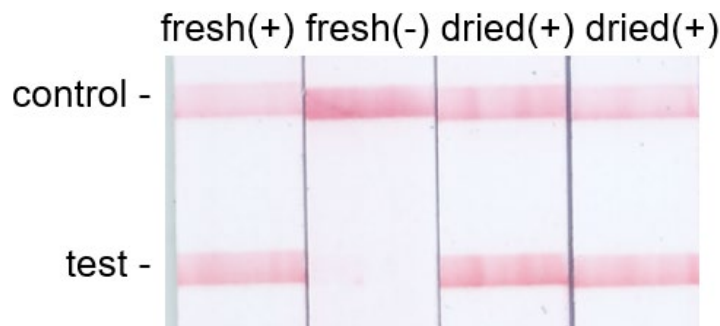


Figure B.5 HIV RT-LAMP reagents stored for 5 months at room temperature.

Dried reagents were reconstituted with 10⁶ virus copies/reaction and rehydrating mixture and amplified for 60 minutes alongside freshly prepared controls. (n=1)

APPENDIX C. SUPPLEMENT TO CHAPTER 4

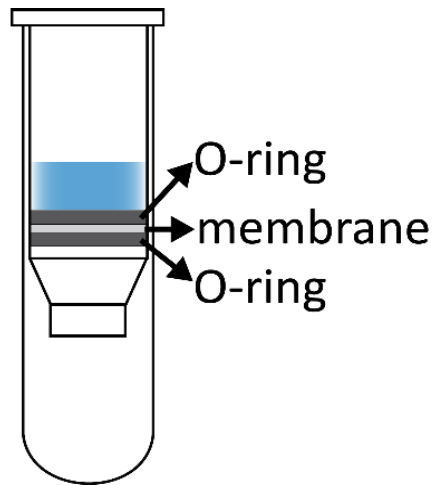


Figure C.1 Vertical filtration setup for testing membrane capture efficiency.

Membrane of interest was placed between two O-rings (after removing commercial filter in Qiagen spin column) and placed into spin column before particle solution was added.

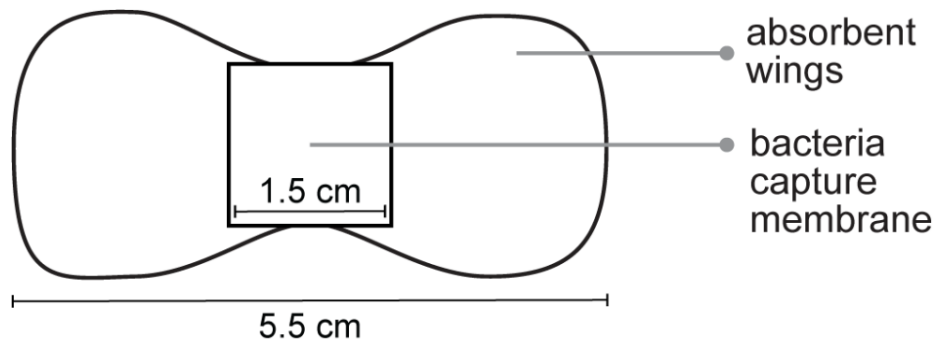


Figure C.2 Water filtration and bacteria capture setup.

Bacteria capture membrane is centered on top of absorbent wings. Water sample is added to the bacteria capture membrane. Water filters vertically through the membrane before wicking outwards into the absorbent wings while bacteria are trapped in the pores of the capture membrane.

Table C.1 Consumable components of *V. cholerae* μ PAD and cost.

	Component	Manufacturer	Product #	Cost/Device
μ PAD	0.22 μ m PES	Millipore	GPWP09050	\$ 0.14
	Glass Fiber	Millipore	GFCP103000	\$ 0.02
	Gel Blotting Paper	Whatman	GB003	\$ 0.01
	Cellulose for Valves	Whatman	3001-861	<\$ 0.01
	LFIA	Ustar Biotechnologies	U40009	\$ 1.80
	PET	Apollo	VPP100CE	<\$ 0.01
	Self-Seal PSA	Swingline	3747307B	\$ 0.05
	Microseal Seals	Bio-Rad	MSB1001	\$ 0.10
			<i>Subtotal</i>	\$ 2.12
SD-LAMP Reagents	Isothermal Buffer	New England Biolabs	B0537S	\$ 0.01
	Bst 2.0	New England Biolabs	M0537L	\$ 0.28
	dNTPs	Agilent Technologies	200415	\$ 0.17
	Betaine	Millipore Sigma	B0300-1VL	\$ 0.07
	B3	Integrated DNA Technologies	Custom	<\$ 0.01
	F3	Integrated DNA Technologies	Custom	<\$ 0.01
	FIP	Integrated DNA Technologies	Custom	<\$ 0.01
	BIP	Integrated DNA Technologies	Custom	<\$ 0.01
	LB-Biotin	Integrated DNA Technologies	Custom	\$ 0.07
	SD-FAM	Integrated DNA Technologies	Custom	\$ 0.04
	SD-Quench	Integrated DNA Technologies	Custom	\$ 0.05
	Dyes, Sucrose, Glycerol, Triton	Various	Various	\$ 0.01
			<i>Subtotal</i>	\$ 0.71
			Total	\$ 2.83

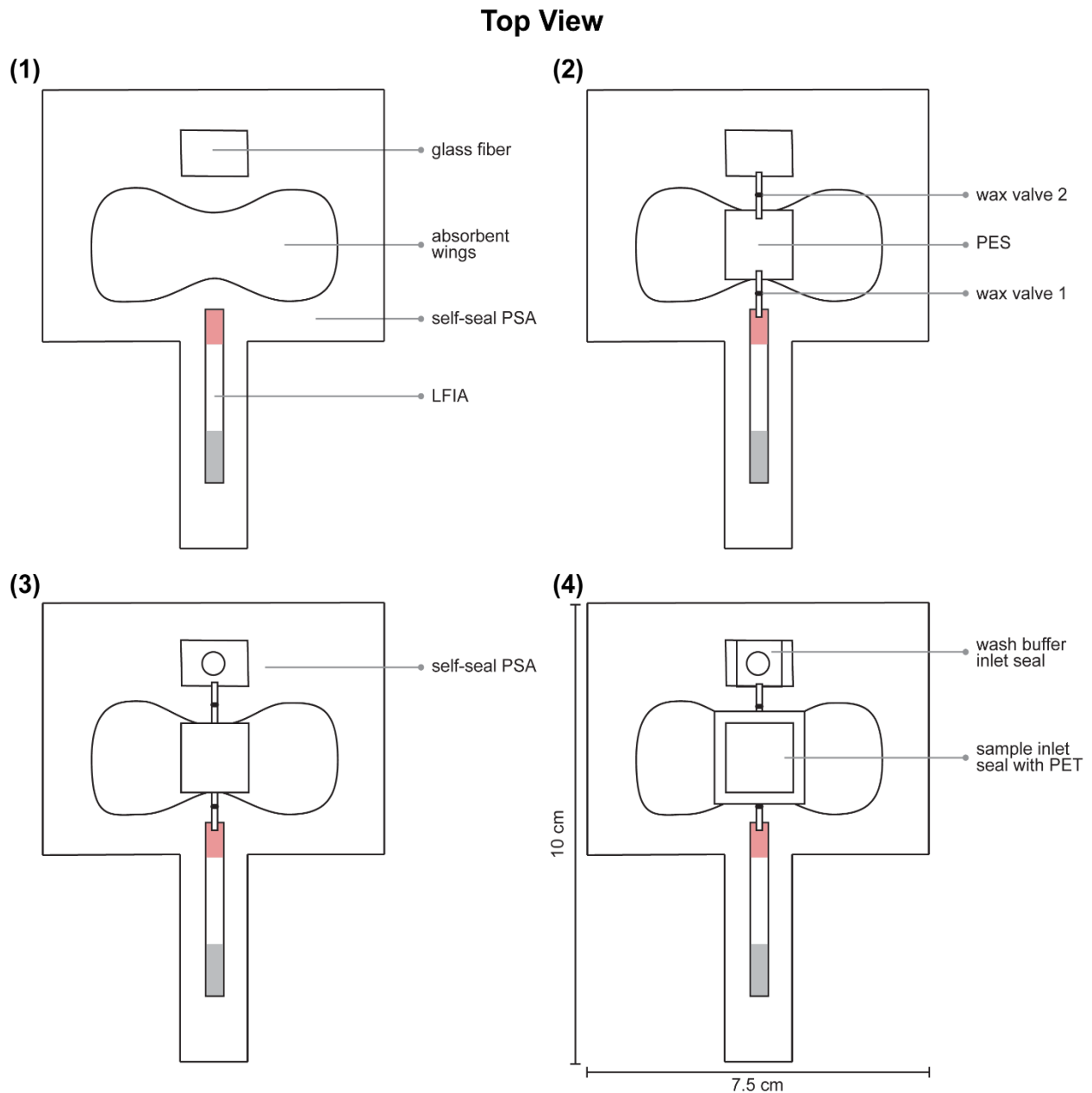


Figure C.3 *V. cholerae* μPAD assembly.

(1) Glass fiber, absorbent wings, and LFIA are placed on bottom self-seal PSA layer. (2) PES and wax valves are added. (3) The top self-seal PSA layer (with inlets for sample and wash buffer) is carefully aligned to seal the membranes. (4) After adding sample and wash buffer, inlets are sealed; sample inlet seal has PET to prevent adhesive from touching the amplification membrane.

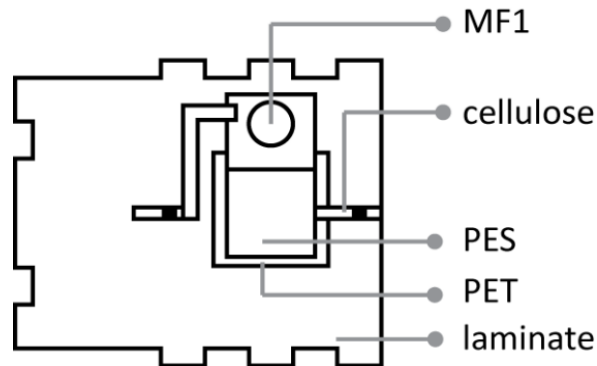


Figure C.4 Schematic of MF1/PES assembly for studies verifying red blood cell and virus separation.

Table C.2 Consumable components of microRAAD and cost.

	Component	Manufacturer	Cost/Device
μPAD	Glass fiber	Millipore	\$ 0.02
	MF1 blood separator	GE Life Sciences	<\$0.01
	0.22 μm polyethersulfone (PES)	Millipore	\$ 0.03
	Wax valve strips	Whatman & Xerox	<\$ 0.01
	Cellulose L	Whatman	<\$ 0.01
	Polyethylene terephthalate (PET)	Apollo	<\$ 0.01
	LFIA	Ustar Biotechnologies	\$ 1.80
	Self-seal PSA	Swingline	\$ 0.05
	Polystyrene gasket	Lohmann Precision Die Cutting	\$ 0.01
	Double-sided adhesive	Silhouette	<\$ 0.01
	<i>Subtotal</i>		<\$ 1.96
RT-LAMP Reagents	Isothermal buffer II	New England Biolabs	\$ 0.03
	dNTPs	Agilent Technologies	\$ 0.05
	Betaine	Millipore Sigma	\$ 0.03
	Primers	Integrated DNA Technologies	\$ 0.01
	Bst 3.0 polymerase	New England Biolabs	\$ 0.14
	Sucrose, Glycerol, TritonX-100, Green Dye, DEPC H ₂ O	Various	\$ 0.01
	<i>Subtotal</i>		\$ 0.27
	Consumable Total		\$ 2.23

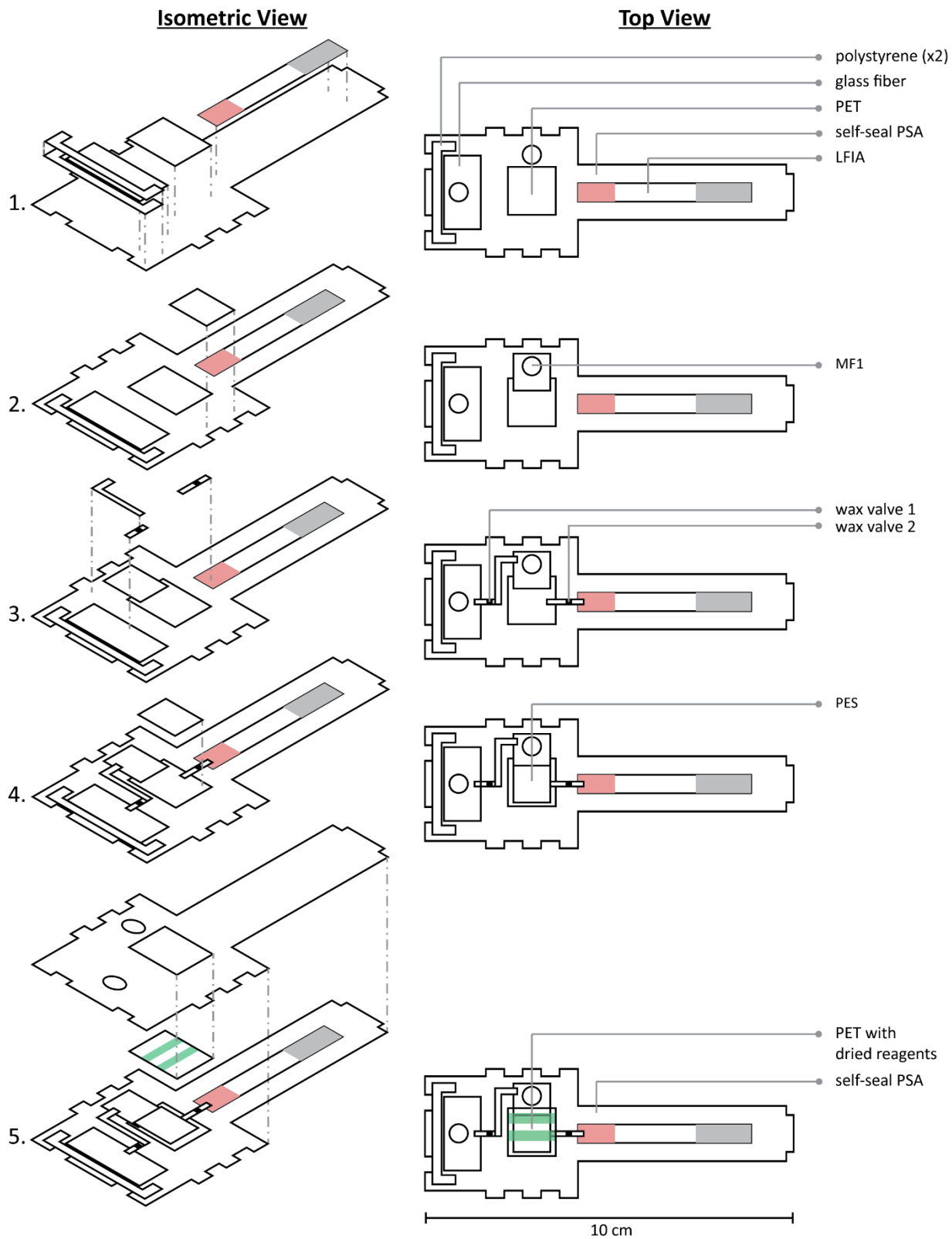


Figure C.5 Assembly of microRAAD μ PAD for HIV detection.

PES was sandwiched with squares of PET to prevent the self-seal PSA from touching the PES.

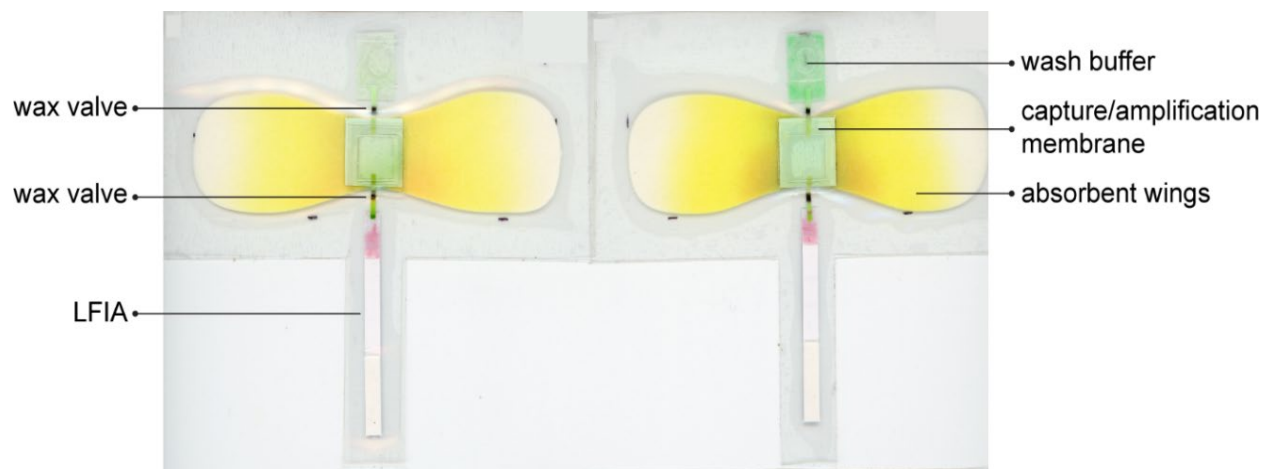


Figure C.6 Fluidic testing of integrated *V. cholerae* μ PAD with large absorbent wings.

Yellow food color solution represents the water sample (added to sample inlet), green food color solution represents the wash buffer (added to wash buffer inlet), and blue food color solution represents the rehydrating mixture (added to sample inlet). After heating the amplification zone and opening the wax valves, there was no flow from amplification zone to LFIA. (n=2)

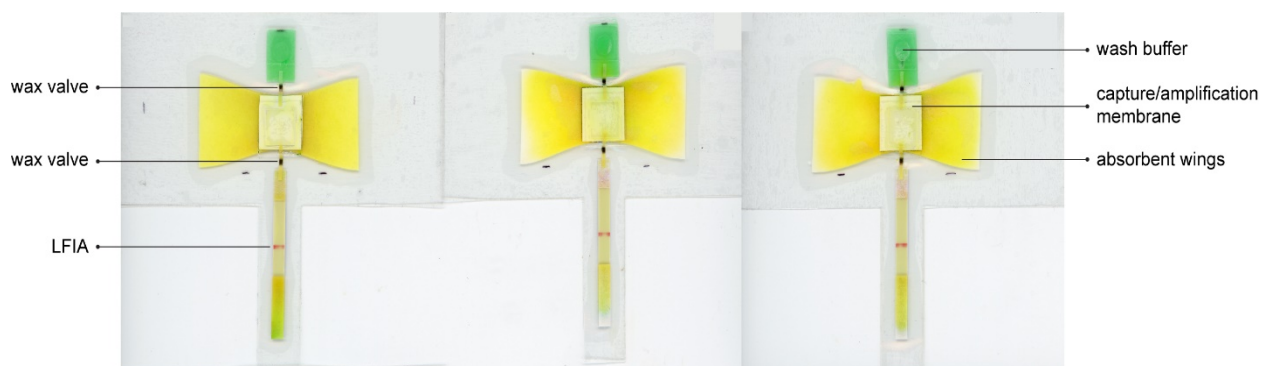


Figure C.7 Fluidic testing of integrated *V. cholerae* μ PAD with small absorbent wings.

Yellow food color solution represents the water sample (added to sample inlet), green food color solution represents the wash buffer (added to wash buffer inlet), and blue food color solution represents the rehydrating mixture (added to sample inlet). After heating the amplification zone and opening the wax valves, the LFIA flow control band confirmed proper flow. (n=3)

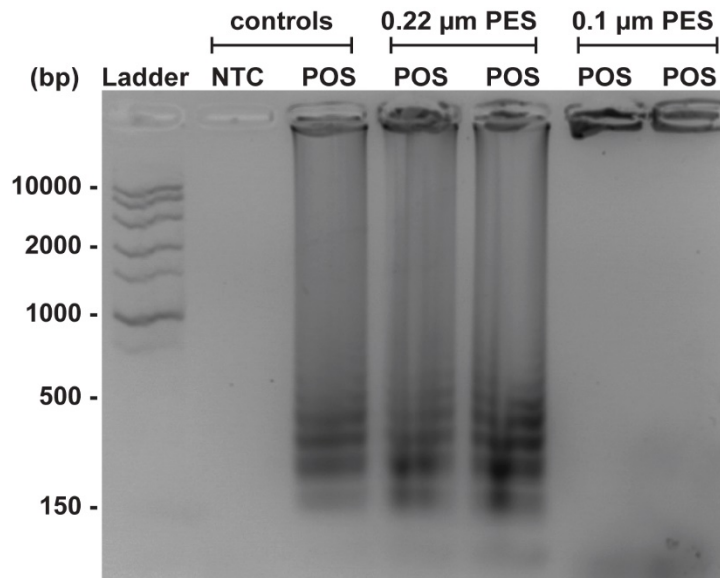


Figure C.8 HIV RT-LAMP in different membranes.

0.22 µm PES (Millipore) and 0.1 µm PES (PALL) membranes were added to tubes containing RT-LAMP master mix and HIV-1 RNA at 10^6 copies/reaction. Samples along with controls (no membrane added) were amplified for 60 minutes. Gel confirms amplification in 0.22 µm PES but not in 0.1 µm PES. (n=1)

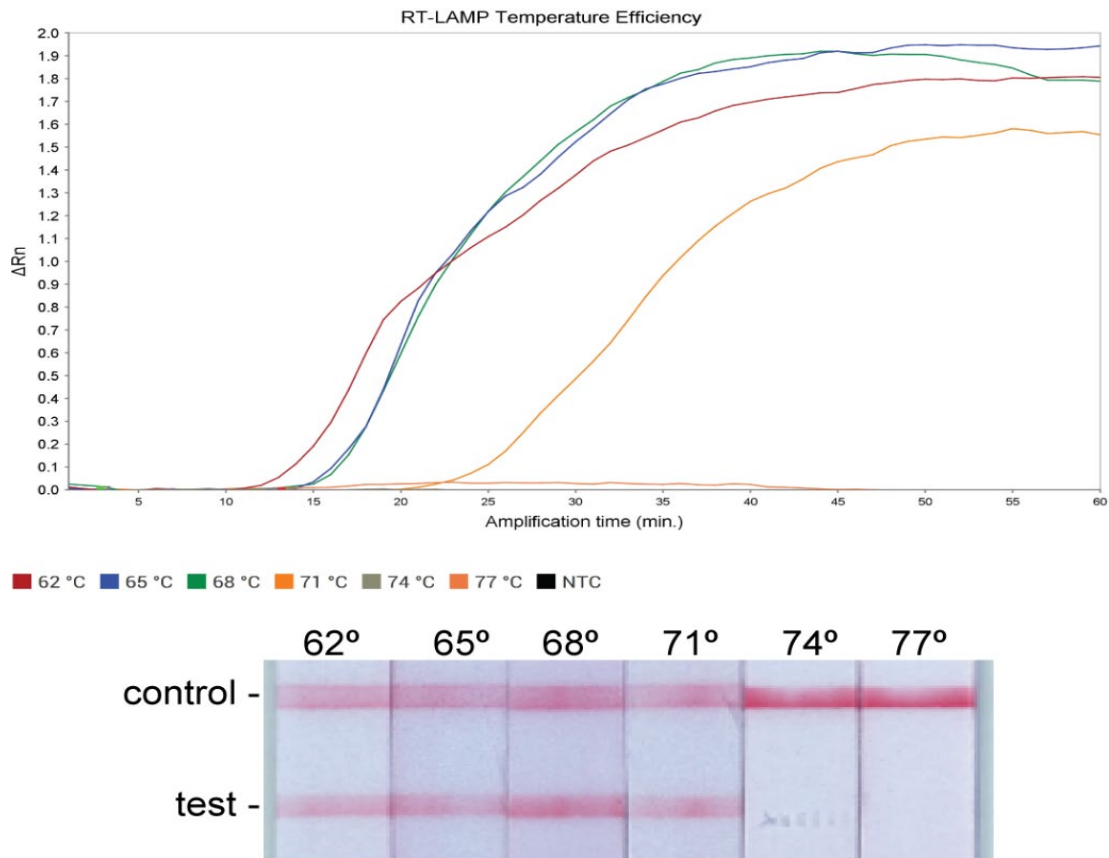


Figure C.9 HIV RT-LAMP assay efficiency at various temperatures.

Amplicons were analyzed via real-time fluorescence and LFIA after 60 minutes of heating at temperatures ranging from 62°C - 77°C. When the 10² RNA copies/reaction was heated between 62°C and 68°C, there was minimal change in time to amplification (real time fluorescence plot). When heated at 71°C, amplification was delayed and when heated above 74°C, no amplification occurred. This result aligns with New England Biolabs' product specification that reverse transcriptase is inactive above 72°C. Together, this indicates that this RT-LAMP assay for HIV is optimal between 62°C and 68°C. (n=1)

APPENDIX D. SUPPLEMENT TO CHAPTER 5

Table D.1 Average data from blinded study.

Particle diffusometry measurements were performed for four different groups. In the table (+) heat indicates the sample contained *V. cholerae* genomic DNA and underwent amplification, (-) heat indicates the sample contained no *V. cholerae* genomic DNA and underwent amplification, (+) no heat is a sample containing *V. cholerae* genomic DNA that did not undergo heating, and (-) no heat is a sample that does not contain *V. cholerae* genomic DNA that did not undergo heating. (n=3)

Sample	(+) heat	(-) heat	(+) no heat	(-) no heat
PD (η/η_0)	1.25±0.01	1.00±0.02	1.02±0.01	1.07±0.01

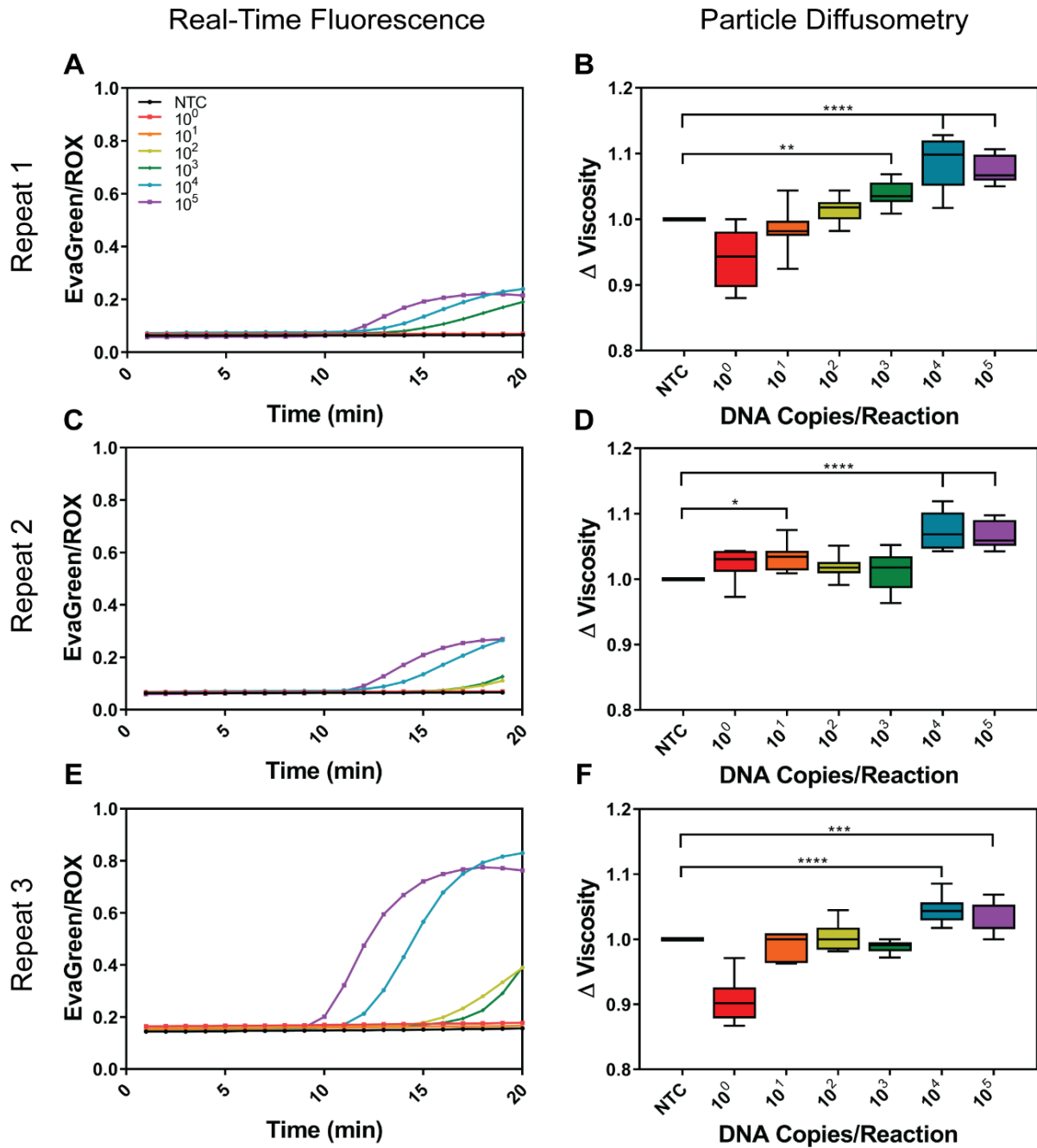


Figure D.1 Real-time fluorescence and PD measurements for DNA dilutions.

(A, C, E) Real-time fluorescence curves. (B, D, F) PD measurements were performed on the same samples as in (A, C, E). (B) PD measurements of viscosity change for the 10^3 , 10^4 , and 10^5 DNA copies/reaction samples are statistically significant (** $p < 0.01$, **** $p < 0.0001$). (D) PD measurements of viscosity change for the 10^1 , 10^4 , and 10^5 DNA copies/reaction samples are statistically significant (* $p < 0.05$, **** $p < 0.0001$). (F) PD measurements of viscosity change for the 10^4 and 10^5 DNA copies/reaction samples are statistically significant (** $p < 0.01$, **** $p < 0.0001$). A one-way ANOVA *post hoc* Dunnett's test was performed for all repeats with multiple comparisons against NTC with a 95% confidence interval.

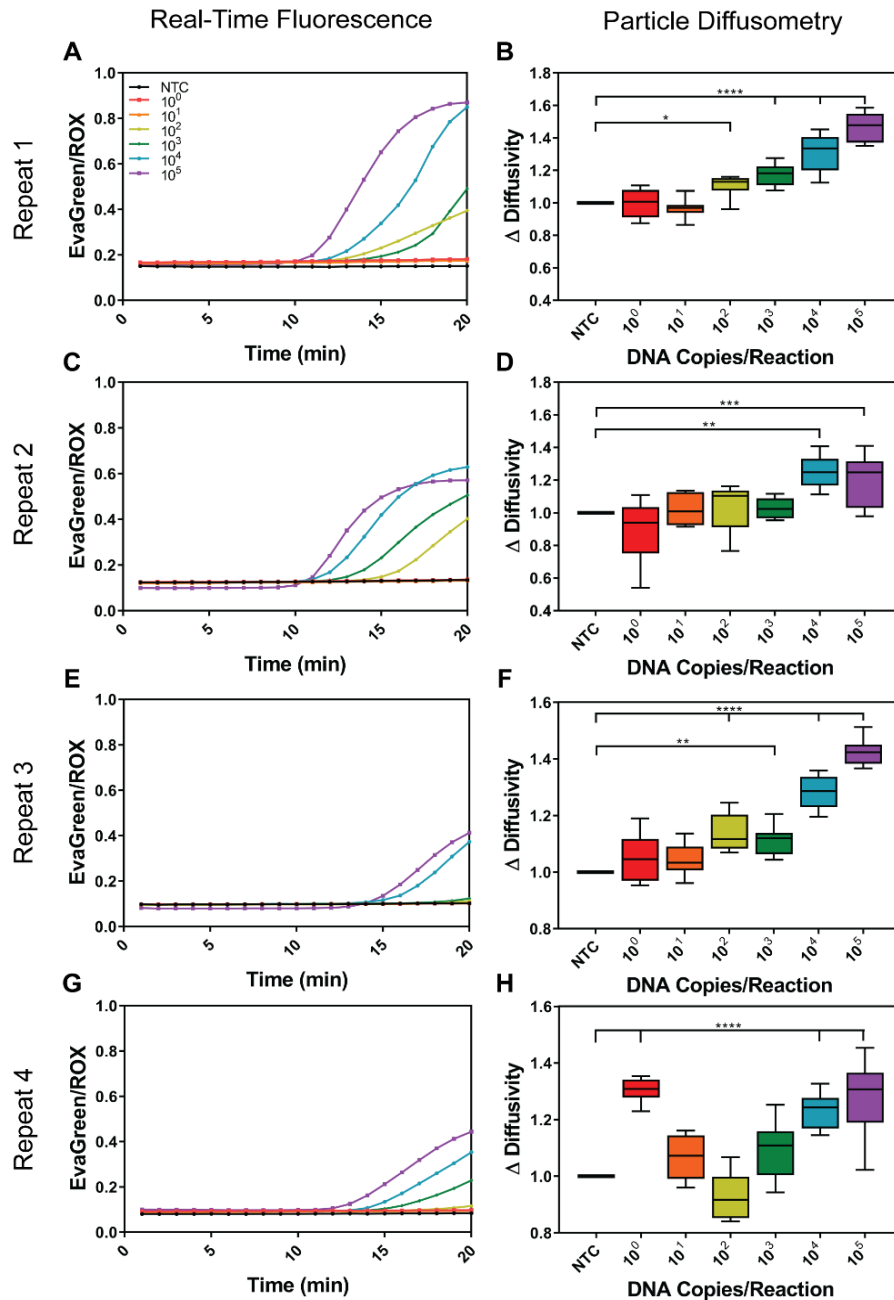


Figure D.2 Real-time fluorescence and PD measurements for biotinylated DNA dilutions.

(A, C, E, G) Real-time fluorescence curves. (B, D, F, H) PD measurements were performed on the same samples as in (A, C, E, G). (B) PD measurements of diffusivity change for the 10^2 , 10^3 , 10^4 , and 10^5 DNA copies/reaction are statistically significant (* $p < 0.05$, **** $p < 0.0001$). (D) PD measurements of diffusivity change for the 10^4 and 10^5 DNA copies/reaction are statistically significant (** $p < 0.01$, *** $p < 0.001$). (F) PD measurements of diffusivity change for the 10^2 , 10^3 , 10^4 , and 10^5 DNA copies/reaction are statistically significant (** $p < 0.01$, **** $p < 0.0001$). (H) PD measurements of diffusivity change for the 10^0 , 10^4 , and 10^5 DNA copies/reaction are statistically significant (**** $p < 0.0001$). A one-way ANOVA *post hoc* Dunnett's test was performed for all repeats with multiple comparisons against NTC with a 95% confidence interval.

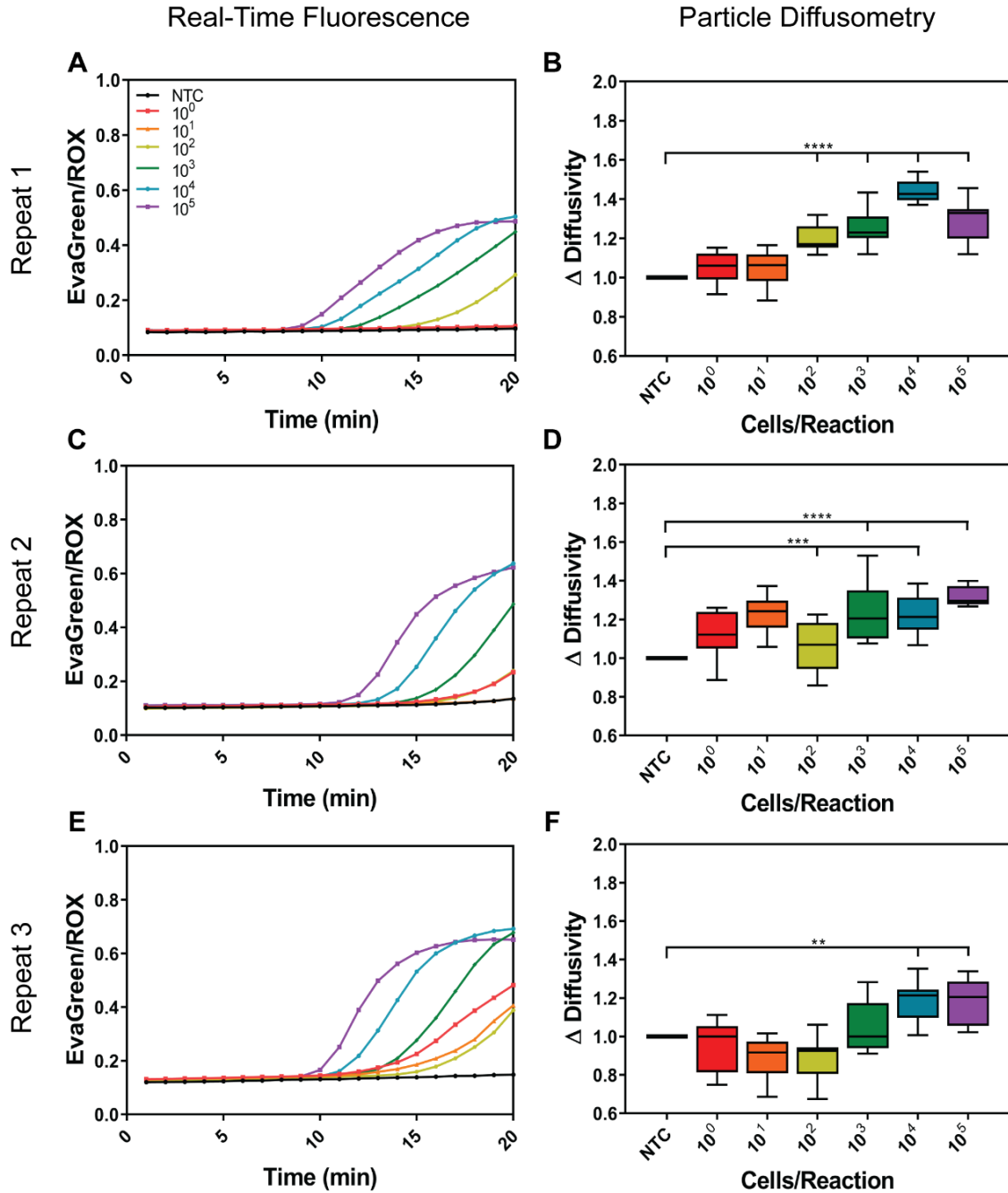


Figure D.3 Real-time fluorescence and PD measurements for biotinylated DNA from whole *V. cholerae* cell dilutions.

(A, C, E) Real-time fluorescence curves. (B, D, F) PD measurements were performed on the same samples as in (A, C, E). (B) PD measurements of diffusivity change for the 10^2 , 10^3 , 10^4 , and 10^5 cells/reaction are statistically significant (**** $p < 0.0001$). (D) PD measurements of diffusivity change for the 10^2 , 10^3 , 10^4 , and 10^5 cells/reaction are statistically significant (** $p < 0.01$, **** $p < 0.0001$). (F) PD measurements of diffusivity change for the 10^4 and 10^5 cells/reaction are statistically significant (** $p < 0.01$). A one-way ANOVA *post hoc* Dunnett's test was performed for all repeats with multiple comparisons against NTC with a 95% confidence interval.

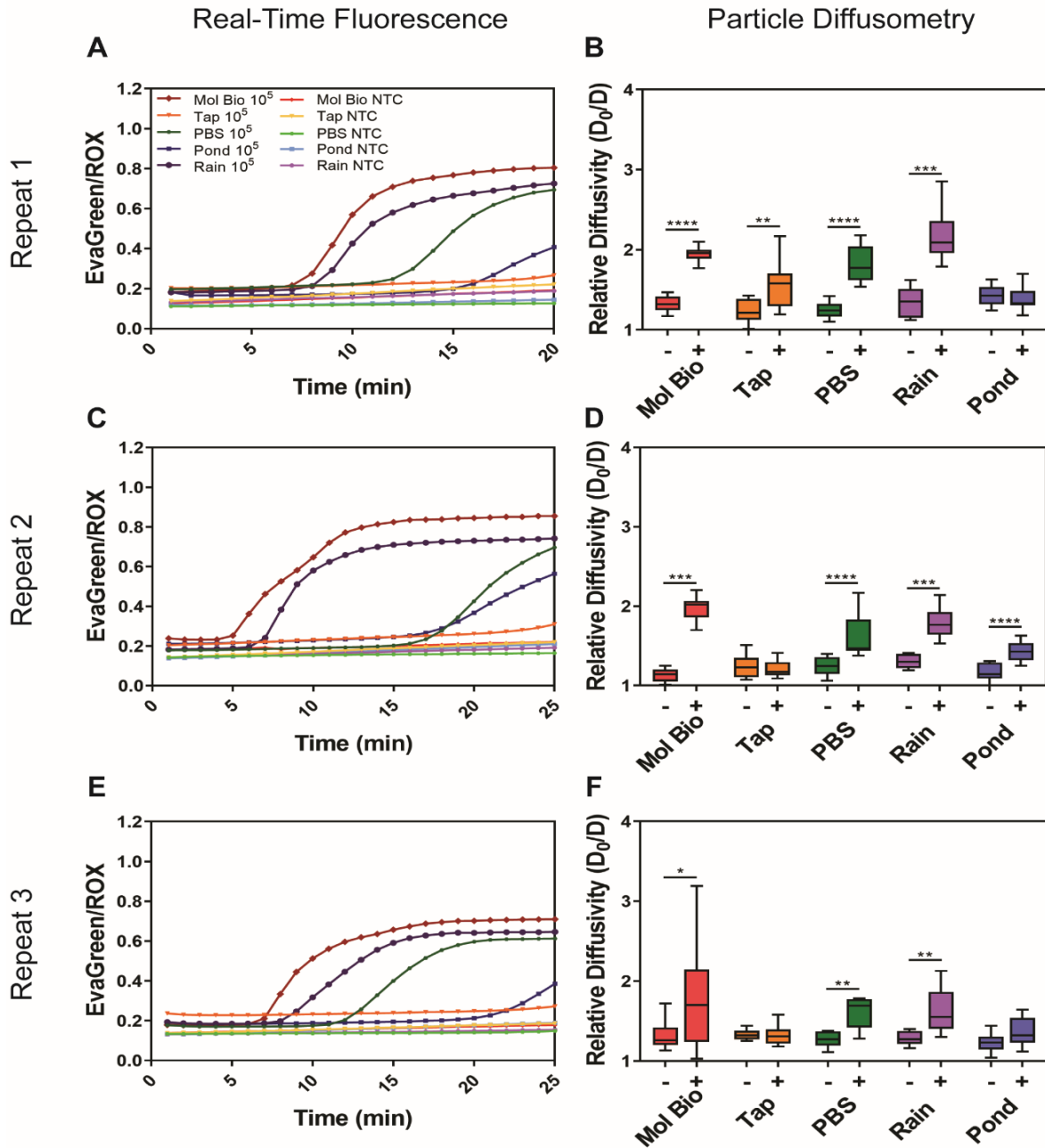


Figure D.4 Real-time fluorescence and PD measurements for biotinylated DNA from whole *V. cholerae* cells spiked in various water samples.

(A, C, E) Real-time fluorescence curves. (B, D, F) PD measurements were performed on the same samples as in (A, C, E). (B) PD measurements of relative diffusivity for Molecular Biology Water (Mol Bio), Tap, PBS, and Rain are statistically significant (** $p < 0.01$, *** $p < 0.001$, **** $p < 0.0001$). (D) PD measurements of relative diffusivity for Mol Bio, PBS, Rain, and Pond are statistically significant (*** $p < 0.001$, **** $p < 0.0001$). (F) PD measurements of relative diffusivity for Mol Bio, PBS, and Rain are statistically significant (* $p < 0.05$, ** $p < 0.01$). A Student's paired t -test with a 95% confidence interval was used when comparing the negative control and positive samples in different water.

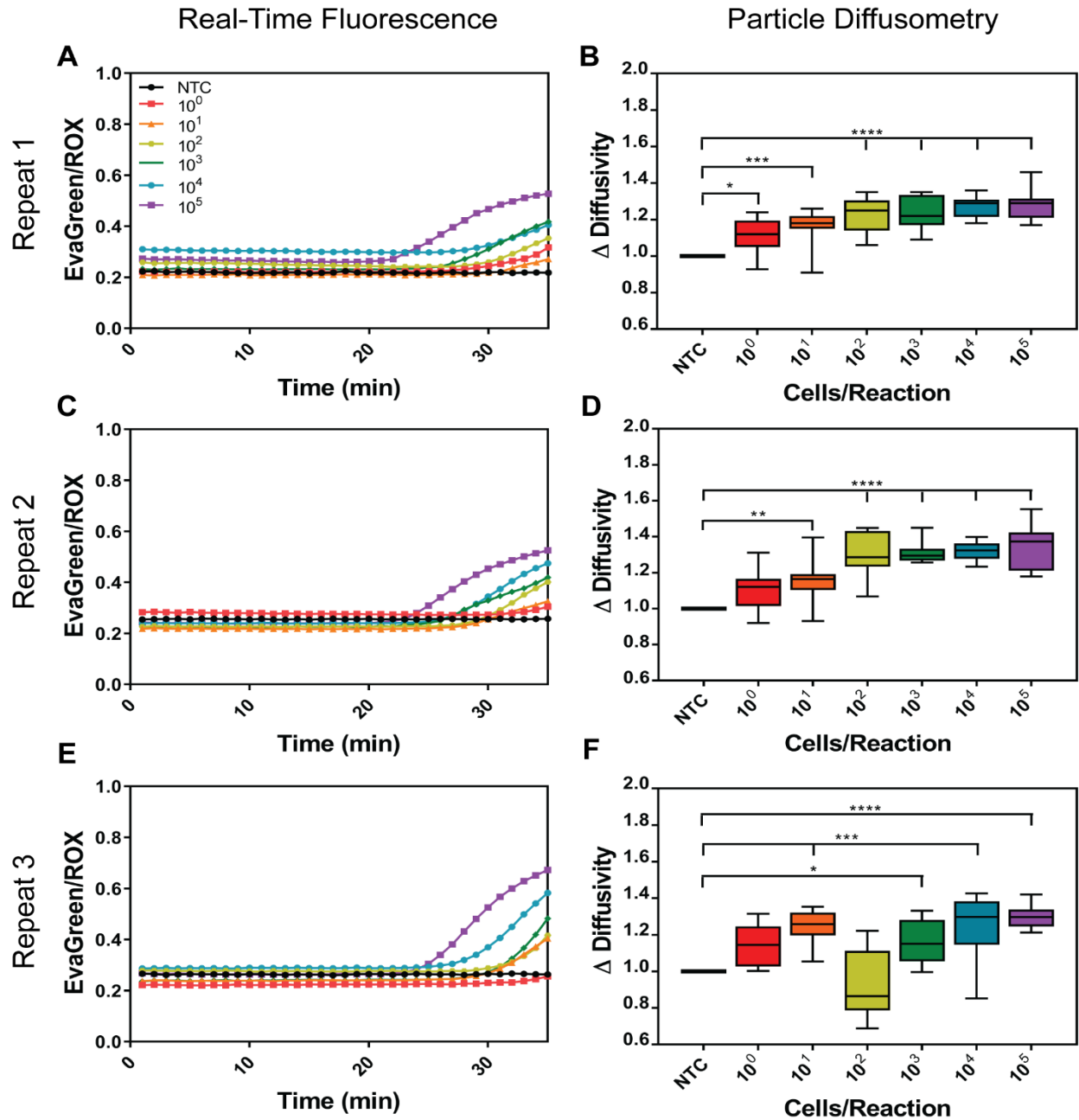


Figure D.5 Real-time fluorescence and PD measurements for biotinylated DNA from whole *V. cholerae* cell dilutions spiked in pond water.

(A, C, E) Real-time fluorescence curves. (B, D, F) PD measurements were performed on the same samples as in (A, C, E). (B) PD measurements of diffusivity change for the 10^0 , 10^1 , 10^2 , 10^3 , 10^4 , and 10^5 cells/reaction are statistically significant (* $p < 0.05$, *** $p < 0.001$, **** $p < 0.0001$). (D) PD measurements of diffusivity change for the 10^1 , 10^2 , 10^3 , 10^4 , and 10^5 cells/reaction are statistically significant (** $p < 0.01$, **** $p < 0.0001$). (F) PD measurements of diffusivity change for the 10^1 , 10^3 , 10^4 , and 10^5 cells/reaction are statistically significant (* $p < 0.05$, *** $p < 0.001$, **** $p < 0.0001$). A one-way ANOVA *post hoc* Dunnett's test was performed for all repeats with multiple comparisons against NTC with a 95% confidence interval.

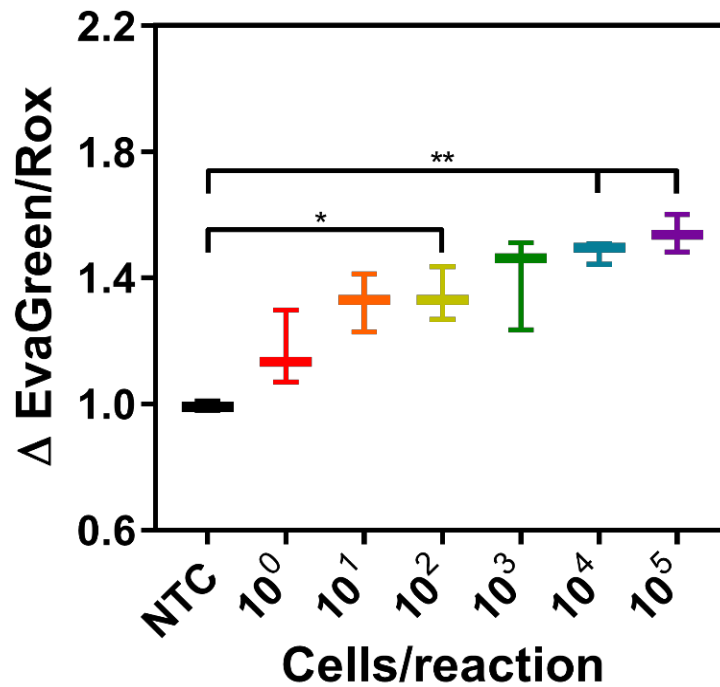


Figure D.6 Fluorescence measurements for biotinylated DNA from whole *V. cholerae* cell dilutions spiked in pond water.

Cells were spiked in pond water at concentrations $10^0 - 10^5$ cells/reaction. The change in EvaGreen/Rox is significant at 10^2 , 10^4 , and 10^5 (* $p < 0.05$, ** $p < 0.01$) cells/reaction compared to NTC. A one-way ANOVA *post hoc* Dunnett's test was performed for all repeats with multiple comparisons against NTC with a 95% confidence interval. (n=3)

APPENDIX E. SUPPLEMENT TO CHAPTER 6

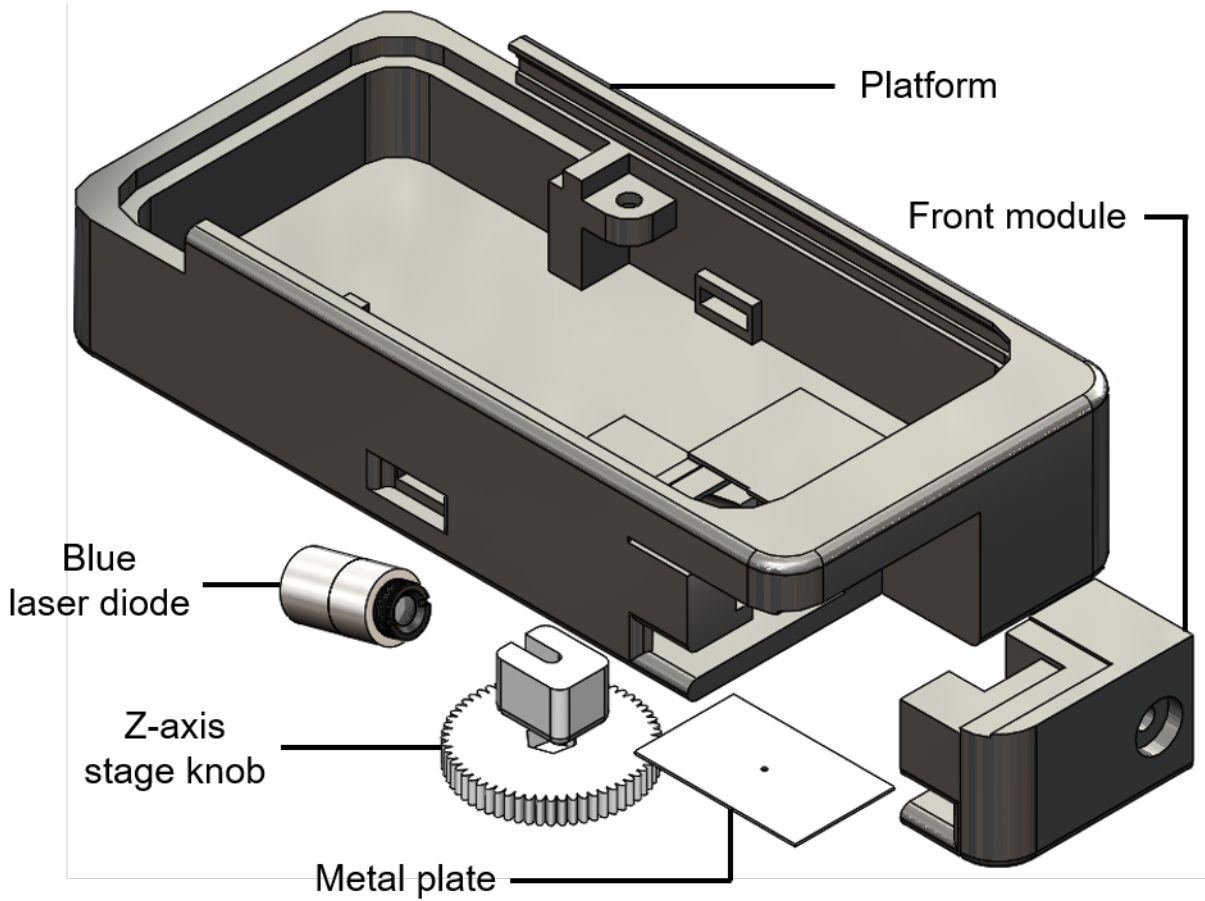


Figure E.1 Exploded CAD model of the platform.

Clockwise: Main platform to house circuitry, front module (used to secure metal plate and z-axis stage knob), metal plate, z-axis stage knob, and blue laser diode.

System Usability Study Survey for Bacterial Concentrator Device

Principal Investigator: Dr. Jacqueline C. Linnes

1. I think that I would like to use this system frequently.

Strongly Disagree						Strongly Agree
1	2	3	4	5		

2. I found the system unnecessarily complex.

Strongly Disagree						Strongly Agree
1	2	3	4	5		

3. I thought the system was easy to use.

Strongly Disagree						Strongly Agree
1	2	3	4	5		

4. I think that I would need the support of a technical person to be able to use this system.

Strongly Disagree						Strongly Agree
1	2	3	4	5		

5. I found the various functions in this system were well integrated.

Strongly Disagree						Strongly Agree
1	2	3	4	5		

6. I thought there was too much inconsistency in this system.

Strongly Disagree						Strongly Agree
1	2	3	4	5		

7. I would imagine that most people would learn to use this system very quickly.

Strongly Disagree						Strongly Agree
1	2	3	4	5		

8. I found the system very cumbersome to use.

Strongly Disagree						Strongly Agree
1	2	3	4	5		

9. I felt very confident using the system.

Strongly Disagree						Strongly Agree
1	2	3	4	5		

10. I needed to learn a lot of things before I could get going with this system.

Strongly Disagree						Strongly Agree
1	2	3	4	5		

Figure E.2 System Usability Study (SUS) survey.

Participant survey for assessment of the *V. cholerae* concentrator device in user-centered design study.

Table E.1 Cost of the consumable components of the smartphone-based PD-LAMP system.

	Component	Manufacturer	Cost/Test
Microfluidic Chip	60 μ m COP	Zeon	\$ 0.02
	188 μ m COP	Zeon	\$0.26
	iCraft Double-Sided Tape	Amazon	\$ 0.01
	400 nm streptavidin particles	Bangs Laboratories	\$ 0.10
<i>Subtotal</i>			<i>\$ 0.39</i>
LAMP Reagents	Isothermal Buffer	New England Biolabs	< \$ 0.01
	dNTPs	Agilent Technologies	\$ 0.10
	Betaine	Millipore Sigma	\$ 0.04
	Primers	Integrated DNA Technologies	\$ 0.05
	Bst 2.0 Polymerase	New England Biolabs	\$ 0.17
	EvaGreen	Biotium	\$ 0.01
	ROX	Thermo Fisher Scientific	\$ 0.02
<i>Subtotal</i>			<i>\$ 0.39</i>
Consumable Total			\$ 0.78

Table E.2 Cost of the reusable components of smartphone-based PD system.

	Component	Manufacturer	Cost/Device
Optics	0.5 mm N-BK7 Ball Lens	Edmund Optics	\$ 29.50
	#12 Straw Cinegel Film Filter	Roscolux	< \$ 0.01
	80-mW Blue Laser Module	LaserLand / Osram	\$ 24.48
	304 Stainless Steel Sheets	McMaster-Carr	\$ 0.04
<i>Subtotal</i>			<i>\$ 54.02</i>
Smartphone-Based Platform	3D printed parts	Stratasys (ABS-M30 / SR-30)	\$ 23.39
	Hex Head Screws	McMaster-Carr	\$ 0.08
	Stainless Steel Hex Nuts	McMaster-Carr	\$ 0.06
	PowerBoost 1000 Charger	Adafruit	\$ 19.95
	Li-Ion Battery 3.7V 2500mAh	Adafruit	\$ 14.95
	Slider Switch	Digikey	\$ 0.48
	iPhone 6	Apple	\$ 150.00
<i>Subtotal</i>			<i>\$ 208.91</i>
Reusable Total			\$ 262.93

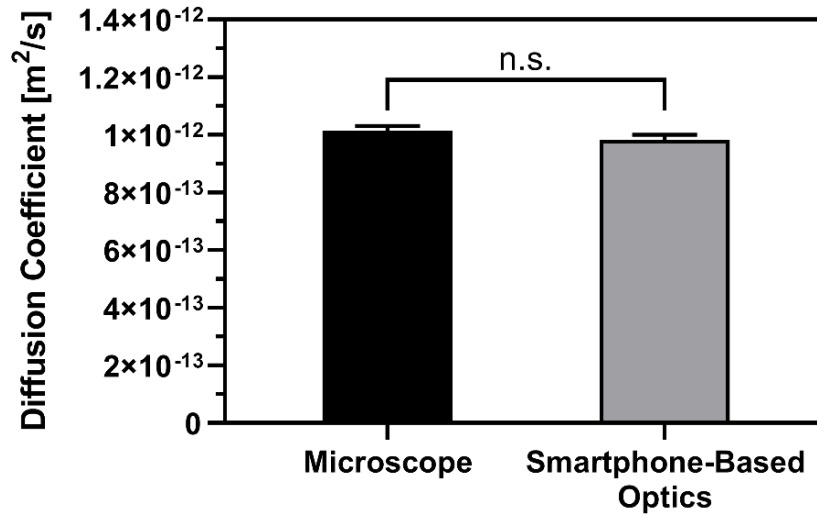


Figure E.3 Comparison of microscope and smartphone-based optical system.

The average diffusion coefficients for water samples using the microscope and the smartphone-based optical system are $1.02 \times 10^{-12} \pm 1.57 \times 10^{-14} \text{ m}^2/\text{s}$ and $9.83 \times 10^{-13} \pm 1.83 \times 10^{-14} \text{ m}^2/\text{s}$, respectively, showing no significant difference (ns = no significance). (n=12)

Table E.3 C_T values from LOD study.

C_T values are not available (NA) for samples that did not amplify. (n=5)

Sample	C _T Values
NTC	NA
6×10^0	25.6 ± 4.5
6×10^1	21.4 ± 2.6
6×10^2	21.1 ± 2.5
6×10^3	18.2 ± 4.5
6×10^4	15.8 ± 4.2

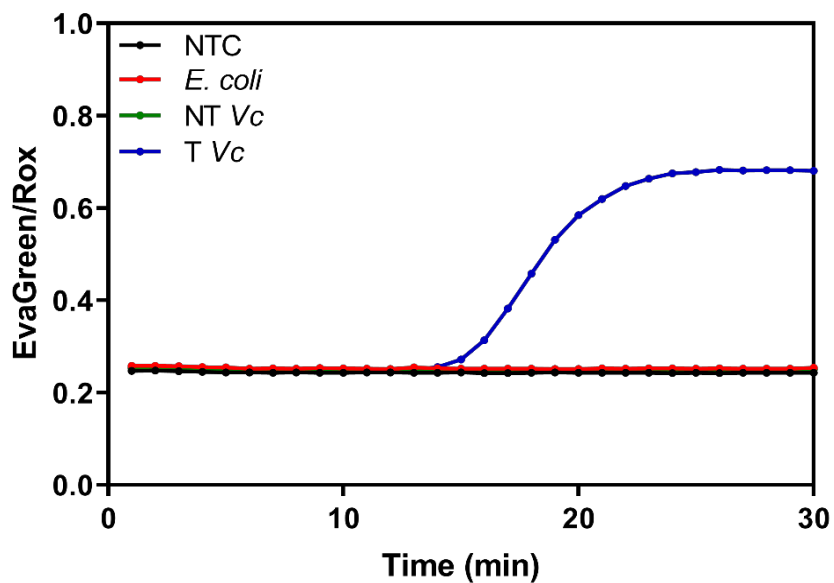


Figure E.4 Representative real-time fluorescence curves over a 30-minute LAMP reaction for selectivity study.

Table E.4 C_T values from selectivity study.

C_T values are not available (NA) for samples that did not amplify. (n=5)

Sample	C _T Values
NTC	NA
<i>E. coli</i>	NA
Non-toxigenic <i>V. cholerae</i>	NA
Toxigenic <i>V. cholerae</i>	14.8 ± 2.7

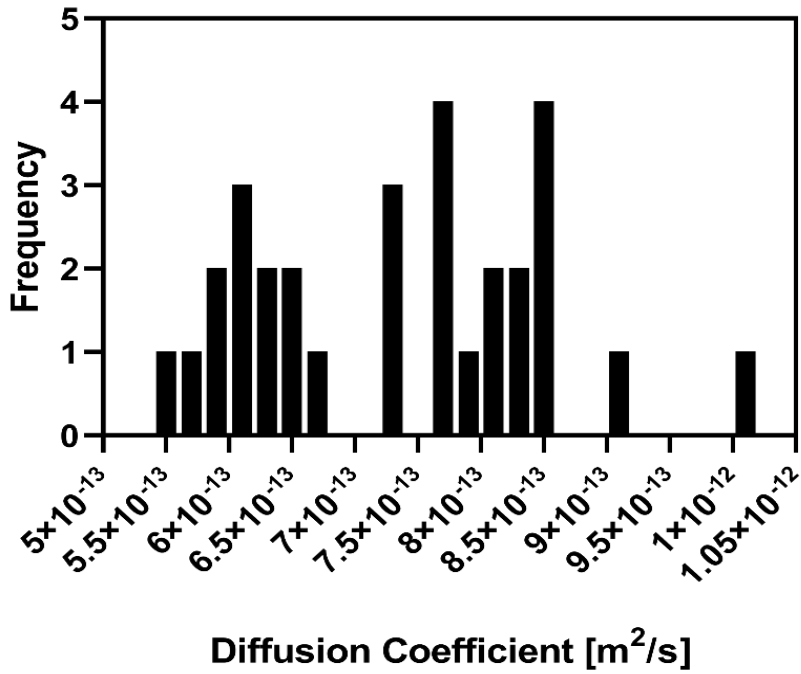


Figure E.5 Diffusion coefficients of training set samples.

The frequency of training set samples plotted in a histogram over a range of averaged diffusion coefficients. (n=30) There is a clear gap (7.0×10^{-13} - 7.5×10^{-13}) between the positive and negative sample clusters.

Table E.5 Real-time fluorescence results and diffusion coefficients for training set samples. (n=30)

Real-Time Fluorescence Result	Diffusion Coefficient
Positive	5.53×10^{-13}
Positive	5.66×10^{-13}
Positive	5.82×10^{-13}
Positive	5.95×10^{-13}
Positive	6.09×10^{-13}
Positive	6.15×10^{-13}
Positive	6.15×10^{-13}
Positive	6.25×10^{-13}
Positive	6.33×10^{-13}
Negative	6.51×10^{-13}
Positive	6.57×10^{-13}
Positive	6.69×10^{-13}
Positive	7.26×10^{-13}
Negative	7.31×10^{-13}
Positive	7.39×10^{-13}
Negative	7.66×10^{-13}
Negative	7.71×10^{-13}
Negative	7.72×10^{-13}
Negative	7.78×10^{-13}
Negative	7.96×10^{-13}
Negative	8.02×10^{-13}
Negative	8.14×10^{-13}
Positive	8.27×10^{-13}
Negative	8.36×10^{-13}
Positive	8.40×10^{-13}
Negative	8.41×10^{-13}
Negative	8.44×10^{-13}
Negative	8.59×10^{-13}
Negative	9.14×10^{-13}
Negative	1.00×10^{-12}

REFERENCES

- (1) Sharma, S.; Zapatero-Rodríguez, J.; Estrela, P.; O’Kennedy, R. Point-of-Care Diagnostics in Low Resource Settings: Present Status and Future Role of Microfluidics. *Biosensors* **2015**, *5* (3), 577–601. <https://doi.org/10.3390/bios5030577>.
- (2) Yager, P.; Domingo, G. J.; Gerdes, J. Point-of-Care Diagnostics for Global Health. *Annu. Rev. Biomed. Eng.* **2008**, *10* (1), 107–144. <https://doi.org/10.1146/annurev.bioeng.10.061807.160524>.
- (3) Yetisen, A. K.; Akram, M. S.; Lowe, C. R. Paper-Based Microfluidic Point-of-Care Diagnostic Devices. *Lab Chip* **2013**, *13* (12), 2210–2251. <https://doi.org/10.1039/C3LC50169H>.
- (4) Shields, D. World In Vitro Diagnostics (IVD) Market - Opportunities and Forecasts, 2013 - 2020 . 2014, pp 1–152.
- (5) Kozel, T. R.; Burnham-Marusich, A. R. Point-of-Care Testing for Infectious Diseases: Past, Present, and Future. *J. Clin. Microbiol.* **2017**, *55* (8), 2313–2320. <https://doi.org/10.1128/JCM.00476-17>.
- (6) Abbott. iSTAT US Cartridge Menu.
- (7) Sperança, M. A.; Suzuki, R. B.; Cabral, A. D.; Carmo, A. M. dos S. Nucleic Acid-Based Diagnosis and Epidemiology of Infectious Diseases. In *Nucleic Acids - From Basic Aspects to Laboratory Tools*; InTech, 2016. <https://doi.org/10.5772/61965>.
- (8) Tomazelli Coltro, W. K.; Cheng, C.-M.; Carrilho, E.; de Jesus, D. P. Recent Advances in Low-Cost Microfluidic Platforms for Diagnostic Applications. *Electrophoresis* **2014**, *35* (16), 2309–2324. <https://doi.org/10.1002/elps.201400006>.
- (9) Abe, K.; Suzuki, K.; Citterio, D. Inkjet-Printed Microfluidic Multianalyte Chemical Sensing Paper. *Anal. Chem.* **2008**, *80* (18), 6928–6934. <https://doi.org/10.1021/ac800604v>.
- (10) Kumar, A. A.; Hennek, J. W.; Smith, B. S.; Kumar, S.; Beattie, P.; Jain, S.; Rolland, J. P.; Stossel, T. P.; Chunda-Liyoka, C.; Whitesides, G. M. From the Bench to the Field in Low-Cost Diagnostics: Two Case Studies. *Angew. Chem. Int. Ed. Engl.* **2015**, *54* (20), 5836–5853. <https://doi.org/10.1002/anie.201411741>.
- (11) Kosack, C. S.; Page, A.-L.; Klatser, P. R. A Guide to Aid the Selection of Diagnostic Tests. *Bull. World Health Organ.* **2017**, *95* (9), 639–645. <https://doi.org/10.2471/BLT.16.187468>.

- (12) Lemaire, J. *Side-by-Side Analysis of HIV POC Early Infant Diagnostic Products*; 2017.
- (13) Rodriguez, N. M.; Wong, W. S.; Liu, L.; Dewar, R.; Klapperich, C. M. A Fully Integrated Paperfluidic Molecular Diagnostic Chip for the Extraction, Amplification, and Detection of Nucleic Acids from Clinical Samples. *Lab Chip* **2016**, *16* (4), 753–763. <https://doi.org/10.1039/C5LC01392E>.
- (14) Lafleur, L.; Bishop, J. D.; Heiniger, E. K.; Gallagher, R. P.; Wheeler, M. D.; Kauffman, P. C.; Zhang, X.; Kline, E.; Buser, J.; Ramachandran, S.; et al. A Rapid, Instrument-Free, Sample-to-Result Nucleic Acid Amplification Test. *Lab Chip* **2016**. <https://doi.org/10.1039/C6LC00677A>.
- (15) Linnes, J. C.; Fan, A.; Rodriguez, N. M.; Lemieux, B.; Kong, H.; Klapperich, C. M.; Boyle, D.; Weigl, B.; Hong, J.; Kohn, D.; et al. Paper-Based Molecular Diagnostic for Chlamydia Trachomatis. *RSC Adv.* **2014**, *4* (80), 42245–42251. <https://doi.org/10.1039/C4RA07911F>.
- (16) Damhorst, G. L.; Duarte-Guevara, C.; Chen, W.; Ghonge, T.; Cunningham, B. T.; Bashir, R. Smartphone-Imaged HIV-1 Reverse-Transcription Loop-Mediated Isothermal Amplification (RT-LAMP) on a Chip from Whole Blood. *Eng. (Beijing, China)* **2015**, *1* (3), 324–335. <https://doi.org/10.15302/J-ENG-2015072>.
- (17) Abbott. i-STAT Handheld Blood Analyzer <https://www.pointofcare.abbott/us/en/offerings/istat/istat-handheld> (accessed Mar 26, 2019).
- (18) Abbott. I-STAT in the Medical Tent. 2018.
- (19) Koydemir, H. C.; Gorocs, Z.; Tseng, D.; Cortazar, B.; Feng, S.; Yan, R.; Chan, L.; Burbano, J.; Mcleod, E.; Ozcan, A. Rapid Imaging, Detection and Quantification of Giardia Lamblia Cysts Using Mobile-Phone Based Fluorescent Microscopy and Machine Learning. *Lab Chip* **2015**, *15*, 1284–1293. <https://doi.org/10.1039/c4lc01358a>.
- (20) Zhdanov, A.; Keefe, J.; Franco-Waite, L.; Konnaiyan, K. R.; Pyayt, A. Mobile Phone Based ELISA (MELISA). *Biosens. Bioelectron.* **2018**, *103*, 138–142. <https://doi.org/10.1016/J.BIOS.2017.12.033>.
- (21) Leavitt, S. A. A Thin Blue Line: The History of the Pregnancy Test Kit. The Office of NIH History 2003.

- (22) Choi, J. R.; Hu, J.; Gong, Y.; Feng, S.; Bakar Wan Abas, W. A.; Pinguan-Murphy, B.; Xu, F. An Integrated Lateral Flow Assay for Effective DNA Amplification and Detection at the Point of Care. *R. Soc. Chem.* **2016**, *141*, 2930–2941.
- (23) Verma, M. S.; Tsaloglou, M.-N.; Sisley, T.; Christodouleas, D.; Chen, A.; Milette, J.; Whitesides, G. M. Sliding-Strip Microfluidic Device Enables ELISA on Paper. **2017**. <https://doi.org/10.1016/j.bios.2017.07.034>.
- (24) Chin, C. D.; Linder, V.; Sia, S. K. Commercialization of Microfluidic Point-of-Care Diagnostic Devices. *Lab Chip* **2012**, *12* (12), 2118–2134. <https://doi.org/10.1039/C2LC21204H>.
- (25) Mothershed, E. A.; Whitney, A. M. Nucleic Acid-Based Methods for the Detection of Bacterial Pathogens: Present and Future Considerations for the Clinical Laboratory. *Clin. Chim. Acta* **2006**, *363* (1–2), 206–220. <https://doi.org/http://dx.doi.org/10.1016/j.cccn.2005.05.050>.
- (26) Lui, C.; Cady, N. C.; Batt, C. A. Nucleic Acid-Based Detection of Bacterial Pathogens Using Integrated Microfluidic Platform Systems. *Sensors (Basel)*. **2009**, *9* (5), 3713–3744. <https://doi.org/10.3390/s90503713>.
- (27) Fakruddin, M.; Mannan, K. S. Bin; Chowdhury, A.; Mazumdar, R. M.; Hossain, M. N.; Islam, S.; Chowdhury, M. A. Nucleic Acid Amplification: Alternative Methods of Polymerase Chain Reaction. *J. Pharm. Bioallied Sci.* **2013**, *5* (4), 245–252. <https://doi.org/10.4103/0975-7406.120066>.
- (28) Garibyan, L.; Avashia, N. Polymerase Chain Reaction. *J. Invest. Dermatol.* **2013**, *133* (3), 1–4. <https://doi.org/http://dx.doi.org/10.1038/jid.2013.1>.
- (29) Yang, S.; Rothman, R. E. PCR-Based Diagnostics for Infectious Diseases: Uses, Limitations, and Future Applications in Acute-Care Settings. *Lancet Infect. Dis.* **2004**, *4* (6), 337–348. [https://doi.org/http://dx.doi.org/10.1016/S1473-3099\(04\)01044-8](https://doi.org/http://dx.doi.org/10.1016/S1473-3099(04)01044-8).
- (30) Baumforth, K. R. N.; Nelson, P. N.; Digby, J. E.; O'neil, J. D.; Murray, P. G. The Polymerase Chain Reaction.
- (31) Jiang, L.; Mancuso, M.; Lu, Z.; Akar, G.; Cesarman, E.; Erickson, D. Solar Thermal Polymerase Chain Reaction for Smartphone-Assisted Molecular Diagnostics. *Nat. Sci. Reports* **2014**, *4* (4137). <https://doi.org/10.1038/srep04137>.

- (32) Lee, D.; Chou, W. P.; Yeh, S. H.; Chen, P. J.; Chen, P. H. DNA Detection Using Commercial Mobile Phones. *Biosens. Bioelectron.* **2011**, *26* (11), 4349–4354. <https://doi.org/10.1016/J.BIOS.2011.04.036>.
- (33) Rajendran, V. K.; Bakthavathsalam, P.; Bergquist, P. L.; Sunna, A. Smartphone Detection of Antibiotic Resistance Using Convective PCR and a Lateral Flow Assay. *Sensors Actuators B Chem.* **2019**, *298*. <https://doi.org/10.1016/j.snb.2019.126849>.
- (34) Al-Soud, W. A.; Rådström, P. Purification and Characterization of PCR-Inhibitory Components in Blood Cells. *J. Clin. Microbiol.* **2001**, *39* (2), 485–493. <https://doi.org/10.1128/JCM.39.2.485-493.2001>.
- (35) Khan, G.; Kangro, H. O.; Coates, P. J.; Heath, R. B. Inhibitory Effects of Urine on the Polymerase Chain Reaction for Cytomegalovirus DNA. *J. Clin. Pathol.* **1991**, *44* (5), 360–365.
- (36) Miyagi, K.; Sano, K.; Morita, C.; Imura, S.; Morimatsu, S.; Goto, T.; Nakano, Y.; Omura, K.; Matsumoto, Y.; Maeda, K.; et al. An Improved Method for Detecting Faecal *Vibrio Cholerae* by PCR of the Toxin A Gene. *J. Med. Microbiol.* **1999**, *48* (10), 883–889. <https://doi.org/doi:10.1099/00222615-48-10-883>.
- (37) Mori, Y.; Notomi, T. Loop-Mediated Isothermal Amplification (LAMP): A Rapid, Accurate, and Cost-Effective Diagnostic Method for Infectious Diseases. *J. Infect. Chemother.* **2009**, *15* (2), 62–69. <https://doi.org/10.1007/s10156-009-0669-9>.
- (38) Jiang, Y. S.; Bhadra, S.; Li, B.; Wu, Y. R.; Milligan, J. N.; Ellington, A. D. Robust Strand Exchange Reactions for the Sequence-Specific, Real-Time Detection of Nucleic Acid Amplicons. *Anal. Chem.* **2015**, *87* (6), 3314–3320. <https://doi.org/10.1021/ac504387c>.
- (39) Nagamine, K.; Hase, T.; Notomi, T. Accelerated Reaction by Loop-Mediated Isothermal Amplification Using Loop Primers. *Mol. Cell. Probes* **2002**, *16*, 223–229. <https://doi.org/10.1006/mcpr.2002.0415>.
- (40) Rolando, J. C.; Jue, E.; Schoepp, N. G.; Ismagilov, R. F. Real-Time, Digital LAMP with Commercial Microfluidic Chips Reveals the Interplay of Efficiency, Speed, and Background Amplification as a Function of Reaction Temperature and Time. *Anal. Chem.* **2019**, *91* (1), 1034–1042. <https://doi.org/10.1021/acs.analchem.8b04324>.
- (41) NEB. Bst 3.0 Activity <https://www.neb.com/faqs/2015/08/05/how-active-is-bst-3-0-at-other-temperatures> (accessed Feb 9, 2019).

- (42) Phillips, E. A.; Moehling, T. J.; Bhadra, S.; Ellington, A. D.; Linnes, J. C. Strand Displacement Probes Combined with Isothermal Nucleic Acid Amplification for Instrument-Free Detection from Complex Samples. *Anal. Chem.* **2018**, *90* (11), 6580–6586. <https://doi.org/10.1021/acs.analchem.8b00269>.
- (43) Clayton, K. N.; Moehling, T. J.; Lee, D. H.; Wereley, S. T.; Linnes, J. C.; Kinzer-Ursem, T. L. Particle Diffusometry: An Optical Detection Method for *Vibrio Cholerae* Presence in Environmental Water Samples. *Nat. Sci. Reports* **2019**, *9* (1), 1739. <https://doi.org/10.1038/s41598-018-38056-7>.
- (44) Mori, Y.; Kanda, H.; Notomi, T. Loop-Mediated Isothermal Amplification (LAMP): Recent Progress in Research and Development. *J. Infect. Chemother.* **2013**, *19* (3), 404–411. <https://doi.org/http://dx.doi.org/10.1007/s10156-013-0590-0>.
- (45) Notomi, T.; Okayama, H.; Masubuchi, H.; Yonekawa, T.; Watanabe, K.; Amino, N.; Hase, T. Loop-Mediated Isothermal Amplification of DNA. *Nucleic Acids Res.* **2000**, *28* (12), e63–e63.
- (46) Whiting, S. H.; Champoux, J. J. Properties of Strand Displacement Synthesis by Moloney Murine Leukemia Virus Reverse Transcriptase: Mechanistic Implications1. *J. Mol. Biol.* **1998**, *278* (3), 559–577. <https://doi.org/http://dx.doi.org/10.1006/jmbi.1998.1720>.
- (47) Iwamoto, T.; Sonobe, T.; Hayashi, K. Loop-Mediated Isothermal Amplification for Direct Detection of Mycobacterium Tuberculosis Complex, *M. Avium*, and *M. Intracellulare* in Sputum Samples. *J. Clin. Microbiol.* **2003**, *41* (6), 2616–2622. <https://doi.org/10.1128/JCM.41.6.2616-2622.2003>.
- (48) Mori, Y.; Nagamine, K.; Tomita, N.; Notomi, T. Detection of Loop-Mediated Isothermal Amplification Reaction by Turbidity Derived from Magnesium Pyrophosphate Formation. *Biochem. Biophys. Res. Commun.* **2001**, *289* (1), 150–154. <https://doi.org/http://dx.doi.org/10.1006/bbrc.2001.5921>.
- (49) Tomita, N.; Mori, Y.; Kanda, H.; Notomi, T. Loop-Mediated Isothermal Amplification (LAMP) of Gene Sequences and Simple Visual Detection of Products. *Nat. Protoc.* **2008**, *3* (5), 877–882. <https://doi.org/10.1038/nprot.2008.57>.
- (50) Connelly, J. T.; Rolland, J. P.; Whitesides, G. M. “Paper Machine” for Molecular Diagnostics. *Anal. Chem.* **2015**, *87* (15), 7595–7601. <https://doi.org/10.1021/acs.analchem.5b00411>.

- (51) Kong, J. E.; Wei, Q.; Tseng, D.; Zhang, J.; Pan, E.; Lewinski, M.; Garner, O. B.; Ozcan, A.; DiCarlo, D. Highly Stable and Sensitive Nucleic Acid Amplification and Cell-Phone-Based Readout. *ACS Nano* **2017**, *11*, 2934–2943. <https://doi.org/10.1021/acsnano.6b08274>.
- (52) Barnes, L.; Heithoff, D. M.; Mahan, S. P.; Fox, G. N.; Zambrano, A.; Choe, J.; Fitzgibbons, L. N.; Marth, J. D.; Fried, J. C.; Soh, H. T.; et al. Smartphone-Based Pathogen Diagnosis in Urinary Sepsis Patients. *EBioMedicine* **2018**, *36*, 73–82. <https://doi.org/10.1016/j.ebiom.2018.09.001>.
- (53) WHO. Cholera Fact Sheet.
- (54) Centers for Disease Control and Prevention. Cholera - *Vibrio cholerae* infection <https://www.cdc.gov/cholera/index.html> (accessed Oct 17, 2018).
- (55) New Horizons Diagnostics. SMART™ Cholera O1 Test Kit http://www.nhdiag.com/cholera_bt.shtml (accessed Mar 27, 2019).
- (56) Arkray. Crystal - VC (Dipstick) http://www.arkray.co.in/english/products/immunodiagnostic_products/rapid_tests/crystal_vc.html (accessed Mar 27, 2019).
- (57) Ley, B.; Khatib, A. M.; Thriemer, K.; von Seidlein, L.; Deen, J.; Mukhopadyay, A.; Chang, N.-Y.; Hashim, R.; Schmied, W.; Busch, C. J.-L.; et al. Evaluation of a Rapid Dipstick (Crystal VC) for the Diagnosis of Cholera in Zanzibar and a Comparison with Previous Studies. *PLoS One* **2012**, *7* (5), e36930. <https://doi.org/10.1371/journal.pone.0036930>.
- (58) LaRocque, R. C.; Krastins, B.; Harris, J. B.; Lebrun, L. M.; Parker, K. C.; Chase, M.; Ryan, E. T.; Qadri, F.; Sarracino, D.; Calderwood, S. B. Proteomic Analysis of *Vibrio Cholerae* in Human Stool. *Infect. Immun.* **2008**, *76* (9), 4145–4151. <https://doi.org/10.1128/IAI.00585-08>.
- (59) Alam, M. T.; Weppelmann, T. A.; Weber, C. D.; Johnson, J. A.; Rashid, M. H.; Birch, C. S.; Brumback, B. A.; Beau de Rochars, V. E. M.; Morris, J. G.; Ali, A. Monitoring Water Sources for Environmental Reservoirs of Toxigenic *Vibrio Cholerae* O1, Haiti. *Emerg. Infect. Dis.* **2014**, *20* (3), 356–363. <https://doi.org/10.3201/eid2003.131293>.
- (60) Maternova. Cholera Rapid Diagnostic Test <https://maternova.net/products/cholera-rapid-test> (accessed Mar 27, 2019).
- (61) World Health Organization. HIV/AIDS <https://www.who.int/news-room/fact-sheets/detail/hiv-aids> (accessed Jan 12, 2019).

- (62) OraSure Technologies. OraQuick In Home HIV Test <http://www.oraquick.com/What-is-OraQuick/How-Oral-Testing-Works> (accessed May 20, 2020).
- (63) Parekh, B. S.; Ou, C.-Y.; Fonjungo, P. N.; Kalou, M. B.; Rottinghaus, E.; Puren, A.; Alexander, H.; Hurlston Cox, M.; Nkengasong, J. N. Diagnosis of Human Immunodeficiency Virus Infection. *Clin. Microbiol. Rev.* **2019**, *32* (1), e00064-18. <https://doi.org/10.1128/CMR.00064-18>.
- (64) Stone, M.; Bainbridge, J.; Sanchez, A. M.; Keating, S. M.; Pappas, A.; Rountree, W.; Todd, C.; Bakkour, S.; Manak, M.; Peel, S. A.; et al. Comparison of Detection Limits of Fourth- and Fifth-Generation Combination HIV Antigen-Antibody, P24 Antigen, and Viral Load Assays on Diverse HIV Isolates. *J. Clin. Microbiol.* **2018**, *56* (8), e02045-17. <https://doi.org/10.1128/JCM.02045-17>.
- (65) Abbott. Alere HIV Combo <https://www.alere.com/en/home/product-details/alere-hiv-combo.html> (accessed May 20, 2020).
- (66) Gurralla, R.; Lang, Z.; Shepherd, L.; Davidson, D.; Harrison, E.; Mcclure, M.; Kaye, S.; Toumazou, C.; Cooke, G. S. Novel PH Sensing Semiconductor for Point-of-Care Detection of HIV-1 Viremia. *Nat. Sci. Reports* **2016**, *6*. <https://doi.org/10.1038/srep36000>.
- (67) Wei, X.; Tian, T.; Jia, S.; Zhu, Z.; Ma, Y.; Sun, J.; Lin, Z.; Yang, C. J. Microfluidic Distance Readout Sweet Hydrogel Integrated Paper-Based Analytical Device (MDiSH-PAD) for Visual Quantitative Point-of-Care Testing. *Anal. Chem.* **2016**, *88* (4), 2345–2352. <https://doi.org/10.1021/acs.analchem.5b04294>.
- (68) Clayton, K. N.; Salameh, J. W.; Wereley, S. T.; Kinzer-Ursem, T. L. Physical Characterization of Nanoparticle Size and Surface Modification Using Particle Scattering Diffusometry. *Biomicrofluidics* **2016**, *10* (5), 1–15. <https://doi.org/10.1063/1.4962992>.
- (69) Clayton, K. N.; Berglund, G. D.; Linnes, J. C.; Kinzer-Ursem, T. L.; Wereley, S. T. DNA Microviscosity Characterization with Particle Diffusometry for Downstream DNA Detection Applications. *Anal. Chem.* **2017**, *89* (24), 13334–13341.
- (70) Clayton, K. N.; Lee, D. H.; Wereley, S. T.; Kinzer-Ursem, T. L. Measuring Biotherapeutic Viscosity and Degradation On-Chip with Particle Diffusometry. *Lab Chip* **2017**, No. 23.
- (71) Denué, B. Evaluation of a Rapid Dipstick Test (Crystal Vc) for the Diagnosis of Cholera in Maiduguri, Northeastern Nigeria. *Arch. Med. Heal. Sci.* **2018**, *6* (1), 24. https://doi.org/10.4103/amhs.amhs_20_18.

- (72) Schrader, C.; Schielke, A.; Ellerbroek, L.; Johne, R. PCR Inhibitors - Occurrence, Properties and Removal. *J. Appl. Microbiol.* **2012**, *113* (5), 1014–1026. <https://doi.org/10.1111/j.1365-2672.2012.05384.x>.
- (73) Mauk, M.; Song, J.; Bau, H. H.; Gross, R.; Bushman, F. D.; Collman, R. G.; Liu, C. Miniaturized Devices for Point of Care Molecular Detection of HIV. *Lab Chip* **2017**, *17* (3), 382–394. <https://doi.org/10.1039/c6lc01239f>.
- (74) Rodriguez, N. M.; Linnes, J. C.; Fan, A.; Ellenson, C. K.; Pollock, N. R.; Klapperich, C. M. Paper-Based RNA Extraction, in Situ Isothermal Amplification, and Lateral Flow Detection for Low-Cost, Rapid Diagnosis of Influenza A (H1N1) from Clinical Specimens. *Anal. Chem.* **2015**, *87* (15), 7872–7879. <https://doi.org/10.1021/acs.analchem.5b01594>.
- (75) Singleton, J.; Osborn, J. L.; Lillis, L.; Hawkins, K.; Guelig, D.; Price, W.; Johns, R.; Ebels, K.; Boyle, D.; Weigl, B.; et al. Electricity-Free Amplification and Detection for Molecular Point-of-Care Diagnosis of HIV-1. *PLoS One* **2014**, *9* (11). <https://doi.org/10.1371/journal.pone.0113693>.
- (76) Miočević, O.; Cole, C. R.; Laughlin, M. J.; Buck, R. L.; Slowey, P. D.; Shirtcliff, E. A. Quantitative Lateral Flow Assays for Salivary Biomarker Assessment: A Review. *Front. Public Heal.* **2017**, *5* (133). <https://doi.org/10.3389/fpubh.2017.00133>.
- (77) Mansfield, M. A. *Design Considerations for Lateral Flow Test Strips*.
- (78) Okada, K.; Chantaroj, S.; Taniguchi, T.; Suzuki, Y.; Roobthaisong, A.; Puiprom, O.; Honda, T.; Sawanpanyalert, P. A Rapid, Simple, and Sensitive Loop-Mediated Isothermal Amplification Method to Detect Toxigenic *Vibrio Cholerae* in Rectal Swab Samples. *Diagn. Microbiol. Infect. Dis.* **2010**, *66* (2), 135–139. <https://doi.org/http://dx.doi.org/10.1016/j.diagmicrobio.2009.09.004>.
- (79) Holstein, C. A. Development of a Novel Paper-Based Flu Test for Improved Diagnosis at the Point of Care, University of Washington, 2015.
- (80) Yamazaki, W.; Seto, K.; Taguchi, M.; Ishibashi, M.; Inoue, K. Sensitive and Rapid Detection of Cholera Toxin-Producing *Vibrio Cholerae* Using a Loop-Mediated Isothermal Amplification. *BMC Microbiol.* **2008**, *8*, 94. <https://doi.org/10.1186/1471-2180-8-94>.
- (81) Zhou, D.; Guo, J.; Xu, L.; Gao, S.; Lin, Q.; Wu, Q.; Wu, L.; Que, Y. Establishment and Application of a Loop-Mediated Isothermal Amplification (LAMP) System for Detection of Cry1Ac Transgenic Sugarcane. *Sci. Rep.* **2014**, *4*. <https://doi.org/10.1038/srep04912>.

- (82) Chander, Y.; Koelbl, J.; Puckett, J.; Moser, M. J.; Klingele, A. J.; Liles, M. R.; Carrias, A.; Mead, D. A.; Schoenfeld, T. W. A Novel Thermostable Polymerase for RNA and DNA Loop-Mediated Isothermal Amplification (LAMP). *Front. Microbiol.* **2014**, *5* (AUG), 395. <https://doi.org/10.3389/fmicb.2014.00395>.
- (83) Reisle, C. LAMP Restriction Digest Fragment Analysis <http://creisle.github.io/creisle.lamprflp/> (accessed Jan 15, 2019).
- (84) Karanis, P.; Thekisoe, O.; Kiouptsi, K.; Ongerth, J.; Igarashi, I.; Inoue, N. Development and Preliminary Evaluation of a Loop-Mediated Isothermal Amplification Procedure for Sensitive Detection of Cryptosporidium Oocysts in Fecal and Water Samples. *Appl. Environ. Microbiol.* **2007**, *73* (17), 5660–5662. <https://doi.org/10.1128/AEM.01152-07>.
- (85) Huq, A.; Sack, R. B.; Nizam, A.; Longini, I. M.; Nair, G. B.; Ali, A.; Morris, J. G.; Khan, M. N. H.; Siddique, A. K.; Yunus, M.; et al. Critical Factors Influencing the Occurrence of Vibrio Cholerae in the Environment of Bangladesh. *Appl. Environ. Microbiol.* **2005**, *71* (8), 4645–4654. <https://doi.org/10.1128/AEM.71.8.4645-4654.2005>.
- (86) Cabral, J. P. S. Water Microbiology. Bacterial Pathogens and Water. *Int. J. Environ. Res. Public Health* **2010**, *7* (10), 3657–3703. <https://doi.org/10.3390/ijerph7103657>.
- (87) Davalieva, K.; Efremov, G. D. Influence of Salts and PCR Inhibitors on the Amplification Capacity of Three Thermostable DNA Polymerases. *Maced. J. Chem. Chem. Eng.* **2010**, *29* (1), 57–62.
- (88) Leung, V.; Brooks, M.; Emerson, S.; Ali, M.; Filipe, C. D. M. Ready-to-use Thermally Stable Mastermix Pills for Molecular Biology Applications. *Biotechnol. Prog.* **2019**, *35* (2), e2764. <https://doi.org/10.1002/btpr.2764>.
- (89) NEB. Bst 2.0 Polymerase <https://www.nebiolabs.com.au/faqs/2012/08/28/why-would-i-use-bst-2-0-warmstart-dna-polymerase1> (accessed May 29, 2020).
- (90) Sigma-Aldrich. Hot Start dNTPs <https://www.sigmaaldrich.com/technical-documents/protocols/biology/cleanamp-dntps.html> (accessed May 29, 2020).
- (91) Wang, W. Lyophilization and Development of Solid Protein Pharmaceuticals. *Int. J. Pharm.* **2000**, *203* (1–2), 1–60. [https://doi.org/10.1016/S0378-5173\(00\)00423-3](https://doi.org/10.1016/S0378-5173(00)00423-3).
- (92) Ota, A.; Matsumura, K.; Lee, J.-J.; Sumi, S.; Hyon, S.-H. StemCell Keep™ Is Effective for Cryopreservation of Human Embryonic Stem Cells by Vitrification. *Cell Transplant.* **2017**, *26* (5), 773–787. <https://doi.org/10.3727/096368916X692654>.

- (93) Hayashida, K.; Kajino, K.; Hachaambwa, L.; Namangala, B.; Sugimoto, C. Direct Blood Dry LAMP: A Rapid, Stable, and Easy Diagnostic Tool for Human African Trypanosomiasis. *PLoS Negl. Trop. Dis.* **2015**, *9* (3), e0003578. <https://doi.org/10.1371/journal.pntd.0003578>.
- (94) NEB. Nonspecific Amplification <https://www.neb.com/faqs/2013/10/24/how-can-i-reduce-nonspecific-or-non-template-amplification> (accessed Jun 1, 2020).
- (95) Einstein, A. *Investigations on the Theory of the Brownian Movement*; 1905.
- (96) Renkin, E. M. FILTRATION, DIFFUSION, AND MOLECULAR SIEVING THROUGH POROUS CELLULOSE MEMBRANES. *J. Gen. Physiol.* **1954**, *38* (2), 225 LP – 243. <https://doi.org/10.1085/jgp.38.2.225>.
- (97) Fournier, R. L. *Basic Transport Phenomena in Biomedical Engineering*, 3rd ed.; CRC Press, 2012.
- (98) Seok, Y.; Joung, H. A.; Byun, J. Y.; Jeon, H. S.; Shin, S. J.; Kim, S.; Shin, Y. B.; Han, H. S.; Kim, M. G. A Paper-Based Device for Performing Loop-Mediated Isothermal Amplification with Real-Time Simultaneous Detection of Multiple DNA Targets. *Theranostics* **2017**, *7* (8), 2220–2230. <https://doi.org/10.7150/thno.18675>.
- (99) Calmy, A.; Ford, N.; Hirschel, B.; Reynolds, S. J.; Lynen, L.; Goemaere, E.; de la Vega, F. G.; Perrin, L.; Rodriguez, W. HIV Viral Load Monitoring in Resource-Limited Regions: Optional or Necessary? *Clin. Infect. Dis.* **2007**, *44* (1), 128–134. <https://doi.org/10.1086/510073>.
- (100) Choi, J. R.; Tang, R.; Wang, S.; Wan Abas, W. A. B.; Pिंगguan-Murphy, B.; Xu, F. Paper-Based Sample-to-Answer Molecular Diagnostic Platform for Point-of-Care Diagnostics. *Biosens. Bioelectron.* **2015**, *74*, 427–439. <https://doi.org/10.1016/j.bios.2015.06.065>.
- (101) Bishop, J. D.; Hsieh, H. V.; Gasperino, D. J.; Weigl, B. H. Sensitivity Enhancement in Lateral Flow Assays: A Systems Perspective. *Lab Chip* **2019**, *19* (15), 2486–2499. <https://doi.org/10.1039/c9lc00104b>.
- (102) Tang, R.; Yang, H.; Gong, Y.; You, M.; Liu, Z.; Choi, J. R.; Wen, T.; Qu, Z.; Mei, Q.; Xu, F. A Fully Disposable and Integrated Paper-Based Device for Nucleic Acid Extraction, Amplification and Detection. *Lab Chip* **2017**, *17* (7), 1270–1279. <https://doi.org/10.1039/C6LC01586G>.

- (103) Phillips, E. A.; Shen, R.; Zhao, S.; Linnes, J. C. Thermally Actuated Wax Valves for Paper-Fluidic Diagnostics. *Lab Chip* **2016**, *16* (21), 4230–4236. <https://doi.org/10.1039/C6LC00945J>.
- (104) Phillips, E. A.; Moehling, T. J.; Ejendal, K. F. K.; Hoilett, O. S.; Byers, K. M.; Basing, L. A.; Jankowski, L. A.; Bennett, J. B.; Lin, L.-K.; Stanciu, L. A.; et al. Microfluidic Rapid and Autonomous Analytical Device (MicroRAAD) to Detect HIV from Whole Blood Samples. *Lab Chip* **2019**. <https://doi.org/10.1039/c9lc00506d>.
- (105) Byers, K. M.; Lin, L. K.; Moehling, T. J.; Stanciu, L.; Linnes, J. C. Versatile Printed Microheaters to Enable Low-Power Thermal Control in Paper Diagnostics. *Analyst* **2020**, *145* (1), 184–196. <https://doi.org/10.1039/c9an01546a>.
- (106) Phillips, E. A. Stimuli-Responsive Valving Mechanisms for Paper-Based Diagnostics, Purdue University, 2020.
- (107) Yanko, W. A.; De Leon, R.; Rochelle, P. A.; Chen, W. *Development of Practical Methods to Assess the Presence of Bacterial Pathogens in Water*; 2004.
- (108) Linnes, J. C.; Rodriguez, N. M.; Liu, L.; Klapperich, C. M. Polyethersulfone Improves Isothermal Nucleic Acid Amplification Compared to Current Paper-Based Diagnostics. *Biomed. Microdevices* **2016**, *18* (2), 30. <https://doi.org/10.1007/s10544-016-0057-z>.
- (109) Aïzel, K.; Agache, V.; Pudda, C.; Bottausci, F.; Fraisseix, C.; Bruniaux, J.; Navarro, F.; Fouillet, Y. Enrichment of Nanoparticles and Bacteria Using Electroless and Manual Actuation Modes of a Bypass Nanofluidic Device. *Lab Chip* **2013**, *13*, 4485. <https://doi.org/10.1039/c3lc50835h>.
- (110) Jing, W.; Zhao, W.; Liu, S.; Li, L.; Tsai, C.-T.; Fan, X.; Wu, W.; Li, J.; Yang, X.; Sui, G. Microfluidic Device for Efficient Airborne Bacteria Capture and Enrichment. *Anal. Chem.* **2013**, *85*, 5255–5562. <https://doi.org/10.1021/ac400590c>.
- (111) Ohlsson, P.; Evander, M.; Petersson, K.; Mellhammar, L.; Lehmusvuori, A.; Karhunen, U.; Soikkeli, M.; Seppä, T.; Tuunainen, E.; Spangar, A.; et al. Integrated Acoustic Separation, Enrichment, and Microchip Polymerase Chain Reaction Detection of Bacteria from Blood for Rapid Sepsis Diagnostics. *Anal. Chem.* **2016**, *88*, 9403–9411. <https://doi.org/10.1021/acs.analchem.6b00323>.

- (112) Cho, B.; Lee, S. H.; Song, J.; Bhattacharjee, S.; Feng, J.; Hong, S.; Song, M.; Kim, W.; Lee, J.; Bang, D.; et al. Nanophotonic Cell Lysis and Polymerase Chain Reaction with Gravity-Driven Cell Enrichment for Rapid Detection of Pathogens. *ACS Nano* **2019**, *13*, 13866–13874. <https://doi.org/10.1021/acsnano.9b04685>.
- (113) Channon, R. B.; Nguyen, M. P.; Henry, C. S.; Dandy, D. S. Multilayered Microfluidic Paper-Based Devices: Characterization, Modeling, and Perspectives. *Anal. Chem.* **2019**, *91* (14), 8966–8972. <https://doi.org/10.1021/acs.analchem.9b01112>.
- (114) Buser, J. R.; Byrnes, S. A.; Anderson, C. E.; Howell, A. J.; Kauffman, P. C.; Bishop, J. D.; Wheeler, M. H.; Kumar, S.; Yager, P. Understanding Partial Saturation in Paper Microfluidics Enables Alternative Device Architectures. *Anal. Methods* **2019**, *11* (3), 336–345. <https://doi.org/10.1039/c8ay01977k>.
- (115) Clennell, M. Ben. *Tortuosity: A Guide through the Maze*; 1997.
- (116) Horst, A. L.; Rosenbohm, J. M.; Kolluri, N.; Hardick, J.; Gaydos, C. A.; Cabodi, M.; Klapperich, C. M.; Linnes, J. C. A Paperfluidic Platform to Detect *Neisseria Gonorrhoeae* in Clinical Samples. *Biomed. Microdevices* **2018**, *20* (2), 35. <https://doi.org/10.1007/s10544-018-0280-x>.
- (117) Rouet, F.; Rouzioux, C. HIV-1 Viral Load Testing Cost in Developing Countries: What's New? *Expert Rev. Mol. Diagn.* **2007**, *7* (6), 703–707. <https://doi.org/10.1586/14737159.7.6.703>.
- (118) Wilson, D. J.; Kumar, A. A.; Mace, C. R. Overreliance on Cost Reduction as a Featured Element of Sensor Design. *ACS Sensors* **2019**, *4* (5), 1120–1125. <https://doi.org/10.1021/acssensors.9b00260>.
- (119) Wu, G.; Zaman, M. H. Low-Cost Tools for Diagnosing and Monitoring HIV Infection in Low-Resource Settings. *Bull. World Health Organ.* **2012**, *90* (12), 914–920. <https://doi.org/10.2471/BLT.12.102780>.
- (120) Wang, D.; Xu, X.; Deng, X.; Chen, C.; Li, B.; Tan, H.; Wang, H.; Tang, S.; Qiu, H.; Chen, J.; et al. Detection of *Vibrio Cholerae* O1 and O139 in Environmental Water Samples by an Immunofluorescent-Aggregation Assay. *Appl. Environ. Microbiol.* **2010**, *76* (16), 5520–5525. <https://doi.org/10.1128/AEM.02559-09>.

- (121) Alam, M. T.; Weppelmann, T. A.; Longini, I.; De Rochars, V. M. B.; Morris, J. G.; Ali, A.; Rashid, M. Increased Isolation Frequency of Toxigenic *Vibrio Cholerae* O1 from Environmental Monitoring Sites in Haiti. *PLoS One* **2015**, *10* (4), e0124098. <https://doi.org/10.1371/journal.pone.0124098>.
- (122) Campbell, G. A.; deLesdernier, D.; Mutharasan, R. Detection of Airborne *Bacillus Anthracis* Spores by an Integrated System of an Air Sampler and a Cantilever Immunosensor. *Sensors Actuators B Chem.* **2007**, *127* (2), 376–382. <https://doi.org/https://doi.org/10.1016/j.snb.2007.04.038>.
- (123) Campbell, G. A.; Mutharasan, R. Detection of Pathogen *Escherichia Coli* O157:H7 Using Self-Excited PZT-Glass Microcantilevers. *Biosens. Bioelectron.* **2005**, *21* (3), 462–473. <https://doi.org/https://doi.org/10.1016/j.bios.2004.11.009>.
- (124) Maraldo, D.; Mutharasan, R. 10-Minute Assay for Detecting *Escherichia Coli* O157:H7 in Ground Beef Samples Using Piezoelectric-Excited Millimeter-Size Cantilever Sensors. *J Food Prot* **2007**, *70* (7), 1670–1677.
- (125) Maraldo, D.; Mutharasan, R. Preparation-Free Method for Detecting *Escherichia Coli* O157:H7 in the Presence of Spinach, Spring Lettuce Mix, and Ground Beef Particulates. *J Food Prot* **2007**, *70* (11), 2651–2655.
- (126) Ilic, B.; Craighead, H. G. Topographical Patterning of Chemically Sensitive Biological Materials Using a Polymer-Based Dry Lift Off. *Biomed. Microdevices* **2000**, *2* (4), 317–322. <https://doi.org/10.1023/A:1009911407093>.
- (127) Zhou, Y.; Ramasamy, R. P. Phage-Based Electrochemical Biosensors for Detection of Pathogenic Bacteria. **2015**. <https://doi.org/10.1149/06938.0001ecst>.
- (128) Xu, X.; Chen, Y.; Wei, H.; Xia, B.; Liu, F.; Li, N. Counting Bacteria Using Functionalized Gold Nanoparticles as the Light-Scattering Reporter. **2012**. <https://doi.org/10.1021/ac302471c>.
- (129) Safavieh, M.; Ahmed, M. U.; Ng, A.; Zourob, M. High-Throughput Real-Time Electrochemical Monitoring of LAMP for Pathogenic Bacteria Detection. *Biosens. Bioelectron.* **2014**, *58*, 101–106. <https://doi.org/10.1016/J.BIOS.2014.02.002>.
- (130) Lu, L.; Sick, V. High-Speed Particle Image Velocimetry near Surfaces. *J. Vis. Exp.* **2013**, No. 76. <https://doi.org/10.3791/50559>.

- (131) Chamrathy, P.; Garimella, S. V.; Wereley, S. T. Non-Intrusive Temperature Measurement Using Microscale Visualization Techniques. *Exp. Fluids* **2009**, *47* (1), 159–170. <https://doi.org/10.1007/s00348-009-0646-1>.
- (132) Adrian, R. J.; Yao, C.-S. Pulsed Laser Technique Application to Liquid and Gaseous Flows and the Scattering Power of Seed Materials. *Appl. Opt.* **1985**, *24* (1), 44–52. <https://doi.org/10.1364/AO.24.000044>.
- (133) Olsen, M. G.; Adrian, R. J. Out-of-Focus Effects on Particle Image Visibility and Correlation in Microscopic Particle Image Velocimetry. *Exp. Fluids* **2000**, *29*, S166–S174. <https://doi.org/10.1007/s003480070018>.
- (134) Chuang, H.-S.; Sie, Y.-S. A Micro-Volume Viscosity Measurement Technique Based on MicroPIV Diffusometry. *Microfluid. Nanofluidics* **2014**, *16*, 65–72.
- (135) Raffel, M.; Willert, C. E.; Wereley, S. T.; Kompenhans, J. *Particle Image Velocimetry: A Practical Guide*; 2007; Vol. 2nd. <https://doi.org/10.1097/JTO.0b013e3182370e69>.
- (136) Meinhart, C. D.; Wereley, S. T.; Gray, M. H. B. Volume Illumination for Two-Dimensional Particle Image Velocimetry. *Meas. Sci. Technol.* **2000**, *11* (6), 809–814. <https://doi.org/10.1088/0957-0233/11/6/326>.
- (137) Leydesdorff, L. Similarity Measures, Author Cocitation Analysis, and Information Theory. *J. Am. Soc. Inf. Sci. Technol.* **2005**, *56* (7), 769–772. <https://doi.org/10.1002/asi.20130>.
- (138) Goodman, A.; Tseng, Y.; Wirtz, D. Effect of Length, Topology, and Concentration on the Microviscosity and Microheterogeneity of DNA Solutions. *J. Mol. Biol.* **2002**, *323*, 199–215. [https://doi.org/10.1016/S0022-2836\(02\)00893-8](https://doi.org/10.1016/S0022-2836(02)00893-8).
- (139) Tian, B.; Qiu, Z.; Ma, J.; Zardán Gómez de la Torre, T.; Johansson, C.; Svedlinh, P.; Strömberg, M. Attomolar Zika Virus Oligonucleotide Detection Based on Loop-Mediated Isothermal Amplification and AC Susceptometry. *Biosens. Bioelectron.* **2016**, *86*, 420–425. <https://doi.org/10.1016/j.bios.2016.06.085>.
- (140) Packard, M.; Wheeler, E.; Alocilja, E.; Shusteff, M. Performance Evaluation of Fast Microfluidic Thermal Lysis of Bacteria for Diagnostic Sample Preparation. *Diagnostics* **2013**, *3* (1), 105–116. <https://doi.org/10.3390/diagnostics3010105>.
- (141) Reidl, J.; Klose, K. E. *Vibrio Cholerae* and Cholera: Out of the Water and into the Host. *FEMS Microbiol. Rev.* **2002**, *26* (2), 125–139. <https://doi.org/10.1111/j.1574-6976.2002.tb00605.x>.

- (142) Steinhubl, S. R.; Muse, E. D.; Topol, E. J. The Emerging Field of Mobile Health. *Sci Transl Med* **2015**, *7* (283), 283–286. <https://doi.org/10.1126/scitranslmed.aaa3487>.
- (143) Hernandez-Neuta, I.; Neumann, F.; Brightmeyer, J.; Ba Tis, T.; Madaboosi, N.; Wei, Q.; Ozcan, A.; Nilsson, M.; Tis, B. T. Smartphone-Based Clinical Diagnostics: Towards Democratization of Evidence-Based Health Care. *J. Intern. Med.* **2019**, *285*, 19–39. <https://doi.org/10.1111/joim.12820>.
- (144) Zhang, D.; Liu, Q. Biosensors and Bioelectronics on Smartphone for Portable Biochemical Detection. *Biosens. Bioelectron.* **2016**, *75*, 273–284. <https://doi.org/10.1016/j.bios.2015.08.037>.
- (145) Zeng, F.; Mou, T.; Zhang, C.; Huang, X.; Wang, B.; Ma, X.; Guo, J. Paper-Based SERS Analysis with Smartphones as Raman Spectral Analyzers. *Analyst* **2018**, *144*, 137–142. <https://doi.org/10.1039/c8an01901k>.
- (146) Wu, T.-F.; Chen, Y.-C.; Wang, W.-C.; Kucknoor, A. S.; Lin, C.-J.; Lo, Y.-H.; Yao, C.-W.; Lian, I. Rapid Waterborne Pathogen Detection with Mobile Electronics. *Sensors* **2017**, *17* (6). <https://doi.org/10.3390/s17061348>.
- (147) Duarte, C.; Salm, E.; Dorvel, B.; Reddy, B.; Bashir, R. On-Chip Parallel Detection of Foodborne Pathogens Using Loop-Mediated Isothermal Amplification. *Biomed. Microdevices* **2013**, *15* (5), 821–830. <https://doi.org/10.1007/s10544-013-9769-5>.
- (148) Cybulski, J. S.; Clements, J.; Prakash, M. Foldscope: Origami-Based Paper Microscope. *PLoS One* **2014**, *9* (6), e98781. <https://doi.org/10.1371/journal.pone.0098781>.
- (149) Palum, R. Image Sampling with the Bayer Color Filter Array. In *Society for Imaging Science and Technology*; 2001; pp 239–245.
- (150) Rosco. myColor Color Comparison <https://us.rosco.com/en/mycolor> (accessed Jul 27, 2019).
- (151) Ishii, S.; Sadowsky, M. J. Escherichia Coli in the Environment: Implications for Water Quality and Human Health. *Microbes Env.* **2008**, *23* (2), 101–108. <https://doi.org/10.1264/jsme2.23.101>.
- (152) Baratloo, A.; Hosseini, M.; Negida, A.; El Ashal, G. Part 1: Simple Definition and Calculation of Accuracy, Sensitivity and Specificity. *Emerg. (Tehran, Iran)* **2015**, *3* (2), 48–49.

- (153) Hajian-Tilaki, K. Receiver Operating Characteristic (ROC) Curve Analysis for Medical Diagnostic Test Evaluation. *Casp. J. Intern. Med.* **2013**, *4* (2), 627–635.
- (154) Brooke, J. System Usability Scale (SUS) <https://www.usability.gov/how-to-and-tools/methods/system-usability-scale.html> (accessed Jun 10, 2020).
- (155) Aguirre-Pablo, A. A.; Alarfaj, M. K.; Li, E. Q.; Hernández-Sánchez, J. F.; Thoroddsen, S. T. Tomographic Particle Image Velocimetry Using Smartphones and Colored Shadows. *Nat. Sci. Reports* **2017**, *7* (1), 3714. <https://doi.org/10.1038/s41598-017-03722-9>.
- (156) Wei, Q.; Qi, H.; Luo, W.; Tseng, D.; Jung Ki, S.; Wan, Z.; Gö rö cs, Z.; Bentolila, L. A.; Wu, T.-T.; Sun, R.; et al. Fluorescent Imaging of Single Nanoparticles and Viruses on a Smart Phone. *ACS Nano* **2013**, *7* (10), 9147–9155. <https://doi.org/10.1021/nm4037706>.
- (157) Apple. iPhone 6 - Technical Specifications https://support.apple.com/kb/SP705?viewlocale=en_US&locale=ko_KR (accessed Jun 29, 2019).
- (158) Besuschio, S. A.; nica Llano Murcia, M.; Benatar, A. F.; Monnerat, S.; Cruz, I.; Picado, A.; de los, M. A.; Curto, N.; Kubota, Y.; Wehrendt, D. P.; et al. Analytical Sensitivity and Specificity of a Loop-Mediated Isothermal Amplification (LAMP) Kit Prototype for Detection of Trypanosoma Cruzi DNA in Human Blood Samples. *PLoS Negl. Trop. Dis.* **2017**, *11* (7). <https://doi.org/10.1371/journal.pntd.0005779>.
- (159) Nliwasa, M.; Macpherson, P.; Chisala, P.; Kamdolozi, M.; Khundi, M.; Kaswaswa, K.; Mwapasa, M.; Msefula, C.; Sohn, H.; Flach, C.; et al. The Sensitivity and Specificity of Loop-Mediated Isothermal Amplification (LAMP) Assay for Tuberculosis Diagnosis in Adults with Chronic Cough in Malawi. *PLoS One* **2016**, *11* (5). <https://doi.org/10.1371/journal.pone.0155101>.
- (160) Alere. *BinaxNOW Influenza A & B Product Instructions*; 2015.
- (161) NCCLS. *Assessment of the Clinical Accuracy of Laboratory Tests Using Receiver Operating Characteristic (ROC) Plots; Approved Guideline*; 1995.
- (162) Zhou, X.-H.; McClish, D. K.; Obuchowski, N. A.; Electronic Book Collection. *Statistical Methods in Diagnostic Medicine*; Wiley, 2011.

- (163) Yeo, S.-J.; Choi, K.; Cuc, B. T.; Hong, N. N.; Bao, D. T.; Ngoc, N. M.; Le, M. Q.; Hang, N. L. K.; Thach, N. C.; Mallik, S. K.; et al. Smartphone-Based Fluorescent Diagnostic System for Highly Pathogenic H5N1 Viruses. *Theranostics* **2016**, *6* (2), 231–242. <https://doi.org/10.7150/thno.14023>.
- (164) Lee, W.-I.; Park, Y.; Park, J.; Shrivastava, S.; Son, Y.-M.; Choi, H.-J.; Lee, J.; Jeon, B.; Lee, H.; Lee, N.-E. A Smartphone Fluorescence Imaging-Based Mobile Biosensing System Integrated with a Passive Fluidic Control Cartridge for Minimal User Intervention and High Accuracy. *Lab Chip* **2019**, *19* (8), 1502–1511. <https://doi.org/10.1039/C8LC01344F>.
- (165) Moehling, T. J.; Lee, D. H.; Henderson, M. E.; McDonald, M. K.; Tsang, P. H.; Kaakeh, S.; Kim, E. S.; Wereley, S. T.; Kinzer-Ursem, T. L.; Clayton, K. N.; et al. A Smartphone-Based Particle Diffusometry Platform for Sub-Attomolar Detection of *Vibrio Cholerae* in Environmental Water. *Biosens. Bioelectron.* **2020**.

PUBLICATIONS

Moehling, T.J.*, Lee, D.H.* , Henderson, M.E., McDonald, M.K., Tsang, P.H., Kaakeh, S., Kim, E.S., Wereley, S.T., Kinzer-Ursem, T.L., Clayton, K.N., Linnes, J.C. A Smartphone-Based Particle Diffusometry Platform for Sub-Attomolar Detection of *Vibrio cholerae* in Environmental Water. *Biosensors and Bioelectronics*. (2020). (In Review).

Meyerson, B.E., **Moehling T.J.**, Agle, J., Coles, H.B., Phillips, J. Layperson access to naloxone at the local level in Arizona and Indiana, 2018. *Journal of Health Care for the Poor and Underserved*. (2020). (In Review).

Byers, K.M., Lin, L.K., **Moehling, T.J.**, Stanciu, L, Linnes, J.C. Versatile Printed Microheaters to Enable Low-Power Thermal Control in Paper Diagnostics. *Analyst*. (2019). DOI: 10.1039/c9an01546a

Phillips, E.A.* , **Moehling, T.J.***, Ejendal, K.F.K., Hoilett, O.S., Byers, K.M., Basing, L.A., Jankowski, L.A., Bennett, J.B., Lin, L.K., Stanciu, L., Linnes, J.C. Microfluidic Rapid and Autonomous Analytical Device (microRAAD) to Detect HIV RNA from Whole Blood Samples. *Lab on a Chip*. (2019). DOI: 10.1039/C9LC00506D

Meyerson, B.E., Agle, J.D., Jayawardene, W., Eldridge, L.A., Arora, P., Smith, C., Vadiiei, N., Kennedy, A., **Moehling, T.J.**, and PharmNet Research Team. Feasibility of a pharmacy-based harm reduction intervention to reduce opioid overdose, HIV, and hepatitis C – Indiana. *Research in Social and Administrative Pharmacy*. (2019). DOI: 10.1016/j.sapharm.2019.08.026

Clayton, K.N.* , **Moehling, T.J.***, Lee, D.H., Wereley, S.T., Linnes, J.C., Kinzer-Ursem, T.L. Particle Diffusometry: An Optical Detection Method for *Vibrio cholerae* Presence in Environmental Water Samples. *Nature Scientific Reports*. (2019). DOI: 10.1038/s41598-018-38056-7

Phillips, E.A., **Moehling, T.J.**, Bhadra, S., Ellington, A.D., Linnes, J.C. Strand displacement probes combined with isothermal nucleic acid amplification for instrument-free detection from complex samples. *Analytical Chemistry*. (2018). DOI: 10.1021/acs.analchem.8b00269

Zhang, Q., Ding, Y., He, K., Li, H., Gao, F., **Moehling, T.J.**, Wu, X., Duncan, J., Niu, Q. Exposure to Alumina Nanoparticles in Female Mice During Pregnancy Induces Neurodevelopmental Toxicity in the Offspring. *Frontiers in Pharmacology*. (2018). DOI: 10.3389/fphar.2018.00253

*indicates co-first author